THERMODYNAMIC BASED FRAMEWORK FOR DETERMINING SUSTAINABLE ELECTRIC INFRASTRUCTURES AS WELL AS MODELING OF DECOHERENCE IN QUANTUM COMPOSITE SYSTEMS

Sergio Cano-Andrade

Dissertation submitted to the Faculty of the
Virginia Polytechnic Institute and State University
In partial fulfillment of the requirements for the degree of

DOCTOR OF PHILOSOPHY
in
Mechanical Engineering

Michael R. von Spakovsky, Chair
Gian Paolo Beretta
Lamine M. Mili
Benjamin F. Hobbs
Michael W. Ellis
Douglas J. Nelson

February 7, 2014, Blacksburg, Virginia

Keywords: sustainability, resiliency, microgrids, multiobjective optimization, entanglement, decoherence, quantum thermodynamics, steepest-entropy-ascent modeling.

Thermodynamic Based Framework for Determining Sustainable Electric Infrastructures as well as Modeling of Decoherence in Quantum Composite Systems

Sergio Cano-Andrade

Abstract

In this dissertation, applications of thermodynamics at the macroscopic and quantum levels of description are developed. Within the macroscopic level, an upper-level Sustainability Assessment Framework (SAF) is proposed for evaluating the sustainable and resilient synthesis/design and operation of sets of small renewable and non-renewable energy production technologies coupled to power production transmission and distribution networks via microgrids. The upper-level SAF is developed in accord with the four pillars of sustainability, i.e., economic, environmental, technical and social. A superstructure of energy producers with a fixed transmission network initially available is synthesized based on the day with the highest energy demand of the year, resulting in an optimum synthesis, design, and off-design network configuration. The optimization is developed in a quasi-stationary manner with an hourly basis, including partial-load behavior for the producers. Since sustainability indices are typically not expressed in the same units, multicriteria decision making methods are employed to obtain a composite sustainability index.

Within the quantum level of description, steepest-entropy-ascent quantum thermodynamics (SEA-QT) is used to model the phenomenon of decoherence. The two smallest microscopic composite systems encountered in Nature are studied. The first of these is composed of two two-level-type particles, while the second one is composed of a two-level-type particle and an electromagnetic field. Starting from a non-equilibrium state of the composite and for each of the two different composite systems, the time evolution of the state of the composite as well as that of the reduced and locally-perceived states of the constituents are traced along their relaxation towards stable equilibrium at constant system energy. The modeling shows how the initial entanglement and coherence between constituents are reduced during the relaxation towards a state of stable equilibrium. When the constituents are non-interacting, the initial coherence is lost once stable equilibrium is reached. When they are interacting, the coherence in the final stable equilibrium state is only that due to the interaction. For the atom-photon field composite system, decoherence is compared with data obtained experimentally by the CQED group at Paris. The SEA-QT method applied in this dissertation provides an alternative and comprehensive explanation to that obtained with the "open system" approach of Quantum Thermodynamics (QT) and its associated quantum master equations of the Kossakowski-Lindblad-Gorini-Sudarshan type.

To

My parents, Silvia and Sergio;

and to those who have already started their journey, Jorge and Braulio

Acknowledgments

I would like to start this lines by thanking my advisor, Dr. Michael R. von Spakovsky for his guidance during my studies of thermodynamics and its application to the models presented in this document. His class lectures, deep and precise discussions on my research, and most important, his example of conduct through the solving of technical problems and leadership in research projects were sources of motivation and apprenticeship. My gratitude also is to Dr. Gian Paolo Beretta for his guidance during the application of the SEA-QT framework to the interesting and stunning phenomenon of entanglement and decoherence, as well as for his effort and perseverance to continue the leading of this novel scheme. Thanks to my committee members: Dr. Lamine Mili, Dr. Benjamin Hobbs, Dr. Michael Ellis, and Dr. Douglas Nelson for their advices during the development of this dissertation.

Special thanks go to Chiara Lo Prete at Harvard University, who developed the early stages of the upper-level SAF during her Ph.D. at The Johns Hopkins University and provided data for the characterization of the Netherlands and the Northwest European electricity market. The development of the upper-level SAF as is presented in this work would not have been possible without her early efforts.

To my colleagues at Virginia Tech: Charles, Omar, Aimen, Guanchen, Alejandro, Martin, and Scott thank you for their support and companionship.

Many thanks go to the von Spakovsky family: Michael, Naomi, Alexis, Sasha, Nicholas and Michael Josef; and to the Dellinger family: Bob, Carole, Beth, Drew, and Matt and his wife Sara for their friendship and hospitality during my stay in Blacksburg.

I am also grateful to the National Council of Science and Technology (CONACyT), México under assistantship ID 213158 and to the U.S. National Science Foundation (NSF) under grant NSF-EFRI-0835879 for financial support of my doctoral studies. I am also thankful to the Mechanical Engineering Department of Virginia Tech for financial support during the last semester of my studies.

Last but not least, I would like to thank all my family, especially to Katyn, for their love and encouragement to continue my journey through the road that lead to the completion of this document.

Contents

List of Figures

List of Tables

Part I

Upper-Level Sustainability Assessment Framework for Sustainable-Resilient Electric Infrastructures

Chapter 1

Introduction to SAF

1.1 Sustainability

Sustainability has been defined as *"the way to meet the needs of the present without compromising the ability of future generations to meet their own needs"* [1]. Although this definition is reasonable from a qualitative point of view, it raises the question of how to treat it quantitatively. It is generally accepted that sustainability is multidimensional, with four principal aspects: technological, economic, environmental, and social [2, 3]. The economic aspect of sustainability generally involves the capital cost of equipment and operation and maintenance costs (O&M). The environmental aspects include SO_2, NO_x, particulates (i.e., PM_{10}, $PM_{2.5}$), unburned hydrocarbons (UHC), and other emissions (i.e., air, water, etc.) treated either as externalities tied to the level of emissions or as internalities tied to the avoidance of emissions to the environment. The social aspects of sustainability include such things as employment, standards of living, reduction in health issues related to pollution, etc. For the technical issues, the efficiency of power producers is taken as a measure as is an increase in the reliability and resiliency of a power network.

Exergy can be applied directly in the technological aspect by utilizing the exergetic efficiency of energy generators as an index. For the environmental aspects, things are a little more unclear, because although exergy can measure qualitatively the environmental impact, the exergy of a pollutant is inadequate for quantifying damage because toxicity and other damage effects play an important role which cannot be directly captured by the exergy.

1.2 Electricity sector

The economic growth of a country has been tied directly to its capacity for meeting the electricity needs of its society. This energy is produced in centralized energy generators fueled by fossil or renewable sources (i.e., coal, oil, nuclear, natural gas, geothermal, solar, wind, and hydro) connected to a main transmission grid. The electricity is then distributed to the customers via distribution lines, which operate at a lower voltage than that of the transmission network. It is in the distribution network in which decentralized producers have the possibility to be connected and contribute to satisfying the electricity demand from the customers, especially those occurring during peak hours or when unexpected failures are present. Decentralized generators as envisioned here are small-scale producers grouped into microgrids (MGs). A MG is a localized group of small electricity and combined heat and power (CHP) producers operating on renewable and non-renewable fuels. The inclusion of MGs is intended to increase the sustainability of the power network by increasing the penetration of renewable-based producers in the overall network. In addition, the resiliency of the power network is increased, since MGs are located near to the customers and in the event of an unanticipated occurrence (e.g., a hurricane, earthquake, terrorist attack, etc.), the MG can be isolated from the network within seconds and diminish the magnitude of the power outage that otherwise would occur if the MG were not present.

MGs have been available mainly for the industrial sector and for some customers in the commercial sector. The general inclusion of MGs in the power network for residential purposes is still being debated and is a focus of the present dissertation research, which seeks to explore the advantages and/or disadvantages that such grids and their associated producers can bring.

1.3 Optimization of power networks and energy producers

The optimization of power networks and energy producers typically occurs at two levels of detail, i.e., at a level of detail in which the energy planning of a power network with respect to its synthesis/design and operation is optimally developed; and at a level of detail at which the optimal synthesis/design and operation of individual producers is developed without taking into account each producer's interaction within the power network. At this second level, a number of well-developed approaches to the optimal synthesis/design and operation of energy systems use exergy (available energy [4]) in addition to energy to account for the technological aspects of the producer.

Once such approach called *exergoeconomics* formulates the cost of resources needed to generate a unit of product (e.g., electricity) on an exergy basis and minimizes this cost by identifying and quantifying the irreversibilities (or exergy destruction) within the components of the producer. Two of the most widely used exergoeconomic approaches are those by Valero and co-workers [5–10] and Tsatsaronis and co-workers [11–14]. The scope of their application is to individual energy producers only.

With the aim of incorporating environmental aspects into the exergoeconomic optimization of individual energy producers, von Spakovsky and Frangopoulos [15], Frangopoulos and co-workers [16–20], and von Spakovsky and co-workers [21–26] proposed an environomic approach, which uses various environmental penalty factors to find syntheses/designs that not only balance resource and equipment costs but reduce emission releases by the energy producer, as well. Recently, Tsatsaronis and co-workers [27–30] included environmental aspects in their exergoeconomic approach without the use of penalty factors. Their approach, called exergoenvironmental analysis, instead use somewhat less sophisticated environmental indices to help identify which syntheses/designs are more environmentally friendly in order to drive the optimal synthesis/design in a more environmentally friendly direction.

At the level of detail permitted for power networks and their associated producers, initial attempts at optimizing the synthesis/design and operation of a power network were those in which one or several producers were required to meet a certain fixed demand [31], i.e., one node of the network was considered in the analysis only. Latter, several nodes were included with a certain number of producers available at each node to meet a fixed demand at each node [32]. In order to include power losses in the transmission lines, a fixed monetary cost directly proportional to the amount of power flowing in a certain transmission line was imposed [33]. A more realistic model that considered several nodes interconnected with each other as well as actual transmission losses based on the amount of power flowing through the transmission lines was reported in [34]. This model was based on the linearized DC load flow model equivalent to Kirchhoff current and voltage laws. In order to expand the modeling, analysis, and optimization of power networks to a 24-hour demand, using several non-commensurable objective functions, the dynamic environmental economic dispatch problem was introduced [35] in which several producers were connected to a single node and forced to meet a required variable 24-hour demand during which the producers could operate either at full load or at part load. More recent developments to extend the analyses

and optimizations to many nodes and the introduction of MGs and renewable energy technologies into the power network with the aim of exploring the technical (e.g., efficiency and reliability) as well as the economic aspects of the network [36–38].

The methodologies developed to date for the optimization of power networks and individual energy producers will be described in some detail in Chapter 2. In this chapter, only an overview is included in order to provide a picture of what has been developed and differentiate the novelties provided in this dissertation with what has already been done.

1.4 High complexity of optimization

The complexity of the analysis of power networks and energy producers has been increasing dramatically because researchers have focused on solving larger problems that involve a large number of degrees of freedom (i.e., decision variables) as well as non-linear as opposed to linear models. The principal problem that is faced with this type of analysis is the computational burden. At the level of energy planning, there is not a clear picture of the path to follow to avoid this type of issue; but at the level of individual energy generators, von Spakovsky and co-workers [39–42] have developed methodologies for the quasi-stationary and dynamic synthesis/design and operation/control optimization (e.g., ILGO and DILGO) of stationary as well as aircraft systems. ILGO and DILGO are methodologies based on decomposition strategies with which the overall system optimization problem is broken into several sub-systems optimizations, the results of which nonetheless lead to an overall system optimum. With this approach, each sub-system is optimized either in series or parallel in an iterative process in which the results obtained from individual sub-systems are linked to those of other sub-systems via coupling functions. The iterative process continues until the variations between subsequent sub-system optimizations meet a convergence requirement and, thus, a final global optimum solution for the overall system. In this way, much larger more complicated models can be optimized than would otherwise be possible.

To date, the optimization methodologies for power networks and individual energy producers have been developed separately. Tying the optimization of network and producers into a single methodology has not been attempted. However, the development of such a methodology and the incorporation of exergy as a common currency is envisioned here in order that the synthesis/design and operation of complex systems, i.e., systems of systems, can become a reality.

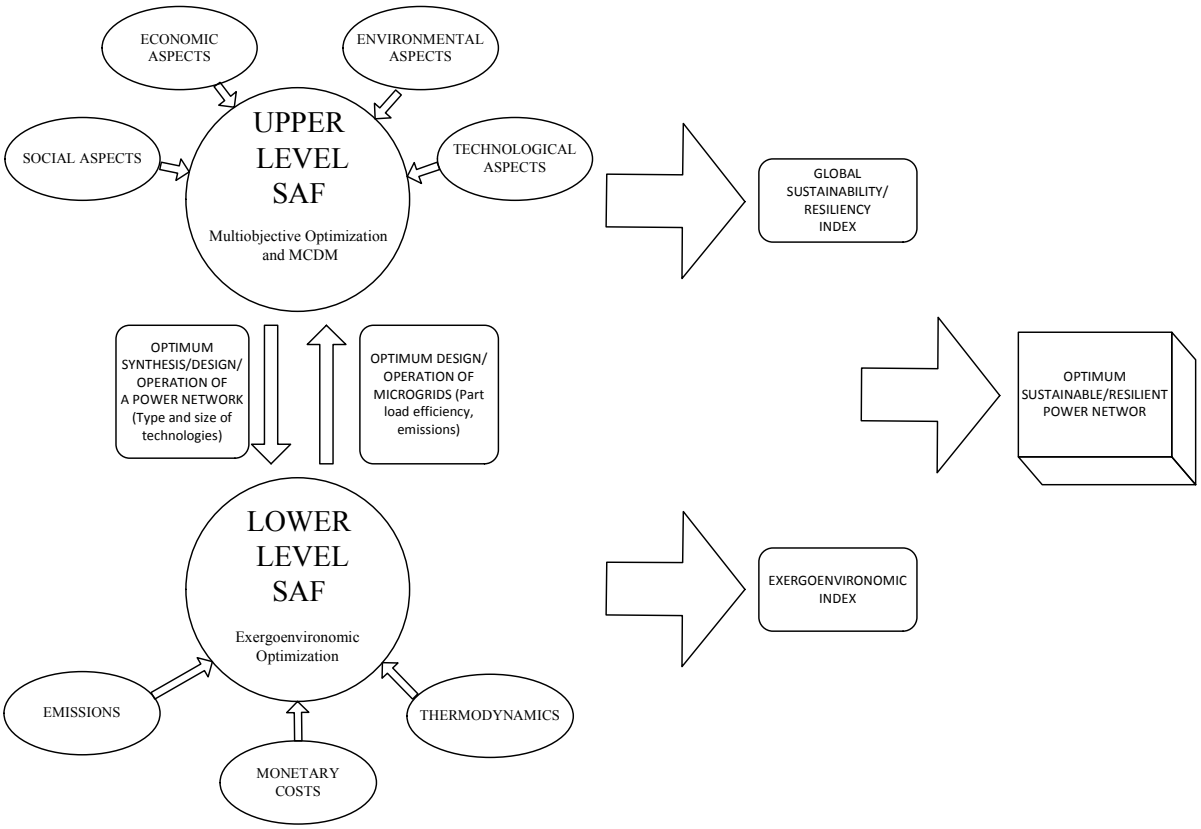

Figure 1.1. Depiction of a SAF for the modeling, analysis, and optimization of a power network and its associated producers. The development of the lower-level and its coupling with the upper-level are not part of the present work.

1.5 Sustainability assessment framework

The development and implementation of such an overarching methodology is the object of this dissertation research as well as that of Fuentes [43]. The methodology envisioned, i.e., a Sustainability Assessment Framework (SAF), is briefly described below and in much greater detail in subsequent chapters.

The SAF as envisioned here is a methodology for modeling, analyzing and optimizing sets of energy producers tied to power networks at different levels of detail based on sustainability considerations. Two possible levels of detail are an upper-level at which the planning of the network and its producers is developed which, of course, limits the detail at which the producers and even the network can be considered, and a lower-level at which every producer is considered in greater detail along with a limited set of interactions such as via a microgrid. The two levels of modeling, analysis, and optimization are coupled via a feedback loop which permits the flow of information between the levels. A SAF as just described is depicted in Figure 1.1.

The analysis and optimization at the upper level of the SAF is based on multiobjective optimization and multicriteria decision making (MCDM) approaches to sustainably and resiliently optimize the synthesis/design and operation of a power network and its producers. The goal of multiobjective optimization is to simultaneously optimize a set of objective functions that may be non-commensurable. As a result, a set of non-dominated solutions (i.e., where an optimum solution is better in at least one attribute than the other solutions in the feasible space) that form a Pareto set is obtained. If the objectives are conflicting with each other, for one optimum solution in the Pareto set, the increase in value of one objective results in the decrease in value of other objectives. From a strictly mathematical point of view, all optimum solutions in the Pareto set are equally important. On the other hand, the goal of MCDM is to aid decision makers (stakeholders) during the process of selecting a most desirable solution from among the optimum solutions in the Pareto set. The selection of a most desirable solution is not an easy task, and different methods have been proposed such as those used in multiobjective programming [44] where a value function is used to obtain the *best solution*. This best solution is a strictly mathematical solution that does not take into account the desires of experts. In this dissertation, it is recognized that the selection of a most desirable solution is ultimately the result of continuous and informed negotiations among decision makers that consider the tradeoffs among objectives in the Pareto set, as is specifically described in [45, 46]. Both the value function and decision-maker approaches are used in this work.

The aim is to obtain the best mix and size of technologies to produce, store, transmit, and distribute electricity via centralized networks and producers as well as via decentralized networks (e.g., MGs) and producers. The lower level SAF being developed by Fuentes [43] is based on the exergy-based thermoeconomic approach developed by Tsatsaronis and co-workers [11–14, 47–49] and the environmental thermoeconomic approach developed by von Spakovsky and Frangopoulos and co-workers [15, 21–24]. The purpose of the lower level is to consider in greater detail than possible at the upper level the effect of similar sustainability considerations on the optimal synthesis/design and operation of the individual and grouped decentralized producers identified by the upper level as the most sustainable and resilient for the power network.

An additional feature of the SAF is to consider a life cycle (cradle-to-grave) point of view and how it impacts the power network and its producers. The cradle-to-grave looks at the sustainability impacts of raw material extractions, equipment manufacture and plant construction, plant operation, and equipment disposal/recycling. The inventory of the life cycle analysis (LCA) of the

SAF is based on exergy so that the amount and also the quality of the different types of energy and materials involved in the processes are taken into account. During plant operation, part load behavior of the producers is considered by introducing nonlinear curves for exergetic efficiencies, emissions, and short run monetary costs (fuel and variable O&M). The life cycle impact to the environment is considered by accounting for the depletion of natural resources and emissions to the environment. For the reduction of emission to the environment, four different actions can be implemented, i.e., removing pollutants from fossil fuels (gasification, liquefaction, pyrolysis) and combustion gases (absorption/scrubbing and electrostatic filters/precipitators), substituting fuels (NG for Coal/Oil), and using renewable resources. The reduction in $\mathrm{CO_2}$ emissions is handled somewhat differently using the following four possible approaches: increasing the efficiency of energy producers, recycling the $\mathrm{CO_2}$, reforesting, and using renewables such as geothermal, solar, wind, wastes, and hydro. The social impacts of MGs can also be included in the multiobjective analyses and optimization (they are not included in this work) in order to assess both the positive (e.g., job creation, life style improvement, etc.) and negative (e.g., land destruction, damage to human health via emissions and noise, etc.) aspects of each power network/producer configuration. Another novel and important social sustainability issue is the acceptance/rejection of MG inclusion by the general public.

In order to apply the two-tiered SAF, the multiobjective optimization of the power network and its producers based on non-commensurable objective functions is developed first in order to obtain the Pareto set of optimum solutions that correspond to optimum network/producer configurations. Next, a multicriteria decision making (MCDM) analysis is developed in order to obtain the best compromise solution among the optimum solutions that constitute the Pareto set, which provides that network configuration with the highest global sustainability/resiliency index. With this upper-level analysis and optimization, the most sustainable/resilient centralized and decentralized producers operating in the power network are targeted for the lower level SAF. The optimal synthesis/design and operation optimization of targeted individual and grouped decentralized producers is then developed using the exergoenvironomic approach of the lower level of the SAF. Finally, the results from the lower level are included into a new upper-level set of optimizations, and the process continued until a globally optimal sustainable and resilient network configuration is obtained.

1.6 Dissertation objectives and originality for SAF

In the present research, the upper-level methodology of the SAF is developed and applied to different grid scenarios in order to determine the most sustainable/resilient power network and producer configuration within a current local or regional society. The goals of the present research are as follow:

- Develop the upper level of the two-tiered SAF briefly described above.
- Apply the upper level of the SAF to test bed scenarios, i.e., the Netherlands and the Northwest European power network.

To accomplish the goals listed above, the following tasks are required:

- Gain a deeper understanding of thermodynamics and in particular the analysis of energy systems.
- Gain a deeper understanding of power engineering in terms of power flow analysis.
- Gain a deeper understanding of economics as it relates to energy markets.
- Develop the modeling characteristics of the upper level of the SAF.
- Research various optimization techniques and packages available for the required multiobjective optimizations.
- Develop a multiobjective optimization model and multicriteria decision making analysis framework using various techniques available in the literature.
- Apply the power network/producer model for the development of the upper level of the SAF (e.g., the Netherlands and the Northwest European Electricity Market Model)

This part of the dissertation research includes a number of original contributions among which is the inclusion of MGs and associated non-renewable and renewable producers into the development of a methodology for the optimal synthesis/design and operation of power networks using technical, economic, and environmental aspects as non-commensurable objective functions in order to search for the advantages or disadvantages that the inclusion of MGs can bring to the network. In addition, the high complexity of the optimization of energy producers coupled to a power network requires the development of a novel approach, which here is proposed via an exergy-based, two-tiered SAF.

1.7 Summary of differences between the present work and that of Lo Prete et al. [37]

The early stages of the upper-level Sustainability Assessment Framework as presented in this dissertation were developed as presented in Lo Prete et al. [37]. This section briefly and specifically discusses the differences between the work developed in [37] and the work of Part I of the present dissertation.

- In Lo Prete et al. [37], the yearly Load Duration Curve (LDC) is divided into six blocks where each block represents a certain number of hours and its load is the average of the load of those individual hours. That is, six independent hours are consider for the analysis.

  In this dissertation, a period of twenty-four hours that represent the day with the highest electricity demand in the network during the year is considered for the analysis; and, as is described below, the decision variables of all twenty-four blocks are part of a single multi-objective optimization problem with each of the off-design operational blocks dependent on the synthesis/design block.
- In Lo Prete el al. [37], the optimal operation configuration is obtained by means of a single objective optimization (minimize $C(\cdot)$) based on the operational cost (economic dispatch) of the system. The rest of the indices (i.e., energetic and exergetic efficiencies, emissions, and LOLP) are obtained from a post-processing analysis after the single optimization is completed.

  In this dissertation, the indices (i.e., total daily costs, network efficiency, emissions, resiliency, and LOLP) are treated as objective functions belonging to the set $\vec{C}$. This set of objective functions is simultaneously optimized in a multiobjective optimization manner (minimize $\vec{C}$) in order to obtain the Pareto set of optimum solutions for the system.
- In Lo Prete el al. [37], a fixed-design configuration is imposed and the optimal operating conditions of the system are obtained. That is, the decision variables $\bar{x}$ in the objective function $C(\bar{x})$ correspond to the set of decision variables for operation optimization only.

  In this dissertation, the synthesis/design/operation optimization of the system is obtained. The model minimize $\vec{C}(\bar{y}^{t=t^{peak}}, \bar{x}^{t\neq t^{peak}})$, where $\bar{y}^{t=t^{peak}}$ is the set of decision variables for synthesis/design optimization corresponding to the peak-hour load demand, and $\bar{x}^{t\neq t^{peak}}$ are

the sets of decision variables for operation optimization corresponding to each of the non-peaking hours.

- In Lo Prete el al. [37], the optimization of one block is independent of the others (i.e., thus, this is not a quasi-stationary approach), and the annual results are obtained by weighing the results of each block by the appropriate number of hours.

  In this dissertation, the decision variables of all twenty-four blocks are interconnected with each other and change their value at every iteration of the optimization (quasi-stationary approach). The decision variables corresponding to the hour with the maximum demand are related to the synthesis/design optimization of the system, and the decision variables of the other twenty-three off-peak hours are related to the operation optimization of the system.
- In Lo Prete el al. [37], linear behavior of the producers is considered during the individual optimization of each of the six blocks considered.

  In this dissertation, the model is able to account for the part-load behavior of the producers by defining the operational costs, SO_2 emissions, and efficiency particular to each producer as a non-linear function of the production.
- The analysis of Lo Prete el al. [37] considers that 50 MG configurations, each with a capacity of 24 MW, are radially connected to the nodes in The Netherlands.

  In this dissertation, the maximum penetration of MGs in the network can be as high as 15% of the total production of the network. In addition, MG configurations are radially connected to the nodes where production and demand is present in the four countries of analysis, i.e., France, Germany, The Netherlands, and Belgium.
- The analysis of Lo Prete el al. [37] considers residential MG configurations only.

  In this dissertation, residential, commercial, and industrial MG configurations are included in the four countries, i.e., France, Germany, The Netherlands, and Belgium, where a different daily Load Demand Profile (LDP) for each of the three different MG sectors, i.e., residential, commercial, and industrial, is employed.
- The analysis of Lo Prete el al. [37] considers that the residential MG configurations have a heating demand. This heating demand is satisfied by CHP producers and NG boilers in the MG configurations in order to study the effect of local cogeneration production on the local market

In this dissertation, cogeneration is not included in the analysis.

- The analysis of Lo Prete el al. [37] includes the cost of CO_2 emissions in the objective function and environmental indices for SO_x and NO_x emissions.

  In this dissertation, the cost of CO_2 emissions in the total cost function and indices for NO_x emissions are not considered.

1.8 Overview of next chapters

In the present chapter, an overview of the motivation to develop this research as well as the goal to develop an upper-level SAF have been presented. Chapter 2 presents a review of the literature for the thermodynamic analysis and optimization of individual energy producers and power networks, including sustainability aspects. The chapter begins with a historical overview of the foundations of thermodynamics, continuing with a description of exergy analysis and the most notable theories to date for thermoeconomic analysis and optimizations as well as subsequent developments to deal with complex system optimizations. Subsequently, available frameworks to include sustainability considerations in the analysis and optimization of energy systems is presented. The chapter closes with a review of the methodologies available for the analysis and interpretation of results via multi-criteria decisions and the research devoted to social considerations in sustainability. Chapter 3 provides the mathematical framework for the upper-level SAF develop in the present work. Three areas of sustainability are included in the model, i.e., those accounting for economic, environmental, and technological issues. Social considerations are not included in the model, although it is suggested to include them in future developments of the SAF. Chapter 4 discusses the results of the application of the SAF to a system that describes a power network at the national level of detail, i.e., the Netherlands, and to a system that describes a power network at the international level, i.e., the northwest European electricity market. Finally, Chapter 5 provides a summary of the research in this part of the dissertation and makes recommendations for future developments and applications of the upper-level SAF developed in the present work.

Chapter 2

Literature Review for SAF

2.1 A brief review of exergy

Available Energy is defined as "*the maximum theoretical energy that can be extracted from a combination of system-environment by bringing the system to mutual stable equilibrium with the environment by means of a reversible adiabatic process*" [4]. Available energy is an extensive property of the system, depends on the state of the system and the state of the environment, is additive, and is defined by the end states of a process. A special case is given when the initial state of the system, viewed as independent and isolated, is that of stable equilibrium. In this particular case, available energy is called 'exergy', and is defined as "*the maximum theoretical useful work obtained if a system is brought into thermodynamic equilibrium with the environment by means of processes in which the system interacts only with its environment*" [50]. Exergy conserves all the characteristics of available energy with the additional characteristic that it exists only for stable equilibrium.

The outline of the conception, growth, and maturing of exergy presented below is based on the very complete description in [50]. The beginnings of exergy can be attributed to the work by Carnot (1824) [51] when he stated that "*the generation of motive power requires not a consumption of caloric, but rather its transportation from a hot to a cold body*". Together with Carnot, the works of Clapeyron (1832) [52] and Clausius (1850,1865) [53, 54] provide the bedrock for exergy and of the second law of thermodynamics in general. Years later, the works of Thomson (Lord Kelvin) (1852) [55], Rankine (1851) [56], Tait (1868) [57], Gibbs (1873) [58], and Maxwell (1871, 1878) [59, 60], among others, provide an advancement in the subject, although the basis had already been

established. From this last list of contributors, note the work by Gibbs in which he introduces for the first time the term *available energy*, the incredibly useful energy-entropy ($E - S$) representations (for equilibrium only, however), and the appreciation that energy is a function of the entropy, parameters $\vec{\beta}$ of the system, and its number and amount of constituents $\vec{n}$ such that

$$E = E(S, \vec{\beta}, \vec{n}) \tag{2.1}$$

When the volume is the only parameter, as, for example, for a piston-cylinder device, the infinitesimal change in energy of a system in going from one stable equilibrium state to a neighboring one on the hypersurface of stable equilibrium states is represented by

$$dU = TdS - PdV + \sum_{j=1}^{r} \mu_j dn_j \tag{2.2}$$

where *T* represents the temperature, *P* the pressure, and μ_j the total potential for the *j*-th constituent.

Years later, Gouy (1889) [61–64] and Stodola (1898) [65] independently of each other quantified the *useful energy* that is lost in a thermodynamic process, thereby, defining the concept of irreversibilities, as

$$I = T_0 S_{irr} \tag{2.3}$$

where T_0 is the temperature of the reference dead state and S_{irr} the entropy generated during the irreversible process.

The important works of Goodenough (1911) [66], Darrieus (1930, 1931) [67, 68], Duhem (1904) [69], Caratheodory (1909) [70], Lorenz (1894) [71, 72], among others, represent the final contributions to the early works on exergy.

In the decade of the 1930s, the concept gained momentum again with the work of two main schools of thought; that by Bosnjakovic [73, 74] in Germany who set the basis for the exergy development in Europe, and the one by Keenan [75, 76] in the United States.

In the decade of the 1950s–1960s, the works by Grassmann [77], Brodyansky [78], Bruges [79], Keenan [75], Tribus [80], Tribus and Evans [81, 82], El-Sayed [83], El-Sayed and Evans [84], Obert [85], Gaggioli [86], Baehr [87], Fratzcher [88], Szargut [89, 90], Petela [91], Knoche [92], and others focused on how to develop exergy balances, the representation of exergy flows in graphics (i.e., Grassmann diagrams), the definition of the reference dead state, different definitions

for the second law efficiency of which the most widely accepted nowadays is given as

$$\eta_{II} = \frac{B_P}{B_F} \tag{2.4}$$

where B_P is the exergy content of the products (e.g., electricity and heat) and B_F that of the fuels. During this time, exergy was considered as a formal but not yet essential part of a thermodynamic analysis.

An important contribution was that of Rant [93], who in 1956 proposed and coined the word exergy, replacing the existing definitions such as availability, available energy, usable energy, work capability, etc., unifying the terms used in Europe and the rest of the world with the exception of the U.S., which deld out much longer with the term availability. The nomenclature, concepts, and balances of exergy were finally unified in the works of Kotas [94], Szargut, Morris and Steward [95], and Moran [96].

In the 1970s, another formidable contribution was made, although this time at the quantum level, when Hatsopoulos and Gyftopoulos [97–100] postulated a unified quantum theory of mechanics and thermodynamics, setting a very general statement of the second law as one of the fundamental postulates of the newborn theory. Between the 1980s–1990s, the major contributions on exergy consisted in a maturing of the second law analysis of engineering processes and chemical systems and, of course, its merging with economic analyses.

From 2000 to the present, researchers in this area have been mainly involved with how to use the second law of thermodynamics in order to use exergy as an index to quantify the environmental effects associated with energy conversion processes. Another open area of research is that of exergy-based synthesis/design/operation optimizations of very large and complex systems. The goal is to sustainably use the resources available in Nature to generate energy the most efficiently, while minimizing the damaging effects on the ecosystem in order to avoid the depletion of available natural resources and a deteriorating environment. Both aspects, sustainability and complex system optimization, are the main focus of the present dissertation.

This section presented a brief overview of the early stages of thermodynamics in order to provide the reader, especially those with expertise in areas other than thermodynamics, a description of the foundations of exergy and exergy-based analyzes. The next section provides a further description of exergy or second law analyzes, its merging with economics, recent theoretical developments, as well an examples of its application to energy production processes.

2.2 Exergy analysis

The objective of an exergy or second law analysis is to determine all the thermodynamic properties of the streams of mass and of energy in a system (temperature, pressure, etc.) as well as their exergy content. With this information, the overall efficiency of the system and those of the different components and the location and quantification of irreversibilities within the components can be obtained [4, 94, 101]. The aim is to quantify the exergy used by a component as well as the amount of exergy destroyed due to the irreversibilities present within each of the components of the system.

To carry out such an analysis, the physical system is schematically decomposed into several components, and then energy and exergy balances are developed for each of the components. It is commonly assumed in these types of analyses that the system and their components operate at steady state conditions, so that the combined rate balance for each component is given as [4]

$$0 = -\sum_{s} \dot{W}_s + \sum_{k} \dot{Q}_k \left(1 - \frac{T_0}{T_k}\right) + \sum_{q} \dot{m}_q \left(h_q + \frac{V_q^2}{2} + g z_q\right) - T_0 \dot{S}_{\text{irr}} \tag{2.5}$$

where the first term represents the rate of exergy transferred by means of work rate interactions $\dot{W}_s$ for $s = 1, 2 \ldots$ where a positive sign is assumed if the work interaction is from the system. The second term represents the rate of exergy transferred by means of heat interactions $\dot{Q}_k$ for $k = 1, 2 \ldots$ and with a source at temperature T_k and a dead state temperature T_0 where a positive sign is assumed if the heat interaction is to the system. The third term represents the rate of exergy transferred by means of a mass interaction $\dot{m}_q$ for $q = 1, 2 \ldots$ and for a flow with enthalpy h_q, kinetic energy $V_q^2/2$, and potential energy $g z_q$ where a positive sign is considered if the mass is entering the system. The fourth term represents the exergy destruction due to irreversibilities, $\dot{S}_{irr}$, with respect to the dead state temperature T_0.

Plenty of work has been done in this area since the 1950s, as is mentioned in the section above. As an ilustration of the application of the methodology of analysis, the work of Anheden and Svedberg [102] is presented in Figure 2.1 where an exergy analysis of a conventional gas turbine is developed. The turbine uses methane (CH_4) as a fuel source and air for the oxidizer in the combustion reaction. Component 1 represents a compressor, component 2 a combustion chamber, component 3 a turbine, component 4 a combustion chamber, and component 5 a turbine. Results are presented in tables, which contain the values of all the properties (i.e., temperature, pressure,

enthalpy, etc.) and the exergy content of each of the streams involved in the process. Results can also be presented as a Grassmann diagram in which the width of the arrows are proportional to the percentage of the total initial exergy flow into the system.

Figure 2.2 depicts the Grassmann diagram for the gas turbine. It is observed in the figure that the compressor has an exergy destruction 2.54% of the initial exergy fuel input to the system, the first combustor of 21.11%, the first turbine of 2.54%, the second combustor of 5.12% and that of the last turbine of 3.8%. In addition, it is also seen via the arrow for the power exiting the system that the exergetic efficiency of this particular gas turbine system is 37.96%.

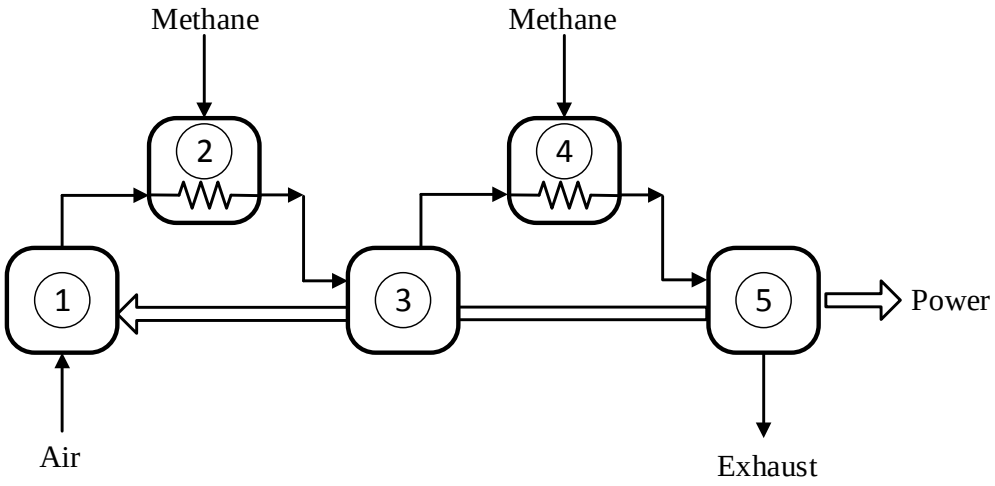

Figure 2.1. Representation of a conventional gas turbine [102].

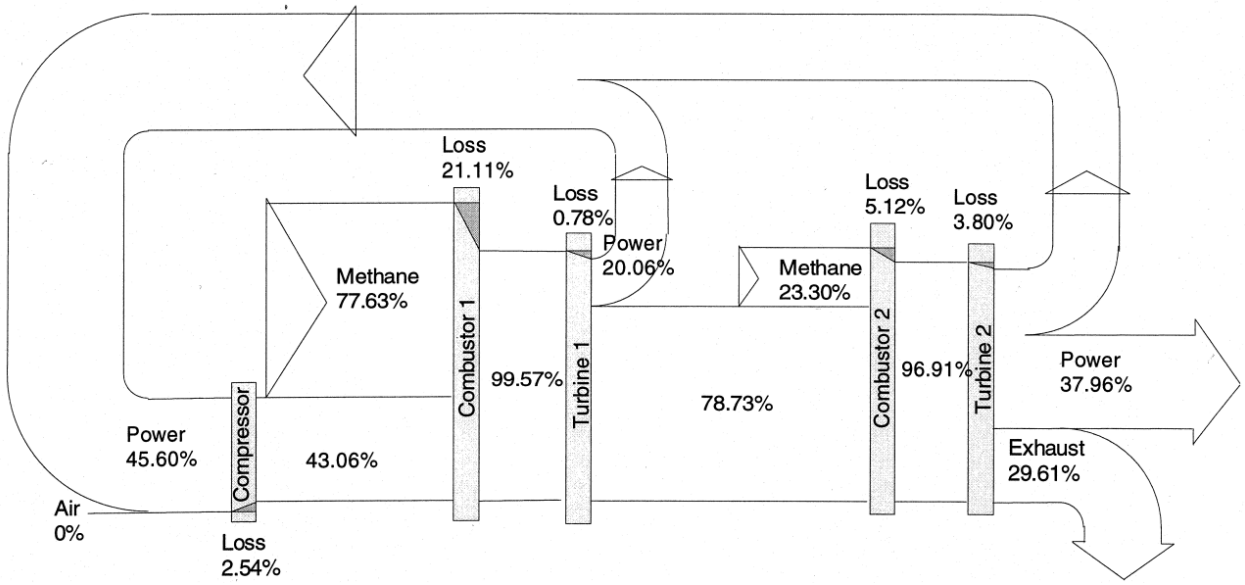

Figure 2.2. Grassmann diagram for the exergy analysis of the gas turbine of Figure 2.1 by Anheden and Svedberg [102]. Reprinted from [102] Copyright © 1998, with permission from Elsevier.

2.3 Exergy and economics

The development of exergy costing started with the work of Keenan [76] when the electricity industry in the U.S. realized that electricity and steam, the products of a CHP plant, should probably not be sold at an equivalent unit price, i.e., one based on the energy content of the streams. Keenan provided them with a methodology to assign costing to the products in terms of their exergy content. In this way, both the quantity and quality of the final energy products are considered in assigning their respective market prices. A few years later, Tribus coined the term *thermoeconomics* and together with Evans and El-Sayed [80–84] developed pioneering work on the thermoeconomic or exergoeconomic analysis applied to desalination processes. Obert and Gaggioli [86] also were pioneers in this emerging area working with optimizing a steam piping system and its insulation. Another group, that of Bergmann and Schmidt [103] worked with steam power plants while Szargut [89, 90] and co-workers worked with chemical and metallurgical processes, providing a methodology for obtaining the exergy reference value for the mineral content of the most common elements in nature [95, 104–106]. Years later Georgescu-Roegen (1971) [107] explained in more detail the relation between economy and the second law of thermodynamics, even to the degree of postulating that "*entropy is the driving force in an economic process of a society*". The work of others could be mentioned. However, since the objective of this dissertation is not about the direct use of exergoeconomic analyses, only the main contributions to the area are discussed here.

In order to refer to a combined analysis of exergy and cost for an energy producer, the terms thermoeconomics and *exergoeconomics* are used interchangeably. Nevertheless, as suggests Tsatsaronis [108, 109], thermoeconomics should be exclusively refer to the development of a combined energy and economic analysis, because the term 'thermo' refers only to heat. However, its wide use, especially by the engineering community, has tagged to it the meaning of an analysis in which monetary costing is assigned to every exergy flow in a system.

The aim of an exergoeconomic analysis is to allocate the monetary cost associated with each component of the system by tracing the cost of the final products through all the flows (i.e., work, heat or mass) connecting the components back to the initial fuel used. The theory is based on assigning a monetary cost to each of the flows according to their corresponding exergy content. For instance, for the gas turbine system depicted in Figure 2.3, the cost assigned to each flow of exergy is given as

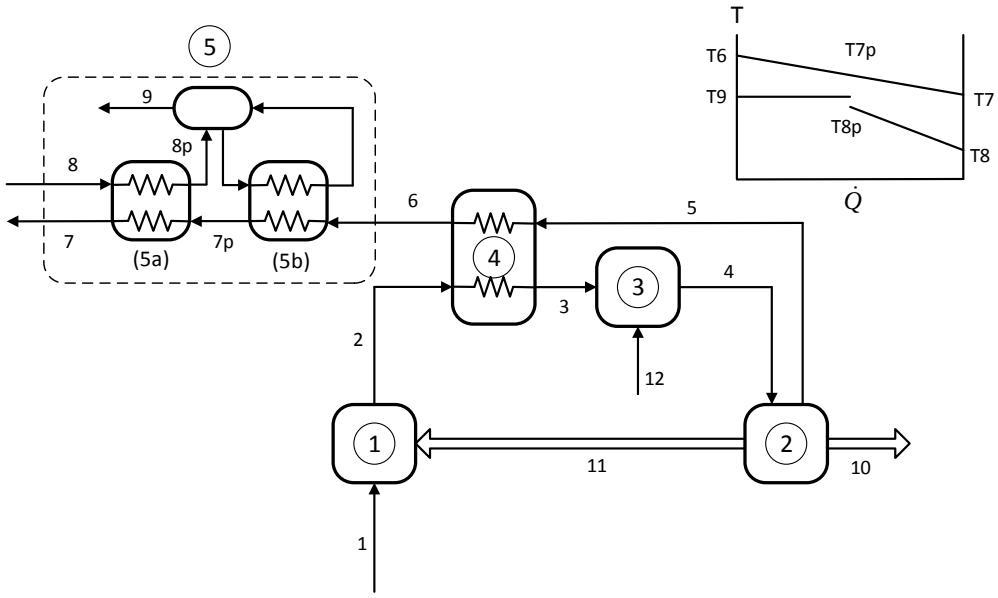

Figure 2.3. Representation of the physical structure of a system and its components in the CGAM problem [110].

$$c_i = \frac{\dot{\Gamma}_i^{\$}}{\dot{B}_i} \tag{2.6}$$

where c_i is the unitary cost associated with flow i, $\dot{\Gamma}_i^{\$}$ the monetary cost rate associated with the exergy flow rate $\dot{B}_i$ of the stream.

Considering a component k of the system, the cost balance is written as

$$0 = -c_{W,k}\dot{B}_{W,k} + c_{Q,k}\dot{B}_{Q,k} + \sum_{\text{in}}(c_{\text{in}}\dot{B}_{\text{in}})_k - \sum_{\text{out}}(c_{\text{out}}\dot{B}_{\text{out}})_k + \dot{\Gamma}_k^{\$} \tag{2.7}$$

where the first term in the right-hand side is the monetary cost rate $\dot{\Gamma}_W^{\$}$ associated with a single flow in the form of work, the second is the monetary cost rate $\dot{\Gamma}_Q^{\$}$ associated with a single flow in the form of heat, the third is the total monetary cost rate $\dot{\Gamma}_{\text{in}}^{\$}$ associated with all the mass flows entering the component, the fourth is the total monetary cost rate $\dot{\Gamma}_{\text{out}}^{\$}$ associated with all the mass flows leaving the component, and the fifth is the monetary cost rate associated with the capital and operation and maintenance costs (O&M) of the component.

In addition to the cost balance relation for each component given by Equation (2.7), auxiliary equations are needed in order to allocate the cost of the products and exergy destruction due to irreversibilities among the different components of the system. These allocation rules are described below when comparing the principal frameworks available for exergoeconomic analyses and optimization.

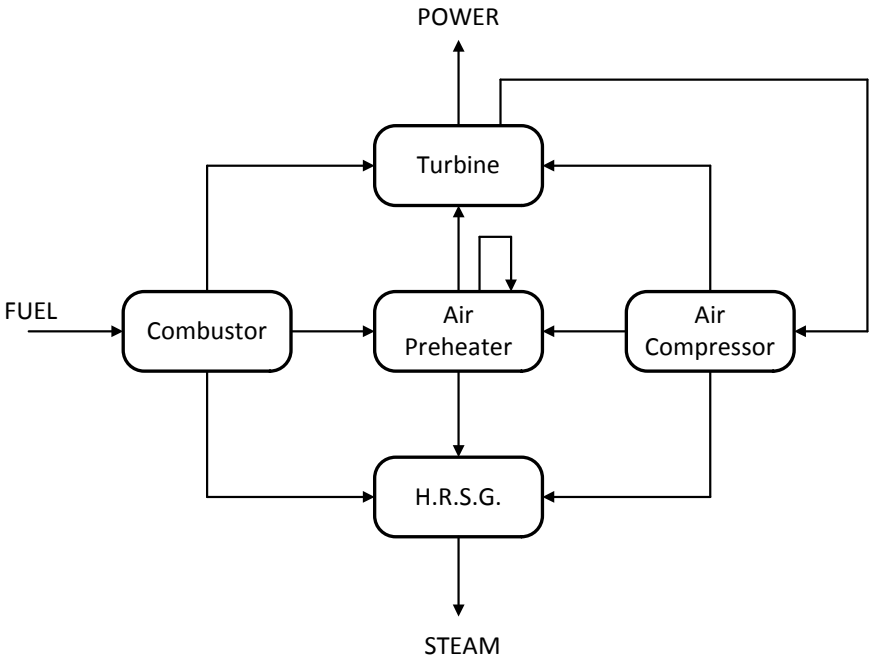

Figure 2.4. Productive Structure of the CGAM problem obtained by Valero et al. [5].

In order to trace the cost of the final products (e.g., work and heat) through the components of a system, a flow structure of the system is formed by schematically representing the physical links of exergy flows between components of the system. This schematic representation shows the distribution of resources among the components. This schematic representation is known as the *productive structure* of the system in the Valero et al. [5] framework and is depicted in Figure 2.4 for the CHP gas turbine of the CGAM[1] problem.

The basis for constructing the productive structure is the *Fuel-Product* concept in which exergy balances are developed for each of the components in order to quantify the total exergy entering (fuel, B_F), and leaving (product, B_P) the component. Every component has only one stream as a product and only one stream as a fuel. Nevertheless, the single product $\dot{B}_{P,i}$ of a component i can serve as a fuel for several other components, such as

$$\dot{B}_{P,i} = \dot{B}_{F,i,0} + \sum_{j=1}^{n} \dot{B}_{F,i,j} \qquad i = 0, 1, \ldots, n \tag{2.8}$$

where $\dot{B}_{F,i,0}$ is the fraction of the product that serves as a fuel to the environment (i.e., final product in the form of a heat, work or mass interaction) and $\dot{B}_{F,i,j}$ the fraction of the product of component

[1]The CGAM problem is a 30 MW and 14 kg/s of saturated steam natural gas cogeneration turbine characterized by **C**hristos Frangopoulos, **G**eorge Tsatsaronis, **A**ntonio Valero, and **M**ichael von Spakovsky in [110]. CGAM is an acronym for the first name of the authors.

i that serves as a fuel for component j in the system. In the same manner, the single fuel stream $\dot{B}_{F,i}$ of the same component i can be formed by the sum of different sources such as

$$\dot{B}_{F,i} = \dot{B}_{F,0,i} + \sum_{j=1}^{n} \dot{B}_{F,j,i} \qquad i = 0, 1, \ldots, n \tag{2.9}$$

where $\dot{B}_{F,0,i}$ is the amount of resources comming from the environment and $\dot{B}_{F,j,i}$ the contribution of the product of component j to the fuel of component i.

In a cost representation, Equations (2.8) and (2.9) are written as

$$\dot{I}^{\$}_{P,i} = \dot{I}^{\$}_{F,i,0} + \sum_{j=1}^{n} \dot{I}^{\$}_{F,i,j} \qquad i = 0, 1, \ldots, n \tag{2.10a}$$

$$\dot{I}^{\$}_{F,i} = \dot{I}^{\$}_{F,0,i} + \sum_{j=1}^{n} \dot{I}^{\$}_{F,j,i} \qquad i = 0, 1, \ldots, n \tag{2.10b}$$

for the product and fuel of a single component of the system, respectively. The total products and amount of resources during the energy production process are defined, respectively, as

$$\dot{B}_{F,total} = \sum_{j=1}^{n} \dot{B}_{F,0,j} \tag{2.11a}$$

$$\dot{B}_{P,total} = \sum_{j=1}^{n} \dot{B}_{F,j,0} \tag{2.11b}$$

In an exergoeconomic optimization, the aim is to obtain the cost-optimal synthesis/design and operation for a system subject to its physical and thermodynamic constraints. Firstly, the productive structure of the system needs to be defined in order to obtain the physical and thermodynamic connections between the components of the system in which the change of the unitary cost of an exergy flow is given by the marginal cost

$$c_{mar,i} = \frac{\partial \dot{I}^{\$}_{i}}{\partial \dot{B}_{i}} \tag{2.12}$$

and secondly, an objective function is constructed based on the total monetary cost rate associated with each component of the system as well as the total cost rate associated with the fuel used.

The principal frameworks or methodologies for exergoeconomic analyses and optimizations to date are those proposed by four main schools of thought, i.e., that of Tsatsaronis and co-workers

[111], Valero and co-workers [5], Frangopoulos [18] and von Spakovsky [25]. The last two theories mentioned had their foundations in the works of El-Sayed and Evans [84]. The main differences among these different frameworks is the method to interconect the different components of the system and their exergy flows by considering differently the allocation of the exergy of the products among the components of the system and also the degree of decomposition of the system for the optimization process.

2.3.1 Comparison of the principal frameworks in the CGAM problem

These four frameworks or methodologies were applied by their originators to the so-called CGAM problem [110] in order to clarify to the broader community the details of each theory in a side-by-side comparison. The CGAM problem is depicted in Figure 2.3 and consists of a CHP natural gas turbine that produces 30 MW of electricity and 14 kg/s of saturated steam at 20 bar. The components are the air compressor (1), gas turbine (2), combustion chamber (3), air pre-heater (4), and heat recovery steam generator (HRSG) (5). As can be seen, the level of physical decomposition of the system is left open to the decision of the analyst, who bases it on the level of detail to be collected from the system (e.g., component five could be physically decomposed into a water preheater (5a) and an evaporator (5b)). Mass flows within the system are the air (1-3), mixture of hot gases (4-7), water (8-9), power (10-11), and fuel (12).

The objective is to

$$\text{minimize} \quad \dot{I}^{\$}_{\text{Total}} = \sum_{f=1}^{\#\text{fuels}} (\dot{I}^{\$}_{\text{Fuel}})_f + \sum_{k=1}^{\#\text{comp}} (\dot{I}^{\$}_{\text{Comp}})_k \tag{2.13}$$

with respect to five independent decision variables, i.e., the pressure ratio of the compressor, P_2/P_1; the isentropic efficiency of the compressor, $\eta_{_{AC}}$; the isentropic efficiency of the turbine, $\eta_{_{GT}}$; the temperature of the air at the inlet of the combustion chamber, T_3; and the temperature of the gases at the inlet of the turbine, T_4. The minimization is subject to physical, economic, and thermodynamic constraints that define the model of the system. In Equation (2.13), $\dot{I}^{\$}_{\text{Total}}$ is the overall cost rate of the system, $\dot{I}^{\$}_{\text{Fuel}}$ is the cost rate of fuel given as

$$\dot{I}^{\$}_{\text{Fuel}} = c_f \dot{m}_f LHV_f \tag{2.14}$$

where c_f is the unit cost, $\dot{m}_f$ the mass flow rate of fuel f, and LHV_f the lower heating value of each of the f fuels used in the energy conversion process. In this particular case, only methane is

used. $\dot{I}^{\$}_{\mathrm{Comp}}$ is the capital amortized costs of each of the k components of the system.

As a reference case, the optimization model is solved using a conventional purely mathematical optimization algorithm. A result of this reference optimization is that the 'mathematical optimum' value is physically not acceptable, because $\Delta T_{\mathrm{pinch}}$ which is the temperature difference between T_{7_p} and T_{8_p} in the HRSG is less than 2 *K*. In addition, the detailed results provided with the four different frameworks for cost allocation are missing from the reference optimization. A sampling of results is given in the following sections. For the detailed results the reader is referred to [5, 18, 25, 111].

2.3.1.1 Exergetic cost theory (ECT)

The ECT framework was developed by Valero and co-workers [112–119] during the 1980s using the exergetic cost concept as the basis for the analysis to allocate these costs to the fuel and product flows in the system. The major strength of ECT is for the design and operation optimization of energy systems where a given synthesis (i.e., configuration) of the system is given beforehand. The symbolic exergoeconomic notation in a matrix form makes it very powerful for obtaining very detail information on the components of the system and their interrelation.

The first step in the analysis is to obtain the productive structure of the system, which mathematically results in a matrix that provides the links between the interactions of the components. The rows indicate the components and the columns indicate the flows from one component to another, that is, an element of the matrix takes a value of 1 if the flow enters a component and -1 if the flow exits the component. If the actual value of the fuel and product of each component are included in this matrix, the matrix corresponds to the Product-Fuel matrix ($\langle PF \rangle$) of the system.

In order to allocate costs to the exergy flows of the system, four main rules or premises are necessary. The first defines the conservation of exergetic cost (P1), the second the cost of external resources (P2), the third a rule for splitting the exergy flow of a product (P3), and the fourth the allocation of fuels by tracing the cost of a stream to the original component where it was generated (P4). Using these cost allocation rules, the optimization problem given by Equation (2.13) is reformulated as [5]

minimize

$$\Pi = c_e F + uZ \tag{2.15}$$

subject to

$$K_D P = F \tag{2.16a}$$

$$P_s + \langle PF \rangle F = P \tag{2.16b}$$

$$P_s = d \tag{2.16c}$$

where Π is the total cost of the system, c_e a vector containing the unit price of resources, u a unit vector, Z a vector containing the monetary costs of each component, P a vector containing the exergy of the product, F a vector containing the exergy of the resources, P_s a vector containing the total product of the plant which is a fixed value d given by the statement of the problem, K_D a unit matrix containing the unit exergy consumption of each component, and $\langle PF \rangle$ the fuel-product matrix containing the physical interconnections of the productive structure of the system.

The problem can be formulated on an exergy cost basis if no investment costs are included or on a monetary cost basis if investment costs are included. Capital costs of equipment can be introduced in to the problem by adding the amortized investment costs vector of the system.

The optimization problem is solved using the Method of Undetermined Multipliers where an iterative optimization of the system is developed by minimizing the exergy destruction of the system. The values for the Lagrange multipliers obtained at the optimum point represent the costs of the flows in the productive structure. At the final iteration of the optimization, an optimum fuel-product-residue matrix for the system is obtained, providing the optimum design configuration for the system as well as the optimum interconnections among the components.

Table 2.1 shows the comparison of the optimum values for the decision variables and other important variables for the problem such as the mass flow of air, $\dot{m}_a$; the mass flow of fuel, $\dot{m}_f$; the temperature difference at the pinch point, ΔT_{pinch}; the work required by the compressor, $\dot{W}_{AC}$; and the net work produced by the turbine, $\dot{W}_{GT}$ [110]. Table 2.2 shows the comparison of the optimum monetary costs obtained with ECT to the reference values provided in [110]. As can be seen, the results obtained with ECT are equal to those provided by the reference optimum in [110].

An additional advantage of ECT is that the total efficiency of the system can be set as a function of the efficiency of the components permitting the real performance of the system to be monitored after the optimum design and operation of the system is obtained. This is done by observing changes in off-design performance via the decrease in efficiency of one of the components and

a quantification of the impact of the malfunction of this component, i.e., its decreased efficiency, on the performance of other components as well as its fuel impact on the system [6–10, 120–123]. Incremental changes in exergy destruction by means of irreversibilities are identified and quantified, and maintenance or improvements scheduled and applied before the malfunction results in a decrease in the overall system efficiency.

Table 2.1. Comparison of the optimum values for the CGAM reference optimization [110] with those obtained with the ECT optimization.

Decision Variables			Selected Variables		
Variable	CGAM [110]	ECT [5]	Variable	CGAM [110]	ECT [5]
P_2/P_1	8.5234	8.5234	$\dot{m}_a$ (kg/s)	99.4559	99.4559
η_{AC}	0.8468	0.8648	$\dot{m}_f$ (kg/s)	1.6274	1.6274
η_{GT}	0.8786	0.8789	$\dot{W}_{AC}$ (kW)	29,692.5	29,692.5
T_3 (K)	914.28	914.28	ΔT_{pinch} (K)	1.64	1.64
T_4 (K)	1,492.63	1,492.63	$\dot{W}_{GT}$ (kW)	59,692.5 (kW)	59,692.5

Table 2.2. Comparison of the optimum costs for the CGAM reference optimization [110] with those obtained with the ECT optimization.

Variable	CGAM [110]	ECT [5]
$\dot{I}^{\$}_{\text{Total}}$ (\$/s)	0.362009	0.36201
$\dot{I}^{\$}_{\text{Fuel}}$ (\$/s)	0.325489	0.32549
$\dot{I}^{\$}_{\text{Comp}}$ (\$/s)	0.036520	0.03652
$\dot{I}^{\$}_{\text{CC}}$ (\$/s)	0.1469×10^{6}	0.1469×10^{6}
$\dot{I}^{\$}_{\text{AC}}$ (\$/s)	0.1348×10^{7}	0.1348×10^{7}
$\dot{I}^{\$}_{\text{GT}}$ (\$/s)	0.1927×10^{7}	0.1927×10^{7}
$\dot{I}^{\$}_{\text{APH}}$ (\$/s)	0.8277×10^{6}	0.8277×10^{6}
$\dot{I}^{\$}_{\text{HRSG}}$ (\$/s)	0.1202×10^{7}	0.1202×10^{7}

2.3.1.2 Exergoeconomic Analysis (EEA)

Tsatsaronis and co-workers (e.g., [11, 108, 124]) developed an exergoeconomic analysis and optimization methodology, and Tsatsaronis and Pisa [111] applied it to the CGAM problem.

Firstly, the authors develop an exergy analysis in order to quantify the properties of all of the streams in the system. Secondly, a cost balance is developed for each of the components as defined by Equation (2.7). The auxiliary equations for the allocation of costs of streams among the

components are developed according to the *fuel* rule, that is, the unitary cost of a stream should be attributed to the component where that stream was originally generated. For the GCAM problem, the unitary cost of the stream of air c_1 and that of the water c_8 are $c_1 = c_8 = 0$ since they are resources from the environment for which no cost is included in the objective function. For the air preheater, $c_5 = c_6$; for the gas turbine, $c_4 = c_5$; and for the HRSG, $c_6 = c_7$ since all these streams are generated at the combustion chamber. For the combustion chamber, on the other hand, a fixed monetary unit cost is assigned to the fuel used for the combustion process consistent with the current price of natural gas, which results in a unitary cost c_{10} \$/GJ.

For the optimization process, the component cost functions are systematically minimized via an intelligent iterative process based on component exergy destruction and on changing one decision variable while keeping the remaining decision variables constant. All decision variables are tested, and the procedure continues until a final physical optimum is obtained. Table 2.3 provides the comparison of the results for EEA [111] compared with those of the CGAM problem [110].

Table 2.3. Comparison of the optimum costs for the CGAM reference optimization [110] with those obtained with the EEA optimization.

Variable	CGAM [110]	EEA [111]
P_2/P_1	8.5234	8.52
η_{AC}	0.8468	0.847
η_{GT}	0.8786	0.879
T_3 (K)	914.28	914.3
T_4 (K)	1,492.63	1,492.6
$\dot{I}^{\$}_{\text{Total}}$ (\$/s)	0.362009	0.362055

Table 2.4. Comparison of the optimum values for the CGAM reference optimization [110] with those obtained by Frangopoulos [18].

		Method proposed in TFA [18]		
Variable	CGAM [110]	GRG2	TFA	Modular
P_2/P_1	8.5234	8.59730	8.59770	8.59050
η_{AC}	0.8468	0.84641	0.84650	0.84653
η_{GT}	0.8786	0.87886	0.87871	0.87878
T_3 (K)	914.28	912.77	913.14	912.93
T_4 (K)	1,492.63	1,491.40	1,491.97	1,491.50
$\dot{I}^{\$}_{\text{Total}}$ (\$/s)	0.362009	0.362014	0.362014	0.362014

2.3.1.3 Thermoeconomic functional approach (TFA)

As a first approach, Frangopoulos [16, 18, 18] solves the original optimization problem with a non-linear optimization algorithm, the generalized reduced gradient method (GRG2), used during his Ph.D. dissertation [19]. Results for the optimum decision variables and selected thermodynamics variables and those for the optimum capital costs are provided in Table 2.4.

As a second approach, TFA is used to obtain the optimal synthesis/design and operation of the system. For the particular case of the CGAM problem, the synthesis is already given and the operation does not change with time so the goal is to find the optimum design for the system. The application of TFA consists of developing the functional analysis of the system by constructing the Functional Diagram. The Functional Diagram can be considered as the productive structure of the system in which the components are connected by input and output streams which represent the fuel and product for a component, respectively, putting a strong emphasis on the function of each component for the allocation of products, i.e., the function of the turbine is to provide power to the compressor and to provide power as a final product. The cost function defined in Equation (2.13) is minimized subject to the equality constraints obtained with TFA that represent the thermodynamic and physical structure of the system and to the inequality constraints that define the operating limits. The method of Lagrange Multipliers is used to obtain an optimum operating cost of the system. In addition, another advantage of TFA is that it can be based on a mathematical decomposition in which the main optimization problem is split into several sub-problems. Obtaining these optima is accomplished by the optimization of each sub-problem in a sequential manner. The advantage is that it decreases the size of each optimization handled by the optimization algorithm. The disadvantage of using this type of decomposition is that the set of decision variables for each sub-problem needs to be disjoint from the set of decision variables of the rest of the sub-problems. Otherwise, the system-level optimum solution cannot be obtained. In order to increase the degree of disjointness, additional decision variables can be included, which enhance the disjointness of these component variable sets but which for large problems may indeed turn out to be impractical. Results for the optimum decision variables and selected thermodynamics variables and those for the optimum capital costs are provided in Table 2.4.

As a third approach, the Modular Simulation and Optimization approach depicted in Figure 2.5 is proposed. In the modular optimization, the system is decomposed into r modules that represent

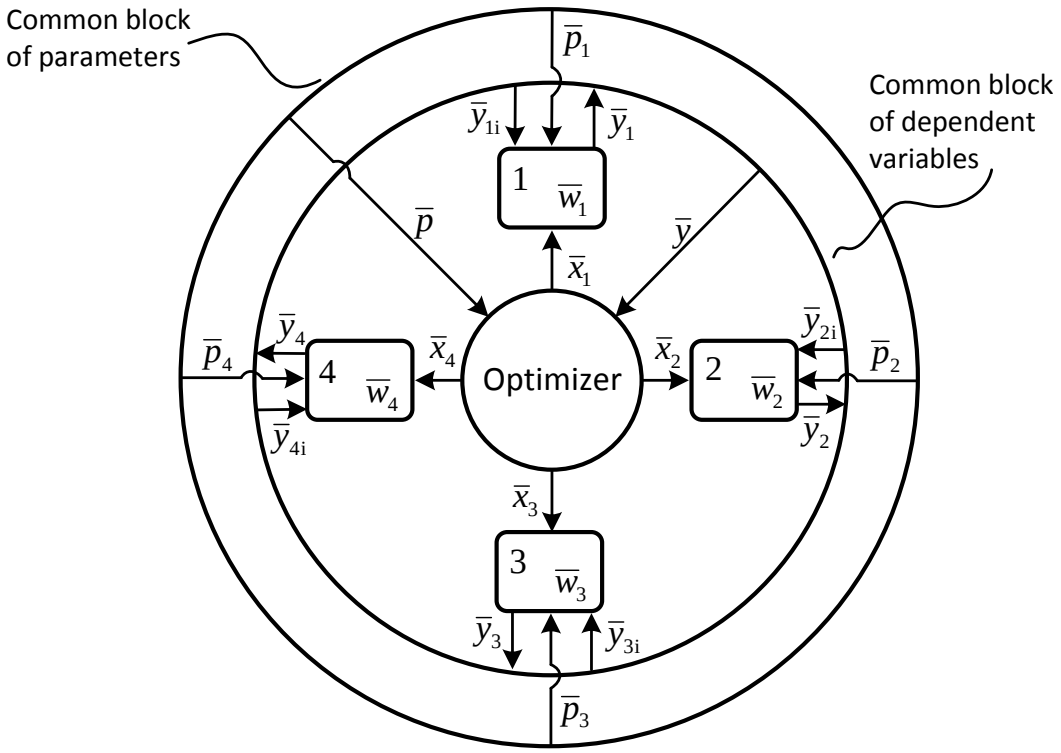

Figure 2.5. Schematic representation of the modular simulation and optimization [18].

a component or a group of components of the system. These modules are coded as subroutines which interact with a central optimizer through a set of independent variables x_r. The modules are also sequentially related by their exergy inputs and outputs, that is, a set of variables y which represent the output of module $r = 1$ serve as inputs for the optimization of module $r = 2$. In addition, every module has its own physical, economic, and thermodynamic optimization model with decision variables w_r.

The optimization starts with a local optimization of the first module after which the optimum set of variables x_1 and the optimum set of variable y_1 are obtained. These variables are communicated to the second module, and the optimization of the second module is developed. This optimization process continues until all the modules are optimized individually, thus, completing the first iteration. Once the iteration is completed, the global objective function is evaluated, and if the convergence criterion has been satisfied, the procedure is stopped; otherwise, the procedure continues until a global optimum solution is obtained. Mathematical decomposition can also be applied to the modular optimization approach, if the condition of the system allows it. The results obtained for the CGAM problem show that the three approaches (i.e., mathematical optimization, TFA and the modular decomposition) give the same optimum, which is very close to that given

by the reference optimization in [110]. Results for the optimum decision variables and selected thermodynamics variables and those for the optimum capital costs are provided in Table 2.4.

2.3.1.4 Engineering functional approach (EFA)

EFA was developed by von Spakovsky [125] and von Spakovsky and Evans [126–129] and was applied by von Spakovsky to the CGAM problem [25]. As is the case with TFA, it is possible to obtain the synthesis/design and operation optimization of a system. The objective is to minimize the total costs of the system with respect to a set of independent decision variables and subject to equality constraints that represent the physical and economic model of the system. Inequality constraints provide physical limits. In EFA, the model can be defined on either a monetary or exergetic cost basis. It is possible to include pollution, scarcity of resource, and the manufacture and recycling of the system costs into the optimization.

The Functional Diagram or thermoeconomic structure of the system is constructed taking into account thermal exergy, mechanical exergy, power, and negentropy loops, interconnecting all the components in the system with physical, economic, and thermodynamic flows. Physical and economic equations are given for every component and flow branches/junctions are used. The internal economy is obtained using the Lagrange Method of Undetermined Multipliers. For the CGAM problem, von Spakovsky proposes five different approaches for the optimization, namely, a direct, a modular, a Lagrangian, a decomposition, and a decentralized approach.

In the direct or centralized approach the optimization algorithm is applied directly to whatever system of equations comprise the objective function and set of inequality constraints of the model. The equality constraints are solved as a separate system of equations, the results of which are fed to the optimization algorithm.

The modular approach closely follows the direct but takes advantage of the modularity or functionality of the thermodynamic calculations which comprise the equality constraints. If in addition, an internal economy (i.e., effectively, a productive structure) of the system is needed as well, the Lagrangian approach can be added to the modular one since the former is used to establish this internal economy. With this third approach, the internal economy is known at every iteration of the optimization algorithm.

The fourth approach, i.e., that of decomposition, divides or decomposes the thermoeconomic

model into subgroups, each of which is optimized in turn around the system in an iterative process which stops once closure or convergence is reached. The effectiveness of this approach depends, as mentioned in the previous section, on the disjointness of each of the decision variable sets associate with each subgroup. As suggested in the previous section, the degree of disjointness can be increased simply with the addition of more of the right type of decision variables, which, however, may become impractical for large-scale optimizations.

The final approach is similar to that of the decomposition approach but now the thermoeconomic model is developed at two levels of optimization, i.e., as a system model basis which captures the physicality of the system, and as subgroup models which capture detailed information of the components that reflect the internal geometry and material structure of each component. With this approach, the individual subgroups can also be economically isolated and optimized individually according to the procedure described by the decomposition approach. How close to the global optimum is the result obtained by the decomposition approach depends on how well the economic isolation was established at the system model level. Of course, this global optimum is an iterative procedure between the system model basis and the detailed models.

The results obtained for the CGAM reference optimization [110] and for the first and second approaches are given in Table 2.5 and show that the optimum solutions obtained are very close to each other. For the third and fourth approaches, the solutions are close but deviate somewhat with the values of T_3 and T_4 even though the difference in the final optimal total cost is 1.8% and 0.37%, respectively.

Table 2.5. Comparison of the optimum values for the CGAM reference optimization [110] with those obtained with the EFA optimization.

		Methods proposed in EFA [25]			
Variable	CGAM [110]	Modular	Lagrangian	Decomposition	Decentralized
P_2/P_1	8.5234	8.59822	8.59859	8.49996	8.49996
η_{AC}	0.8468	0.84678	0.84675	0.84991	0.84991
η_{GT}	0.8786	0.87874	0.87900	0.88000	0.87991
T_3 (K)	914.28	912.601	912.281	924.764	900.09
T_4 (K)	1,492.63	1,491.566	1,491.4400	1,528.970	1,480.153
$\dot{I}^{\$}_{\text{Fuel}}$ (\$/s)	0.325489	0.32552	0.32546	0.32110	0.32869
$\dot{I}^{\$}_{\text{Comp}}$ (\$/s)	0.036520	0.03653	0.03658	0.04740	0.03467
$\dot{I}^{\$}_{\text{Total}}$ (\$/s)	0.362009	0.36204	0.36204	0.36850	0.36336

2.3.2 Other developments on energy system analysis and optimizations

Almost a decade after the conception and first application of the CGAM Problem, the TADEUS[2] problem was developed by Valero and co-workers [6–10, 120–123] in order to extend the ECT approach to account for malfunctions and disfunctions in order to diagnosis the operation of energy systems and individual energy producers. The goal is to quantify the effect of the change in the exergy destruction of one component on the exergy destruction of the other components, and as a consequence, its effect on the overall efficiency of the system. By knowing the response of each component to these perturbations, preventive maintenance can be scheduled for each component of the system, accordingly.

Tsatsaronis and co-workers (e.g., [12, 13, 47, 130–132]) also proposed to split the exergy destruction due to irreversibilities into endogenous and exogenous parts. The endogenous irreversibilities are those caused in the component itself, and the exogenous ones are those caused by irreversibilities in other components. In addition, they proposed to split the exergy destruction of a component into avoidable and unavoidable. The unavoidable exergy destruction is that needed to generate a certain product, while the avoidable exergy destruction is that which can be reduced or eliminated completely leading to increased system efficiency. This splitting clarifies the margin of improvement possible for a system or component. These concepts of splitting the exergy destruction due to irreversibilities had already been proposed earlier for the concepts of malfunctions and disfunctions by Valero and co-workers (e.g., [6–10, 120–123]) as an extension of their ECT.

In terms of applications, exergoeconomic analyses and optimizations have been developed for steam plants [133], solar heating systems [134], CHP plants [135], coal plants [25, 136], hydrogen systems and hydrogen production [48, 137, 138], petroleum processes [139], district heating/district cooling systems [140], ventilation systems [141], heating and cooling systems [142], fuel cell and hybrid fuel cell systems [143, 144], etc.

Moreover, with regard to the complex optimization of energy systems, the optimization of an energy system can be developed at three different levels, namely, that of synthesis (configuration), design (component characteristics), and operation [145]. Obtaining the synthesis of the system is usually the most complex part of the process, and three main approaches are available in the liter-

[2]The TADEUS problem is a combined cycle power plant consisting of two 125 MW gas turbines and a 110 MW steam turbine [7]. It was named after **Tadeus** J. Kotas, author of the book: "*The exergy method of thermal plant analysis*" [94].

ature, i.e., heuristic and evolutionary methods to reach targets identified by physical rules and use of a superstructure[3] which is reduced during an optimization to an optimal configuration. Among these three approaches, the third one, starting with a superstructure, is the most robust, although, the computational burden associated with this type of optimization is highly complex.

As a solution to deal with the computational burden associated with the optimization of highly complex models of energy systems, several techniques have been developed. Those of decomposition have proven to be very successful. Decomposition can be divided into different types, namely, disciplinary, conceptual, time, and physical. Two particular forms of decomposition found in the literature are local-global optimization (LGO), e.g., [146, 147], and iterative and dynamic iterative local-global optimization (ILGO/DILGO) [148–160]. It is only, however, with the last of these, namely ILGO/DILGO that a real effective disjointness, i.e., that of so-called "thermodynamic isolation", is achieved [148].

2.4 Sustainability considerations

Even before the conception and acceptance of a formal definition for sustainability, the engineering community had been searching for ways to minimize damage to the ecosystem in the production of electricity, while satisfying the energy needs of society. However, how to utilize the exergy concept in order to deal with sustainability issues, particularly the environmental ones, is still an open question [50]. To try to answer this question, Wall and Gong [161] and Gong and Wall [162] assert that exergy can be directly linked to the environment and sustainable development by dividing the environment into five main groups, that is, biosphere, lithosphere, atmosphere, hydrosphere, and sociosphere. Every event that takes place in the environment is related to a cause-effect concept in which, however, a clear link between the cause and effect cannot be drawn, i.e., the effect perceived can be produced by many causes, and a cause can lead to multiple effects.

In terms of exergy, the fuel to the environment is that from the sun coming in the form of radiation, while that from fossil fuels stored in deposits in the earth's crust is only a small percentage of the total when compared to that of the sun. Nonetheless, it is the latter, the exergy from deposits,

[3] A "superstructure" or "superconfiguration" is a system configuration with all the possible components and interconnections physically available for the optimal system configuration (or superconfiguration) [145]. The optimal system configuration is obtained by synthesizing this superstructure or superconfiguration and is restricted to the initially available characteristics.

that in part measures the level of sustainability of a society. Any misuse of these deposits can lead to a non-sustainable society, because any abuse causes uncontrolled depletion of resources and an excess of emissions with a high exergy content relative to the damage caused to the environment. Therefore, entropy production or exergy destruction is a direct index to measuring sustainability; and, thus, exergy destruction and losses need be taken into account beginning with the extraction of raw materials and continuing through the disposal/recycle of equipment. The accounting should also include the amount and which renewable and no-renewable energy source is used as well as the amount of each. One approach for tackling the sustainability issue in energy systems synthesis, design, and operation is that of increasing the efficiency of such systems through a detailed exergy or second law analysis by identifying and quantifying the sources and causes of exergy destruction within each component. The goal of this type of analysis in its early stages was to reduce the costs of production, but later those using this type of analysis realized that environmental issues were also an important aspect of the analysis.

2.4.1 Environomic analysis

Some of the pioneers in tackling the environmental aspect with respect to energy production systems were von Spakovsky and Frangopoulos [15, 163–165], Frangopoulos and co-workers (e.g., [17, 20, 166]), and von Spakovsky and co-workers (e.g., [21–24]). This was done in part by introducing pollution penalty factors that penalize a system synthesis/design relative to the amount of pollutants emitted, accounting in the process for prescribed societal limits and existing environmental conditions. The methodologies developed by these researchers called environomics are able to drive the synthesis/design and operation optimization of a system towards a configuration with the least environmental damage relative to thermodynamic and economic constraints on system efficiency and cost. This environmental aspect is, of course, balanced with the system's technical and economic ones.

The pollution costs are added to the original optimization problem defined by Equation (2.13) such that

$$\sum_{p=1}^{\#\mathrm{pol}} \dot{I}^{\$}_{\mathrm{Pollutant}} = c_{_{\mathrm{Pollutant}}} f_{\mathrm{pPollutant}} \dot{p}_{_{\mathrm{Pollutant}}} \tag{2.17}$$

where $c_{_{\mathrm{Pollutant}}}$ is the unit damage cost of the pollutant, $\dot{p}_{_{\mathrm{Pollutant}}}$ is the rate of pollutant emission,

and $f_{\mathrm{pPollutant}}$ is the pollution penalty factor. One proposal for pollution penalty factor is given as [165]

$$f_{\mathrm{pPollutant}} = \frac{\alpha_{\mathrm{Pollutant}} - \alpha_{0_{\mathrm{Pollutant}}}}{\bar{\alpha}_{\mathrm{Pollutant}} - \alpha_{0_{\mathrm{Pollutant}}}} \tag{2.18}$$

where $\alpha_{\mathrm{Pollutant}}$ is the intensive property characteristic of the pollutant, $\alpha_{0_{\mathrm{Pollutant}}}$ the intensive property of the pollutant in the reference environment, and $\bar{\alpha}_{\mathrm{Pollutant}}$ the harmfulness limit of the pollutant [165].

A second proposal for pollution penalty factor is expressed as [165]

$$f_{\mathrm{p}_{\mathrm{Pollutant}}}(\dot{\phi}_{\mathrm{Pollutant}}) = \left(1 + \frac{\dot{\phi}_{\mathrm{Pollutant}}}{\dot{\phi}_{c_{\mathrm{Pollutant}}}} \exp\left(\frac{\dot{\phi}_{\mathrm{Pollutant}} - \dot{\phi}_{o_{\mathrm{Pollutant}}}}{\dot{\phi}_{c_{\mathrm{Pollutant}}}}\right)\right) \tag{2.19}$$

where $\dot{\phi}_{\mathrm{Pollutant}}$ is the degree of pollution, $\dot{\phi}_{c_{\mathrm{Pollutant}}}$ the critical value, and $\dot{\phi}_{o_{\mathrm{Pollutant}}}$ the natural purification rate. The degree of pollution is given as [165]

$$\dot{\phi}_{\mathrm{Pollutant}} = \frac{1}{V}\frac{dS_{\mathrm{Pollutant}}}{dt} \tag{2.20}$$

where V is the total volume of the affected region and $dS_{\mathrm{Pollutant}}/dt$ the rate of increase in entropy in the affected region.

Table 2.6. Optimal results of the environomic framework applied to the CGAM problem [165].

Variable	CGAM [18, 25]	Environomic I [165]	Environomic II [165]
P_2/P_1	8.59822	9.50524	9.12781
η_{AC}	0.84678	0.85356	0.85093
η_{GT}	0.87874	0.88711	0.88353
T_3 (K)	912.601	884.816	897.360
$\dot{m}_{NO_x}$ (kg/s)	0.00254	0.00234	0.00242
c_{NO_x}	0.0000216	0.0000207	0.0000212
$f_{P_{NO_x}}$	-	1.535	0.4059
$\dot{I}^{\$}_{\mathrm{Pollution}}$ ($/s)	0.0	0.02686	0.01811
$\dot{I}^{\$}_{\mathrm{Fuel}}$ ($/s)	0.32552	0.32273	0.32341
$\dot{I}^{\$}_{\mathrm{Comp}}$ ($/s)	0.03653	0.04068	0.03909
$\dot{I}^{\$}_{\mathrm{Total}}$ ($/s)	0.36204	0.39026	0.38060

These pollution factors are applied to the natural gas CHP cycle of the CGAM problem [18, 25] with data for the newest technology as of that date and with $\mathrm{NO_x}$ as the only emissions product

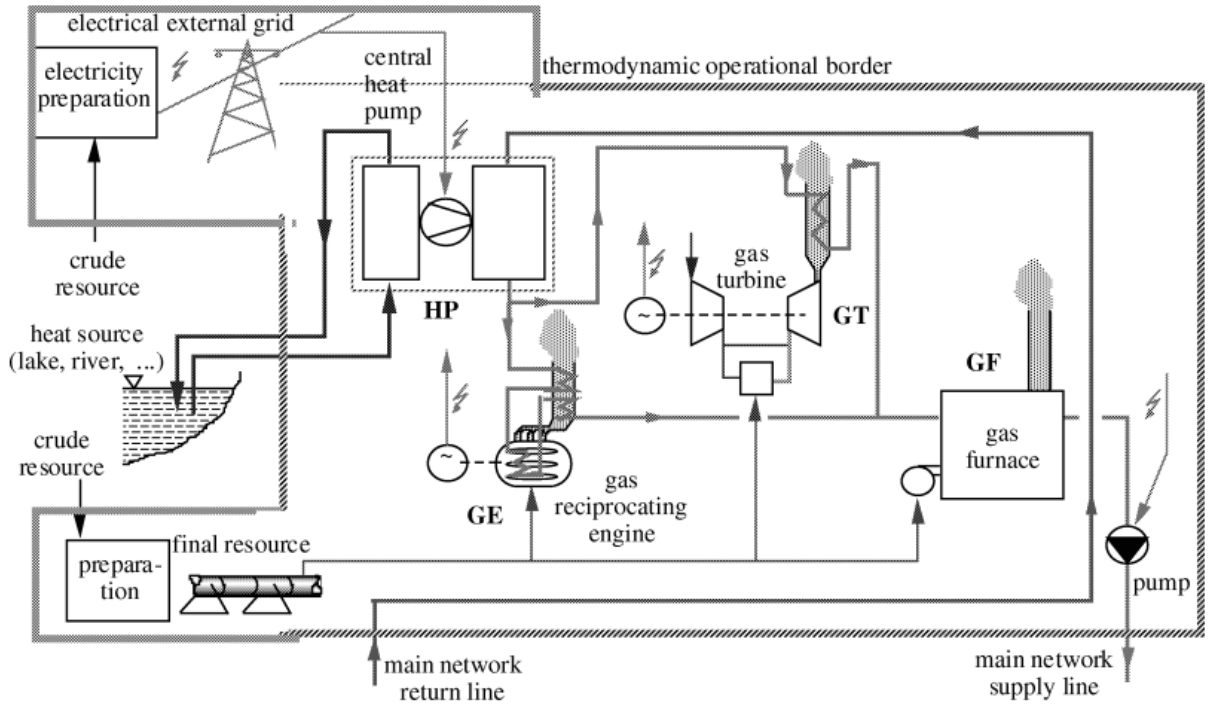

Figure 2.6. Configuration of the district heating system optimized using the environomic framework by Curti, von Spakovsky, and Favrat [21]. This figure was published in [21] Copyright © 2000 Elsevier Masson SAS. All rights reserved. Reprinted with permission.

of the energy conversion process. Table 2.6 shows the results obtained using these two pollution penalty factors (i.e., Environomic I defined by Equation 2.18 and Environomic II defined by Equation 2.19) compared to the exergoeconomic optimizations developed earlier for the CGAM problem [18, 25]. The environomic optimization is developed using EFA only. As expected, the total costs of the system increase significantly, i.e., by about 5.13 % for the first factor and by about 7.8 % for the second factor when pollution costs are included. Another observation is that the cost rate of fuel is reduced by a small percentage of less than 1% for the two pollution factors, and the air preheater temperature T_3 is reduced as well.

Pelster, Favrat, and von Spakovsky [23] applied the environomic optimization approach to the synthesis/design and operation optimization of a combined cycle power plant, while Curti, Favrat, and von Spakovsky [21, 22] applied it to the synthesis/design and operation optimization of a district heating system in the city of Laussane, Switzerland. As an example of the application to a complex system, the application of Curti, Favrat, and von Spakovsky [21, 22] is discussed here. The application of the environomic optimization framework is for the district heating system depicted in Figure 2.6. In this model, it is assumed that the district heating demand of the system is supplied by natural gas boilers, heat pumps, and CHP gas turbines and reciprocating engines.

Pollutants such as NO_x and NO_2 are considered in the optimization model, and two different scenarios are modeled, i.e., that of low heat rate demand at high temperature, and that of high heat rate demand at low temperature.

Results for the optimum heat rate by component are provided in Table 2.7 for the two scenarios where it can be seen that when no pollution penalties are added to the model, the district heating needs are mainly supplied by boilers while for the case when they are included, the production of the boilers is reduced by over 40%, and natural gas CHP generators and heat pumps driven by electricity from the grid provide the rest of the district heating demand resulting in an increase of the costs.

Table 2.7. Heat rate values for the district heating system optimized using environomics by Curti, von Spakovsky and Favrat [21, 22]. The costs are given in the Swiss currency CHcts/kWh.

	Low heat rate demand at high temperature		High heat rate demand low temperature	
Electricity Price (13 CHcts/kWh) Gas Price (5 CHcts/kWh)	Without pollution cost	With pollution costs	Without pollution cost	With pollution costs
Network Temperature (^{o}C)	85.8	69.5	89.8	52.0
Heat Pump (MW)	29.0	50.9	31.7	61.1
CHP Gas Turbine (MW)	12.7	0.0	14.6	0.0
CHP Gas Engine (MW)	0.0	0.0	0.0	0.0
Gas Furnace (MW)	20.9	11.4	16.4	0.0

2.4.2 Exergoenvironmental analysis

Tsatsaronis and his co-workers (e.g. [27–30]) introduced environmental aspects into their exergoeconomic analyses without the use of penalty factors. This new methodology is called exergoenvironmental analysis. The exergoenvironmental analysis is applied in parallel and in a similar way to the exergoeconomic analysis of EEA by obtaining environmental balance equations for each component k of the system [29, 30], such that

$$b_{P,k}\dot{B}^{\mathrm{env}}_{P,k} = b_{F,k}\dot{B}^{\mathrm{env}}_{F,k} + \dot{Y}_k \tag{2.21}$$

where $b_{P,k}$ and $b_{F,k}$ are the unitary environmental cost of the product and fuel of a component, respectively; $\dot{B}^{\mathrm{env}}_{P,k}$ and $\dot{B}^{\mathrm{env}}_{F,k}$ are the environmental impact rates associated with the product and

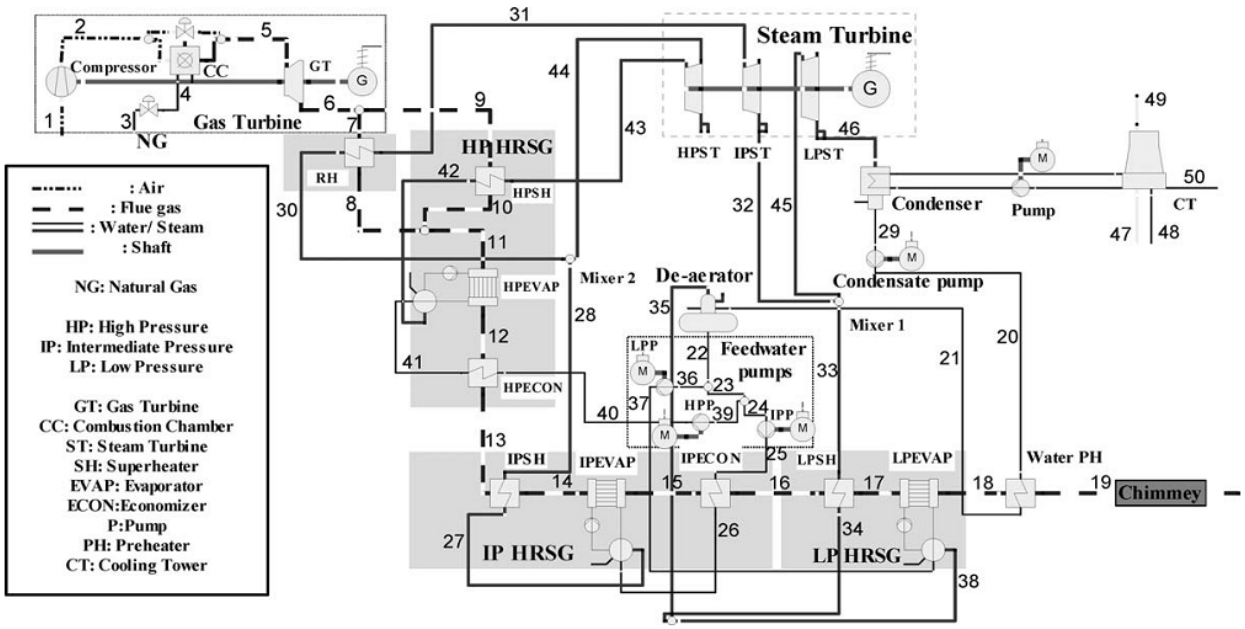

Figure 2.7. Combined cycle system analyzed with an exergoenvironmental approach by Petrakopoulou et al. [28]. Reprinted from [28] Copyright © 2011, with permission from Elsevier.

fuel of a component, respectively; and $\dot{Y}_k$ is the environmental impact rate associated with the life cycle of the component given by

$$\dot{Y}_k = \dot{Y}_k^{CO} + \dot{Y}_k^{OM} + \dot{Y}_k^{DI} \tag{2.22}$$

where $\dot{Y}_k^{CO}$, $\dot{Y}_k^{OM}$ and $\dot{Y}_k^{DI}$ are the environmental impact rates associated with the construction, life time operation and maintenance, and disposal of the component. The auxiliary equations for the exergoenvironmental analysis are obtained applying the Fuel-Product concepts in a fashion similar to EEA [29].

Meyer et al. [27] applied this methodology to a high-temperature fuel cell system integrated with an allothermal biomass gasification process and Petrakopoulou et al. [28] to a combined cycle power plant with and without chemical looping combustion. The schematic of the system for the combined cycle without the chemical looping combustion analyzed by Petrakopoulou et al. [28] is depicted in Figure 2.7. A life time of the system of 20 yr with 2012 data for the characterization of the plant and the Eco-indicator 99[4] [167] for the environmental life impacts (i.e., human health, ecosystem and depletion of resources) are considered for the analysis.

The main results of the exergoeconomic analysis shows that the total cost rate of the plant is

[4]The Eco-indicator 99 is the final weighted result of the life impact assessment of a production process with units of Eco-indicator points (Pts)

16,513 €/hr including the costs caused by exergy destruction due to irreversibilities and the amortized capital costs and operation and maintenance costs. For the exergoenvironmental analysis, the production of electricity and the impact of NO_x and SO_2 emissions is considered. The result, given in Table 2.8, shows that the total impact on the environment is of 39,585,477 mPts/hr, including those of the exergy destruction due to irreversibilities in the operation of the system and the impact rate associated with the life cycle of the components of the plant.

Table 2.8. Results of the analysis for the combined cycle plant developed by Petrakopoulou et al. [28].

Exergoeconomic Analysis		Exergoenvironmental Analysis	
Variable	Results [28]	Variable	Results [28]
c_F (€/GJ)	9.2	b_F (mPts/GJ)	3,599
c_P (€/GJ)	20.5	b_P (mPts/GJ)	6,398
$\dot{I}^{\$}_{\mathrm{Irr}}$ (€/h)	10,053	$\dot{B}^{\mathrm{env}}_{\mathrm{Irr}}$ (mPts/h)	39,536,056
$\dot{I}^{\$}_{\mathrm{Comp}}$ (€/h)	6,460	$\dot{Y}_{\mathrm{Total}}$ (mPts/h)	49,422
$\dot{I}^{\$}_{\mathrm{Total}}$ (€/h)	16,513	$\dot{B}^{\mathrm{env}}_{\mathrm{Irr}} + \dot{Y}_{\mathrm{Total}}$ (mPts/h)	39,585,477

2.4.3 The reference environment and the exergoecology concept

Szargut and co-workers [104–106] were pioneers in proposing exergy as the accounting unit for all the resources used during the process of a certain product, including the quantification of the damage to the environment due to the depletion of resources and emissions to the environment. This method is called a thermo-ecological analysis.

As an extension to the thermo-ecological analysis, Valero and co-workers [168–174] extended Szargut's thermo-ecological analysis by providing a methodology to quantify the resources needed to restore the minerals and natural resources used in an industrial process to their pristine state. This is develop by extending the database of reference mineral elements in the earth's crust [168, 173] provided by Szargut [106] and subsequently proposing the *exergoecology* concept [169], which is an exergy-based methodology to account for the mineral capital of the Earth [169]. Valero and co-workers [170] also propose two indices for the their application to the mineral capital of the Earth, i.e., the exergy replacement cost and exergy abatement cost. The exergy replacement cost is the amount of exergy needed to restore a given amount of natural resource back to its pristine state using the most efficient current technology while the exergy abatement cost is that needed to

eliminate the excess of pollutants emitted (e.g., those that exceed the maximum limit that nature can abate by itself) using the most efficient current technology. As an example of the application of the methodology, Valero and Valero [169] applied the exergoecology analysis for the process of bauxite-aluminum and limestone-lime production. Table 2.9 provides the results of the analysis. Total production in 2007 is taken into account as is the respective cost of production including the exergy cost needed to restore each of the minerals back the Earth's crust using the most current technology as of that date.

This section has presented methodologies developed to date to account for the energy, resources, and emissions of an energy production process from extraction to production and restoration of the natural environment. Section 2.4.2 in particular introduced the Eco-indicator 99, which is a single index accounting for the resources used and damage to the environment from extraction to disposal. In addition to the Eco-indicator 99, there are other methodologies available in the literature for the life cycle analysis of energy production systems. The next section provides a general overview of the ISO guidelines for developing life cycle analysis and exergy-based life cycle analysis methodologies.

Table 2.9. Results of the exergoecology analsysis develop by Valero and Valero [169].

	World Production in 2007 (tons)	Total exergy costs (Gtoe)
Bauxite	1.99×10^8	0.17
Alumina	7.60×10^7	0.23
Aluminum	3.80×10^7	0.44
Limestone	4.99×10^8	0.0149
Calcite	2.99×10^8	0.0163
Lime	2.77×10^8	0.0544

2.4.4 Overview of exergy-based life cycle analysis

The goal of a Life Cycle Analysis (LCA) is to assess the environmental impact of a process from the extraction of minerals for the manufacture of equipment to the dismantling and disposal of the equipment at the end of its useful life. This process includes the process of raw material acquisition, manufacture, use/reuse/maintenance and recycle/disposal of the goods, as well as transportation between the stages of the process as is depicted in Figure 2.8(a). The guidelines for developing an LCA are properly establish according to the ISO 14000 series normative [175–178].

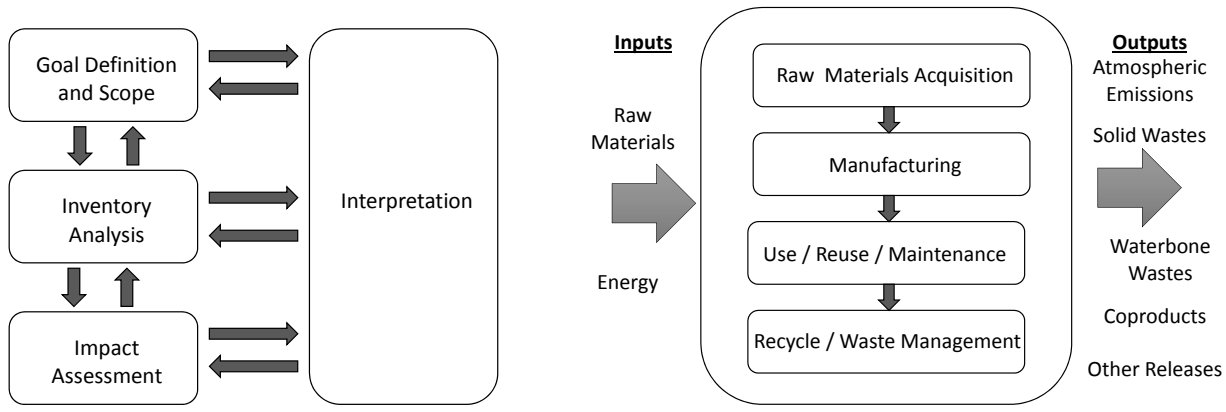

(a) Life Cycle Analysis Methodology. (b) Boundaries of the Life Cycle Analysis.

Figure 2.8. Representation of the methodology for developing a Life Cycle Analysis.

The LCA development consist of four stages (see Figure 2.8(b)), i.e., *goal definition and scope*, *life cycle inventory analysis (LCI)*, *life cycle impact assessment (LCIA)*, and *life cycle interpretation* [175–178]. These stages are developed in a series process but are not independent of each other. Once results from one stage are obtained, interpretation of the results are necessary and feedback is provided to the previous stages. The process continues iteratively until a desired level of accuracy is reached.

In the first stage of the analysis, the boundaries, scope, and objectives of the analysis are clearly described. In the second stage, an exhaustive collection of data accounting for materials, use of natural resources, and emissions to the environment is developed according to the physical flow structure of the particular process. The extent to which the data collection is developed depends on the objective of the study provided in the previous stage. The third stage consists of a detailed analysis of the data by grouping it into different impact categories reflecting the total amount of natural resources and damage to the environment during the process. In this stage, the different impact categories are grouped and weighted in order to obtain a certain number of indices that reflect the impact of the particular process. Since this process involves the use of weights, all the assumptions and decisions have to be clearly provided in order to reduces the subjectivity of the analysis. The last stage consist of translating the results so that they are comprehensive to decision makers.

Several databases are available around the world for LCA practitioners, but two of the main databases available are the open US-EPA database supported by the US-Environmental Protection Agency and hosted by the National Renewable Energy Laboratory [179] and the *ecoinvent* database

[180] which is a not-for-profit project develop in Switzerland.

In order to include exergy in the assessment of the LCA of a process, Szargut proposed the *Cumulative Exergy Content* (CEC) method [106] to account for the total exergy use during a certain process, including the quantification of the exergy damage to the environment due to the depletion of resources and emissions to the environment. In the CEC it is assumed that exergy is increased or decreased from the initial exergy content of the raw materials at every stage of the process due to the thermodynamic structure of the particular process by means of heat, work, or mass interactions. As a final result, the product contains a particular amount of exergy equivalent to the exergy used during the process.

Other methodologies, which use exergy as an index for assessing the impact of the life cycle of a process on the environment, have been developed recently and are available in the literature such as the CEENE methodology [181–185], the life cycle analysis (LCA) method [186], the exergetic life cycle analysis (ELCA) method [183], the life cycle exergy analysis (LCEA) method [187], and the extended exergy accounting method [188]. These exergy-based methodologies are mentioned here as a reference for further research on the Sustainability Assessment Framework proposed in this dissertation.

2.4.5 Criticisms on the use of exergy as an index of sustainability

Exergy is a robust and well-established thermodynamic quantity, which can be used for assessing various aspects of sustainability such as, for example, the quantification of the primary energy resources needed for the production of a good in a certain production process. For the particular case of energy production processes, it entails the analysis of fossil and non-fossil (e.g., solar energy, wind, etc.) fuels.

However, the use of exergy as a sustainability index has also been strongly criticized in the literature [189–192]. A number of these criticisms are addressed here. For instance, it is suggested that because of the use of a reference environment, the results of two identical analyses using different reference states may not be directly comparable. This criticism fails to recognize the nature of any thermodynamic analysis. All such analyses whether based on exergy or energy or some other thermodynamic property require consistency in the choice of references since properties such as energy, exergy, entropy, enthalpy, Gibbs free energy, Helmholtz free energy, etc. all

depend on a reference or set of references and, thus, are relative properties and not absolute. The point of making a comparison between two different exergy or for that matter energy analyses is to discern the relative differences in performance and not the absolute differences. Thus, of course, the reference states chosen must be consistent to make the comparisons.

Another criticism leveled is that an exergy-based methodology can identify the amount and location of irreversibilities but cannot identify the causes of these irreversibilities. The response to this criticism is that an energy analysis by itself, for example, cannot even identify the amount and location much less the causes of irreversibilities. Whether or not the exergy analysis can do the latter or not is beside the point since it is the designer who identifies the causes guided by the exergy analysis.

The criticism leveled that an exergy methodology puts more emphasis on the environmental aspects of sustainability by considering that the most valuable process is that which uses fewer resources, failing in the process to account for socioeconomic considerations in the analysis, also misses the point. In a similar vein, the criticism is made that an exergy-based methodology converts the cost of every resource consumption into exergetic costs, providing an understanding of when and where the system needs to be modified, but fails to decide if the modification is truly convenient from a purely economic standpoint. These are not really criticisms but simply a recognition already long held by the principal practitioners of exergy analysis (e.g., [4, 101, 110, 136]) of the limitation of the analysis as posed. None of these practitioners would ever make a claim that the analysis is sufficient in and of itself. All would agree that socioeconomic considerations whether posed in exergy or some other terms may be needed and can indeed be added as some have (e.g., [50, 188, 191]).

An additional criticism states that exergy as a property is not a good indicator for externalities such as those due to emissions, since the exergy content of emissions does not represent the actual damage to the environment. Again, this was recognized by exergy practitioners at least two decades ago (e.g, [163–165]) and was addressed through, for example, the use of pollution penalty functions and unit damage costs coupled to the exergy content of the emissions. Obviously, such an approach may not be sufficient to deal with all aspects of human health, aesthetics, material damage, ecosystem effects, etc., and, thus, other indices could be used that directly address the external effects of concern. In fact, most advocates of exergy recognize that the use of exergy should simply be part of an overall multicriteria analysis with an array of indices addressing various con-

cerns, and, thus, the criticism leveled is not applicable to how exergy is used in this dissertation or in most other applications.

Another common criticism leveled is that the rules for allocation of resources to the different products of the process are not rigorous in the sense that they depend on the decision of the analyst. The collection of data for the accurate description of a production process for a very large system is sometimes very complicated (this is not a problem for small systems). The excessive use of assumptions for the analysis of large and complex systems increases the uncertainty of the results. Unfortunately, this criticism fails to recognize that such an allocation whether via exergy or energy or emergy or some other property is part and parcel of any design process and simply cannot be avoided. If an allocation is to be made, assumptions will be required, which is why the design of a system whether from a thermodynamic or economic or environmental or sustainability standpoint is *not* and *never* will be a science but is instead the practice of engineering.

A final set of criticisms is that people's preferences are not taken into account in the analysis (which, by the way, actually makes the result of an exergy-based methodology more objective) and the general public is not well informed about the basis of the framework, making general acceptance of the methodology for those outside the group difficult. Indeed, the first of these criticisms is simply a variation of an earlier one and is not applicable to how an exergy-based methodology would be applied in practice as a part of a multicriteria analysis with a full range of indices that account for the economic, environmental, and societal aspects of system synthesis, design, and operation. In considering tradeoffs among all of these indices including exergy, subjective preferences play a crucial and indeed inescapable role. Regarding the criticism that the general public is not well informed, this is a challenge for users of exergy indices; but the information exergy indices provide is sufficiently valuable and distinct from other indices that it is well worth the effort to educate potential users.

From the previous discussion, and as is also described in [189–192], it should be obvious by now that no single index or property captures all aspects of sustainability and that there is a need to include at least one index for each of the pillars of sustainability, i.e., economic, environmental, technological and societal, in the analysis. In addition, although the aggregation of indices into a single index for sustainability helps with the interpretation of the results by the decision maker, the problem arises that if the aggregation does not reflect the true preferences of stakeholders, the results may be untrusted. For this reason, stakeholder involvement should be present as much as is

practically possible beginning in the early stages of the analysis. Moreover, instead of obtaining a single aggregated sustainability index, it may be more beneficial to study the trade-offs among the multiple indices considered in order to arrive at a clearer understanding of the problem. Similarly, the development of a sensitivity analysis to rule out the indices that do not affect the final decision may be of help in order to avoid any extraneous information that can pollute the results by providing unnecessary information to the stakeholder.

In summary, exergy alone (or any other index by itself for that matter) cannot provide a complete representation of sustainability (in fact, it was never intended to do so) because sustainability is multidimensional. Furthermore, the approach of using multiple indices to understand sustainability outcomes may be more robust, while the involvement of stakeholders beginning in the early stages of a particular analysis should result in a more complete description of the sustainability of a given synthesis, design, and operation.

2.5 Sustainability of complex networks of energy producers

At the level of power networks, improvements in the concept of sustainability have been developed, especially with the use of multi-criteria decision making (MCDM) analysis and optimization [45, 46, 193]. The details of the analyses vary in terms of whether or not only producers, only producers/transmission, or producers/transmission/distribution are taken into account. These types of analyses are part of energy planning and market models [34, 37, 194–200].

Vera and Langlois [201] develop a study to emphasize the importance of quantitative metrics for the energy development of a country. In their study, they propose interrelated social, economic, and environmental considerations as the basis for indices to measure the sustainability of energy systems. It is assumed that energy at affordable prices is essential for supporting social aspects; that availability and reliability are essential for economic aspects; and that the effects of the use and generation of electricity on the atmosphere, water, and land are the backbone of the environmental aspect. These researchers suggest that increasing the efficiency of processes for electricity generation is one of the most, if not the most, important measure for assuring sustainability. The indices proposed are those developed by five main international organizations [202] dealing with health, safety (accidents), generation efficiency, prices, and pollution (e.g., air quality).

Afgan and co-workers [203–205] propose a methodology for energy system assessment un-

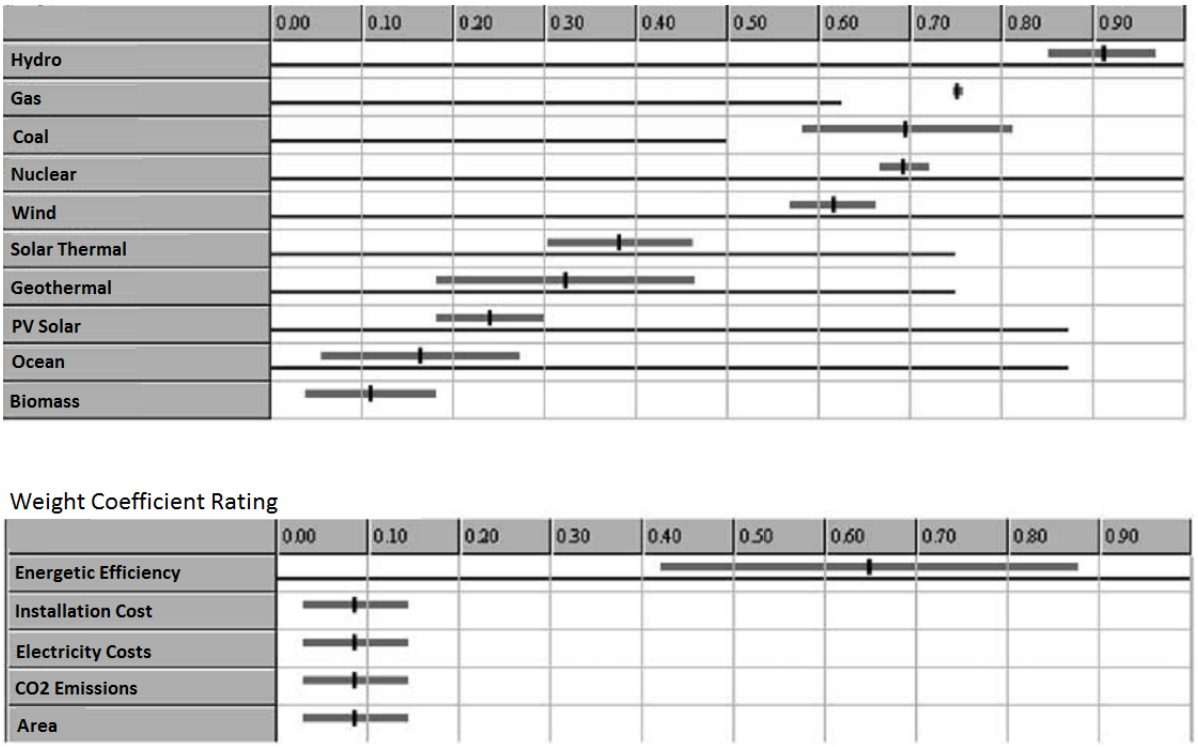

Figure 2.9. Results of prioritizing the energetic efficiency obtained by Afgan and Carvalho [204]. Reprinted from [204], Copyright © 2002, with permission from Elsevier.

der sustainability considerations based on a multicriteria analysis. Only energy-based indices are considered with the aim of evaluating the quality of energy systems. Firstly, the system needs to be described. Secondly, a set of energy-based indices is selected covering the environmental, technological, economic, and social aspects of sustainability. After that, a collection of data is developed with the quantitative characteristics of the technologies considered in the analysis. The indices are then normalized, and a general sustainability index is obtained by using weights for the different aspects of sustainability. Weights are found using a method in which all the possible weight combinations are given consistent with the number of indices and a possible number of weight vectors, although equal weighting is employed usually. In other cases, a high importance is given to one index, and the same low weight is given to the rest of the indices. Another variation is to give importance to one index, while giving importance by the order of numbering to the rest of the indices.

Table 2.10 shows the different technologies used in the analysis including renewable and non-renewable producers as well as the indices used for the evaluation. Figure 2.9 shows the results obtained when a priority has been given to the energetic efficiency of the producers. As a result, the producers based on hydro power have a very high priority compared with the rest of the tech-

nologies. This clearly indicates that the use of energetic efficiency as an index does not give a clear idea of the best technology when analyzing renewable and non-renewable energy technologies.

Evans, Strezov and Evans [206] made an exhaustive search of the literature to obtain the characteristics of renewable energy technologies (photovoltaic, wind, hydro, and geothermal), looking for seven principal characteristics or indices such as the price of electricity over the full life cycle ($/kWh); life cycle greenhouse gas emissions (CO_2-eq); availability when the technology is required; fist law efficiency; land requirement (foot print index, km^2/TWh); water consumption (water lost from circulation, kg/kWh); and social impacts reflected in toxins and visual aesthetics for photovoltaic; bird strikes, noise, and visual for wind; displacements, agricultural, and river damage for Hydro; and seismic activity, odor, pollution, and noise for geothermal. These technologies and their respective values for the indices are provided in Table 2.11.

The four renewable technologies are then ranked for each index from one to four as given in Table 2.12 where one corresponds to the best technology and four to the worst. It is assumed that all the indices have the same importance and the ranking corresponds to international considerations. Afterward the indices for each technology are added, and a global sustainability index is obtained. Wind is ranked the best sustainable technology followed by hydro and then photovoltaic. Geothermal is found to be the least sustainable. The sustainability assessment in this work is simple and straightforward and is used to assess what is available in terms of renewable energy sources. Another valuable contribution of this work is the exhaustive literature review of current available renewable generators.

Table 2.10. Technologies and sustainability indices studied by Afgan and Carvalho [204].

	Energetic Efficiency (%)	Installation Cost($/kW)	Elect. Cost (¢/kWh)	CO_2 Emissions (kg/kWh)	Area (km^2/kW)
Coal	43	1,000	5.4	0.82	0.4
Solar Thermal	15	3,500	17	0.1	0.08
Geothermal	8	2,500	8	0.06	0.03
Biomass	1	2,500	14	1.18	502
Nuclear	33	2,300	4	0.025	0.01
PV Solar	10	4,500	75	0.1	0.12
Wind	28	1,100	7	0.02	0.79
Ocean	3	10,000	25	0.02	0.28
Hydro	80	2,000	8	0.04	0.13
Natural Gas	38	650	4	0.38	0.04

Table 2.11. Technologies and sustainability indices studied by Evans, Strezov, and Evans [206].

	Photovoltaic	Wind	Hydro	Geothermal
Price of Elect. ($/kWh)	0.24	0.07	0.05	0.07
Emissions (CO_2-eq)	90	25	41	170
Efficiency (%)	4-22	24-54	>90	10-20
Water Consumption (kg/kWh)	10	1	36	12-300
Land Use (km^2/TWh)	28-64	72	750	18-74

Table 2.12. Results of the ranking for the study of Evans, Strezov, and Evans [206].

	Photovoltaics	Wind	Hydro	Geothermal
Price	4	3	1	2
Emissions	3	1	2	4
Availability	4	2	1	3
Efficiency	4	2	1	3
Land Use	1	3	4	2
Water Consumption	2	1	3	4
Social Impacts	2	1	4	3
TOTAL	20	13	16	21

Frangopoulos and Keramioti [207] propose a multicriteria approach using sustainability indices for the analysis of three different cogeneration units. Emphasis is placed on the difficulty of measuring sustainability and on what their quantitative metrics would be. Sustainability is divided into four main categories, i.e., technical, environmental, monetary, and social issues. All the pillars can be measured quantitatively with the exception of the social. In their work, they describe a methodology to quantify the first three indices and put aside the social issues. The first step is to select the indices for the analysis after which they are grouped according to their sustainability category. Since the indices are non-commensurable, it is necessary to use normalization and then weight the indices in order to obtain a sub-index for each of the four main groups. The sub-indices are weighted again, and a final sustainability index is obtained. Final indices are compared with the different scenarios, and a final decision can be taken.

Frangopoulos and Keramioti compared three different systems to satisfy the electric and heating demand of an industrial unit using the framework proposed, i.e., electricity from the network and heat from a natural gas boiler (System A), a CHP natural gas turbine similar to that provided

in [110] (System B), and a CHP reciprocating engine operated with 90 % NG and 10 % diesel coupled to a natural gas boiler (System C). The values of the indices for the three different systems are given in Table 2.13. Four sub-indices for technological considerations, six sub-indices for environmental considerations, and two sub-indices for economic considerations are included in the analysis. Table 2.14 provides the results obtained for the three sustainability indices considered, as well as the total composite sustainability index for each technology.

Table 2.13. Technologies and sub-indices evaluated by Frangopoulos and Keramioti [207].

Index	System A	System B	System C
Energetic electric Efficiency (%)	0.38	0.3761	0.47
Energetic total efficiency (%)	0.56	0.8483	0.86
Exergetic electric efficiency (%)	0.36	0.36	0.451
Exergetic total efficiency (%)	0.337	0.513	0.522
Annual NO_x emissions (kg/yr)	209,856.8	319,209	483,574.1
Annual CO emissions (kg/yr)	74,814.7	19,388	1,124,668.8
Annual UHC emissions (kg/yr)	0	14,923	673,199
Annual PM_{10} emissions (kg/yr)	13,963	10,441	8,485.8
Annual CO_2 emissions (kg/yr)	182,559,976.6	120,547,231	118,790,310
Annual SO_x emissions (kg/yr)	0	0	15,035
Total costs (€)	319,384,905.1	181,429,678	232,009,565.8
total cost with externalities (€)	357,593,745	211,828,489.5	278,628,728.5

Table 2.14. Global sustainability indices for the analysis of Frangopoulos and Keramioti [207].

Index	System A	System B	System C
I_{tech}	0.433	0.548	0.605
I_{env}	0.658	0.866	0.333
I_{econ}	0	1	0.587
I_{total}	0.364	0.805	0.508

In order to obtain an index for each aspect of sustainability as well as the total sustainability index and for purposes of illustration, Frangopoulos and Keramioti assume that the sub-indices within their respective group (i.e., economic, environmental, and technological) have the same importance and that the three aspects of sustainability have the same importance as well. From the total composite index for each system, it can be seen that the use of combined heat and power plays a very important role in the energy conversion process, since the CHP gas turbine has the highest

total sustainability index. The sustainability index decreases when the cogeneration percentage is reduced and boilers are introduced into the system. The least sustainable technology is that in which boilers are used to satisfy the entire heat demand for the industrial unit.

Sheinbaum, Ruiz, and Rodríguez [208] develop a sustainability analysis of the Mexican energy sector based on the indices proposed by the Economic Commission for Latin America and the Caribbean (CEPAL) [209]. Eight main indices are proposed, e.g., energy autarky (capacity to satisfy energy needs with ones own resources in the long term), robustness, productivity, electricity coverage, coverage of basic energy needs, relative purity in the use of energy (SO_2 emissions), use of renewable energy sources, and depletion of fossil fuels. These indices correspond to the four pillars of sustainability, that is, social, environmental, technical, and economic. The eight indices are equally weighted in order to obtain a general sustainability index. A comparison of the energy sector in 2008 to that in 1990 is made.

Results of the comparison are given in Table 2.15 where it can be seen that a decrease in all the indices other than those for productivity and the coverage of basic energy needs occurs. These two areas of improvement are basically related to population growth and the electrification of rural areas, while the others are mainly related to the mismanagement of natural resources relative to regulations adopted in 1990. The global sustainability index is obtained by considering that the eight indices have the same importance, resulting in a global sustainability index in 1990 of 0.73 and in 2008 of 0.56 (clearly this shows that the energy sustainability of the country has decreased considerably).

Table 2.15. Results of the analysis by Sheinbaum, Ruiz, and Rodríguez [208].

	Autarky	Robustness	Productivity	Electricity Coverage	Coverage of basic Energy Needs	Relative Purity	Renewable Energy ources	Depletion of Fossil Fuels
1990	0.96	0.94	0.50	0.88	0.33	1.00	0.27	0.97
2008	0.78	0.57	0.57	0.98	0.39	0.45	0.23	0.54

2.6 Social aspects of sustainability

Social aspects are considered as the fourth pillar of sustainability. These aspects account for job creation, increments in life quality, etc.; and their significance should be included in a detailed

sustainability analysis, because in order for a technology to be socially sustainable, it should at least be accepted by society [201].

Assefa and Frostell [201] develop an analysis in the town of Kil in central Sweden based on knowledge about energy production and the different energy production technologies available to date, acceptance of the inclusion of new types of energy production technologies such as fuel cells and photovoltaics into the network, and fear about the inclusion of these new types of energy production technologies. Their analysis is based on questionnaires sent to the community only under local analysis. Their results indicate that society is not well educated with regards to energy production technologies, which they find alarming, because this lack of knowledge contributes to delays in the implementation of state-of-the-art energy generators. Out of all of the questionnaires distributed, only 39 % were returned. In the questionnaires, questions about the priorities of the customer were also included. The result is that reliability of supply and the price of electricity were the most important aspects followed by environmental concerns and only then by the social issues involved with the production of electricity.

Another major contribution is that of Gallego and Mack [210], who develop a set of social indices as part of the NEEDS project [211]. Their indices are based on an exhaustive search of the available social indices in the literature which are accepted and enriched by experts in different disciplines in four countries. In a first step, 1320 indices are adopted and in a second step, this number is filtered to only 26 indices which satisfy nine characteristics that a social index must exhibit. Table 2.16 gives the nine different characteristics for filtering the indices while Table 2.17 groups the final 26 indices in four different areas, i.e., continuity of energy service, political stability, risk, and quality of life. In the next step of the process, 6 experts from France, 9 from Germany, 10 from Italy, and 10 from Switzerland are asked to answer questionnaires and participate in a two-day workshop to discuss the acceptability of the social indices selected and to suggest any other indices, if necessary. The last step of the analysis is one of evaluation by the same set of experts who rate 16 different energy production technologies (renewable and non-renewable) on a range of 1 to 5, where a value of one indicates high acceptance and a value of five indicates no acceptance. This survey expresses the opinion of societal experts for their expectations to the year 2050. Table 2.18 provides the results of the opinion of the experts on the different technologies according to the social indices included in the analysis. The 16 technologies are grouped into 7 fuel-based technologies, and only 9 out of the 26 original social indices are evaluated.

Table 2.16. Characteristics for filtering the social indices considered by Gallego and Mack [210].

Are the indices clear in value?
Are the indices coherent and consistent (logical)?
Are the indices appropriate in scale?
Are the indices sufficient in information?
Can the indices be applied throughout Europe?
Are the indices capable of linking social impacts to energy system-related aspects (exclusiveness and exhaustiveness)?
Do the indices discriminate between the specific energy technologies that have been included in our analysis?
Are data or data collection methods available for each of the indices?
Can data be disaggregated on the national or even regional level?

Table 2.17. Social indices obtained by Gallego and Mack after the filtering process [210].

Continuity of energy service over time	Political stability and legitimacy
+ Need of reserve capacity	+ Potential of energy system induced conflicts that may endanger the cohesion of societies
+ Market concentration in the supply of primary sources of energy	+ Willingness of NGOs and other citizen movements to act for or against the realization of an option
+ Time span for known reserves and assumed resources for each energy system if used at present rate	+ Reliance on participative decision-making process for different kinds of technologies
+ Probability of the not-in-time availability of a complete waste management concept	+ Empirical survey results concerning citizens acceptance of power plants
+ System flexibility to react to market changes, in particular sudden fuel price fluctuations	
+ Flexibility to incorporate new technological developments	
Social components of risk	**Quality of life**
+ Qualitative risk characteristics (risk perception variables)	+ Share of the effective electricity costs in a social welfare recipients budget
+ Subjective expected health consequences of normal operation	+ Technology specific job opportunities (direct)
+ Trust in risk management agencies	+ Perception of fairness of risk distribution and benefits in neighboring communities
+ Mortality due to normal operation	+ Land use caused by the energy system
+ Mortality due to severe accidents	+ Inaccessible public area due to energy system
+ Potential for a successful attack	+ Percentage of population perceiving aesthetic impairment of the landscape
+ Maximum potential effects of a successful assault	+ Subjective satisfaction of inhabitants with the power plant
	+ Number of residents feeling highly affected by noise caused by energy production
	+ Contribution to congestion in traffic peak periods through transports to energy facility

Table 2.18. Results of the analysis develop by Gallego and Mark [210].

	Innovative ability	Waste disposal	Conflict	Participation	Health concerns	Familiarity	Catastrophic potential	Functional impact	Aesthetic impact
Coal power steam	3.64	2.30	2.91	3.91	3.35	3.33	2.45	3.41	3.70
Carbon separation and sequestration	2.44	3.47	2.57	4.00	2.94	3.64	3.12	2.94	3.00
Gas turbine combined cycle	3.12	1.67	2.56	3.54	2.46	3.12	2.32	2.46	3.03
Nuclear power	3.05	3.64	4.50	4.63	4.18	3.70	4.77	3.13	3.54
Hydro power	3.92	1.38	2.56	3.76	1.69	3.06	2.71	3.23	3.18
CHP fuel cell	1.63	1.68	1.39	2.29	1.75	2.85	1.74	1.51	1.56
Photovoltaic	1.61	1.74	1.51	2.43	1.17	2.62	1.32	2.06	2.53

The major conclusions of the analysis is that of these technologies, nuclear is the least accepted, while combined heat and power (CHP) fuel cell and solar photovoltaic (PV) are the most accepted. In addition, the major weaknesses of this study (also recognized by the authors) is that no general population is included in the analysis, which leaves an open opportunity of research for social aspects on the sustainability of energy production technologies in general and of these technologies coupled to power networks via microgids in particular.

Chapter 3

System Description and Modeling Scheme for SAF

3.1 Power network system

The power network system considered in this dissertation is depicted in Figure 3.1. It is represented by a total of N nodes or areas interconnected by a total of Q high-voltage transmission corridors, setting up a total of L arcs or loops. Production and demand of energy (electricity and/or heat) can exist at a node. If production of energy exists at a node *n*, there is a maximum of W producers from which it can be generated and supplied to the network.

In order to describe the synthesis/design/operation optimization of the network from a sustainability and resiliency standpoint, two different scenarios at both the national- and international-level of description are considered. The first scenario, *Scenario 1*, considers the network at the transmission level with only centralized energy producers generating power to meet all of the energy demand. The second scenario, *Scenario 2*, considers the network at the transmission level with centralized producers as well as decentralized energy producers via microgrids (MGs) satisfying the energy requirements of the network. The electricity demand on the network in *Scenario 2* is equal to that in *Scenario 1*. The MG producers in *Scenario 2* are in direct competition with the centralized producers located in the main network.

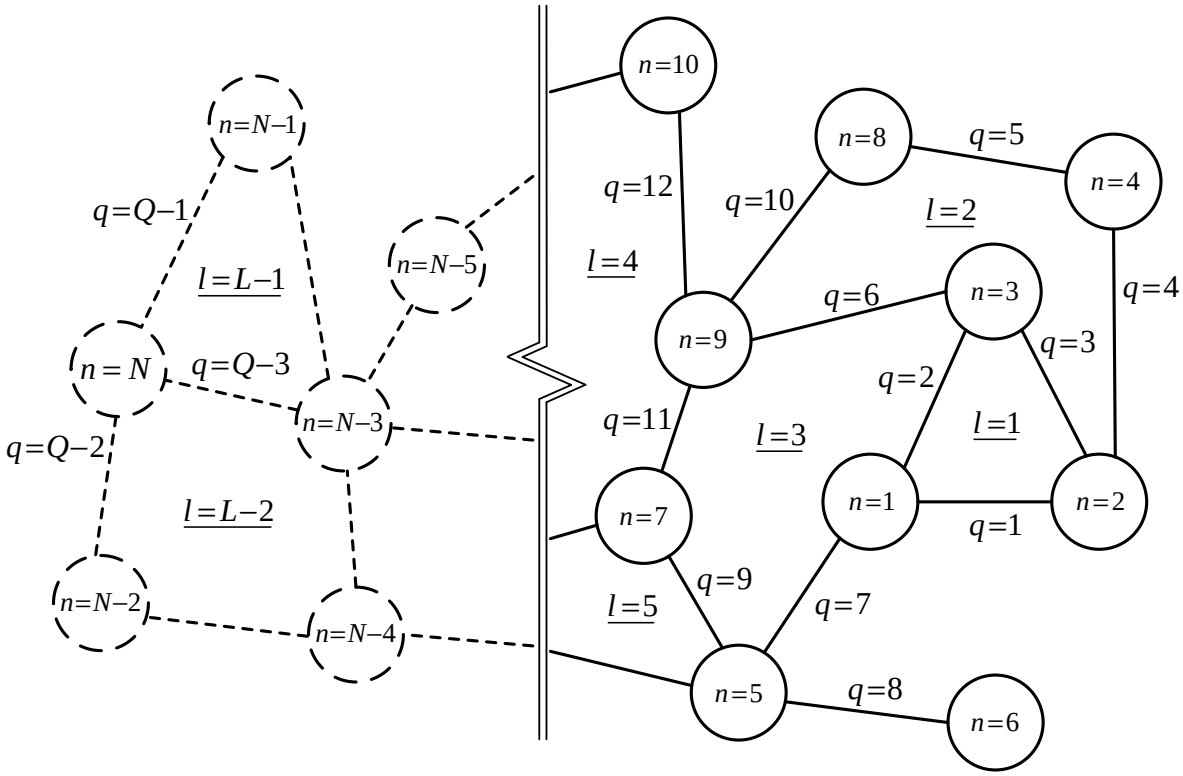

Figure 3.1. Schematic representation of the power network.

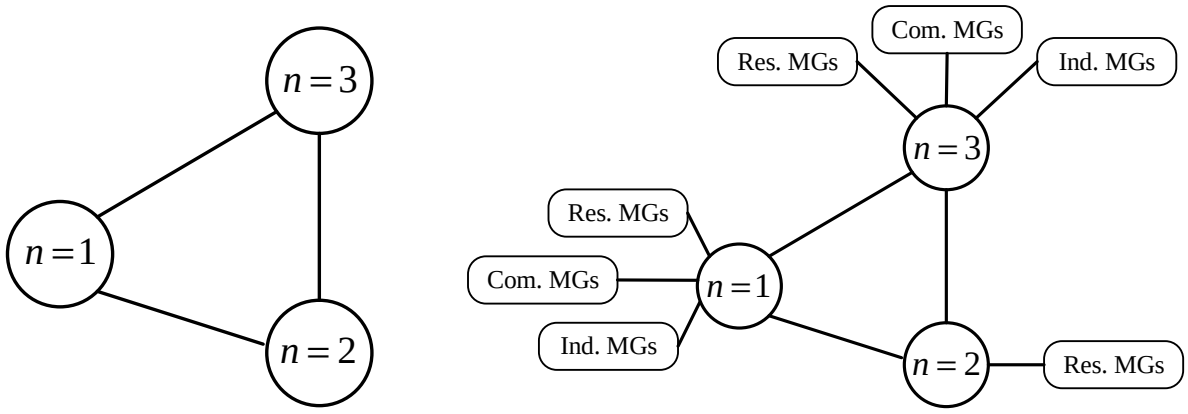

(a) Grid. (b) Grid and MGs.

Figure 3.2. Schematic representation of a) The Netherlands power network system and b) the same network system but with attendent MGs [212].

3.1.1 National level: The Netherlands

3.1.1.1 Scenario 1: Grid only

The system considered in a first application of *Scenario 1* is a power network that represents The Netherlands in the Northwest European Electricity Market, depicted in Figure 3.2(a). A description

of the Netherlands power network is obtained from a more detailed network simulator described by COMPETES (**CO**mprehensive **M**arket **P**ower in **E**lectricity **T**ransmission and **E**nergy **S**imulator) [195]. *Scenario 1* for The Netherlands consists of three nodes ($n = 1, \ldots, 3$) connected by three high-voltage transmission lines ($q = 1, \ldots, 3$) setting up one loop ($l = 1$) in which demand and supply of electricity are present. It is assumed that the power network is capable of satisfying its load with no need for importing power from neighboring countries. Five main firms compete in the market. A maximum number of generators ($w = 1, \ldots, W$) is initially available at every node, n. Table 3.1 shows the percentage of each of the main producers by fuel type available in this system.

A sustainable optimum configuration of producers that satisfies the power demand can be determined during the simultaneous optimization of a set of different objectives. As a result, a non-dominated curve of optimum solutions representing the Pareto set of non-dominated solutions for the set of different objectives is obtained. In this Pareto set, non-dominated solutions are those that perform better than some others in at least one criterion, that is, if the objectives are non-commensurable, the improvement in value of one objective leads to a decrease in value of other objectives.

Table 3.1. Percentage of centralized available capacity in The Netherlands [212].

	Node 1 (%)	Node 2 (%)	Node 3 (%)	Grid (%)
Nuclear	5.21	-	-	2.87
Coal	36.18	-	13.21	24.26
Natural Gas (NG)	37.48	86.18	83.70	58.56
Oil	0.18	-	-	0.10
Hydroelectric	0.16	1.89	0.07	0.34
Waste	20.80	11.93	3.02	13.88

Table 3.2. Characteristics of the centralized technologies in The Netherlands [212].

	Capital Costs ($/kW)	Efficiency (%)	SO_2 Emissions (kg/kWh)
Nuclear	3,000	35.00	0.0000
Coal	2,000	38.14	0.0021
NG	800	41.33	1.94×10^{-6}
Oil	350	43.00	0.0016
Hydroelectric	1,700	100.00	0.0000
Waste	2,200	52.00	0.0020

A period of twenty-four hours is considered ($t = 1, \ldots, 24$). The twenty-four hour demand of electricity from the system represents a Load Demand Profile (LDP) of a winter day in The Netherlands (Dec. 01, 2010) [213]. The LDP of a node, *n*, is different than the LDPs of the remaining nodes in the network.

Data for the short run costs (fuel and variable operation and maintenance (O&M)) and the capacity of the centralized generators at full load are available from COMPETES and can be obtained from the Energy Research Center of The Netherlands (ECN) [214]. This data has been updated by Lo Prete et al. [37] in order to account for transmission resistance losses, first and second law efficiencies, $\mathrm{SO_2}$ and $\mathrm{NO_x}$ emissions, forced outage rates (FORs), and updated production capacities and 2008 costs. In this dissertation, data from Lo Prete et al. [37] is updated to take into account the non-linearity in part-load performance for first law efficiency, short run costs, and $\mathrm{SO_2}$ emissions of the producers. The conversion factor from Euro to USD used is 1.3269, corresponding to the average exchange rate for 2010 [215]. It is assumed that the productive life of every centralized generator is 20 years. The average hours of operation during the year for a generator is obtained from [216]. Table 3.2 shows the average capital costs of equipment, average full load efficiency, and average full load $\mathrm{SO_2}$ emissions by fuel.

3.1.1.2 Scenario 2: Grid and MGs

In *Scenario 2*, various sectors of the grid representing residential, commercial, and industrial customers are grouped and radially connected via MGs to the main grid described in *Scenario 1* (see Figure 3.2(b)). A different load demand profile for each of the three different MG sectors – residential, commercial and industrial– is employed. The total load demand of the system is equal to that for *Scenario 1* in order to have a valid comparison between MG producers and those in the main grid, allowing the customers to get electricity from the main grid only, from the MGs only, or from both. Data for residential, commercial, and industrial load curves is under confidentiality agreement and cannot be published here.

Five residential, two commercial, and three industrial MG configurations are tied to Node 1; ten residential MG configurations are tied to Node 2; and six residential, two commercial, and one industrial MG configurations are tied to Node 3. In total, the system for *Scenario 2* is composed of thirty-two nodes of which twenty-nine are MG nodes and three main grid nodes. The capacity of every residential MG configuration is 20 MW, for a commercial MG configuration 110 MW,

and for an industrial MG configuration 200 MW. Table 3.3 shows the percentage of producers by fuel type available for the MGs. If MGs are isolated or islanded from the grid, they can satisfy the total demand of their customers. In addition, MG producers can operate during off-peak as well as during peak hours. The average hours of operation during the year for decentralized technologies is also taken from [216].

Average capital costs, average full load energetic efficiencies, and average full load SO_2 emissions for MG producers are provided in Table 3.4. The total life time of operation for these technologies is considered to be 20 years, except for SOFCs where 10 years is assumed.

Table 3.3. Percentage of available capacity for MG nodes in The Netherlands [212].

	Node 1 (%)	Node 2 (%)	Node 3 (%)	MGs (%)
NG	37.07	70.00	44.63	43.49
Coal	51.20	-	36.48	40.24
Oil	8.70	12.00	13.04	10.51
Wind	1.96	18.00	4.00	4.55
Solar	1.09	-	1.85	1.20

Table 3.4. Average characteristics of the decentralized production technologies for The Netherlands [212].

	Capital Costs ($/kW)	Efficiency (%)	SO_2 Emissions (kg/kWh)
Solid Oxide Fuel Cell (SOFC)	4,700	50.00	0.000000
Diesel reciprocating Engines (REs)	350	34.00	0.000206
NG Microturbines (MT)	1,100	26.00	0.000003
NG-Combined Cycles (NGCC)	1,532	48.00	0.000000
Coal Fired	2,043	36.00	0.000370
Integrated Gasification (IGCC)	2,500	38.00	0.000304
Wind Turbines	900	18.00	0.000000
Solar Photovoltaic (PV)	5,884	18.00	0.000000

3.1.2 International level: COMPETES

3.1.2.1 Scenario 1: Grid only

The system considered in *Scenario 1* is a power network that represents the Northwest European electricity market as described by COMPETES [195] and depicted in Figure 3.3. *Scenario 1*

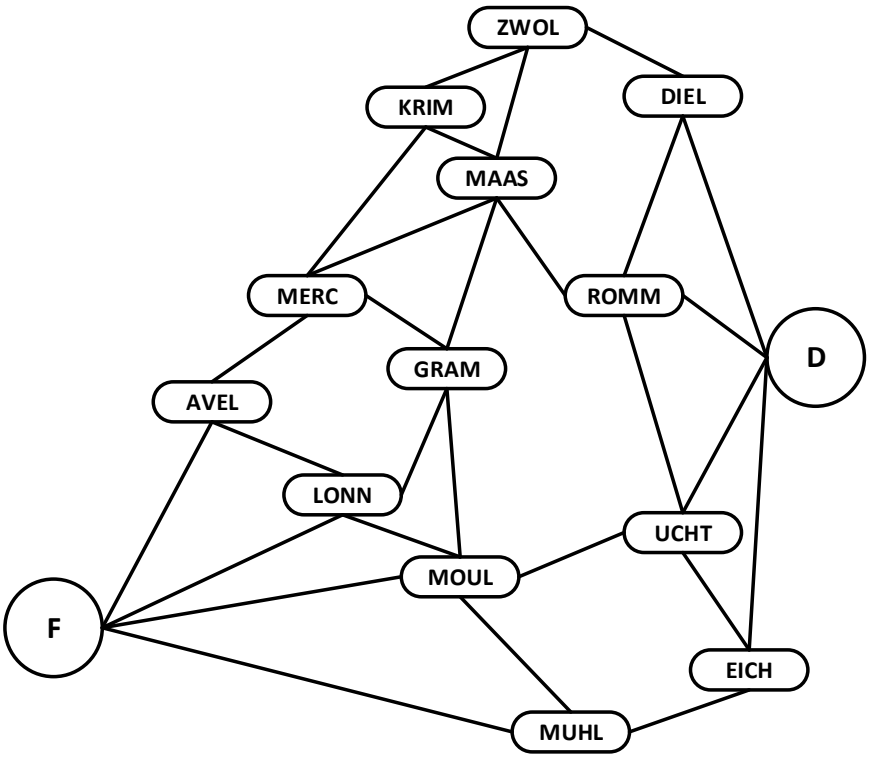

Figure 3.3. Schematic representation of the Northwest European electricity network [195, 214].

consists of fifteen nodes ($n = 1, \ldots, 15$) connected by twenty eight high-voltage transmission lines ($q = 1, \ldots, 28$) setting up fourteen arcs or loops ($l = 14$). Demand and generation of electricity exists at seven nodes located in four countries, namely, Zwol, Krim and Maas in The Netherlands, Merc and Gram in Belgium, F in France, and G in Germany. Four of the remaining nodes are intermediate nodes between France and the rest of the network, and the last four remaining nodes do the same for Germany. These intermediate nodes are necessary to construct the linearized direct current (DC) model for the network [34]. At the intermediate node Avel in France, a constant export of electricity to a region outside the market is present. It is assumed that the power network is capable of satisfying its load with no need of importing power from other neighboring countries. Twelve main firms compete to supply the electricity needs for this market.

Initially, a maximum number of generators ($w = 1, \ldots, W$) is available at every node n to form a superstructure. Table 3.5 shows the average characteristics of each of the main producers by fuel type initially available in the system. A sustainable optimum configuration of producers that satisfies the power demand is determined during the optimization process, via the minimization (maximization) of a set of objectives. A period of twenty-four hours is considered ($t = 1, \ldots, 24$). The twenty-four-hour electricity demand for the system represents a LDP for the most demanding

day in Nortwest Europe (Dec. 14, 2010 [213]). The LDP of a node, *n*, is different than the LDPs of the remaining nodes in the network. The LDP for each node is determined according to the country in which it is located as is the maximum energy demand at that node.

Data for the short run costs (fuel and variable O&M) and the capacity of the centralized generators at full load are available from COMPETES and can be obtained from the Energy Research Center of The Netherlands (ECN) [214]. This data has been updated by Lo Prete et al. [37] in order to account for transmission resistance losses, first and second law efficiencies, SO_2 and NO_x emissions, FORs, and updated production capacities and 2008 costs. In addition, data from Lo Prete et al. [37] is updated in this dissertation to take into account the non-linearity in part-load performance for the first law efficiency, short run costs, and SO_2 emissions of the producers. The conversion factor from Euro to USD is as before 1.3269 [215]. The average productive life, average capital costs of equipment, average full load efficiency, and average full load SO_2 emissions the centralized producer by fuel is given in Table 3.5. The average hours of operation during the year for a producer is obtained from [216].

Table 3.5. Average characteristics of the centralized technologies for COMPETES.

	Available[a] Capacity (MW)	Useful Life[b] (years)	Capital Costs[c] ($/kW)	Exergetic[d] Efficiency (%)	SO_2 Emissions[e] (kg/kWh)
Nuclear	101,584	40	3,000	47.67	0.00129
Coal	72,752	30	1,900	34.44	0.00146
NG	37,758	20	700	37.43	1.94×10^{-6}
Oil	15,550	25	350	30.91	0.00225
Hydroelectric	4,722	80	1,700	89.60	0.00000
Waste	1,144	30	2,200	50.93	0.00000

Note: [a]Ref. [214], [b]Ref. [212, 217, 218], [c]Ref. [37, 214], [d]Ref. [37, 214], [e]Ref. [37, 214].

3.1.2.2 Scenario 2: Grid and MGs

In *Scenario 2*, various sectors of the grid representing residential, commercial, and industrial customers are grouped and radially connected via MGs to the main grid described in *Scenario 1* for COMPETES. A different LDP for the three different MG sectors –residential, commercial and industrial– is assumed. As for the case of The Netherlands only network, the total load demand of this larger system is equal to that for *Scenario 1* in order to have a valid comparison between MG

producers and those in the main grid, allowing the customers to get electricity from the main grid only, from the MGs only, or from both.

The number of MGs at each node in the network is given in Table 3.6. In total, the system for *Scenario 2* is composed of 443 nodes of which 428 are MG nodes and 15 main grid nodes. The capacity of every MG is 20 MW for a residential configuration, 110 MW for a commercial configuration, and 200 MW for an industrial configuration. Table 3.7 shows the available producers capacity for each type of the MG configurations. If MGs are isolated or islanded from the grid, they can satisfy the total demand of their customers. In addition, MG producers can be operating during off-peak as well as during peak hours. The average hours of operation during the year for decentralized technologies is taken from [216]. Average capital costs, average full load energetic efficiencies, and average full load SO_2 emissions for MG producers are the same as in the case for The Netherlands only network (see Table 3.4).

Table 3.6. Number of MGs by node and type in COMPETES.

	Residential	Commercial	Industrial
Merc	8	6	2
Gram	6	3	2
Krim	7	5	4
Maas	10	1	0
Zwol	10	4	1
D	89	65	35
F	80	58	32

Table 3.7. Available producer capacities for each type of MG.

	Residential (MW)	Commercial (MW)	Industrial (MW)
SOFC	10	6	17
RE	13	100	35
MT	68	67	162
Wind	2	0	0
Solar	0	5	0
NGCC	0	1	1
Coal	0	1	1
IGCC	0	0	5

3.2 Synthesis/design/operation optimization model

The problem considered in [34, 37, 219] is modified here to include multiple objectives as well as the part-load performance of the producers in a quasi-stationary optimization. The optimization is developed over a period of time which corresponds to the most demanding day of the year 2010.

Initially, a superstructure is considered where a number of producers is available to be chosen to be part of the final optimum network configuration. This superstructure is synthesized or reduced to a network configuration that satisfies the demand from the customers. At the same time, this reduced network is optimized at the peak-demand (design) and during the off-peak hours (operation). It is assumed that producers targeted to be part of the optimal configuration are operated at full load during the peak hour and at full or part load or not at all during the off-peak hours.

The problem mathematically represents a quasi-stationary, multiobjective optimization problem with non-linear constraints. The objective of the problem is to

Minimize

$$\vec{C} = [\pm C_1, \pm C_2, \ldots, \pm C_{k-1}, \pm C_k]^T \tag{3.1}$$

with respect to nonnegative $\mathrm{P}^t_{w,n}$ and $f^t_{m,n}$ and subject to

$$\sum_{n=1}^{N} S_{n,m,l}(f^t_{n,m,l} - f^t_{m,n,l}) = 0 \quad \text{for all } l \text{ and } t \tag{3.2a}$$

$$P^t_{D_n} - \sum_{w=1,n}^{W} P^t_{w,n} - \sum_{m=1,n}^{M} [f^t_{m,n}(1 - \alpha_{m,n} S_{m,n} f^t_{m,n}) - f^t_{n,m}] \leq 0 \quad \text{for all } n \text{ and } t \tag{3.2b}$$

$$P^{min}_{w,n} \leq P_{w,n} \leq P^{max}_{w,n} \quad \text{for all } w \text{ and } n \ \text{(generation limits)} \tag{3.2c}$$

$$f^{min}_{m,n} \leq f_{m,n} \leq f^{max}_{m,n} \quad \text{for all } m \text{ and } n \ \text{(transmission limits)} \tag{3.2d}$$

The objective functions C_k in Equation (3.1) are defined in Section 3.3. A minus sign for the *k*-th element of the objective function vector represents a maximization. $P^t_{w,n}$, and $f^t_{m,n}$, are the decision variables of the problem and represent the power produced by technology *w* at node *n* and time *t* and the flow transmitted from node *m* to node *n* at time *t*, respectively.

The equality constraint, Equation (3.2a), is the linearized DC load flow model equivalent of Kirchhoff's voltage law (KVL). The assigning of a positive or negative value to the reactance depends on the direction of the power flow vectors in each voltage loop *l*, (see Figure 3.4(a)) and

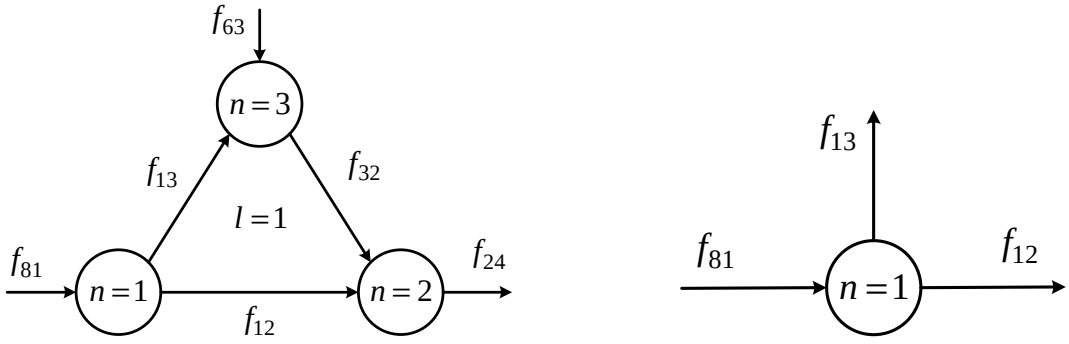

(a) Second law (Loop). (b) First law (Node).

Figure 3.4. Schematic representation of the linearized DC Kirchhoff circuit laws for the network depicted in Figure 3.1.

is determined by the term inside the parenthesis of Equation (3.2a). For the case of *Scenario 2*, it is assumed that the MGs are radially connected to a main node in the network.

The first inequality constraint, Equation (3.2b), is the linearized DC load-flow model equivalent of Kirchhoff's current law (KCL). As is shown in Figure 3.4(b) the first term, $P^t_{D_n}$, represents the load demand at node *n* during time *t*. The second term represents the total power generated at node *n* during time *t* while the third term is the net power input to node *n* during time *t*, where $f^t_{m,n}\left(1-\alpha_{m,n}S_{m,n}f^t_{m,n}\right)$ is the net import of electricity to node *n* from every neighboring node *m* with $S_{m,n}$ being the reactance of a high voltage flow line, $\alpha_{m,n}$ a constant used to account for transmission losses (assuming resistance is approximately proportional to reactance) [37], $f^t_{n,m}$ the export of power from node *n* to a neighboring node *m* to which *n* is directly connected, and $f^t_{m,n}$ the corresponding import of power to node *n* from a neighboring node *m*. For the case of *Scenario 2*, each MG represents an extra node, *n*, in the network; and since they are located near to the customers, no transmission losses are considered when supplying electricity to their corresponding main grid node.

As to the second and third inequality constraints, Equation (3.2c) sets restrictions on the capacity of each producer, *w*, at node *n*. The minimum capacity for every producer is set equal to zero (although a more general formulation that recognizes minimum loading constraints could be adopted instead), and the maximum capacity is set to the full-load capacity of a producer. Equation (3.2d) restricts the flow through the transmission lines. The minimum power flow capacity is equal to zero, while the maximum flow capacity is set equal to the maximum capacity available to flow from node *m* to node *n*.

3.3 Sustainability indices included in the model

3.3.1 Economic indices

Capital costs and O&M costs comprise the principal aspects of sustainability. Those considered in this work are described below.

3.3.1.1 Monetary costs

The objective function that accounts for the economic aspects in Equation (3.1) is that which accounts for capital and fuel costs. Capital costs account for the investment in acquiring the equipment, including its manufacture and installation, while fuel costs account for the cost of the fuel used during the operation of the energy producer. The fuel costs are directly related to the efficiency of the equipment. The monetary objective function of this model, for which $k = \$$, is given as

$$C_k = C_\$ = \sum_{t=1}^{t^{\max}} \sum_{n=1}^{N} \sum_{w=1}^{W} (C^{\text{cap}}_{w,n,\$} + C^{t}_{w,n,\$}) \tag{3.3}$$

where $C^{\text{cap}}_{w,n,\$}$ is the capital cost of a producer. These costs are amortized, accounting for interest, depreciation, and taxes. The annualization factor is $\phi\,(1+\phi)^{yr} \,/\, ((1+\phi)^{yr} - 1)$ where ϕ is the discount rate, and *yr* is the useful life of the producer. $C^{t}_{w,n,\$}$ is the fuel cost of the producer expressed as [220]

$$C^{t}_{w,n,\$} = \varphi_{w,n,\$} + \beta_{w,n,\$} P^{t}_{w,n} + \gamma_{w,n,\$} \left(P^{t}_{w,n}\right)^2 \tag{3.4}$$

Here, the real positive constants $\varphi_{w,n,\$}$, $\beta_{w,n,\$}$, and $\gamma_{w,n,\$}$ are the nonlinear coefficients particular to each producer, *w*, at each node, n. In this way, the model is able to account for the part-load behavior of the producers. These are assumed to be nonnegative to maintain the convexity of the cost functions. In order to obtain these constants, fuel costs are scaled according to the standard off-design efficiency curves obtained from the literature [221–231] for every type of technology, and a regression analysis is applied to obtain the values pertaining to each producer. The constants are the same for two or or more producers if and only if they use the same fuel and are rated at the same capacity.

3.3.2 Environmental indices

Emissions to the environment such as $\mathrm{SO_x}$, $\mathrm{NO_x}$, UHC, PM, CO, and $\mathrm{CO_2}$ are considered as environmental aspects of sustainability. In the present work, only $\mathrm{SO_2}$ emissions are considered, so that $k = \mathrm{SO_2}$.

3.3.2.1 $\mathrm{SO_2}$ Emissions

The objective function in Equation (3.1) that accounts for environmental emissions is written as follows:

$$C_k = C_{\mathrm{SO_2}} = \sum_{t=1}^{t^{\max}} \sum_{n=1}^{N} \sum_{w=1}^{W} C^t_{w,n,\mathrm{SO_2}} \tag{3.5}$$

The emissions of a producer can be expressed as [220]

$$C^t_{w,n,\mathrm{SO_2}} = \varphi_{w,n,\mathrm{SO_2}} + \beta_{w,n,\mathrm{SO_2}} P^t_{w,n} + \gamma_{w,n,\mathrm{SO_2}} \left(P^t_{w,n}\right)^2 \tag{3.6}$$

Here, the real positive constants $\varphi_{w,n,\mathrm{SO_2}}$, $\beta_{w,n,\mathrm{SO_2}}$, and $\gamma_{w,n,\mathrm{SO_2}}$ are the nonlinear coefficients particular to each producer, *w*, at each node, n. In this way as before, the model is able to account for the part-load behavior of the producers. Again, these are assumed to be nonnegative to maintain the convexity of the cost functions. In order to obtain these constants, $\mathrm{SO_2}$ emissions are scaled according to standard off-design curves obtained from the literature [221–231] for every type of technology, and a regression analysis is applied to obtain the values pertaining to each producer. The constants are the same for two or or more producers if and only if they use the same fuel and are rated at the same capacity.

3.3.3 Technological indices

Factors such as system energetic efficiency, exergetic efficiency, reliability, resiliency, etc. are commonly used to assess the technological aspects of sustainability. The ones used in this work are described below.

3.3.3.1 Efficiency

Another objective function in Equation (3.1) is that for network efficiency (first or second law). The inclusion of network efficiency as an objective function in the sustainability assessment frame-

work provides additional information that the minimization of total (capital and operational) cost and SO_x emissions do not capture such as, for example, information about transmission losses as well as cogeneration when CHP production units are present in the network. With respect to the latter, the allocation of fuel costs and avoided emissions to the products (electricity and heat) of a CHP plant can be done, as is clearly explained in [232], by assigning the increment of fuel consumption to the production of electricity only, by assigning the increment of fuel consumption to the production of heat only, by assigning the increment of fuel consumption of a CHP unit based on the ratio of fuel needed to produce heat only and fuel needed to produce electricity only as if they were produced in separate units, or allocating the fuel based on the exergy content of the products. In these methods, the allocation is done with a constant factor without taking into account the surroundings of the CHP unit.

As an extension of these allocation methods, Beretta, Iora, and Ghoniem [232] propose to account for the penetration of cogeneration in the local area of interest in order to fairly allocate the fuel consumption among the products of cogeneration. The resulting alloation factor is a dynamic ratio of primary energy factors for heat and electricity that changes when the penetration of cogeneration becomes more (less) important in the area of interest. When heat use becomes more important, a higher fraction of fuel use (avoided emissions) is allocated to the production of heat.

Now, the efficiency of the network defined as [101]

$$C_k = C_\eta = \frac{P^{\mathrm{Tot}}}{F^{\mathrm{Tot}}} \tag{3.7}$$

where P^{Tot} is the total power produced in a certain period of time and F^{Tot} is the total fuel needed to produce that amount of power. P^{Tot} is given by

$$P^{\mathrm{Tot}} = \sum_{t=1}^{t^{\max}} (P_L^t + P_D^t) = \sum_{t=1}^{t^{\max}} \sum_{n=1}^{N} \sum_{w=1}^{W} P_{w,n}^t \tag{3.8}$$

where P_L^t represents the total transmission losses in the high-voltage transmission lines and P_D^t the total demand. F^{Tot} is expressed as

$$F^{Tot} = \sum_{t=1}^{t^{\max}} \sum_{n=1}^{N} \sum_{w=1}^{B} F_{w,n}^t = \sum_{t=1}^{t^{\max}} \sum_{n=1}^{N} \sum_{w=1}^{W} \frac{P_{w,n}^t}{\eta_{w,n}^t} \tag{3.9}$$

Here, the fuel $F_{w,n}^t$ needed to produce $P_{w,n}^t$ can be expressed in terms of its energy or exergy content in order to obtain an energy- or exergy-based index, respectively. The fuel $F_{w,n}^t$ used

by renewable producers is set equal to zero. The energetic as well as exergetic efficiency of an individual producer in Equation (3.9) is written as [220]

$$\eta_{w,n}^{t} = \varphi_{w,n,\eta} + \beta_{w,n,\eta} P_{w,n}^{t} + \gamma_{w,n,\eta} \left(P_{w,n}^{t}\right)^{2} \tag{3.10}$$

Here, the real positive constants $\varphi_{w,n,\eta}$, $\beta_{w,n,\eta}$, and $\gamma_{w,n,\eta}$ are the nonlinear coefficients particular to each producer, *w*, at each node, n. Thus, the model is able to account for the part-load behavior of the producers. These constants are obtained by scaling the efficiencies according to standard off-design curves obtained from the literature [221–231] for every type of technology, and a regression analysis is applied to obtain the values pertaining to each producer. The constants are the same for two or or more producers if and only if they use the same fuel and are rated at the same capacity.

3.3.3.2 Reliability indices

A second technological objective function in Equation (3.1) is that for the reliability of the system. Reliability is the probability that the power demand is higher than the available power capacity in the system. The reliability index used is the Loss-of-Load Probability (LOLP), which represents the expected number of hours that the system is not able to supply the demand in a certain period of time [233]. The objective function for reliability is defined in [37] as

$$C_k = C_{LOLP} = \sum_{z=1}^{Z} p_z f_{LOLP_z} \tag{3.11}$$

where p_z and f_{LOLP_z} are the probability and LOLP value of the *z*-th mixture of the normal approximation (MONA) [234]. MONA is used for the first time in this context in [37] to approximate the 2008 LDC of the Northwest European electricity market in order to obtain the capacity reliability analysis of the network. The term f_{LOLP_z} is obtained from Lo Prete et al. [37] and is given as

$$f_{LOLP_z} = \mathbb{P}\left(P_{D_z} - P_Q^t - P_{\mathrm{W}}^t \geq 0\right) = \int_0^{\infty} \left(f_{P_{D_z} - P_Q^t}(x) F_{W_z^t}(x)\right) dx \tag{3.12}$$

Note that in this expression, wind production in the main grid is taken into account since it is significant fraction of the total production [37]. For example, average wind production for the year 2010 in The Netherlands was 381 MW [235]. In Equation (3.12), $\mathbb{P}$ is the probability, P_{D_z} the demand, P_Q^t the power produced by non-wind technologies, P_{W}^t the power produced by wind

technology, $f_{P_{D_z}-P_Q^t}(x)$ the normal distribution function of the production capacity deficit, x is equal to $P_{D_z} - P_Q^t$, and $F_{W_z^t}(x)$ is the exponential cumulative distribution function evaluated at x given by

$$F(x) = 1 - e^{-\lambda x} \tag{3.13}$$

Here, the parameter λ equals the average wind production during the day. In the absence of detailed data, it is assumed that the daily wind production is the ratio between the yearly average production and the number of days in the year.

3.3.3.3 Resiliency indices

The third objective function in Equation (3.1) is that for resiliency. Resiliency is defined as the ability of a system to recover to a new normal state from a failure caused by an unanticipated catastrophic event. If a power outage occurs due to a failure in the main grid resulting from, for example, a snow storm, hurricane, terroristic attack, etc. and there are no MGs present in the network, the amount of electricity not supplied to the customers within a period of time is taken into account and corresponds to one hundred percent of the power outage described by a Descriptive Resiliency Metric [236]. If, on the other hand, MGs are present, they can be isolated or islanded within a matter of seconds since MGs can operate in island mode and provide the electricity needs of at least the local customers tied to the MGs, minimizing the extent of the power outage caused by the unexpected event. There are any number of measures that could be used for resiliency from a descriptive standpoint. For example, the time elapsed to restore the network to a normal operation, the amount of power that a utility cannot deliver to the final customer (or total number of customers affected), and the total monetary cost that the outage brings to the utility [236].
In this work, it is assumed that the resiliency of the system is directly proportional to the amount of energy produced by the MGs and is described by the MG penetration index given by

$$C_k = C_{\text{Resiliency}} = \sum_{t=1}^{t^{\max}} \sum_{n=1}^{N} \sum_{w=1}^{W} \frac{P_{w,n}^{t,\text{MGs}}}{P_{w,n}^{t,\text{MGs}} + P_{w,n}^{t,\text{Grid}}} \tag{3.14}$$

The maximum possible penetration of MGs is restricted in the present work to be only 15% of the total production of the system, since it is well known that a high penetration of MGs could cause instability problems in the network if no voltage and load frequency regulation is present

[36]. Clearly, with the inclusion of state-of-the-art power electronics in the network, this problem could be overcome (and, in fact, contribute to network stability) in which case one would not need to restrict maximum MG penetration to such a low percentage.

3.3.4 Social indices

Social issues are those that account for job creation, increments in life quality, etc. Social indices are not considered in this work, since at least based on the sensitivity analysis found in [37], they may not substantially affect the final results of a quantitative energy sustainability assessment. Thus, as a first cut, we ignore the social indices. However, their significance should be reexamined in more detail in future work.

3.4 Multiobjective optimization and Pareto optimality concepts

3.4.1 Time dependency in optimization

Three possible approaches for the optimization of a system can be used to determine its optimal synthesis/design and operation. The first is time independent, while the latter is two are time dependent. The time-independent approach is based on the optimization of the system at the peak-hour demand only, while the second is based on a quasi-stationary optimization over twenty-four hours during the same day as described below. The third approach is a transient optimization based on the same twenty-four hour period in which transitions from one time period to the next are taken into account. These transitions are absent in the quasi-stationary approach. The need to account for them and, thus, use a transient as opposed to quasi-stationary approach is when the transition times become comparable to or dominate the non-transition times. In this work, it is assumed that they are not comparable nor dominant.

3.4.1.1 Stationary or peak-hour optimization

In this approach, an optimum configuration is obtained by for example, minimizing the total life cycle costs of the system to satisfy the peak-hour load demand of the day, t^{peak}, shown in Figure 3.5. After that, the short run costs for the optimum configuration over the twenty-three off-peak hours are, as in [219], determined proportionally based on the peak-hour. Note that in [219], the year

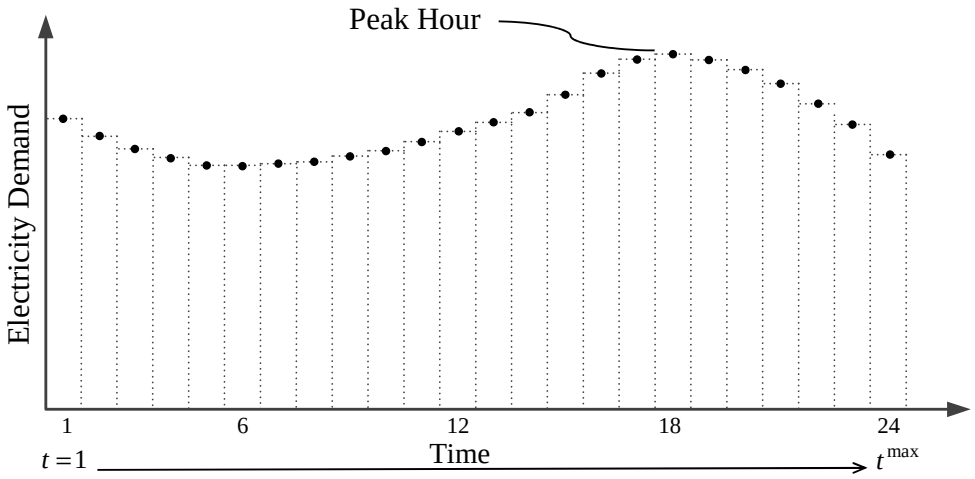

Figure 3.5. Representation of a daily load demand curve [212].

is divided into 4 periods, i.e., summer-peak and -off peak and winter-peak and -off peak and the minimum short run costs (operational costs) for the performance of the system are obtained for each single hour, and the costs are then averaged and added to the capital costs to obtain the total yearly costs. Thus, system operation at off-peak hours is optimized as a post-processing task that does not affect the optimal synthesis/design of the system which is already fixed.

3.4.1.2 Quasi-stationary optimization

In this second approach the optimum configuration of the system and its performance over the twenty-four hours is obtained in a single optimization, e.g., minimization of the total costs over the entire twenty-four-hour period. Thus, both the synthesis/design and the operation are simultaneously optimized instead of, as in the previous approach, first optimizing the former and then only at the end in a post-processing step optimizing the latter. Of course, the major disadvantage is that the problem becomes much larger, making it more expensive in terms of computational resources. Nonetheless, it is the more correct of the first two approaches for determining the optimal synthesis/design, and operation since each of these system characteristics are not independent of each other.

3.4.1.3 Transient optimization

This third approach is more focused on the control of the instantaneous response of producers to particular events within the power network. As in the second approach, the synthesis/design, and the operation are optimized simultaneously; but instead of assuming steady state operation in each

time interval the behavior of the system in modeled in a transient fashion. As mentioned above, this approach is only useful when transient events are important.

3.4.2 Optimization algorithms

In the sustainability assessment of a system with a single objective optimization, the nature of the analysis is not conserved because all the objectives are grouped into a single measurement unit. In a multiobjective optimization, on the other hand, a Pareto set of non-dominated solutions for different non-commensurable objectives is found. As part of the post-processing, the analyst can make a decision as to which optimal solution to use based on the importance assigned to each objective (weighting) [45] or based on the minimization (maximization) of an objective or value function [220].

3.4.2.1 Gradient-based methods

Now, to optimize a system of non-commensurable objective functions, derivative-based [237, 238] and non-derivative-based methods [239–241] are available. Derivative-based optimization methods, such as Sequential Quadratic Programming (SQP), are less computationally expensive, although there is the possibility of getting stuck in local optima if the problem is non-convex. To overcome this problem, different initial decision variable sets are used to try and span the feasible space in order to ensure that the algorithm reaches the global optimum.

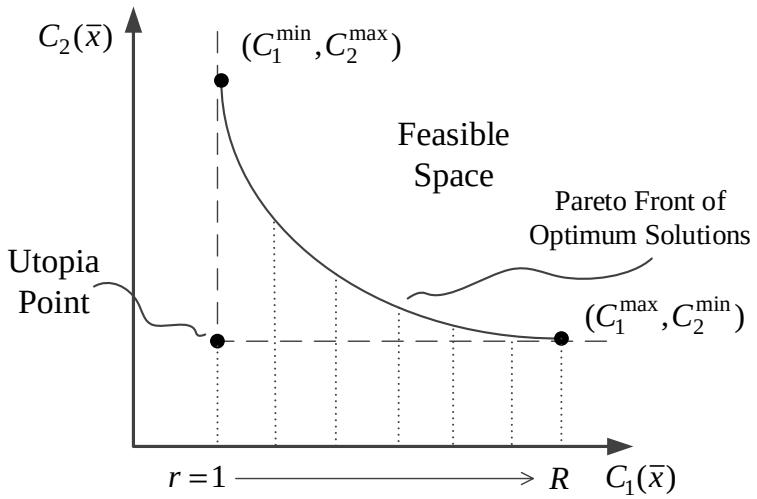

Figure 3.6. Representation of the Pareto front of optimum solutions [212]. Reprinted from [212] Copyright © 2012 by ASME, with permission.

3.4.2.2 Non-gradient-based methods

A non-derivative based method, such as a Genetic Algorithm (GA), is a robust method for optimization in which a number of final optimum values are provided (individuals). The initial values are allowed to interchange part of their binary chain (genes) through the optimization process in order to minimize (maximize) the objective functions. The problem is converged when a certain number of generations is reached and/or the objective function convergence criteria are met. Although it is a robust method of solution, it is very computationally expensive when used for large problems [39].

3.4.2.3 Optimization algorithm used

It is the derivative-based method, a SQP algorithm [242–244], which is used here. To optimize a set of non-commensurable objective functions, the maximum and minimum feasible values of the functions are obtained by optimizing each objective function independently of all of the others. This provides the so-called utopia point shown in Figure 3.6. Once this is done, the continuous feasible space of an objective function is discretized and the function used as a constraint in the optimization of another objective function. This process is repeated for all combinations of objective functions. The Pareto set resulting from this process is represented by a $r \times k$ matrix where the $k = 1, \ldots, K$ are the indices of the objective functions and the $r = 1, \ldots, R$ are the number of intervals into which the feasible space is discretized.

3.5 Making decisions

3.5.1 Value functions

Once the non-dominated set of solutions forming the Pareto front is obtained, a decision-making procedure is applied to obtain the most desirable solution from among all the optimum solutions forming the Pareto front (see Figure 3.6). Value functions do not explicity weight the objective functions in order to find the best compromise solution but instead requires the minimization (maximization) of an objective function. Nevertheless, it is understood that a set of optimum weights is obtained when a best compromise solution is reached. Numerically, the set of non-dominated solutions is represented by a matrix C with matrix elements $c_{r,k}$ where the r index the number of

intervals into which the feasible space is discretized and the k index the objective functions. To implement the a value function the r^{th} value of the k^{th} objective function, $c_{r,k}$, is first normalized to eliminate the difference in units between objective functions. This is accomplished by using

$$\bar{c}_{r,k} = \begin{cases} 1 & c_{r,k} \leq c_{r,k}^{min} \\ \dfrac{c_{r,k}^{max} - c_{r,k}}{c_{r,k}^{max} - c_{r,k}^{min}} & c_{r,k}^{min} < c_{r,k} < c_{r,k}^{max} \\ 0 & c_{r,k} \geq c_{r,k}^{max} \end{cases} \tag{3.15}$$

when minimizing objectives, e.g., emissions and costs, and by using

$$\bar{c}_{r,k} = \begin{cases} 0 & c_{r,k} \leq c_{r,k}^{min} \\ \dfrac{c_{r,k} - c_{r,k}^{min}}{c_{r,k}^{max} - c_{r,k}^{min}} & c_{r,k}^{min} < c_{r,k} < c_{r,k}^{max} \\ 1 & c_{r,k} \geq c_{r,k}^{max} \end{cases} \tag{3.16}$$

when maximizing objectives, e.g., efficiencies [220]. Here $\bar{c}_{r,k}$, $c_{r,k}^{max}$, and $c_{r,k}^{min}$ are the normalized value of $c_{r,k}$ and the maximum and minimum values of the $c_{r,k}$ in the k^{th} vector of solutions of an objective function C_k, respectively.

The next step is to take each element $\bar{c}_{r,k}$ of $\bar{C}$ and use them to reduce the matrix to a column vector according to the expression

$$c_r = \frac{\sum_{k=1}^{K} \bar{c}_{r,k}}{\sum_{r=1}^{R} \sum_{k=1}^{K} \bar{c}_{r,k}} \tag{3.17}$$

The best compromise solution is found by selecting the objective function set with the maximum value of c_r, i.e., c_r^{max}.

3.5.2 Involvement of decision makers

If instead of using value functions a weighting post-processing approach is used, an interaction between the analyst and the decision makers (DM) is required. Decision makers such as scientists, investors, the general public, etc., can be polled to assess their priorities among the different objectives considered in the analysis based on their perceptions or interests [45]. The polls are then used

to determine an assignment of a weight, Φ_k, for each objective function. The best compromise solution c_r^{max} is then obtained from the set of values given by

$$c_r = \sum_{k=1}^{K} \Phi_k C_k \tag{3.18}$$

where

$$\sum_{k=1}^{K} \Phi_k = 1 \tag{3.19}$$

To determine the weights for each objective function in this work, the methodology proposed in [245] is used. A total of six decision makers, all of them involved in academia but in different disciplines, are asked to rate the five sustainability indices in descending order, starting from what they consider to be the most important one. A value of 5 is then assigned to the most important index, and a value of 1 is assigned to the least important.

A $K \times J$ index-DM weight matrix, Ω, is determined from the information obtained, and its elements are normalized according to the expression

$$\Omega_{ij}^N = \frac{\Omega_{ij}}{\sum_i \Omega_{ij}} \tag{3.20}$$

where in this case, $i = 1, \ldots K$ and $j = 1, \ldots, J$, were K is the number of objective functions and J is the number of decision makers, respectively. The normalized weighting matrix, Ω^N, results.

In order to manage the fuzziness introduced by the respondents, a $J \times M$ DM-characteristic reliability matrix, Ψ, is determined. The characteristics used to evaluate the expertise of the respondents, as well as the values given to each characteristic are shown in Table 3.8. Here the elements of Ψ are $\Psi_{j,m}$ where $j = 1, \ldots, J$ and $m = 1, \ldots, M$, and M is the total number of characteristics for each decision maker. Then multiplying the Ω^N and Ψ matrices together yields a $K \times M$ matrix such that

$$\Pi = \Omega^N \Phi \tag{3.21}$$

Taking the elements of this product matrix then results in the needed weights Φ_k for each objective function C_k, i.e.,

$$\Phi_k = \frac{\sum_m \Pi_{k,m}}{\sum_i \sum_m \Pi_{i,m}} \tag{3.22}$$

where it has been assumed that all the criteria used to evaluate the reliability of the respondents have the same importance.

The validity of these weights Φ_k depend on issues such as how questions are formulated, knowledge and understanding of stakeholders about the particular problem, failure of stakeholders to truly represent the community, etc. as is clearly described in [45, 46, 246]. Thus, the formulation of weights comes with varying levels of subjectivity and uncertainty.

Table 3.8. Characteristics to measure the reliability of a DM [212].

Rank	Value	Experience (yr)	Value
Professor	5	≤ 25	5
Associate Professor	4	$18 \leq x < 25$	4
Assistant Professor	3	$11 \leq x < 18$	3
Instructor	2	$5 \leq x < 11$	2
Graduate Student	1	< 5	1
Reputation	Value	Self-confidence	Value
Known by many, internationally	5	Very High	5
Known by many, nationally	4	High	4
Known by many, regionally	3	Average	3
Known by many, locally	2	Low	2
Known by a few	1	Very Low	1

3.6 Verification of the model

3.6.1 Single node: Environmental-economic dispatch problem

The economic dispatch problem proposed originally by Wood and Wollenberg [247] was complemented with environmental aspects and latter was used by King and Rughooputh [220] as a test-bed for their elitism multiobjective optimization algorithm. This environmental-economic dispatch problem used in [220] is used here as a test-bed for a first verification of the SAF model for a single node. The reason for considering the environmental-economic dispatch problem as a verification are its simplicity in that it considers only three fossil-fueled producers satisfying a fixed

power demand; and its complexity in that it introduces two types of conflicting objectives (economic and environmental) as well as the nonlinearities to account for the part-load performance of the producers.

The model of the problem is expressed as a multiobjective (non-commensurable), non-linear optimization problem with non-linear constraints. The first objective function, C_1, corresponds to the minimization of fuel costs (economic objective, \$/hr), the second objective function, C_2, corresponds to the minimization of SO_2 emissions (environmental objective, ton/hr), and the third objective function, C_3, corresponds to the minimization of $\mathrm{NO_x}$ emissions (environmental objective, ton/hr). The decision variables of the model are $P_{w,n}$, and represent the real power generated by each producer, *w*, at a node, *n*. Mathematically, the problem can be written as

Minimize

$$\vec{C} = [C_1, C_2, C_3]^T \tag{3.23}$$

with respect to nonnegative $P_{w,n}$ and is subject to

$$\sum_{w=1}^{3} P_{w,n} - P_n^D - P_{n,m}^L = 0 \quad \text{for all } n \ \text{ (power balance)} \tag{3.24a}$$

$$P_{w,n}^{min} \leq P_{w,n} \leq P_{w,n}^{max} \quad \text{for all } n \ \text{ (generation limits)} \tag{3.24b}$$

where the subscript m refers to the number of each transmission line connected to node n. For the present problem $m = 1$ even though for the present model no transmission lines are explicitly included.

The objective functions in Equation (3.23) are

$$C_k = \sum_{w=1,n,k}^{3} \left(\varphi_{w,n,k} + \beta_{w,n,k} P_{w,n} + \gamma_{w,n,k} P_{w,n}^2\right) \tag{3.25}$$

where $n = 1$ for this problem and $k = 1, 2, 3$. The real positive constants $\varphi_{w,n,k}$, $\beta_{w,n,k}$, and $\gamma_{w,n,k}$ are the nonlinear coefficients particular of each objective function, *k*, each producer, *w*, at each node, n. For the particular case presented, Table 3.9 provides the coefficients for fuel cost ($k = 1$), Table 3.10 the coefficients for SO_2 emissions ($k = 2$), and Table 3.11 the coefficients for $\mathrm{NO_x}$ emissions ($k = 3$).

Table 3.9. Fuel cost coefficients [220].

Producer, w	$\varphi_{w,k=1,n=1}$	$\beta_{w,k=1,n=1}$	$\gamma_{w,k=1,n=1}$
1	561	7.92	0.001562
2	310	7.85	0.00194
3	78	7.97	0.00482

Table 3.10. SO_2 emission coefficients [220].

Producer, w	$\varphi_{w,k=2,n=1}$	$\beta_{w,k=2,n=1}$	$\gamma_{w,k=2,n=1}$
1	0.5783298	0.00816466	0.0000016103
2	0.3515338	0.00891174	0.0000021999
3	0.0884504	0.00903782	0.0000054658

Table 3.11. NO_x emission coefficients [220].

Producer, w	$\varphi_{w,k=3,n=1}$	$\beta_{w,k=3,n=1}$	$\gamma_{w,k=3,n=1}$
1	0.04373254000000	– 0.000094868099	0.00000014721848
2	0.05582171300000	– 0.000097252878	0.00000030207577
3	0.02773152400000	– 0.000353737340	0.00000193385310

Variable P_n^D in Equation (3.24a) is the fixed power demand and is 850 MW for the case considered here. The $P_{n,m}^L$ in the same equation represent the power flow losses in the transmission lines and are given by

$$P_{n,m}^L = P_{w,n} B_{n,m} P_{w,m} \tag{3.26}$$

where $B_{n,m}$ are the elements of the transmission losses matrix. For the present case $B_{n,m} = [0.00003, 0.00009, 0.00012]$ and the total transmission power loss is

$$P^L = 0.00003\mathrm{P}_1^2 + 0.00009\mathrm{P}_2^2 + 0.00012\mathrm{P}_3^2 \tag{3.27}$$

Finally, the $P_{w,n}^{min}$ and $P_{w,n}^{max}$ in Equation (3.24b) are the minimum and maximum real power that each producer is allowed to provide, respectively. Their values are given in Table 3.12 for each producer.

Once the non-dominated set of solutions forming the Pareto front for this problem is obtained, Equations (3.15) to (3.17) are applied to obtain the most desirable solution from among all the

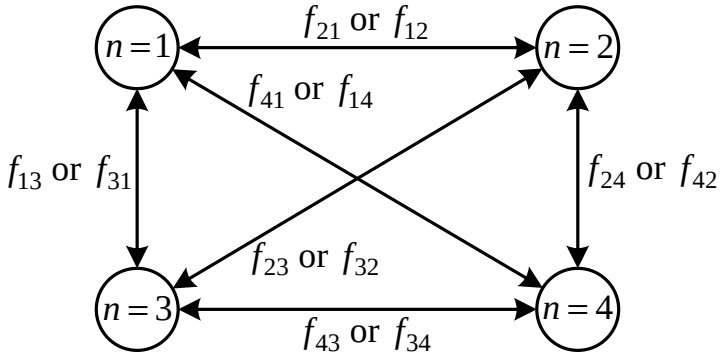

Figure 3.7. Representation of a model with various nodes and transmission lines [248].

optimum solutions forming the Pareto front. The use of a value function for making the decisions in this particular case is justified by King and Rughooputh [220] that the decision maker (or operator) only has a very short period of time to take a critical decision to operate each producer at a certain load in order to satisfy the demand. It is this short period of time that contributes to the operator having imprecise (fuzzy) goals for each objective (cost and emissions).

Table 3.12. Limit values for the producer technologies [220].

Producer, w	$P^{min}_{w,n=1}$	$P^{max}_{w,n=1}$
1	150	600
2	100	400
3	50	200

3.6.2 Multiple nodes: Multi-area economic dispatch (MAED)

The model used for verification purposes in this dissertation of a problem consisting of power production in a multi-area (or multi-node) region which allows the sharing of power (transmission or flow) among nodes, is that presented by Streiffert [248]. The terms area and node are used here interchangeably to represent a region where generation and demand of electricity or heat or both are required. The model consists of four nodes interconected by transmission lines as depicted in Figure 3.7. Each node has four producers, $P_{w,n}$, and each node is connected by a flow line $f_{m,n}$. Mathematically, the model can be written as

Minimize

$$C = \sum_{w,n=1}^{N} \sum_{w=1,n}^{W} \left(\beta_{w,n} P_{w,n} + \gamma_{w,n} P_{w,n}^2\right) + \sum_{m,n=1}^{N} \sum_{m=1,n}^{M} \left(\alpha_{m,n} f_{m,n}\right) \tag{3.28}$$

with respect to nonnegative $P_{w,n}$ and $f_{m,n}$ and subject to

$$P_n^D - \sum_{w=1,n}^{W} P_{w,n} - \sum_{m=1,n}^{M} (f_{m,n} - f_{n,m}) = 0 \quad \text{for all } n \text{ (power balance)} \tag{3.29a}$$

$$P_{w,n}^{min} \leq P_{w,n} \leq P_{w,n}^{max} \quad \text{for all } n \text{ (generation limits)} \tag{3.29b}$$

$$f_{m,n}^{min} \leq f_{m,n} \leq f_{m,n}^{max} \quad \text{for all } n \text{ (transmission limits)} \tag{3.29c}$$

Decison variable $f_{n,m}$ represents the export of power from node *n* to its neighboring node *m* to which *n* is directly connected, and $f_{m,n}$ represents the import of power to node *n* from its neighboring node m to which n is directly connected. Decision variable $P_{w,n}$ is the power produced by technology w at node n; and as before, the real positive constants $\beta_{w,n}$ and $\gamma_{w,n}$ are the nonlinear coefficients particular of each producer. Since the focus of this particular case is to model the exchange of power among nodes only, variable $\alpha_{m,n}$ in Equation (3.28) is set to zero.

The characteristics of each producer as well as those for the transmission lines are given in Table 4.3. The demand for Node-1 is $P_1^D = 400$ MW, for Node-2 $P_2^D = 200$ MW, for Node-3 $P_3^D = 350$ MW, and for Node-4 $P_2^D = 300$ MW. Results for this verification are given in Chapter 4.

3.6.3 Multiple nodes and transmission losses: COMPETES

The model for the Northwest European electricity market, COMPETES [195], is used here for further verification of the model with transmission losses developed in the present research. This model is developed by Lo Prete et al. [37] to investigate the effects of introducing MGs into the Northwest European Electricity Market. The work of Lo Prete et al. [37] entails a performance optimization of the electricity grid (i.e., the system is economically dispatched) consisting primarily of fossil fuel producers and sets of CHP small-scale producers connected to the grid via MGs. The sustainability indices for the analysis and optimization are the energetic and exergetic efficiencies, fuel costs, and NO_x and SO_2 emissions proposed by Frangopoulos and Keramioti [207] as well as the Loss-of-Load Probability (LOLP) and Expected Loss of Energy (ELOE) indices for the reliability of the power network. The model can be written as

Minimize

$$C_\$ = \sum_{n=1}^{N} \sum_{w=1}^{W} C_{w,n,\$} P_{w,n} \tag{3.30}$$

with respect to nonnegative $\mathrm{P}_{w,n}$ and $f_{m,n}$ and subject to

$$\sum_{n=1}^{N} S_{n,m,l}(f_{n,m,l} - f_{m,n,l}) = 0 \quad \text{for all } l \tag{3.31a}$$

$$P_{D_n} - \sum_{w=1,n}^{W} P_{w,n} - \sum_{m=1,n}^{M} [f_{m,n}(1 - \alpha_{m,n} S_{m,n} f_{m,n}) - f_{n,m}] \leq 0 \quad \text{for all } n \tag{3.31b}$$

$$P_{w,n}^{min} \leq P_{w,n} \leq P_{w,n}^{max} \quad \text{for all } w \text{ and } n \ \text{(generation limits)} \tag{3.31c}$$

$$f_{m,n}^{min} \leq f_{m,n} \leq f_{m,n}^{max} \quad \text{for all } m \text{ and } n \ \text{(transmission limits)} \tag{3.31d}$$

The objective function $C_\$$ in Equation (3.30) is the total monetary cost of generation for the network. $P_{w,n}$, and $f_{m,n}$, are the decision variables of the problem and represent the power produced by technology *w* at node *n* and the flow transmitted from node *m* to node *n*, respectively. Equation (3.31a) is the linearized DC load flow model equivalent of Kirchhoff's voltage law (KVL), Equation (3.31b) is the linearized DC load-flow model equivalent of Kirchhoff's current law (KCL), and Equation (3.31c) and Equation (3.31d) set restrictions on the capacity of each producer and the flow through the transmission lines, respectively. The constant $\alpha_{m,n}$ (assuming resistance is approximately proportional to reactance) is set to a value wich corresponds to the transmission losses being approximately 2% of the total generation during the peak hour [37].

In the analysis of Lo Prete et al. [37], the 2008 Load Duration Curve (LDC) is divided into six blocks where each block represents a certain number of hours and its load is the average of the load of those individual hours. A common system design configuration is imposed on all six blocks, and the optimum production configuration of each block is obtained by optimizing the cost of generation (i.e., the system is economically dispatched). The optimization of one block is develop independently of the others. Thus, this is not a quasi-stationary approach. The annual results are obtained by weighing the results of each block by the appropriate number of hours. The rest of the indices (i.e., energetic and exergetic efficiencies, emissions, and LOLP) are obtained from a post-processing analysis after the single optimization is developed. In the present work, the verification of the model using that of Lo Prete et al. [37] is developed for the case where CO_2 emissions are not considered. Results for this verification are given in Chapter 4.

Chapter 4

Results and Discussion for SAF

4.1 Results for verification of the model

4.1.1 Single node: Environmental-economic dispatch problem

The model for the environmental-economic dispatch problem is described in section 3.6.1. It is expressed as a multiobjective, non-linear optimization problem with non-linear constraints. The objective functions are defined by Equation (3.25) and represent the fuel costs, SO_2 emissions, and NO_x emissions. The equality and inequality constraints representing the model and system operational limits are defined in Equations (3.24a) and (3.24b), respectively. King and Rughooputh [220] optimize their model using a Non-Sorted Genetic Algorithm (NSGA-II) developed by Deb et al. [239]. In the present work, the model is optimized by using a derivative-based Sequential Quadratic Programming (CFSQP) optimization algorithm developed by Tits and co-workers [242–244]. In addition, the NSGA-II [239] algorithm obtained from Deb [249] is used here as well for purposes of comparison between performance of the two different algorithms.

Table 4.1 shows the results of minimizing each of the three objectives individually. The first column for each objective function provides the results from King and Rughooputh [220], and the second column for each objective shows the results obtained by the present author using the CFSQP algorithm. As is evident for the case of minimizing the three objective functions individually, the difference between the values of the cost functions from King and Rughooputh [220] and the results obtained in this work are negligible. The losses are similar for the two cases. For the minimization of the fuel costs and NO_x emissions, the power generated by the three producers is very similar.

For the minimization of SO_2 emissions, generators P_2 and P_3 produce less power than in [220], but P_1 generates a larger amount.

Figure 4.1 shows the Pareto front for this environmental-economic dispatch problem. Figure 4.1(a) is the Pareto front obtained by King and Rughooputh [220] while Figure 4.1(b) shows the non-dominated solutions obtained in the present work using the CFSQP and NSGA-II algorithms. The blue circles corresponds to the solution obtained using the latter algorithm. The optimization using the NSGA-II algorithm is based on the characteristics obtained from King and Rughooputh [220], that is, a population of 500 individuals, a crossover probability of 0.99, a mutation probability of 0.01, a distribution index for crossover equal to 5, a mutation crossover equal to 50, and an initial seed of 0.125. The optimal solution is obtained at the 20,000-th generation. The red squares correspond to the values obtained using the CFSQP algorithm. In order to use the derivative-based method, the feasible space is discretized into 21 intervals, and an optimization for each individual set is obtained.

Table 4.1. Minimization of the individual objective functions for the environmental-economic dispatch problem.

	Fuel Cost		SO_2 emissions		NO_x emissions	
	Ref. [220]	CFSQP	Ref. [220]	CFSQP	Ref. [220]	CFSQP
P_1	431.680	435.198	538.527	551.962	508.367	507.002
P_2	302.925	299.970	227.817	219.574	250.444	251.971
P_3	131.314	130.661	98.185	92.980	105.934	105.796
Losses, P^L	15.919	15.829	14.528	14.516	14.745	14.769
Fuel Cost	8344.651	8344.593	-	-	-	-
SO_2 emissions	-	-	8.97870	8.96594	-	-
NO_x emissions	-	-	-	-	0.09599	0.09593

Table 4.2. Most desirable solution for the environmental-economic dispatch problem when the three objective functions are optimized simultaneously.

	Ref. [220]	CFSQP	NSGA-II
P_1	496.328	503.462	493.398
P_2	260.426	252.935	262.785
P_3	108.144	108.374	108.754
Losses (P^L)	14.898	14.771	14.938
Fuel Cost (C_1)	8358.896	8362.355	8357.581
SO_2 emissions (C_2)	8.97870	8.97558	8.98009
NO_x emissions (C_3)	0.09599	0.09594	0.09602

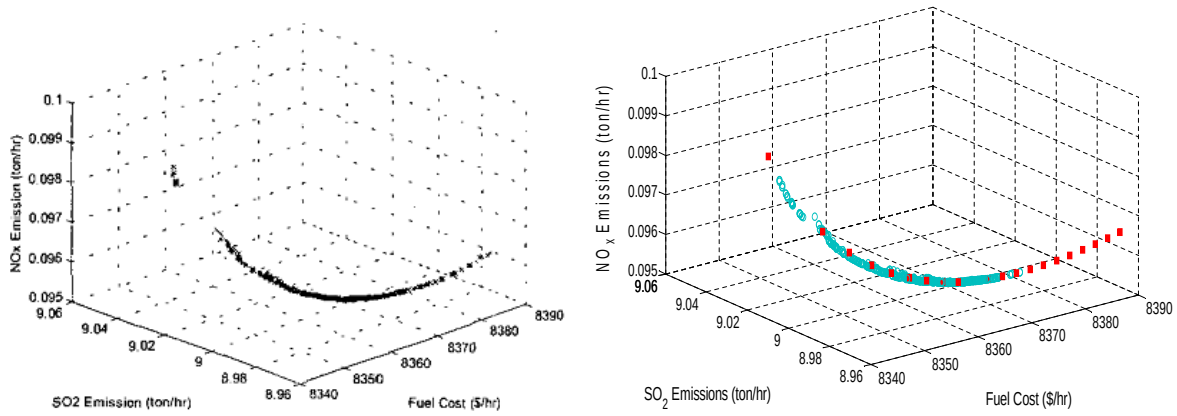

(a) Results from King and Rughooputh [220]. Reprinted from [220] Copyright © 2003 IEEE, with permission.

(b) Present work.

Figure 4.1. Pareto frontier for the environmental-economic dispatch problem; in part (b), the blue circles are the solutions obtained using the NSGA-II algorithm, and the red squares the solutions obtained with the CFSQP algorithm.

Table 4.2 presents a comparison of the results of solving the dispatch problem as a multiobjective optimization, minimizing the three objectives at the same time. The second column shows the results given in [220], and the third and fourth columns show the results obtained in the present work using the CFSQP and NSGA-II algorithms, respectively. As can be seen, the most desirable solution differs somewhat more than before using a derivative-based algorithm as compared to a genetic algorithm. With the CFSQP algorithm, the accuracy of the solution is highly dependent on the number of intervals into which the feasible space is discretized. If a small number of sets is used, the error is high. If a large number of discrete points is used, the spacing between non-dominated solutions is reduced; and the most desired solution is closer to that obtained using the genetic algorithm. For the purposes of the study developed in the present work, the accuracy provided by a derivative-based algorithm such as CFSQP [242–244] is more than acceptable, considering the significant reduction in computational burden which is realized with highly complex optimization problems.

4.1.2 Multiple nodes: Multi-area economic dispatch (MAED)

The model for the multi-area economic dispatch problem is described in section 3.6.2. It represents a power network where generation and demand of electricity or heat or both are required in

each node. The system is depicted in Figure 3.7 and consists of four nodes, with four producers in each node, interconnected by transmission lines. MAED model is expressed as a non-linear single objective optimization problem. The objective function is defined by Equation (3.28) and represent the fuel costs of generation. The equality constraints representing the model are defined by Equations (3.29a), and the inequality constraints representing the operational limits of the system are defined by Equations (3.29b) and (3.29c). Results for the MAED provided by Streiffert [248] and those of the optimal values obtained in the present work are provided in Table 4.3. As can be seen, the results obtained here using the CFSQP algorithm are in good agreement with those found in [248].

Table 4.3. Results of the verification using the Streiffert model [248].

Node	Prod.	$P_{w,n}^{max}$ [248]	$P_{w,n}^{min}$ [248]	$\beta_{w,n}$ [248]	$\gamma_{w,n}$ [248]	$P_{w,n}$ [248]	C [248]	$P_{w,n}$	C
N_1	$P_{1,1}$	150	50	4	0.01	150	825	150	825
	$P_{2,1}$	100	25	2	0.03	100	500	100	500
	$P_{3,1}$	100	25	3	0.05	66.97	425	67.01	425.53
	$P_{4,1}$	100	25	1	0.04	100	500	100	500
N_2	$P_{1,2}$	150	50	4	0.05	56.97	390	57.01	390.53
	$P_{2,2}$	100	25	2	0.04	96.25	563	96.26	563.16
	$P_{3,2}$	100	25	3	0.08	41.87	266	41.88	265.96
	$P_{4,2}$	100	25	1	0.06	72.52	388	72.51	387.94
N_3	$P_{1,3}$	150	50	4	0.1	50	450	50	450
	$P_{2,3}$	100	25	2	0.12	36.27	230	36.25	230.22
	$P_{3,3}$	100	25	3	0.1	38.49	264	38.50	263.77
	$P_{4,3}$	100	25	1	0.13	37.32	218	37.31	218.28
N_4	$P_{1,4}$	150	50	4	0.01	150	825	150	825
	$P_{2,4}$	100	25	2	0.03	100	500	100	500
	$P_{3,4}$	100	25	3	0.05	57.05	334	57.01	333.52
	$P_{4,4}$	100	25	1	0.04	96.27	467	96.26	466.90
Node	Line	f_{mn}^{max}	f_{mn}^{min}	α_{mn} [248]	-	f_{mn} [248]	C [248]	f_{mn}	C
N_1	f_{21}	100	0	1	-	0	0	0	0
	f_{31}	100	0	1	-	0	0	0	0
	f_{41}	100	0	1	-	1.21	1	3.23	3.23
N_2	f_{12}	100	0	1	-	0	0	0	0
	f_{32}	100	0	1	-	0	0	0	0
	f_{42}	100	0	1	-	2.11	2	0.04	0.04
N_3	f_{13}	100	0	1	-	18.18	18	20.24	20.24
	f_{23}	100	0	1	-	69.73	70	67.70	67.70
	f_{43}	100	0	1	-	100	100	100	100
N_4	f_{14}	100	0	1	-	0	0	0	0
	f_{24}	100	0	1	-	0	0	0	0
	f_{34}	100	0	1	-	0	0	0	0
Total:							\$7,337.00		\$7,337.01

4.1.3 Multiple nodes and transmission losses: COMPETES

The model for a system with multiple nodes and transmission losses that describes a power network model for the Northwest European electricity market represented by COMPETES [195] is given in section 3.6.3. The model is expressed as a non-linear single objective optimization problem for the performance optimization of the electricity grid consisting primarily of fossil fuel producers and sets of CHP small-scale producers connected to the grid via MGs [37]. The objective function is defined by Equation (3.30) and represent the short run costs of the network. The equality and inequality constraints representing the model are defined by Equations (3.31a) and (3.31b), respectively, and the inequality constraints representing the operational limits of the system are defined by Equations (3.31c) and (3.31d).

Table 4.4 provides results for the verification using the COMPETES model. The optimization of the monetary optimal costs varies from that in Lo Prete et al. [37] by 2.07% for the scenario in which the grid alone is optimized (*Scenario 1*) and by 1.35% for the scenario in which MGs are included in the model (*Scenario 2*). For both cases, the result obtained with the SQP algorithm is lower that the result reported in [37].

Based on the comparison of results given in Table 4.4 and the information available to the author of the model by Lo Prete et al. [37], it is believed that this small difference in the results is due to the optimization algorithm only, although this conjecture cannot be totally affirmed. In the case of [37], the model is written in ILOG OPL 6.3 and the Cplex 12 optimizer [250] used, while in the present work the model is written in C language and the CFSQP algorithm [242–244] is used for the optimization.

Table 4.4. Results of the verification with the model for COMPETES.

	Scenario 1 - No MG		*Scenario 2* - MG	
	Ref. [37]	verification	Ref. [37]	verification
Efficiency, η_I (%)	45.84	45.77	45.83	45.81
Efficiency, η_{II} (%)	44.40	44.31	44.39	44.36
SO_x Emissions (kton/yr)	289.44	224.54	281.55	215.35
NO_x Emissions (kton/yr)	347.76	253.78	343.15	249.52
Cost (M€/yr)	15,291.00	14,974.26	15,180.00	14,973.88
Cost (M$/yr)	20,289.63	19,869.34	20,142.34	19,868.84
LOLP (hr/10-yr)	7.70	7.70	5.53	5.53

4.2 National level: The Netherlands

4.2.1 Single objective-peak hour versus quasi-stationary optimization

In order to compare the peak-hour versus the quasi-stationary optimization approaches, a *single-objective* optimization minimization of the total life cycle costs of the model for the Netherlands described in Section 3.1.1.1 and depicted in Figure 3.2(a) (*Scenario 1*) is obtained. A period of twenty-four hours representing the day with the highest energy consumption of the year is considered. Using one day as a representative period has the advantage that the most stressful scenario is considered only, reducing the computational burden associated with the optimization. On the other hand, it represents a very small sample of events (as opposed to the total operating time of 8760 hrs) and may not fully capture the reality of the scenario, particularly with renewable-based energy producers such as wind and photovoltaics. This, nonetheless, is a reasonable approach since the added computational burden which would be involved could well render the problem computationally impossible.

For the peak-hour optimization, the model of the system is described in Section 3.6.3, where the objective function is defined by Equation (3.30) and represents the short run costs of the nerwork. The equality and inequality constraints representing the model are defined by Equations (3.31a) and (3.31b), respectively, and the inequality constraints representing the operational limits are defined by Equations (3.31c) and (3.31d). In order to obtain the performance of the system, the short-run costs of every non-peaking hour are proportionally determined relative to the load demand profile using the peak-hour value as the basis. That is, the cost of each non-peaking hour is equivalent to the product of the cost for the peak hour and the ratio of load demand of the non-peaking hour of interest and that of the peak hour. The sum of the twenty four-hour short-run costs plus the capital costs (on a levelized $/day basis) determined at the peak in order to meet peak demands represents the total life cycle costs for the system over the twenty-four hour period.

In contrast, for the quasi-stationary optimization, the model of the system is described in Section 3.2, where the objective function is defined by Equation (3.3) considering the term $C^t_{w,n,\$}$ that represent the short run costs of the network and defined by Equation (3.4), where φ and γ are equal to zero for this particular case. The equality and inequality constraints representing the model are defined by Equations (3.2a) and (3.2b), respectively, and the inequality constraints representing the operational limits are defined by Equations (3.2c) and (3.2d). For this quasi-stationary optimiza-

tion approach, the decision variables of each non-peaking hour are linked to those of the peaking hour; and as a result, all decision variables for the system are updated at every iteration of the optimization. Thus, the short-run costs of every non-peaking hour are determined based on the values obtained for the decision variables of each non-peaking hour for each iteration of the optimization.

Table 4.5 shows the results for the total life cycle costs of the peak-hour optimization strategy versus the total life cycle costs of the quasi-stationary optimization strategy. The minimum costs for the peak-hour optimization approach are 84,035 Million USD (MM-$) and those obtained from the quasi-stationary optimization approach are 75,114 MM-$, a difference of about 12%. This is not surprising, since the quasi-stationary optimization sets aside the most expensive generation sources during low-load periods, while the peak-hour optimization approach assumes that all generators reduce their output proportionally. Table 4.5 also shows the results for total life SO_2 emissions, efficiency, and LOLP. In the averaging scheme, the LOLP represents the minimum outage hours/10-yr of the system during the peak hour, while that of the quasi-stationary scheme is based on the optimum configuration of the entire period. As can be seen, a higher efficiency for that of the quasi-stationary approach is obtained, while total life SO_2 emissions are better for the peak-hour strategy, noting, of course, that this strategy is not a reflection of reality. Reliability is similar for both approaches. The differences with the peak-hour optimization results are attributable to the fact that the part-load performance of the system for the peak-hour strategy is not determined directly but are instead based on averages.

Table 4.5. Single objective optimization results for the peak-hour averaging approach versus the quasi-stationary approach for the Netherlands [212].

	Peak-hour Optimization	Quasi-stationary Optimization	Difference (%)
Total Life Cycle Costs (MM-$)	84,035	75,114	11.88
Total Life Cycle SO_2 Emissions (Ton)	264,314	324,833	-18.63
Network Efficiency (%)	43.36	43.71	0.79
LOLP (Outage, hr/10-yr)	3.21	3.24	-1.07
Resiliency (%-MGs)	-	-	-

Another approach used to obtain the part-load performance of the system, when optimizing only the peak-hour, is that of using the optimal peak-load configuration obtained to optimize the twenty-three non-peaking hours separately. Using this approach, the optimum values are almost

identical with those obtained by the quasi-stationary approach, *but* the optimum configuration and its part-load performance are different. Thus, although the quasi-stationary optimization is more computationally expensive, it does make a difference in the correctness of the results obtained. This difference becomes even more important when optimizing the synthesis/design performance of a transient system [153].

4.2.2 Quasi-stationary multi-objective optimization results

4.2.2.1 Limits on the objective functions

Two scenarios are considered for the quasi-stationary *multi-objective* optimization of the Netherlands. *Scenario 1* is described in Section 3.1.1.1 and depicted in Figure 3.2(a), and *Scenario 2* is described in Section 3.1.1.2 and depicted in Figure 3.2(b). The quasi-stationary multi-objective optimization problem is given by Equations (3.1) and (3.2). The objective functions C_k in Equation (3.1) are the total life cycle costs of the system defined by Equation (3.3); the total life cycle SO_2 emissions of the system defined by Equation (3.5); the efficiency of the system defined by Equation (3.7); the reliability of the system given by the LOLP and defined by Equation (3.11); and the resiliency of the system defined as the microgrid penetration in the system and given by Equation (3.14). The minimum and maximum values for the objective functions representing the feasible space for the synthesis/design/operation are provided in Table 4.6 for *Scenario 1* and Table 4.7 for *Scenario 2*. As seen, the feasible space is larger for *Scenario 2*. This is because of the addition of renewable-based production technologies such as photovoltaic (PV) and wind turbines as well as more fuel-expensive reciprocating engines and natural gas (NG) microturbines.

The next sections present the Pareto sets for two objective functions at a time. Visualizing more than two at a time is difficult, since a *k*-dimensional space is required for *k* objective functions. When using more than three objectives, the Pareto sets are shown with numerical values.

Table 4.6. Feasible space for *Scenario 1* for the quasi-stationary, multiobjective optimization problem described in Section 3.1.1.1 and given by Equations (3.1) and (3.2) [212].

	Minimum	Maximum
Total Life Cycle Costs (MM-$)	75,126	104,144
Total Life Cycle SO_2 Emissions (Ton)	96,401	324,833
Network Efficiency (%)	41.40	44.31
LOLP (Outage, hr/10-yr)	2.781	3.274
Resiliency (%-MGs)	-	-

Table 4.7. Feasible space for *Scenario 2* for the quasi-stationary, multiobjective optimization problem described in Section 3.1.1.2 and given by Equations (3.1) and (3.2) [212].

	Minimum	Maximum
Total Life Cycle Costs (MM-$)	71,113	108,912
Total Life Cycle SO_2 Emissions (Ton)	77,088	368,936
Network Efficiency (%)	40.81	44.43
LOLP (Outage, hr/10-yr)	4.53	23.44
Resiliency (%-MGs)	4.41	12.17

4.2.2.2 Capital – O&M life cycle costs

Figure 4.2 shows a view of the Pareto set for the capital costs versus the total life cycle short run costs (variable O&M and Fuel). Capital life cycle costs denote the investment made for the total capacity of each optimum configuration, assuming that each network configuration is fully built with no capacity expansion. It can be seen that as the capital cost of the grid decreases, the total short run costs increase. This trend is observed because coal and waste plants are replaced by natural gas technologies in the most expensive optimum configurations, as can be seen in Figure 4.3 for *Scenario 1* and Figure 4.4 for *Scenario 2*. Coal plants are expensive to build but relatively cheap to operate, while natural gas technologies are relatively cheap to build but more expensive to operate.

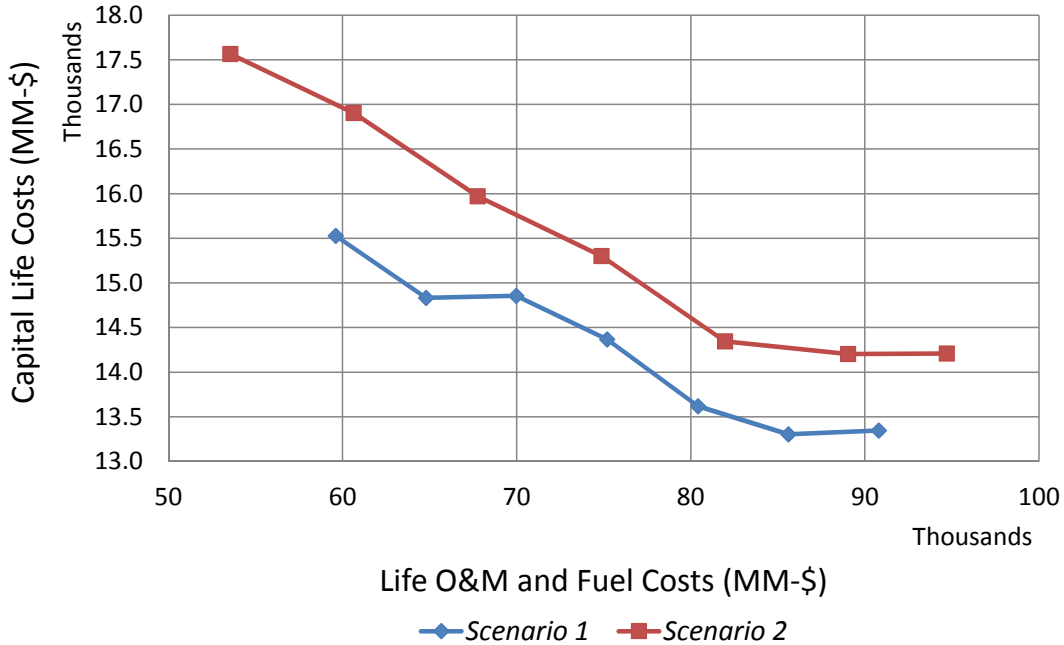

Figure 4.2. Optimal capital versus life cycle O&M costs [212]. Reprinted from [212] Copyright © 2012 by ASME, with permission.

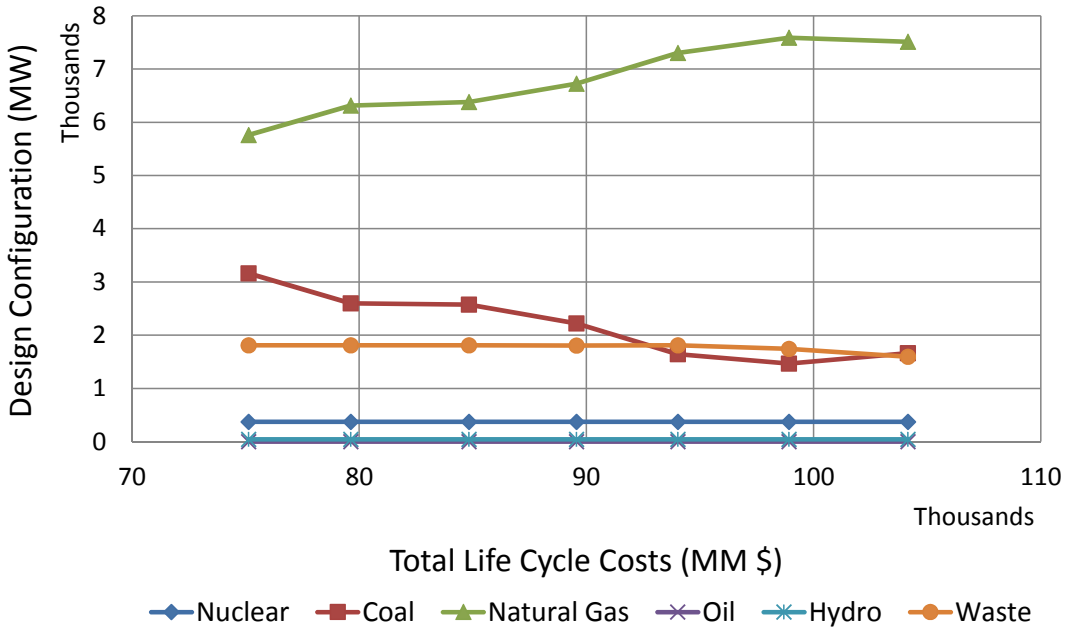

Figure 4.3. Sizes of the optimum network configuration in the Pareto set for *Scenario 1* [212]. Reprinted from [212] Copyright © 2012 by ASME, with permission.

Comparing both scenarios, as seen in Figure 4.2, *Scenario 2* is more expensive than *Scenario 1* for all possible optimum configurations in the synthesis/design/operation space. This is because of the higher unit capital cost of distributed generation technologies such as fuel cells, photovoltaics, and small coal plants, as well as the higher operating costs of diesel reciprocating engines, NG microturbines, and solid oxide fuel cells.

4.2.2.3 Total life cycle costs – efficiency

Figure 4.5 shows a view of the Pareto set for the network efficiency. An optimum efficiency point is shown at about 79,000 MM-$ for *Scenario 1* and about 83,000 MM-$ for *Scenario 2*. Beyond these points for both scenarios, the efficiency of the system decreases as the total life cycle costs increase. This is because smaller less efficient technologies begin to play a role in the production of electricity, while the base-load technologies, such as coal, decrease their participation in the optimum configurations. For *Scenario 1*, efficiency decreases to the left of the optimum point because the penetration of NG-based technologies decreases, while the penetration of coal-based ones increases. This is due to the fact that the life cycle O&M costs of the coal-based technologies are lower even though their capital costs are higher and their efficiencies lower than those of the NG-based generators. For *Scenario 2*, the same trend as for *Scenario 1* is followed with the addi-

tion of capital intensive oil-, PV-, and wind-based generators, the latter two having the advantage of almost negligible O&M life cycle costs.

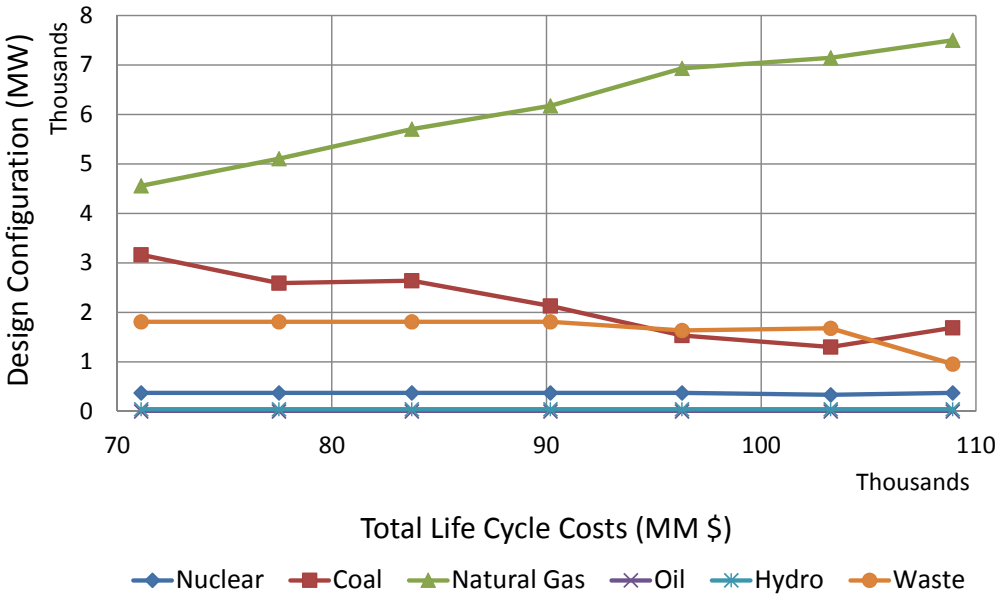

(a) Grid.

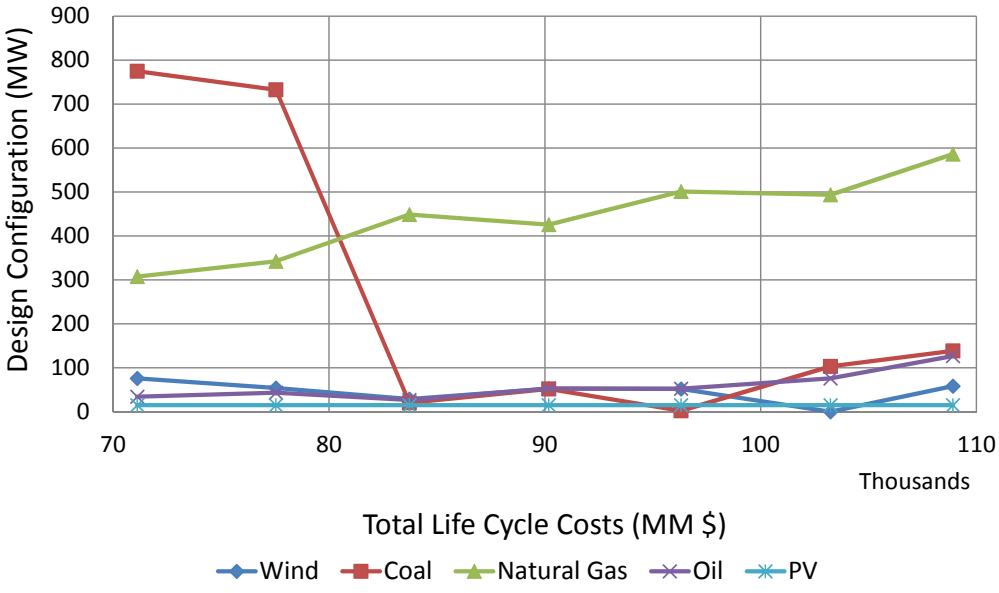

(b) MGs.

Figure 4.4. Sizes of the optimum network configuration in the Pareto set for *Scenario 2* [212]. Reprinted from [212] Copyright © 2012 by ASME, with permission.

In addition, it is shown that *Scenario 2* has a better network efficiency than *Scenario 1* for almost all the optimum points, except for a range between 91,000-97,000 MM-$. In this range, coal reduces significantly its role in the network for both scenarios. Approximately 1.2 GW of

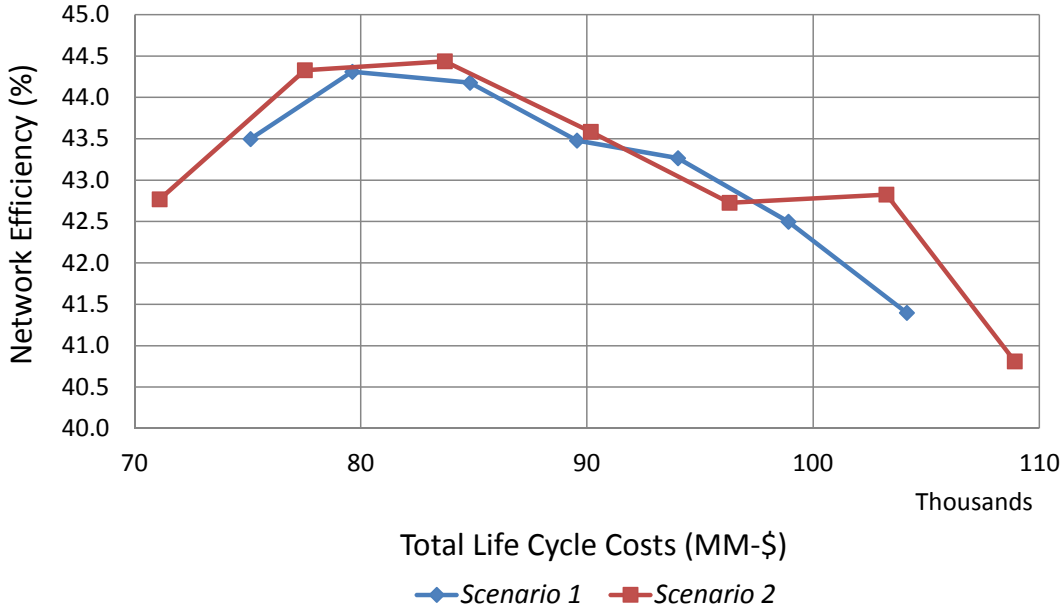

Figure 4.5. Optimal network efficiency versus optimal total life cycle costs [212]. Reprinted from [212] Copyright © 2012 by ASME, with permission.

centralized NG is replaced by distributed generation in *Scenario 2*. Nuclear, oil, waste, and hydro technologies produce almost the same amount of power in both scenarios. In addition, transmission losses are reduced in *Scenario 2*, because of the local power generation, which improves the performance of the power network system.

4.2.2.4 Total life cycle costs – SO_2 emissions

Figure 4.6 shows the total life cycle SO_2 emissions versus total life cycle costs for the optimal configurations. For both scenarios, it is seen that emissions decrease while the cost of production increases. This is because technologies using cheaper fuels with higher emissions of SO_2, such as coal and wastes, decrease production costs, while cleaner and more expensive technologies such as natural gas increase production costs. Technologies fueled with nuclear and hydro maintain the same production costs. Oil does not play a role in any configuration for the centralized system; it is required for the MGs only. In MG configurations, natural gas and oil technologies increase their penetration in the system for the most expensive cases.

Figure 4.6 also shows that the optimal total life cycle SO_2 emissions are lower for *Scenario 2*, because PV, wind turbines, and fuel cells play a role in the optimum configurations. For the most expensive cases, the emissions are lower for *Scenario 1* because oil starts to increase its contribution in the MG configurations.

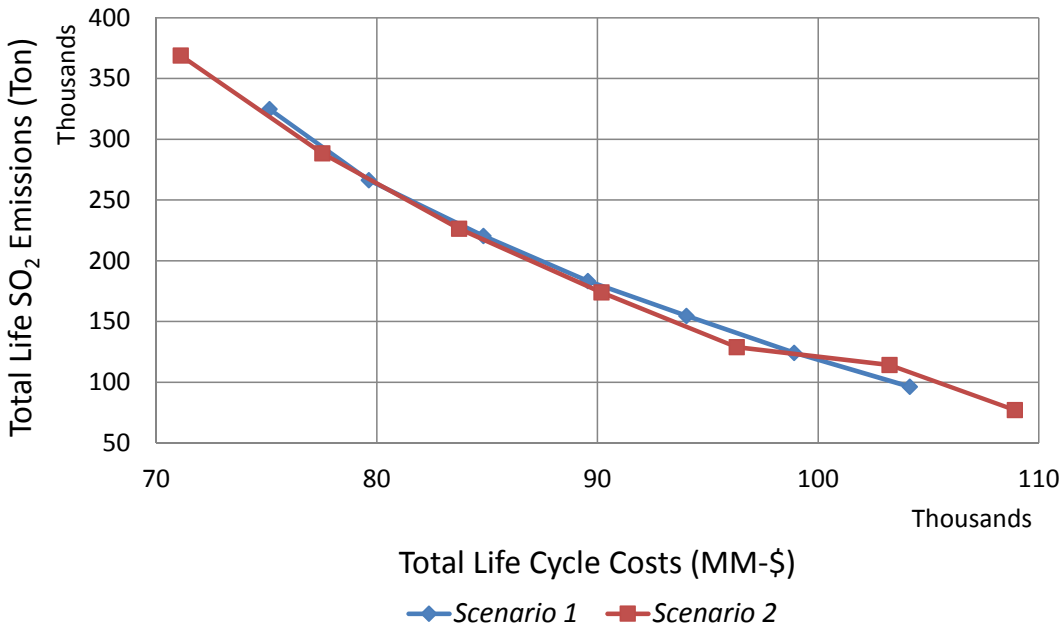

Figure 4.6. Optimal total life cycle SO_2 emissions versus optimal total life cycle costs [212]. Reprinted from [212] Copyright © 2012 by ASME, with permission.

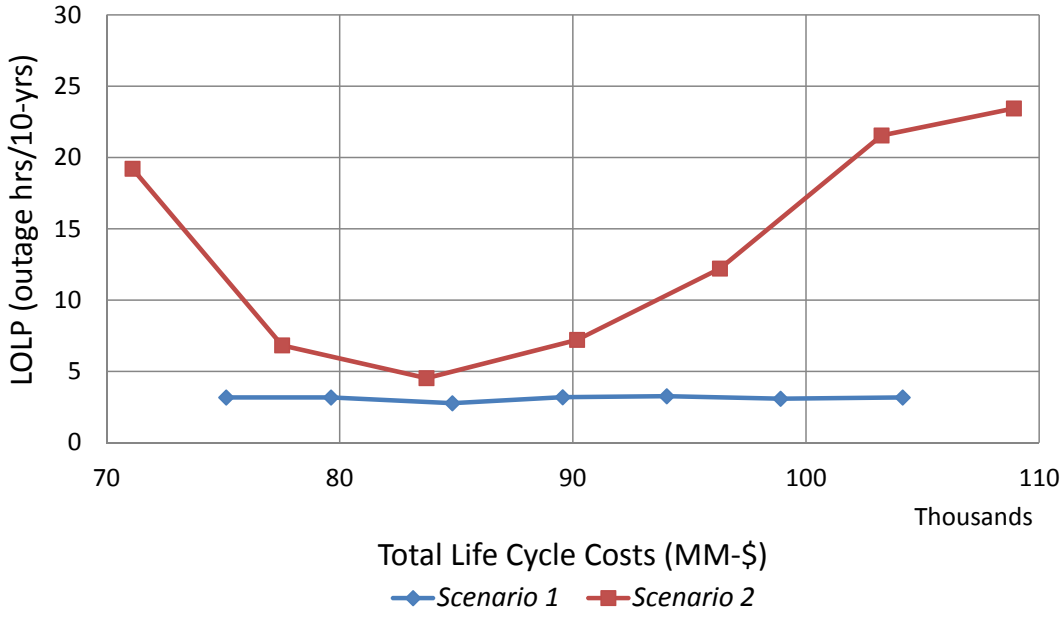

Figure 4.7. Optimal LOLP versus optima total life cycle costs [212]. Reprinted from [212] Copyright © 2012 by ASME, with permission.

4.2.2.5 Total life cycle costs–reliability

Figure 4.7 shows the Pareto set for optimal reliability versus optimal total life cycle costs. The LOLP is almost independent of costs for *Scenario 1* so that little variation in the reliability of the optimal system occurs. This is due to the fact that although the configurations are changing at

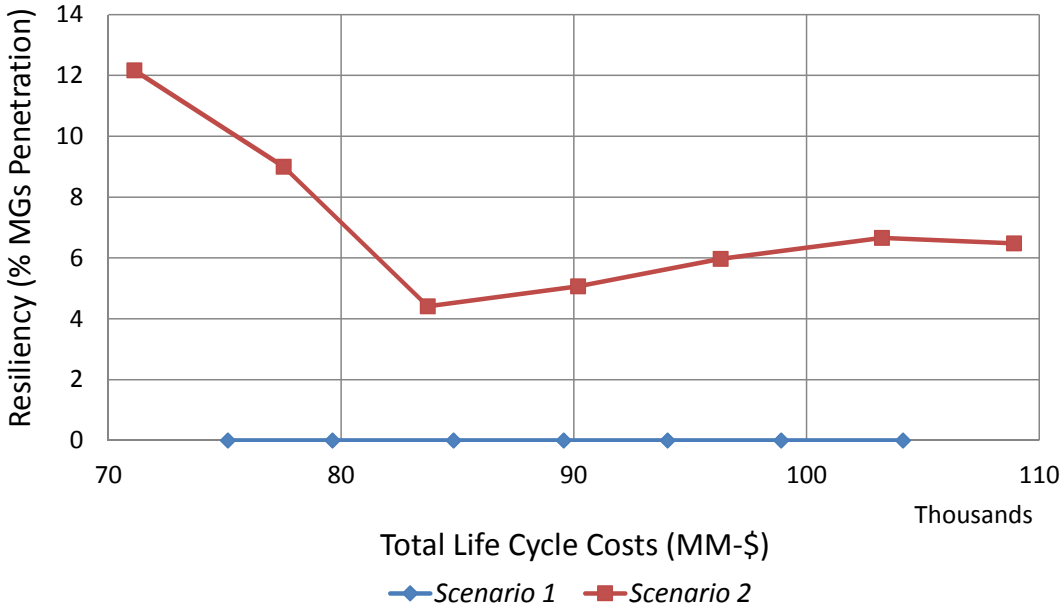

Figure 4.8. Optimal resiliency (penetration of MGs) versus optimal total life cycle costs (capital and O&M) [212]. Reprinted from [212] Copyright © 2012 by ASME, with permission.

every point in the Pareto set, they always include a large amount of base- and intermediate-load power plants.

The figure also shows that reliability is better for *Scenario 1* than for *Scenario 2*. A high penetration of wind and PV results in uncertainties in the power available to the grid due to the intermittent nature of these technologies; thus, their availability is low. There is an optimum point for *Scenario 2* at about 84,000 MM-$, when the MG penetration is the lowest of all the possible optimum configurations. Note that the LOLP reported here is only that for the capacity reliability and does not include the transmission line.

4.2.2.6 Total life cycle costs–resiliency

Figure 4.8 shows the view of the Pareto set for resiliency versus total life cycle costs for the optimal configurations. Since resiliency is defined to be directly proportional to MG penetration, *Scenario 1* has a resiliency of zero for all the possible optimum solutions. On the other hand, *Scenario 2* shows the highest resiliency at the lowest optimal total life cycle costs, when small coal technologies provide their maximum contribution to the network. This indicates that at this optimum point, if a disruption of the transmission grid were to occur, MGs could be isolated from the network within seconds and provide electricity locally to residential, commercial, and industrial customers, thus, minimizing by about 12% the amount of power outage that otherwise would occur

if no MG capacity at all were included in the network.

4.2.2.7 Post–processing analysis

Table 4.8 and Table 4.9 show the numerical values for the Pareto front of optimum solutions for *Scenario 1* and *Scenario 2*, respectively, presented and discussed in previous sections. For sake of comparison, two methods of decision making are used in order to obtain the most desirable solution among the set of optimum solutions in the Pareto front. The first approach is that described in Section 3.5.1, in which a value function is applied directly in order to obtain the most desirable solution. The second approach is that described in Section 3.5.2, in which decision makers are asked to give their suggestion for the importance of the different objective functions used in the problem in order to obtain the weights for the sustainability indices.

Table 4.8. Objective function values for selected Pareto optimal solutions for *Scenario 1* [212].

Total Life Cycle Costs (MM-$)	Efficiency (%)	Total Life Cycle SO_2 Emissions (Ton)	LOLP (hr/10-yr)	Resiliency (%-MGs)
75,126	43.50	324,833	3.178	-
79,627	44.31	266,435	3.173	-
84,826	44.18	220,530	2.781	-
89,561	43.48	183,275	3.203	-
94,024	43.27	154,562	3.274	-
98,907	42.50	124,240	3.099	-
104,144	41.40	96,401	3.187	-

Table 4.9. Objective function values for selected Pareto optimal solutions for *Scenario 2* [212].

Total Life Cycle Costs (MM-$)	Efficiency (%)	Total Life Cycle SO_2 Emissions (Ton)	LOLP (hr/10-yr)	Resiliency (%-MGs)
71,113	42.77	368,936	19.216	12.17
77,533	44.33	288,398	6.836	9.00
83,725	44.43	226,374	4.528	4.41
90,177	43.58	173,953	7.209	5.07
96,308	42.73	128,960	12.222	5.97
103,236	42.82	114,170	21.541	6.66
108,912	40.81	77,088	23.443	6.48

If the first approach is used, that is, using value functions, the sustainability-resiliency sub-indices are obtained with the value functions given by Equation (3.15) for minimizing objectives, and by Equation (3.16) for maximizing objectives, and the global sustainability-resiliency index is obtained with the methodology given in Section 3.3 of Chapter 3. Table 4.10 shows the results for *Scenario 1* and Table 4.11 for *Scenario 2*. The global sustainability-resiliency index is indicated in bold and represents the most desirable solution among the optimum solutions in the Pareto set. As seen, the most desirable solution for *Scenario 1* has a composite sustainability-resiliency index of 0.07945, while that for *Scenario 2* has one of 0.09351. Table 4.12 lists the actual values corresponding to the objective functions of the global composite sustainability-resiliency index. As can be seen in Table 4.12, the most desirable solution for *Scenario 2* shows that the inclusion of MGs into the network leads to a better overall efficiency, a reduction in monetary costs, and an improved network resiliency. On the other hand, total life cycle SO_2 emissions and network reliability are not improved, i.e., they are slightly better in *Scenario 1*.

Table 4.10. Sustainability-resiliency indices for *Scenario 1* using value functions [212].

Total Life Cycle Costs	Efficiency	Total Life Cycle SO_2 Emissions	LOLP	Resiliency	Composite Index
0.8938	0.7431	0.1511	0.9806	-	0.07149
0.7747	0.9669	0.3512	0.9811	-	0.07937
0.6372	*0.9309*	*0.5085*	*1.0000*	-	***0.07945***
0.5119	0.7376	0.6362	0.9797	-	0.07399
0.3939	0.6796	0.7345	0.9763	-	0.07189
0.2647	0.4669	0.8384	0.9845	-	0.06596
0.1261	0.1630	0.9338	0.9802	-	0.05689

Table 4.11. Sustainability-resiliency indices for *Scenario 2* using value functions [212].

Total Life Cycle Costs	Efficiency	Total Life Cycle SO_2 Emissions	LOLP	Resiliency	Composite Index
1.0000	0.5414	0.0000	0.2043	1.0000	0.07090
0.8302	*0.9724*	*0.2760*	*0.8035*	*0.7395*	***0.09351***
0.6663	1.0000	0.4885	0.9153	0.3624	0.08863
0.4956	0.7652	0.6681	0.7856	0.4166	0.08085
0.3334	0.5304	0.8223	0.5431	0.4906	0.07023
0.1502	0.5552	0.8729	0.0920	0.5472	0.05726
0.0000	0.0000	1.0000	0.0000	0.5325	0.03957

Table 4.12. Values of the objective functions corresponding to the most desirable solution [212].

Objective	*Scenario 1*	*Scenario 2*
Total Life Cycle Costs (MM-$)	84,826	77,533
Efficiency (%)	44.18	44.33
Total Life Cycle SO_2 Emissions (Ton)	220,530	288,398
LOLP (hr/10-yr)	2.781	6.836
Resiliency (%-MGs)	0.00	9.00

Table 4.13. Responses from the consultants to the ranking of objectives [212].

	DM1	DM2	DM3	DM4	DM5	DM6
Costs	5	2	1	5	5	1
Efficiency	2	4	3	2	4	3
Emissions	3	5	5	3	3	5
Resiliency	1	3	2	1	1	2
Reliability	4	1	4	4	2	4

Table 4.14. DM-characteristic reliability matrix [212].

	Rank	Experience	Self-confidence	Reputation
DM1	3	2	5	3
DM2	5	3	5	3
DM3	2	1	5	1
DM4	1	1	5	1
DM5	2	1	5	1
DM6	5	5	5	5

Now, if instead of value functions the weighting post-processing approach proposed by [207] and described in Section 3.5.2 of Chapter 3 is used, sustainability sub-indices and a composite sustainability-resiliency index for each of the optimum solutions in the Pareto set are obtained. To establish the weights, the values for the responses from the experts in Table 4.13 are used as is the DM-characteristic reliability matrix given in Table 4.14. Note that a very high self-confidence is assumed for all the consultants.

Table 4.15 shows the results for *Scenario 1* and Table 4.16 for *Scenario 2*. As seen, the most desirable solution for *Scenario 1* has a composite sustainability-resiliency index of 0.5562, while that for *Scenario 2* has one of 0.6446. These two most desirable solutions are also the ones found using

value functions (see Table 4.10 and Table 4.11) although the values of the composite sustainability-resiliency indices are different. Figure 4.9 shows the normalized indices of the most desirable solution for both scenarios using value functions and DM inputs for the Netherlands. Note that since the transmission reliability is not included, the results for reliability given here are not conclusive.

Table 4.15. Sustainability-resiliency index for *Scenario 1* using DM suggestions [212].

Economic Sub-index	Environmental Sub-index	Technological Sub-index	Composite Index
0.8938	0.1511	0.4696	0.5194
0.7747	0.3512	0.5144	0.5553
0.6372	*0.5085*	*0.5134*	***0.5562***
0.5119	0.6362	0.4682	0.5379
0.3939	0.7345	0.4556	0.5231
0.2647	0.8384	0.4159	0.4975
0.1261	0.9338	0.3539	0.4586

Table 4.16. Sustainability-resiliency index for *Scenario 2* using DM suggestions [212].

Economic Sub-index	Environmental Sub-index	Technological Sub-index	Composite Index
1.0000	0.0000	0.6477	0.5659
0.8302	*0.2760*	*0.8069*	***0.6446***
0.6663	0.4885	0.6707	0.6106
0.4956	0.6681	0.6070	0.5867
0.3334	0.8223	0.5157	0.5489
0.1502	0.8729	0.3995	0.4622
0.0000	1.0000	0.2518	0.4019

4.2.2.8 24-hr performance for the best optimum solution

Figure 4.10 shows the twenty-four hour performance of the best compromise solution for *Scenario 1*. Coal, nuclear, waste, and hydro technologies serve as base-load technologies, while NG provides intermediate-load and peaking. This is expected, since coal, nuclear, hydro, and waste are typically large power plants that are cheap to operate, although more capital intensive.

Figure 4.11 shows the performance of the best compromise solution for *Scenario 2*. Compared with *Scenario 1*, the main grid for *Scenario 2* is producing about 1,000 MW less electricity from NG technologies. Nuclear, coal, waste, and hydro produce the same electricity in both scenarios. In the MGs, NG technologies such as fuel cells and microturbines produce a constant amount of electricity throughout the day, while small coal plants produce most of the electricity, especially for industrial applications. Diesel reciprocating engines operate during peak hours only.

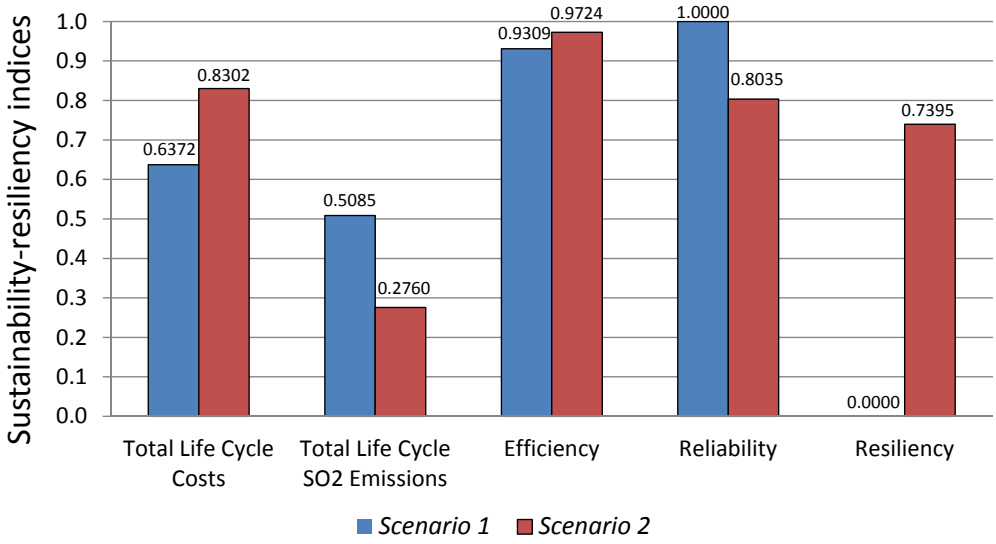

Figure 4.9. Normalized values or indices for the best compromise solution in the Pareto set for the Netherlands [212]. Reprinted from [212] Copyright © 2012 by ASME, with permission.

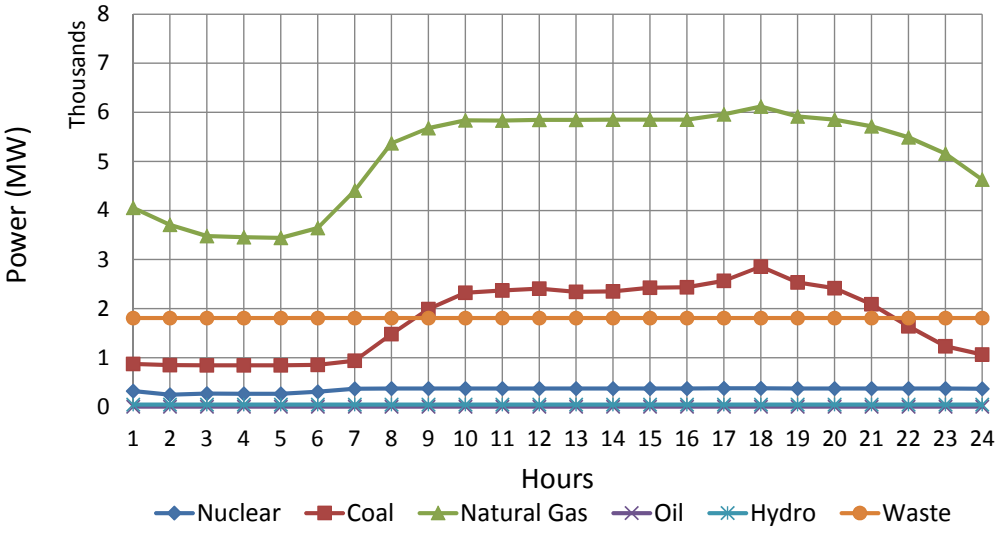

Figure 4.10. Power production throughout the day for the best fuzzy logic compromise solution for *Scenario 1* [212]. Reprinted from [212] Copyright © 2012 by ASME, with permission.

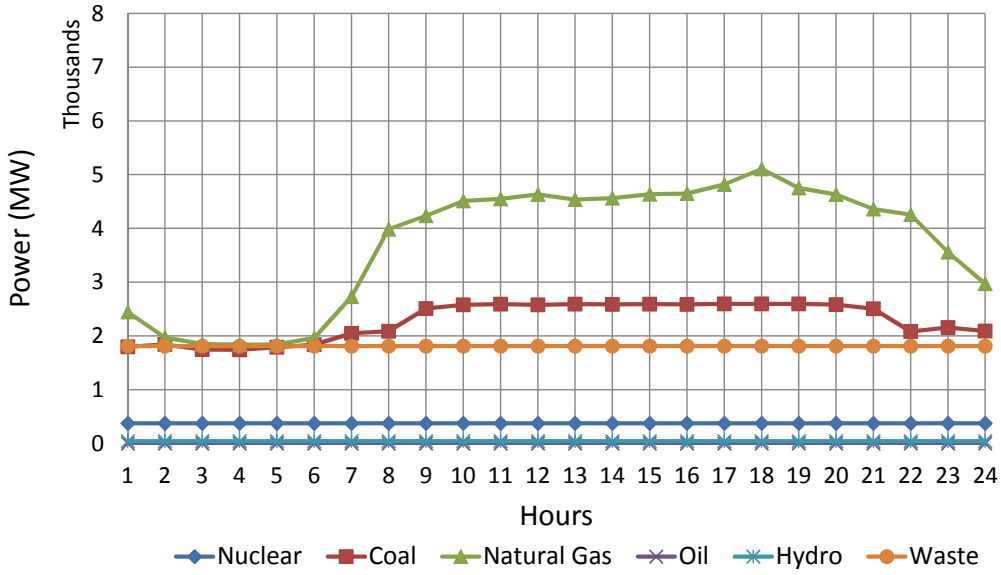

(a) Production of the Grid.

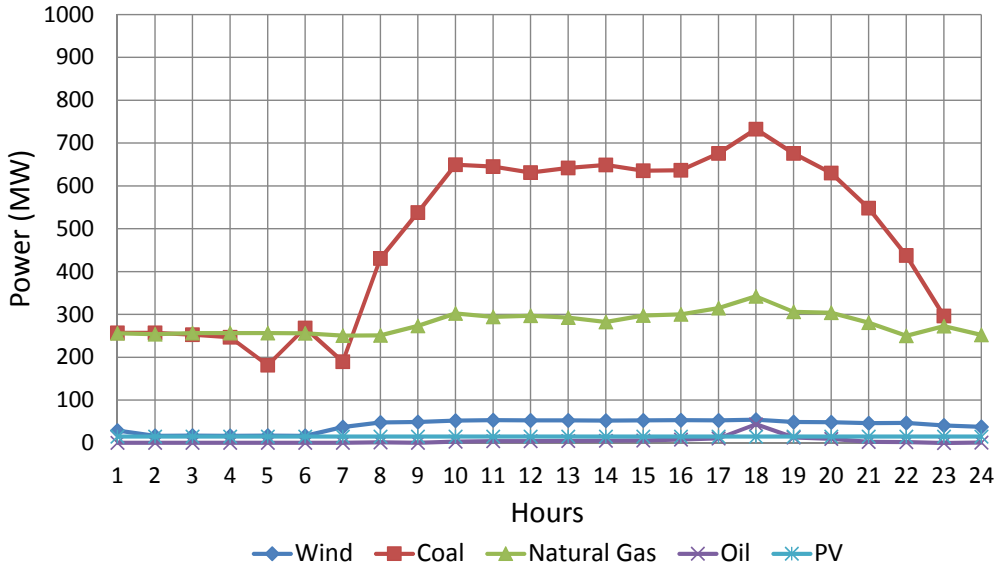

(b) Production of the MGs.

Figure 4.11. Power production throughout the day for the best fuzzy logic compromise solution for *Scenario 2* [212]. Reprinted from [212] Copyright © 2012 by ASME, with permission.

4.3 International-level power network system: COMPETES

The Northwest European electricity market is represented by the system described in Section 3.1.2. Two different scenarios are considered in order to provide a description of the effects of the inclusion of localized power producers via microgrids. *Scenario 1* is the reference case and consists of the power network with centralized power production as described in Section 3.1.2.1. In *Scenario*

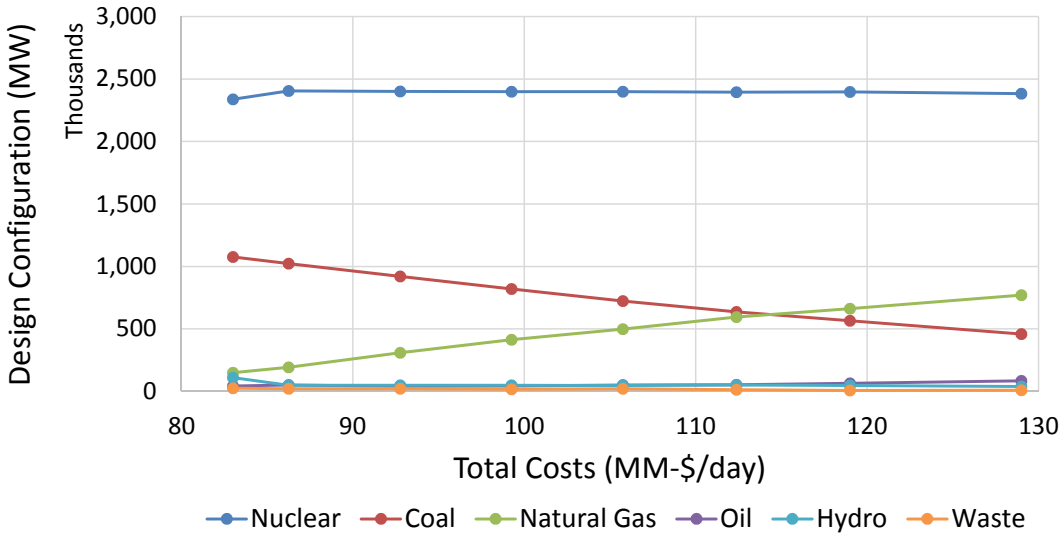

Figure 4.12. Sizes of the optimum network configurations in the Pareto set for *Scenario 1*.

2 (see Section 3.1.2.2), the model of *Scenario 1* is modified by including localized power producers via microgrids at the different nodes of the system where energy production exists.

The quasi-stationary multi-objective optimization model for the synthesis/design/operation of the system is described in Section 3.2 and is given by Equations (3.1) and (3.2). The objective functions of Equation (3.1) are the total daily costs defined by Equation (3.3); the total daily SO_2 emissions of the system defined by Equation (3.5); the efficiency of the network, represented by the exergy of the fossil fuels used for the generation of electricity and defined by Equation (3.9); and the resiliency of the system, i.e., the degree of microgrid penetration in the system, given by Equation (3.14). The equality and inequality constraints representing the model are defined by Equations (3.2a) and (3.2b), respectively, and the inequality constraints representing the operational limits are expressed by Equations (3.2c) and (3.2d).

The next sections present the Pareto sets for two objective functions at a time because visualizing more than two simultaneously is difficult, since a k-dimensional space is required for k objective functions.

4.3.1 Design/ configurations

Figure 4.12 depicts the design configurations for *Scenario 1*. It can be seen that the power production of nuclear technologies is increased for the second configuration and remains constant through the rest of them. In contrast, the production of hydro technologies is decreased for the

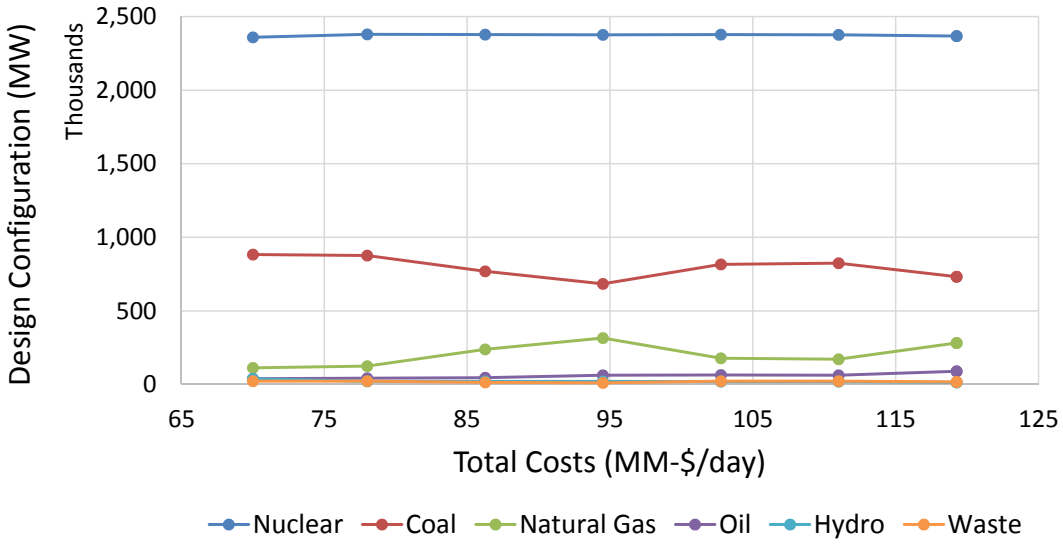

(a) Grid.

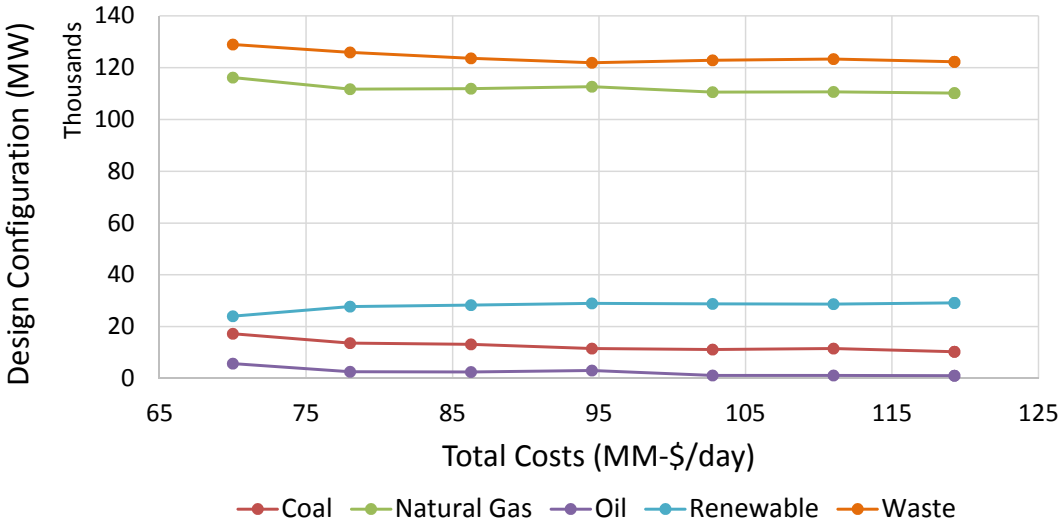

(b) Microgrids.

Figure 4.13. Sizes of the optimum network configurations in the Pareto set for *Scenario 2*.

second configuration and remains constant for the rest of the configurations. The production of oil technologies increases gradually for the most expensive cases, while the production of waste technologies remains constant for all the design configurations, although their production is not comparable to the other technologies such as coal, NG, and nuclear.

The most significant changes occur for the production of coal and NG technologies. The production of operationally cheaper coal technologies decreases significantly for the most expensive scenarios, while that by the NG technologies which are more expensive to operate increases.

Figure 4.13 shows the design configurations for *Scenario 2*. It is seen that production of nuclear technologies located in the centralized network remain constant for all the design configurations.

Their production is also equivalent to that produced for nuclear technologies in *Scenario 1*. The production of waste technologies remain almost constant for all the design configurations in the main grid, but the production of waste technologies is dominant in the MG configurations primarily because of the production of IGCC technologies in the industrial MGs. This high penetration of waste technologies in the MGs increases significantly the total production of waste technologies in *Scenario 2* to that of the waste technologies of *Scenario 1*. The production of coal technologies in the grid decreases to that for the fourth design configuration at about 95 MM-$/day and then increases again at about 111 MM-$/day after which it decreases. In the MGs the production of coal technologies decreases gradually for the most expensive design configurations. The total production for coal technologies for *Scenario 2*, i.e., grid and MGs, is higher compared with the total production of coal technologies for *Scenario 1*.

The production of NG technologies follows an apposite trend to that of the coal technologies in the main grid. In the MGs, NG technologies are the second dominant producers just behind waste technologies, with almost a constant production for all design configurations. The total production of NG technologies, i.e., grid and MGs, remain almost constant for *Scenario 2*, opposite to the case of *Scenario 1* where NG technologies increase their production dramatically for the most expensive design configurations. Production of oil technologies is about the same for both scenarios where their production is small compared to the other more dominant technologies. For the case of renewable technologies, the production of photovoltaics (PV) and wind in the MGs and hydro in the main grid increases the penetration of renewable energy sources for Scenario 2, as compared to Scenario 1 where the production of renewable energy sources is small.

4.3.2 Total daily costs – SO_2 emissions

Figure 4.14 shows the total daily SO_2 emissions versus total daily costs for the optimal configurations. For both scenarios, it is seen that emissions decrease while the total costs increase. This decrease in total daily SO_2 for *Scenario 1* at higher costs is mainly due to the inclusion of technologies such as coal which use cheaper fuels with higher emissions of SO_2, while cleaner and more expensive technologies such as those using natural gas are a larger percentage of the total production. Technologies fueled with oil maintain the same level of production and emissions while renewable technologies such as hydro help decrease the cost of production. Nuclear technologies

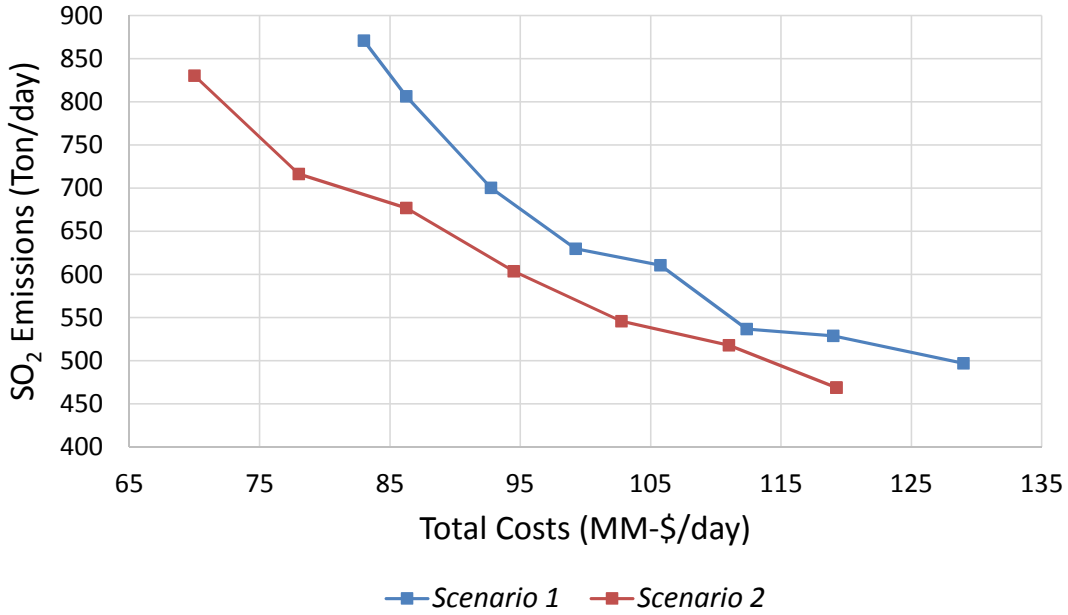

Figure 4.14. Optimal daily SO_2 emissions versus optimal total daily costs (capital and O&M).

increase these costs. For *Scenario 2*, this decrease in total daily SO_2 emissions at higher costs is because the power production of coal technologies in both the main grid and MGs is replaced by more expensive cleaner technologies such as NG and waste gasification (IGCC). Cleaner technologies in the MG configurations such as PV, wind turbines, and fuel cells play an important role in the optimum configurations.

4.3.3 Total daily costs – daily exergy use

Figure 4.15 shows a view of the Pareto set for the exergy use by fossil fueled technologies. An optimum efficiency point is shown at about 93,000 MM-$ for *Scenario 1* and about 78,000 MM-$ for *Scenario 2*. Beyond these points for both scenarios, the efficiency of the system decreases (exergy use increases) as the total daily costs increase. This is because smaller less efficient technologies begin to play a role in the production of electricity, while the base-load technologies, such as coal, decrease their participation in the optimum configurations. This effect is even more significant for *Scenario 2* where MG technologies play a role, especially for the waste gasification technologies. In addition, since MG technologies are allowed to sell their production to the main grid, an increase in energy exchange among nodes is noted bringing as a consequence an increase of the transmission losses, provoking a decrease in the efficiency of the network for *Scenario 2* as compared to *Scenario 1*.

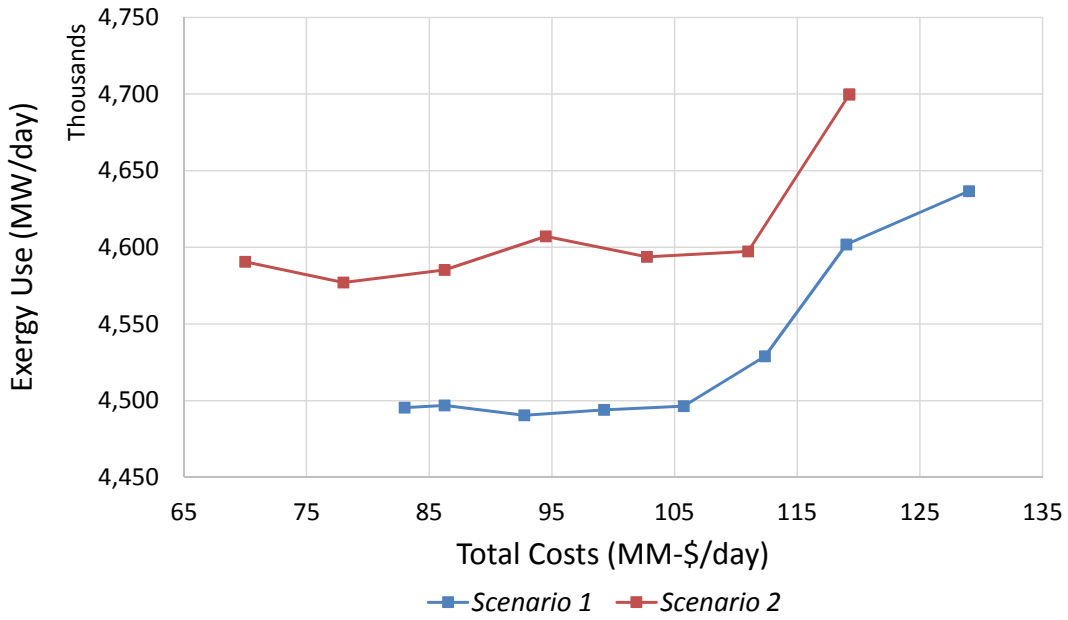

Figure 4.15. Optimal daily exergy use versus optimal total daily costs (capital and O&M).

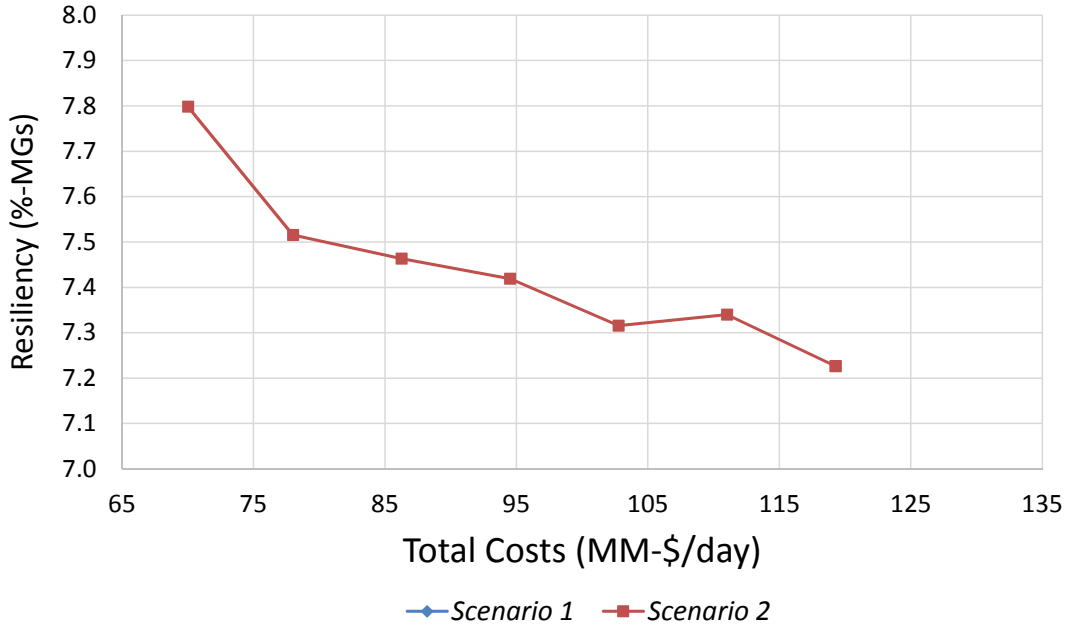

Figure 4.16. Optimal resiliency (penetration of MGs) versus optimal total daily costs (capital and O&M).

4.3.4 Total daily costs – resiliency

Figure 4.16 shows the view of the Pareto set for resiliency versus total daily costs for the optimal configurations. Since resiliency is defined to be directly proportional to MG penetration, *Scenario 1* has a resiliency of zero for all the possible optimum solutions. On the other hand, *Scenario 2*

shows the highest resiliency at the lowest optimal total daily costs when small coal, oil, natural gas and waste gasification technologies provide their maximum contribution to the network. This indicates that at this optimum point, if a disruption of the transmission grid were to occur, MGs could be isolated from the network within seconds and provide electricity locally to residential, commercial, and industrial customers, thus, minimizing by about 7.8% the amount of power outage that otherwise would occur if no MG capacity at all were included in the network.

4.3.5 Post–processing analysis

Table 4.17 and Table 4.18 show the numerical values for the Pareto set of optimum solutions for *Scenario 1* and *Scenario 2*, respectively, presented and discussed in previous sections. The rows indicate the optimal synthesis/design/operation configurations representing the Pareto set of optimum solutions. Appendix A shows the optimal configuration synthesis/design variable values for the eight optimal solutions in the Pareto set for *Scenario 1*. It is seen that nuclear has the highest production, followed by coal and NG. Oil, hydro and waste have the lowest production. In addition, hydro and NG serve as peaking producers, while the rest of the technologies serve as base- and intermediate-load technologies. Appendix B shows the optimal configuration synthesis/design variable values for the eight optimal solutions in the Pareto set for *Scenario 2*. The main grid performs in a similar manner as that of *Scenario 1*, but now NG technologies decrease their production in the network. On the other hands, MG technologies play an important role in the production of electricity. Coal and waste technologies serve as base- and intermediate-load producers, while NG, oil, and renewables such as wind and PV serve as peak-load producers. As for the case of the Netherlands system presented in Section 4.2, two methods of decision making are used in order to obtain the most desirable solution among the set of optimum solutions in the Pareto set. The first approach is that described in Section 3.5.1 in which a value function is applied using fuzzy logic directly in order to obtain the most desirable solution. The second approach is that described in Section 3.5.2 in which decision makers are asked to give their suggestion for the importance of the different objective functions used in the problem in order to obtain the weights for the sustainability indices.

If the first approach is used, that is, using value functions, the sustainability-resiliency sub-indices are obtained with the value functions given by Equation (3.15) for minimizing objectives

and by Equation (3.16) for maximizing objectives, while the global sustainability-resiliency index is obtained with the methodology given in Section 3.3 of Chapter 3. Table 4.19 shows the results for *Scenario 1* and Table 4.20 for *Scenario 2*.

Table 4.17. Objective function values for selected Pareto optimal solutions for *Scenario 1*.

	Total daily costs ($/day)	Total daily SO_2 Emissions (kg/day)	Total daily exergy use (MW/day)	Resiliency (% MGs)
Config. 1	83,000,000	870,899	4,495,467	0
Config. 2	86,250,000	806,442	4,496,929	0
Config. 3	92,750,000	700,113	4,490,475	0
Config. 4	99,250,000	629,728	4,494,020	0
Config. 5	105,750,000	610,535	4,496,364	0
Config. 6	112,375,000	536,695	4,528,906	0
Config. 7	119,000,000	528,736	4,601,784	0
Config. 8	129,000,000	496,748	4,636,658	0

Table 4.18. Objective function values for selected Pareto optimal solutions for *Scenario 2*.

	Total daily costs ($/day)	Total daily SO_2 Emissions (kg/day)	Total daily exergy use (MW/day)	Resiliency (% MGs)
Config. 1	70,000,000	830,106	4,590,638	7.80
Config. 2	78,000,000	716,432	4,577,014	7.52
Config. 3	86,250,000	676,977	4,585,251	7.46
Config. 4	94,500,000	603,540	4,607,182	7.42
Config. 5	102,750,000	545,605	4,593,740	7.32
Config. 6	111,000,000	517,934	4,597,256	7.34
Config. 7	119,254,232	468,739	4,699,697	7.23
Config. 8	119,254,232	468,739	4,699,697	7.23

The global sustainability-resiliency index and its associated sub-indices are indicated in bold and represent the most desirable solution among the optimum solutions in the Pareto set. As seen, the most desirable solution for *Scenario 1* has a composite sustainability-resiliency index of 0.0703, while that for *Scenario 2* has one of 0.0884. Table 4.21 lists the actual values corresponding to the objective functions of the global composite sustainability-resiliency index. As can be seen in Table 4.21, the most desirable solution for *Scenario 2* shows that the inclusion of MGs into the network leads to a reduction in monetary costs and an improved network resiliency. On the other

hand, total daily SO_2 emissions and network efficiency are not improved, i.e., they are somewhat better in *Scenario 1*. Appendix C shows the performance decision variables of the most desirable configuration for *Scenario 1* and Appendix D shows the performance decision variables of the most desirable configuration for *Scenario 2* obtained using value functions.

Table 4.19. Sustainability-resiliency indices for *Scenario 1* using value functions (fuzzy logic).

	Total Costs Sub-Index	SO_2 Emissions Sub-Index	Total exergy use Sub-Index	Resiliency Sub-Index	Composite Index
Config. 1	0.7797	0.0000	0.9761	-	0.0592
Config. 2	0.7246	0.1603	0.9691	-	0.0625
Config. 3	0.6144	0.4247	1.0000	-	0.0687
Config. 4	***0.5042***	***0.5997***	***0.9831***	-	***0.0703***
Config. 5	0.3941	0.6474	0.9719	-	0.0679
Config. 6	0.2818	0.8310	0.8163	-	0.0650
Config. 7	0.1695	0.8508	0.4679	-	0.0502
Config. 8	0.0000	0.9304	0.3012	-	0.0415

Table 4.20. Sustainability-resiliency indices for *Scenario 2* using value functions (fuzzy logic).

	Total Costs Sub-Index	SO_2 Emissions Sub-Index	Total exergy use Sub-Index	Resiliency Sub-Index	Composite Index
Config. 1	***1.0000***	***0.1014***	***0.5212***	***1.0000***	***0.0884***
Config. 2	0.8644	0.3841	0.5863	0.5048	0.0789
Config. 3	0.7246	0.4822	0.5470	0.4136	0.0730
Config. 4	0.5847	0.6648	0.4421	0.3364	0.0683
Config. 5	0.4449	0.8089	0.5064	0.1550	0.0645
Config. 6	0.3051	0.8777	0.4896	0.1978	0.0630
Config. 7	0.1652	1.0000	0.0000	0.0000	0.0393
Config. 8	0.1652	1.0000	0.0000	0.0000	0.0393

Table 4.21. Values of the objective functions corresponding to the most desirable solution using both using value functions (fuzzy logic).

Objective	*Scenario 1*	*Scenario 2*
Total Daily Costs ($)	99,250,000	70,000,000
Total Daily SO_2 Emissions (kg)	629,728	830,106
Daily Exergy Use (%)	4,494,020	4,590,638
Resiliency (%-MGs)	0.00	7.80

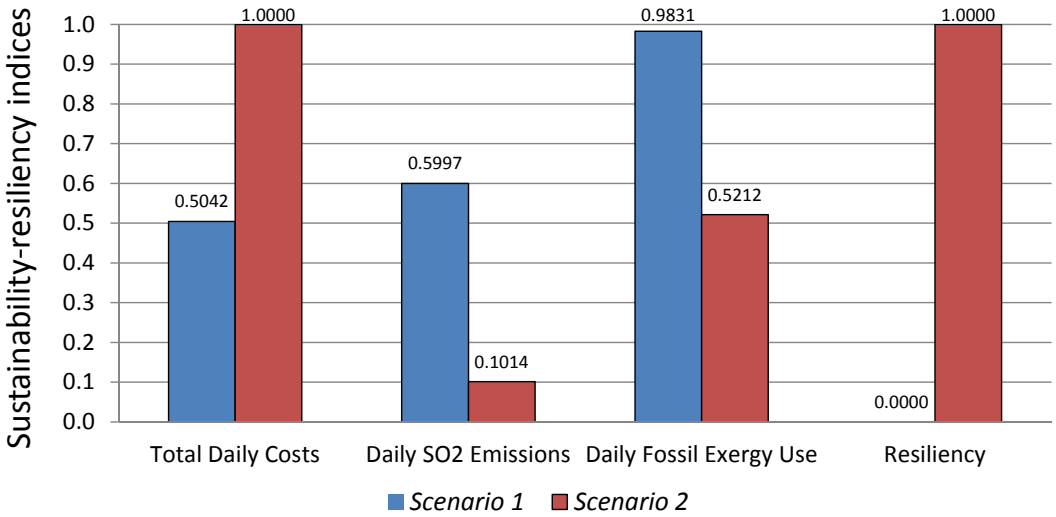

Figure 4.17. Normalized values or indices for the best compromise solution in the Pareto set for the Northwest European electricity market obtained using value functions.

Figure 4.17 shows the normalized indices of the most desirable solution for both scenarios using value functions for the Northwest European electricity market. As seen, the inclusion of MGs improves the total daily costs and increase the resiliency of the network. Nevertheless, the scenario in which MGs are not included is better in terms of daily SO_2 emissions and daily fossil-exergy use.

Now, if instead of value functions, the weighting post-processing approach proposed by [207] and described in Section 3.5.2 of Chapter 3 is used, another set of sustainability sub-indices and composite sustainability-resiliency index for each of the optimum solutions in the Pareto set is obtained. To establish the weights, the values for the responses given in Table 4.13 are used as is the DM-characteristic reliability matrix given in Table 4.14.

Table 4.22 shows the results for *Scenario 1* and Table 4.23 for *Scenario 2*. As seen, the most desirable solution for *Scenario 1* has a composite sustainability-resiliency index of 0.4700 (shown in bold), while that for *Scenario 2* has one of 0.7542 (shown in bold). The most desirable solution for *Scenario 1* is different from that obtained using value functions (see Table 4.19) while that for *Scenario 2* is the same as that found using value functions (see Table 4.20).

Figure 4.18 shows the normalized indices of the most desirable solution for both scenarios using DM inputs for the Northwest European electricity market. As seen, the inclusion of MGs improves the total daily costs and increase the resiliency of the network. Nevertheless, the scenario in which MGs are not included is better in terms of daily SO_2 emissions and daily fossil-exergy use.

Table 4.22. Sustainability-resiliency indices for *Scenario 1* using DM weighting.

	Total Costs Sub-Index	SO_2 Emissions Sub-Index	Total exergy use Sub-Index	Resiliency Sub-Index	Composite Index
Config. 1	0.1663	0.0613	0.2425	–	0.4477
Config. 2	0.1961	0.0231	0.2350	–	0.4542
Config. 3	***0.1663***	***0.0613***	***0.2425***	–	***0.4700***
Config. 4	0.1364	0.0865	0.2384	–	0.4614
Config. 5	0.1066	0.0934	0.2357	–	0.4357
Config. 6	0.0762	0.1199	0.1980	–	0.3941
Config. 7	0.0459	0.1228	0.1135	–	0.2821
Config. 8	0.0000	0.1343	0.0731	–	0.2073

Table 4.23. Sustainability-resiliency indices for *Scenario 2* using DM weighting.

	Total Costs Sub-Index	SO_2 Emissions Sub-Index	Total exergy use Sub-Index	Resiliency Sub-Index	Composite Index
Config. 1	***0.2706***	***0.0146***	***0.1264***	***0.3426***	***0.7542***
Config. 2	0.2339	0.0554	0.1422	0.1730	0.6045
Config. 3	0.1961	0.0696	0.1326	0.1417	0.5400
Config. 4	0.1582	0.0959	0.1072	0.1152	0.4766
Config. 5	0.1204	0.1167	0.1228	0.0531	0.4130
Config. 6	0.0826	0.1267	0.1187	0.0678	0.3957
Config. 7	0.0447	0.1443	0.0000	0.0000	0.1890
Config. 8	0.0447	0.1443	0.0000	0.0000	0.1890

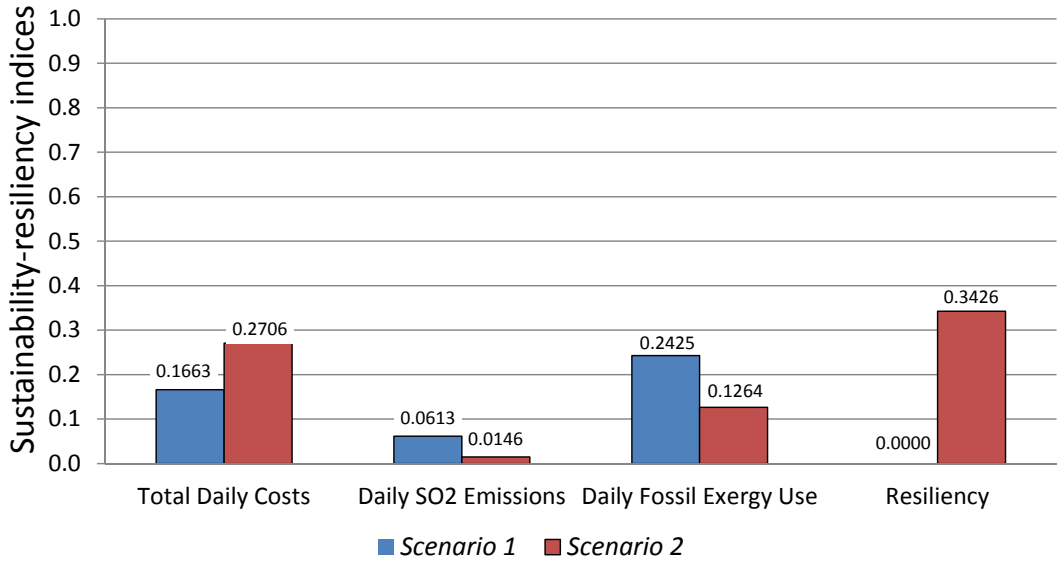

Figure 4.18. Normalized values or indices for the best compromise solution in the Pareto set for the Northwest European electricity market obtained using DM weighting.

Chapter 5

Conclusions for SAF

In this dissertation, a multi-objective, quasi-stationary, non-linear optimization approach is proposed as an upper-level of a two-tired Sustainability Assessment Framework (SAF) in which the synthesis/design/operation of a power network system is obtained. The methodology proposed is applied to two different scenarios, i.e., a base case scenario that considers the power network with centralized producers and a second scenario which integrates localized distributed energy producers using a mix of renewable and non-renewable energy sources via microgrids for the study of the effect of microgrids on a power network at both national and international levels of detail.

At the national level, a three-node network system representing the Netherlands in the Northwest European electricity market with and without MG configurations is presented. Results show that decentralized power generation brings improvements to the network, especially relative to the technological and monetary aspects of sustainability-resiliency. Coal, nuclear, hydro, and waste fueled technologies serve as base- and intermediate-load technologies, while NG serves as a peak-load technology only in both scenarios for this particular case. The inclusion of MGs replaces part of the NG production in the main grid. Industrial MGs play an important role in the synthesis/design/performance of the network, because the load demand of this specific set of MG configurations has small variations throughout the day and is supplied by small coal technologies in most cases. At the international level, the Northwest European electricity market described by COMPETES with and without MG configurations is presented. Results show that decentralized power generation brings improvements to the network, especially relative to the monetary aspects, and to the resiliency of the network which in this work is considered as the percentage of MG penetration in the network. The inclusion of MGs replaces part of the coal and a high percentage

of NG production in the main grid, indicating that, as for the case of a three node system, industrial MGs play an important role in the synthesis/design/performance of the network, because the load demand of this specific set of MG configurations has small variations throughout the day and is supplied by integrated gasification (IGCC) technologies based on waste in most cases. Renewable energy sources, i.e., PV, hydro and wind, located in the MGs play an important role in the production of the total load of the network. Note that although generation reliability considerations are included in the national level results, they are not at the international level.

As to social sustainability considerations, they are not included in the analysis developed in this work due to the fact the prior work in the literature suggests that they are unlikely to alter the final quantitative results. It is nonetheless important to understand the perceptions of different stakeholders and most important, the users, towards the inclusion of decentralized technologies into the main grid. Furthermore, although the use of value functions and a weight assignment process are potentially useful tools for obtaining a most desirable solution from among the optimum solutions in the Pareto set, a detailed analysis in agreement with [45] applying multicriteria decision making methods to analyze the trend of the Pareto sets is necessary when dealing with more complex systems.

As a final remark, the methodology presented here must eventually be coupled with the lower-level SAF in order to obtain the global optimum for the synthesis/design/operation of the network configuration system. In the lower-level SAF [43], the detailed exergo-environomic optimization of individual energy producers and storage technologies acting in concert within a microgrid is obtained. The producers and microgrids optimized at this lower level depends on the optimum results found at the upper level and vice versa. Thus, an iterative process is required to converge the results of these two levels of assessment. This is left for future work.

Part II

Steepest-Entropy-Ascent Quantum Thermodynamic Modeling of Decoherence in Two Quantum Composite Systems

Chapter 6

Introduction to SEA-QT

The beginnings of Intrinsic Quantum Thermodynamics (IQT) from which the mathematical framework of Steepest-Entropy-Ascent Quantum Thermodynamics (SEA-QT) derives can be traced back to the work of Hatsopoulos and Keenan [251] who provide a precise and general definition of the second law of thermodynamics in 1965 from which all other statements such as that of Clausius, that of Kelvin and Planck, and that of Caratheodory follow as theorems. Eleven years later, in 1976, IQT sees the light for the first time as a fundamental theory when Hatsopoulos and Gyftopoulos [252–255] publish their seminal series of papers postulating the *Unified Quantum Theory of Mechanics and Thermodynamics* (i.e. IQT) with the aim of reconciling Quantum Mechanics (QM) and Equilibrium (Classical) Thermodynamics (ET) into a single theory with a single kinematics and dynamics. Within this new theory, Hatsopoulos and Gyftopoulos address a fundamental need to which Park [256] points for a density operator which recovers the concept os state of system lost when the density operator of Quantum Statistical Mechanics (QSM) is used as the so-called "state operator" for mixed or non-pure states. Hatsopoulos and Gyftopoulos do so by postulating a density operator based on an ensemble of identical systems unambiguously prepared [255]. In 1981, Beretta [257] complets the dynamical postulate of this theory when he postulats a new equation of motion based on the principle of Local-Steepest-Entropy-Ascent, which incorporates both the first and second laws of thermodynamics and completes what is missing in QM, namely, a description of irreversible relaxation to stable equilibrium. The Hatsopoulos-Gyftopoulos-Park-Beretta theory is subsequently renamed Quantum Thermodynamics by Beretta and colleagues [258] and then Intrinsic Quantum Thermodynamics [259] to distinguish this theory from the use of the term *Quantum Thermodynamics* (QT) which has been adopted by others to

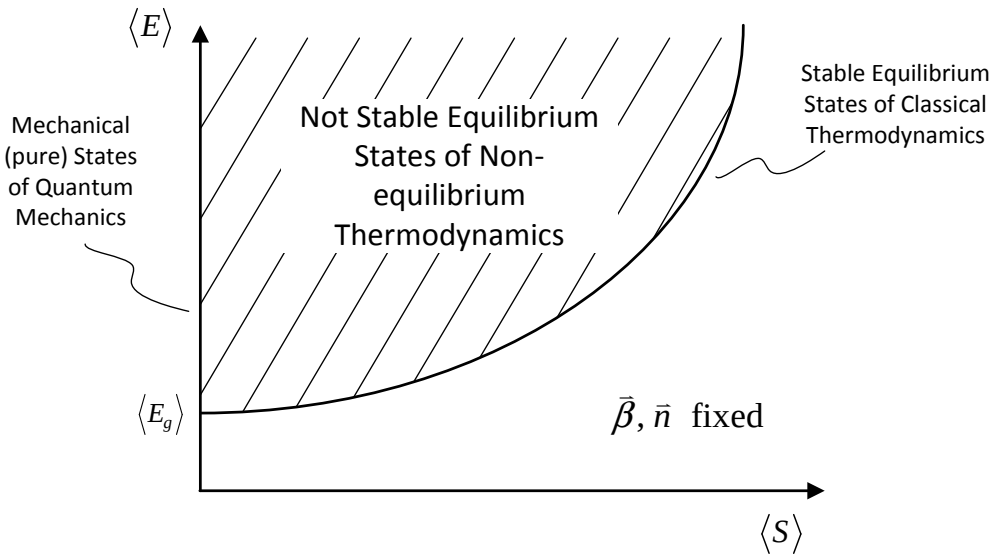

Figure 6.1. Depiction of all possible system states in the energy-entropy plane. $\vec{\beta}$ is the set of all parameters (e.g., volume, magnetic field strength, etc.), and $\vec{n}$ the set of constituents [4].

describe the field of Dissipative Quantum Dynamics (DQD) [260, 261]. More recently, Beretta and co-workers [262] have adopted the name SEA-QT to distinguish the fundamental theory of IQT from the mathematical framework applied to the modeling of non-equilibrium irreversible processes of atomistic-level systems.

6.1 Quantum Mechanics (QM)

QM and ET are fundamental theories of physical reality which were developed independently and have enjoyed great success. QM using a fundamental level of description describes the kinematics of pure system states, that is, all possible states represented by the vertical axis of the Energy ($\langle E\rangle$)–Entropy ($\langle S\rangle$) diagram depicted in Figure 6.1 . The governing equation for the evolution of these system states is given by the Schrödinger wave equation, namely,

$$i\hbar\frac{\partial}{\partial t}\Psi(\vec{q},t) = H(\vec{q},t)\,\Psi(\vec{q},t) \tag{6.1}$$

where $\Psi(\vec{q},t)$ is the state or wave function, $\vec{q} = \{q_1, q_2, \ldots, q_n\}$ the set of Q orthogonal spatial coordinates that constitute the Q-dimensional Hilbert space, $\mathscr{H}$, t the time, $\hbar$ Planck's modified constant[1], and H is the Hamiltonian operator given by the sum of the kinetic (T) and potential (V) energy operators of the system, i.e.,

[1] $\hbar$ =h/2π where Planck's constant is $h = 6.626069 \times 10^{-34}$ kg m^2 s^{-1}.

$$H(\vec{q},t) = T + V = -\frac{\hbar^2}{2m}\nabla^2 + V(\vec{q},t) \tag{6.2}$$

where ∇^2 represents the Laplacian operator. When the Hamiltonian of the system is independent of time, that is $H = H(\vec{q})$, the state function can be separated as the product of a time-independent function, $\phi(\vec{q})$, and a time-dependent function, $\psi(t)$, such that

$$\Psi(\vec{q},t) = \phi(\vec{q})\,\psi(t) \tag{6.3}$$

Applying the method of separation of variables [263], Equation (6.1) can be represented by the two-equation set

$$H(\vec{q})\,\phi(\vec{q}) = \varepsilon\,\phi(\vec{q}) \tag{6.4a}$$

$$i\hbar\frac{\partial}{\partial t}\psi(t) = \varepsilon\,\psi(t) \tag{6.4b}$$

Equation (6.4a) is the time-independent Schrödinger equation or energy eigenvalue equation where $\phi(\vec{q})$ is the energy eigenfunction that provides the stationary energy eigenstates of the system, and ε is the energy eigenvalue[2] of the Hamiltonian operator that represents the numerical result obtained from a measurement of the energy (physical observable) of the system. The solution to this eigenvalue equation provides information about the degrees of freedom available for distributing the energy of the system, i.e., it provides the energy spectrum (energy eigenlevels) as well as the corresponding state vectors of the quantum system.

Equation (6.4b) is the time-dependent Schrödinger equation or equation of motion of QM. The solution to this Hamilton-Jacobi differential equation provides information on how the phase of the energy is distributed among the different energy eigenlevels of the system as the system state evolves in time from some initial state, $\psi(t_0) = \psi(0)$, to a subsequent state, $\psi(t > t_0) = \psi(t)$. In other words, knowing the energy structure of the quantum system found from a solution of Equation (6.4a), the evolution of the state of the system can be known by integrating the equation of motion, resulting in

$$\psi(t) = e^{-\frac{i}{\hbar}Ht}\,\psi(0) \tag{6.5}$$

[2]An energy eigenvalue is always a real number for the case when $H = H^\dagger$, where $H^\dagger$ is the Hermitian conjugate or self-adjoint operator of the Hamiltonian. The numerical value of the eigenvalues of the system is predicted using Equation (6.4a). Every time that a measurement is performed on the system, the numerical value of one of the eigenvalues of the system is obtained; nevertheless, it is not possible to know exactly what eigenvalue, among all the possible, is going to be obtained before the measurement is performed.

This evolution in time represents a unitary transformation as expressed by

$$U(t, t_0) = e^{-\frac{i}{\hbar}H(t-t_0)} \tag{6.6}$$

The general solution to Equation (6.1) is then given by the product of the solutions to the static and dynamic Schrödinger equations

$$\Psi(\vec{q}, t) = \phi(\vec{q})\, e^{-\frac{i}{\hbar}H(t-t_0)}\, \psi(0) \tag{6.7}$$

6.2 Mathematical concepts of QM and Dirac notation

Heisenberg and Schrödinger developed the mathematical language for the representation of QM based on the fundamental work postulated by Planck and Bohr. Heisenberg, using a matrix language, developed his work in order to describe the discrete behavior (quantized space) of matter, while Schrödinger, using the mathematics of the wave function, developed his work in order to provide a description for the spectrum behavior (continuous space) of matter. Years later, Dirac developed a mathematical framework that encompasses both Heisenberg's and Schrödinger's notation, using a *ket–bra–operator* representation.

The ket, $|\alpha\rangle$, is represented by a column matrix which contains the elements of a state vector (eigenvector) that belongs to a Hilbert space. The bra, $\langle\gamma|$, is represented by a row matrix which contains the elements of a vector that belongs to a dual Hilbert space. The bra and ket have a one-to-one correspondence, that is, for a given ket there exists one and only one bra. Using the scalar product, $(\alpha, \gamma) = \langle\alpha|\gamma\rangle$ [3], Equation (6.3) can be rewritten as

$$\Psi(\vec{q}, t) = \langle\vec{q}, t|\Psi\rangle \tag{6.8}$$

which indicates that the state or wave function $\Psi(\vec{q}, t)$ is the projection of $|\Psi\rangle$ onto the space $\langle\vec{q}, t|$. In addition, every physical observable of a system is represented by a linear Hermitian operator, A, for which the classical value of that observable corresponds to the expectation or mean value, $\langle A\rangle$, of an infinite number of measurements taken over an infinite number of identical systems, respectively, each in some state. For the case of the energy, its expectation value is given as

$$E = \langle E\rangle = \sum_{i=1}^{\infty} |c_i(t)|^2\, \varepsilon_i \tag{6.9}$$

[3]The scalar product is non-commutative, that is, $(\alpha, \gamma) \neq (\gamma, \alpha)$.

where ε_i are the energy eigenvalues corresponding to the $|\phi_i\rangle$ eigenvectors or eigenstates that represent the basis in the Hamiltonian representation, $|c_i(t)|^2$ is the probability density or the probability that the system will be found in a given eigenstate, and $c_i(t)$ is the probability amplitude given by

$$c_i(t) = \langle \phi_i | \psi(t) \rangle \tag{6.10}$$

where the normalization condition $\langle \psi(t) | \psi(t) \rangle = \sum_{i=1}^{\infty} |c_i(t)|^2 = 1$ must be satisfied.

According to the Heisenberg uncertainty principle, the wave function cannot be measured directly. Nevertheless, using the concept of wave packet, the state of a quantum system can be described as a linear combination of the eigenstates in which the system can be found. For a quantum system with n discrete energy eigenlevels, the state vector is given by

$$|\psi(t)\rangle = c_1\phi_1 + c_2\phi_2 + \ldots + c_n\phi_n = \sum_{i=1}^{n} c_i(t)\,|\phi_i\rangle \tag{6.11}$$

6.3 Equilibrium Thermodynamics

Several definitions are presented below in order to provide a clear reading of what follows. These definitions are based on those provided by Gyftopoulos and Beretta [4], and the reader is encouraged to review this source for further clarifications. The first definition is that of a *system*, which is a collection of constituents subject to internal and external forces. The constituents are specified by the type and amount n_i of each of the distinguishable species (e.g., particles, fields, etc.) The internal forces correspond to those of attraction and repulsion among the constituents for which the magnitude and range of application of these forces need to be specified. The external forces correspond to every external restriction imposed on the system (parameters, $\vec{\beta}$) such as the volume delimited by the walls of a container. The magnitude and range of application of these forces need to be specified. The second definition is that of a *property* as an intrinsic characteristic of the system whose value is specified at a given instant of time. The numerical value of each property corresponds to the expectation (mean) value of an infinite number of measurements performed on an ensemble of identical systems. The third definition is that of *state*, characterized by the values of all the independent intensive properties of the system at a given instant of time. In order to go from some initial state to some final state, the system undergoes a *process*. The evolution of the state of a system in time is given by the equation of motion of SEA-QT, or alternatively by

the conservation and entropy balances which result from the first and second laws of thermodynamics. Using a phenomenological level of description, ET describes the evolution in state of a system whose initial and final states are in stable equilibrium, i.e., which for a system with fixed parameters, $\vec{\beta}$, and fixed amount of constituents, $\vec{n}$, fall on the convex curve shown in Figure 6.1 represented by $E = E(S, \vec{\beta}, \vec{n})$. For variable $\vec{\beta}$ and $\vec{n}$, $E = E(S, \vec{\beta}, \vec{n})$ in fact represents the hypersurface of possible stable equilibrium states in which the system can be. Note that knowledge of $E = E(S, \vec{\beta}, \vec{n})$ along with differentiation and algebraic manipulation is sufficient for deriving all thermodynamic stable equilibrium properties.

The first law of thermodynamics, as formulated by Gyftopoulos and Beretta [4], implies the existence of the property *energy* which can be proven to be additive as well as conservative. The second law of thermodynamics, as formulated by Hatsopoulos and Keenan [251], asserts the existence and uniqueness of stable equilibrium states and leads to general definitions of the non-conserved properties of generalized adiabatic availability and generalized available energy. A general definition for the entropy valid for all states and systems then results from a combination of the first and second laws [264, 265]. As to the *adiabatic availability*, it represents the maximum energy that can be extracted in a reversible adiabatic process from a closed system with fixed $\vec{\beta}$ and $\vec{n}$, is non-additive, and has a value of zero at stable equilibrium. In a similar fashion, the *available energy* represents the maximum energy that can be extracted in a reversible adiabatic process from the composite of a closed system with fixed $\vec{\beta}$ and $\vec{n}$ and a reservoir, is additive, and has a value of zero when the system is in a state of mutual stable equilibrium with the reservoir. The generalized versions of these las two properties allow for variable $\bar{\beta}$ and $\bar{n}$.

6.4 Motivation to use the SEA-QT framework of IQT

The mathematical foundations of Quantum Statistical Mechanics (QSM) were developed by von Newmann [266] based on the concept of the state operator of a system with the purpose of describing the non-pure states of a system in the region of not-stable equilibrium states depicted by the hashed region in Figure 6.1. According to von Newmann, the state operator contains all the information of a quantum mechanical system at a given instant of time. In QSM, the state operator, ρ_{QSM}, of the system is provided by an ensemble of identical systems ambiguously prepared, that is, a heterogeneous ensemble [255] within which each member system is prepared in a different

pure state represented by ρ_i^{QSM}, so that ρ_{QSM} is expressed as the statistical average given by

$$\rho_{QSM} = \sum_{i=1}^{N} w_i \rho_i^{QSM} \tag{6.12}$$

where

$$\rho_{QSM} \neq \rho_1^{QSM} \neq \rho_2^{QSM} \neq \dots \tag{6.13a}$$

$$\rho_i^{QSM} = (\rho_i^{QSM})^2 = |\psi_i\rangle \langle\psi_i| \tag{6.13b}$$

The w_i are the weights or statistical mechanical probabilities corresponding to the contribution of each of the ensemble members and must satisfy the normalization condition

$$\sum_{i=1}^{N} w_i = 1 \tag{6.14}$$

In order to obtain the entropy of the system at a given state, von Newmann proposed the following expression

$$\langle S(\rho_{QSM})\rangle = -k_B \mathrm{Tr}\left(\rho_{QSM} \ln \rho_{QSM}\right) \tag{6.15}$$

where k_B is Boltzmann's constant[4].

However, a state operator based on a heterogeneous ensemble is inconsistent with the second law of thermodynamics and leads to a perpetual motion machine of the second kind (PMM2), i.e., there is a contradiction between the state of the ensemble and the states of the members of the ensemble relative to the thermodynamic property, the adiabatic availability [4]. This property is not conserved and is a measure of the quality of the energy of the system at any given instant of time, providing with a measure of the maximum amount of energy which can be extracted from the system in a reversible adiabatic work interaction.

The PMM2 arises when the state of the ensemble as represented by ρ_{QSM} is in an equilibrium state for which the adiabatic availability is necessarily zero. However, all members of the ensemble are in pure states, all with an adiabatic availability greater than zero, thus, suggesting that energy can be extracted from the members of the ensemble yet not from the ensemble as a whole. This, of course, cannot be.

[4]Boltzmanns constant is $k_B = 1.380648 \times 10^{-23}\ \mathrm{kg\ m^2\ s^{-2}\ K^{-1}}$

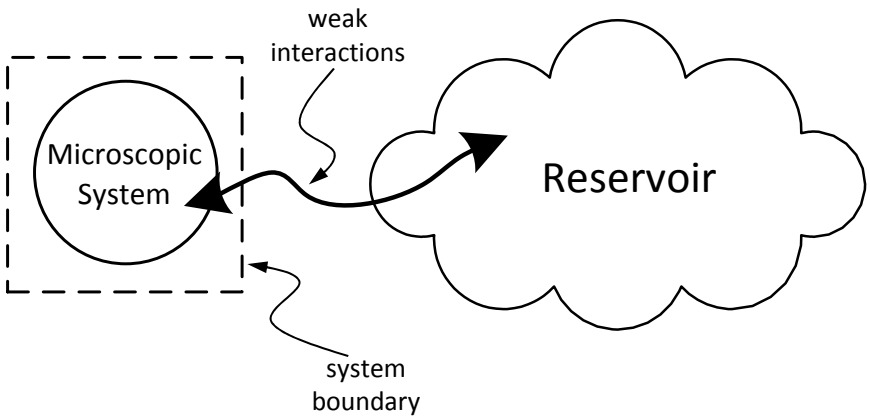

Figure 6.2. Depiction of the "open system" model of DQD which consists of a closed system reservoir coupled by weak interactions.

Another fundamental weakness of the QSM state operator unlike its classical statistical mechanical counterpart for which the state of the ensemble coincides with the state of the system is that in QSM this is no longer the case [256]. Thus, a bedrock of physical though, "the state of the system" is lost.

A final point is that even though the state operator of QSM was developed to represent non-pure states, the equation of motion of QM, the time-dependent von Newmann equation, cannot describe the irreversible evolution in state of a system described with such a state operator from one non-pure state to another.

Two different approaches to address this lacune have been phenomenological modifications of the time-dependent Schrödinger (or equivalent von Newmann) equation to include so-called frictional terms that introduce a non-linear dynamics into the equation of motion able to describe irreversible relaxations in state [256, 266–271] and the development of the so-called master equations of Dissipative Quantum Dynamics (DQD) often now referred to as Quantum Thermodynamics (QT). Among the weaknesses of the first of these is the use of phenomenological terms to describe the non-linear dynamics absent from the exclusively linear dynamical description of the time-dependent Schrödinger equation. Such a phenomenological description fails to capture the fundamental character of the irreversible phenomena if present at the atomistic level.

The second approach which comes from DQD or QT modifies the time-dependent von Newmann equation using the so-called "open system" model depicted schematically in Figure 6.2 and consisting of a closed system plus reservoir[5]. The level of description remains at a fundamental

[5]The term "closed system" here takes the meaning used in thermodynamics of a system which may be isolated or not, and if not, can undergo work and heat interactions but not mass interactions.

level, but the non-linear dynamics is mimicked with a linear dynamics intended to describe the irreversible phenomena present. The latter are assumed to result from weak interactions between the system and reservoir which build up correlations between the two that "dissipate" in a time frame significantly shorter than that of the system's state relaxation to stable equilibrium, i.e., the so-called Born-Markov approximation [260, 261].

A major problem with this approach is that it is not general since, as pointed out by Nakatani and Ogawa [272], the Born-Markov approximation fails when the coupling becomes strong, thus, negating the very mechanism assumed to be the cause of the irreversible relaxation to stable equilibrium. Furthermore, the dissipative behavior which this model describes is one of a "loss of information", i.e., loss of correlations, relative to the exogenous statistics of the coupling and leads at a quantum level to the so-called Loschmidt paradox[6] [273].

Nonetheless, despite these problems, a number of quantum master equations (QMEs) have been developed and used with some success [274–278]. Among these is that provided by Kossakowski and Lindblad [279–281] given by

$$\frac{\mathrm{d}\rho_{QT}}{\mathrm{d}t} = -\frac{i}{\hbar}\left[H, \rho_{QT}\right] + \sum_{j}^{N} h_j \left(L_j \rho_{QT} L_j^{\dagger} - \{L_j^{\dagger} L_j, \rho_{QT}\}\right) \tag{6.16}$$

where the first term on the right hand side provides the linear dynamics to the von Newmann equation of motion, while the second models the weak interactions (loss of information) of the system with the reservoir. N is the dimension (degrees of freedom) of the system. The h_j are constants used to model the strength of the dissipation dynamics and depend on the specific system under analysis. The L_j are the Lindblad operators and represent the effects on the system caused by the system-reservoir interaction. The dissipative dynamics in this equation are strictly linear.

The results obtained with QT have been useful in treating irreversible and non-unitary evolutions in physics and chemical kinetics [282]. Nevertheless, the fundamental weakness is still there, i.e., that the irreversible relaxation of system state is due to the loss of information attributable to an exogenous statistics and is, thus, merely a mathematical and not physical characteristic of the system.

IQT uses and is a similar mathematical framework as QSM and QT but with fundamental changes in the conceptual bedrock, especially in the type of ensemble used to represent the state of

[6]The Loschmidt paradox (or irreversibility paradox) states that the extraction of irreversible, non-unitary information from an intrinsically reversible (unitary) process is a contradiction.

the system. Consequently, the state operator is based on a homogeneous preparation of identically prepared systems so that the state of the ensemble is reflected in the state of each of the sub-ensembles or systems, namely,

$$\rho = \rho_1 = \rho_2 = \dots \tag{6.17}$$

preserving the bedrock physical concept of the state of the system since the state of the ensemble coincides with that of the system itself [256][7]. In this view, the entropy is an intrinsic property of the system, which at any given instant of time is a measure of how the system energy is distributed among the different degrees of freedom (energy eigenlevels) of the system, while the generation of entropy reflects the internal redistribution of system energy resulting from a change in state with a consequent destruction of system adiabatic availability. Thus, the state of an isolated system is viewed as spontaneously relaxing to stable equilibrium as a result of this redistribution of energy within its own internal quantum structure and not as the consequence of some sort of external interaction with a reservoir or environment.

The entropy of IQT [283] is defined by the von Newmann entropy equation with the difference that the state operator of QSM is replaced by the state operator of IQT [283] such that

$$\langle S(\rho) \rangle = -k_B \mathrm{Tr} \left(\rho \ln \rho \right) \tag{6.18}$$

In general, the non-linear IQT equation of motion used in the SEA-QT framework consists of two terms, the first of which captures the unitary, Hamiltonian dynamics of the Schrödinger-von Neumann equation, and the second which models the non-linear dynamics of the dissipative evolution in state based on the principle of SEA subject to the relevant dynamical constraints [284–287]. In particular, for the case of a system composed of two or more distinguishable (separable or non-separable, i.e., interacting or non-interacting) subsystems, the form of the IQT/SEA-QT equation ensures that the evolution in state follows in correlated or uncorrelated local states the path of locally-perceived SEA [288].

Within the SEA-QT framework, the dissipative aspects of the time evolution emerge from the non-Hamiltonian term in the equation of motion. Thus, instead of focusing on the non-Hamiltonian

[7] As pointed out by Park [256], initially, when the density operator is based, as it is in Equation (6.12), on an ambiguous preparation of states, i.e., on a so-called heterogeneous ensemble of identical systems in differing states, the state of the ensemble no longer coincides with that of the system.

effects of the interactions between the microscopic system and its surroundings, the SEA-QT description assumes the composite system to be isolated and its time evolution to be intrinsically non-Hamiltonian. In so doing, the equation predicts a loss of quantum entanglement or coherence consistent with that observed in recent experiments [289–292]. Note that the dissipative dynamics in the equation of motion are strictly non-linear.

6.5 Dissertation objectives and originality for SEA-QT

The overall objective of this part of this doctoral research is to apply the alternative and comprehensive framework of SEA-QT and its dynamical law of time evolution along the locally perceived direction of SEA, which effectively implements on a local basis maximal entropy production (LMEP) [257]. This is used to model the non-linear dynamic behavior of a general (closed and adiabatic) microscopic system as its state evolves in time towards stable equilibrium. In particular, the purpose is to provide a description of the phenomenon of the decoherence and loss of correlations existent among the different constituents of the composite microscopic system.

Two different models of application are considered: one in which the general system is composed of two particles of type spin-$^1/_2$ (quantum bit or qubit [8]), and the other in which the general system consists of a particle and a photon field. These models represent two of the simplest compsite systems encountered in Nature.

The aim is to demonstrate that for a general quantum system in any non-equilibrium state, the entanglement and correlations, which may exist among the states of the constituents (i.e., distinguishable and indivisible particles) that comprise the system, disappear as the system evolves towards a state of stable equilibrium. To demonstrate the generality of the postulated decoherence, and using the particle-particle composite system, a scheme for randomly generating the initial non-

[8]The principle of quantum computing relies on the superposition principle of QM, that is, the simplest quantum computer is that composed of one pair of two-level systems (quantum bits or qubits) interacting with each other. If one of the systems (the driver) remains unchanged, the other qubit (the slave) remains unchanged as well. On the other hand, if the state of the driver is switched to its exited state, the slave undergoes a well-defined change of state as well. However, if the driver is in a superposition state (the states of a qubit are 0 and 1), the output of the system is entangled; and the two qubits are correlated (i.e., they are in a nonseparable state) so that the interaction among qubits can lead to a transfer of information at a quantum level. In this way real problems can be solved in parallel. Nevertheless, this massive transfer of information relies on how well the entanglement or correlation (transfer of information) is performed so that if the correlation between the qubits is lost, the ability to transfer information between the qubits is diminished as well, and the performance of the quantum computer is lowered, possibly even to the point of inoperability.

equilibrium states is developed and the time evolution of a well-chosen subset of all such possible states studied.

In order to achieve the overall objective outlined above, the following set of tasks is envisioned:

- Gain a deep understanding of the foundations, concepts, and mathematical framework of IQT and its mathermatical framweork SEA-QT.
- Study and understand the behavior of spin-$^1/_2$ and quantum harmonic oscillator systems within the framework of QM.
- Study the principles of Cavity Quantum Electrodynamics (CQED).
- For the particle-particle composite system, develop and apply a methodology to obtain a general initial non-equilibrium state based on a random and homogeneous mapping of the local two-dimensional geometrical spaces of each constituent.
- Deveop a particle-photon field model for the CQED experiments performed by Haroche and co-workers [291–293].
- Predict the evolution of state for the particle-particle and particle-photon field systems using the equation of motion of SEA-QT.
- Demonstrate in a general fashion that the irreversible evolution in state of the system results in a spontaneous decoherence, i.e., a loss of the entanglement and correlation between the states of the constituents of the composite systems.
- For the particle-photon field system, compare the numerical results obtained with SEA-QT framework to experimental data available from the literature (i.e., that generated by Haroche and co-workers [291–293]).
- Analyze the results and draw general conclusions of the cause of decoherence and its impact on nano-scale applications; suggest ways to mitigate it.

An original contribution to the literature of the research proposed in this dissertation is the use of the SEA-QT framework to numerically model as generally as possible the phenomenon of decoherence and its causes using particle-particle and particle-photon field systems. In addition, for the particle-particle composite system, a heuristic analysis of the rate of change of the correlation functional corresponding to the contribution of the dissipative term of the equation of motion is developed. This heuristic analysis aims to confirm (not prove) that this term is always non-negative as long as the composite system relaxes to a state of stable equilibrium starting from any non-pure,

non-equilibrium state, i.e., that the dissipative term of the equation of motion only destroys correlations between the constituent parts of the system. Furthermore, for the particle-photon field composite system, the decoherence results are compared with experimental data found in the literature. The analysis is a first application for this equation, which has never been applied nor experimentally compared with experimental data. Finally, a suggestion for mitigating the decoherence of general quantum systems also represent an original contribution to the literature.

6.6 Overview of next chapters

In the present chapter, an overview of the motivation to develop this research as well as the goal to provide an alternative and comprehensive description of the phenomenon of decoherence at atomistic levels have been presented. Chapter 7 presents a description of the foundations of IQT and its mathematical framework SEA-QT with a brief introduction to the *Unified Quantum Theory of Mechanics and Thermodynamics* as well as the dynamical postulate and the postulation of the equation of motion. In addition, recent theoretical developments and applications to specific problems, including chemically reactive systems, hydrogen storage in carbon nanotubes, and the modeling of the relaxation of other isolated single constituent systems is presented. Also, comparison of previous SEA-QT modeling predictions with experimental data from the literature is presented. To conclude the chapter, a description of the phenomenon of coherence and its modeling using the DQD or QT approach available in the literature are provided. Chapter 8 provides the mathematical description of the composite systems considered here, namely, those for particle-particle and particle-photon field. A review of the approaches to model a two-level-type particle and a quantum harmonic oscillator that describe particles and photon fields, respectively, are given. A methodology to randomly generate initial non-equilibrium states for the particle-particle general system is presented. To conclude the chapter, the method and computational programs used to solve the system of differential equations is outlined. Chapter 9 discusses the results of the modeling of decoherence for the two different general microscopic systems under analysis. Finally, Chapter 10 provides a summary of the research in this part of the dissertation and makes recommendations for mitigating the decoherence between the constituents of composite systems.

Chapter 7

Literature Review for SEA-QT

In this chapter, the essence of the seminal papers of Hatsopoulos and Gyftopoulos [252–255] is discussed in order to outline the foundations on which IQT and its mathematical framework SEA-QT rest. The principal application of this theory by Beretta [257, 258, 284–288, 294–300] as well as the applications and extensions developed by von Spakovsky and co-workers [259, 262, 301–306] in recent years are presented. In addition, experimental validations of SEA-QT framework for single constituent quantum systems is provided. To date and to the best knowledge of this author, the application of the SEA-QT framework has been restricted to single constituent quantum systems. This has led to the present motivation of developing an application of the SEA-QT equation of motion for a composite quantum system with the goal of gaining an understanding not only of this equation but of the behavior of this type of system. The application developed here is that of modeling such systems, particularly from the stand point of the decoherence, coherence, and entanglement between the constituents of the system. In addition, anther goal is to provide a heuristical analysis of the dissipative term of the SEA-QT equation of motion to show that it drives the non-negative rate of the entropy correlation functional to zero as the state of the system relaxes to stable equilibrium. Previous work devoted to entanglement, coherence, and decoherence is presented at the end of this chapter together with the most relevant applications of these phenomena to quantum computing and quantum information.

7.1 Foundations of SEA-QT

Recalling Hatsopoulos and Beretta [307], the challenge in the 19^{th} century was to set the foundations of entropy and the second law of thermodynamics which Clausius, Carnot, Joule, Watt,

Kelvin, Plank, Caratheodory, and others did, stating, for example that *"it is impossible to transfer energy from a low temperature body to a high temperature body"* (Clausius statement) [308]. The Clausius statement together with that of Kelvin-Planck and Caratheodory were probably the most widely accepted statements of the second law of thermodynamics throughout the 19^{th} and 20^{th} centuries. Even today, most scientists still view these statements as the formal statements of the second law.

During the 20^{th} century, however, the second law challenge turned on explaining entropy at a microscopic level. A principal outcome of this effort was the bridge between to describe the bridge between QM and ET that was formulated by von Newmann with the development of QSM [266]. An alternative approach was that provided in 1976 by Hatsopoulos and Gyftopoulos with their *"Unified Quantum Theory of Mechanics and Thermodynamics"* [252–255], now known as IQT, proposing a unification of QM and Thermodynamics in which all the possible states of QM and ET are only a subset of this more general theory.

In 1976, the theory of IQT was proposed in a series of four papers. The first [252] presents the postulates of IQT. The first three of these correspond to the postulates of QM, that is, the correspondence principle, the mean-value postulate, and the dynamical postulate. The fourth is the stable equilibrium postulate, which is a formulation of the second law of thermodynamics at a quantum level. The rigorous and general definition of the second law is that postulated in 1965 by Hatsopoulos and Keenan stating that *"for a system with a given energy, with fixed amounts of constituents $\vec{n}$ and parameters $\vec{\beta}$, there exists one and only one stable equilibrium state"* [309]. Previous statements of the second law (e.g., those of Clausius, Kelvin and Planck, and Caratheodory) are simply theorems provable from this most general statement.

The second paper [253] introduces the definition of a property called the *adiabatic availability* which is the *"maximum energy that can be extracted adiabatically from a system by bringing it to stable equilibrium by means of a reversible weight process"*[253]. Adiabatic availability is an extensive property that depends on the state of the system only, is obtained by statistically averaging an infinite number of measurements on the energy of the system, and is less than or equal to the total energy content of the system. Definitions of the extensive properties *available energy* and *entropy* follow naturally from the definition of adiabatic availability. Available energy is defined as *"the maximum energy that can be extracted from a composite of a system-reservoir by bringing the system to mutual stable equilibrium with the reservoir by means of a reversible*

adiabatic weight process" [253], while entropy is defined to be the *internal distribution of system energy among the possible energy eigenlevels of the system*.

The third paper [254] is a continuation of the second in which the second law of thermodynamics and all its consequences, including a definition of stable equilibrium states and mutual and partially mutual stable equilibrium states between systems. The fourth and last paper in the series [255] establishes the basis for the definition of the density or state operator. The state of a system is fully represented by the density operator of IQT which is based on an ensemble of identical systems identically prepared, i.e., the socalled homogeneous ensemble. This definition of *density or state operator* recovers the fundamental physical concept of 'state of the system' lost in QSM as shown by Park [256] and Park and Simmons [310] and avoids the violation of the second law built into the density operator of QSM, which bases the definition of state on a density operator based on an ensemble of identical system ambiguously prepared, i.e., the so-called heterogeneous ensemble.

The four papers of the theory of IQT provide the necessary kinematics and requirements that a dynamical postulate should satisfy for a complete thermodynamic theory applicable to all systems and all states. An equation of motion capable of describing all possible state evolutions of a system, however, was as of yet not discovered.

Five years later, in 1981, Beretta [257] completes the dynamical postulate of the Hatsopoulos and Gyftopoulos paradigm when he postulates an equation of motion to describe the evolution of the state of an isolated single constituent microscopic system [284] and a more general form of this equation to describe the evolution of state of an isolated general microscopic system composed of two or more distinguishable and indivisible constituents [288].

7.2 Further developments and applications of SEA-QT

7.2.1 Recent theoretical extensions of the SEA-QT framework

During the 1990s, an important contribution to the SEAQT framework was that of Gyftopoulos and Cubukcu [283] who provided an analysis of the pletora of entropy relations which exist in the literature and are claimed to represent the entropy of thermodynamics. To distinguish between these relations and verify these claims, the authors propose eight different characteristics that any expres-

sion for the entropy of thermodynamics must satisfy. They are as follow [283]: *"(1) The expression must be well defined for every system (large or small) and every state (stable equilibrium or not stable equilibrium). (2) The expression must be invariant in all reversible adiabatic processes and increase in any irreversible adiabatic process. (3) The expression must be additive for all systems and all states. (4) The expression must be non-negative and vanish for all states encountered in mechanics. (5) For given values of the energy, amounts of constituents, and parameters, one and only one stable equilibrium state must correspond to the largest value of the expression. (6) For given values of the amounts of constituents and parameters, the graph of entropy versus energy of stable equilibrium states must be concave and smooth. (7) For a composite C of two subsystems A and B, the expression must be such that the entropy maximization procedure for C yields identical thermodynamic potentials for all three systems A, B and C. (8) For stable equilibrium states, the expression must reduce to relations that have been established experimentally and that express the entropy in terms of the values of the energy, amount of constituents, and parameters, such as the relation for ideal gases"*.

Table 7.1. Analysis of different entropy relations claimed to be the entropy of thermodynamics [283]. A ✕ indicates that the characteristic is not satisfied; consequently, the subsequent characteristics are not evaluated.

Entropy Relation	Characteristic							
	(1)	(2)	(3)	(4)	(5)	(6)	(7)	(8)
Daróczy [311]: $S = \frac{1}{2^{1-\alpha}-1}(\mathrm{Tr}\rho - 1)$ where $\alpha > 0$, and $\alpha \neq 1$	✓	✓	✕					
Hartley [312]: $S = k_B \ln N(\rho)$ where $N(\rho)$ is the number of positive eigenvalues of ρ	✓	✓	✓	✓	✕			
Infinite norm [312]: $S = -k_B \ln \|\rho\|_\infty$ where $\|\rho\|_\infty = \rho_{\mathrm{largest}} =$ largest eigenvalue of ρ	✓	✓	✓	✓	✓	✕		
Rényi [313]: $S = \frac{k_B}{1-\alpha}\ln(\mathrm{Tr}\rho^\alpha)$ where $\alpha > 0$, and $\alpha \neq 1$	✓	✓	✓	✓	✓	✓	✕	
von Newmann [314]: $S = -k_B \mathrm{Tr}\rho \ln \rho$	✓	✓	✓	✓	✓	✓	✓	✓

The entropy relations analyzed by Gyftopoulos and Cubukcu are shown in Table 7.1. Entropy expressions based on temperature and heat, expressions proposed in statistical classical mechanics, and expressions from statistical quantum mechanics that depend on variables other than the eigenvalues of the density or 'state' operator ρ are excluded because they are defined for stable equilibrium states only and are, thus, not general; or the density operator for the system is a statistical mixture of zero-entropy operators corresponding to each element of an ensemble and is, thus, inconsistent with the second law of thermodynamics; or fail criterion (2), respectively.

Of those evaluated in Table 7.1 with respect to the eight characteristics listed above, only the von Newmann entropy relation exhibits all eight characteristics provided that the density operator is that obtained from a homogeneous ensemble of identical systems identically prepared.

During the 2000s, the developments of the SEA-QT framework gained momentum again when Gheorghiu-Svirschevski [315, 316] derived the equation of motion using a variational principle, rediscovering the novel approach for nonlinear quantum dynamics that was postulated twenty years earlier by Beretta [257]. Caticha [317] and Lemanska and Jaeger [318] also made attempts to derive the equation of motion for quantum and non-quantum probability distributions, respectively. The result of the work of Caticha is the equivalent of the equation of motion of SEA-QT for a continuous probability density function, while that of Lemanska and Jaeger provides a description of the state evolution for a state operator with non-zero probabilities only, i.e., it does not maintain unpopulated a probability whose value is zero initially as is demonstrated in [286]. In addition, the equation of motion of the Lemanska and Jaeger framework only represent a semi-group (unlike the SEA-QT equation of motion which represents a full group) and is, thus, not reversible in time [286].

After the rediscovery of the dynamical law of SEA-QT by Gheorghiu-Svirschevski [315, 316], several other important contributions to SEA-QT were developed by Beretta such as the derivation of Onsager's reciprocity and Callen's fluctuation-dissipation relations, a description of the internal-relaxation time compatible with the time-energy Heisenberg uncertainty principle providing a lower bound for this internal-relaxation time constant or functional of the state operator, the implication of the local maximum entropy production principle in the constituents of composite systems, a description of the necessary conditions for the Schrödinger-von Newmann equation to be compatible with the laws of thermodynamics, numerical results for the SEA-QT state evolution of a closed and single-particle system forward and backwards in time from an initial

non-equilibrium state, numerical comparisons of the SEA-QT equation of motion for an isolated closed system with other dynamical equations such as that proposed by Lemanska and Jaeger [318], numerical results for the visualization of the behaviour of the equation of motion for a single constituent system in order to corroborate that the equation of motion satisfies all the characteristics postulated in [257, 284, 288], explaination of the importance of providing a description of the internal-relaxation time functional and the extension of the nonlinear dynamics to systems composed of two or more particles interacting whith each other in wich entanglement and correlations are present, reformulation of the steepest-entropy-ascent framwork in terms of square-root probabilities, description of the Onsager reciprocity relations far from equilibrium, and a phenomenological description of heat interactions for a single constituent system interacting with a heat reservoir. [258, 286, 287, 295–300]. Note that the nomenclature used in previous publications by Beretta in [257, 284, 285, 288, 294] is changed to a more compact form. The underlying theory, however, is the same.

The geometrical construction of the dynamical postulate of SEQ-QT is described in [257, 258, 284–288, 294–300]. A brief description of the derivation of the equation of motion using this geometrical construction is provided below using the nomenclature developed in [287, 319]. To begin with, the state operator ρ is represented as

$$\rho = \gamma^{\dagger}\gamma \tag{7.1a}$$

where

$$\gamma = U\sqrt{\rho} \tag{7.1b}$$

and

$$U^{\dagger} = U^{-1} \tag{7.1c}$$

in order to assure that the density operator is positive at all times. The operator U can be assumed to be equal to the identity matrix, I. From unitary Hamiltonian dynamics, the equation of motion in the square root of the density operator representation is expressed as

$$\dot{\gamma}_H = \frac{i}{\hbar}\gamma\,\Delta H \tag{7.2}$$

or equivalently

$$\dot{\rho}_H = -\frac{i}{\hbar}[H, \rho] \tag{7.3}$$

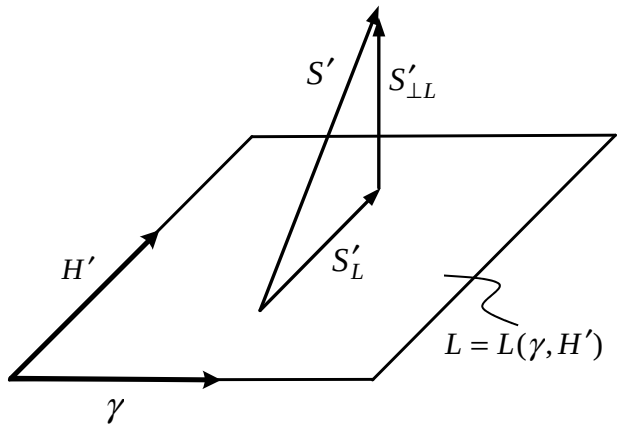

Figure 7.1. Representation of the steepest-entropy-ascent geometrical construction [319].

where

$$\Delta H = H - \langle H \rangle I \tag{7.4}$$

is the deviation operator of H.

Now, if it assumed that

$$\dot{\gamma} = \dot{\gamma}_H + \dot{\gamma}_D \tag{7.5}$$

where $\dot{\gamma}_D$ is in the direction of steepest entropy ascent but restricted in such a way that the energy is conserved (i.e., for an isolated system, $\dot{\gamma}_D \cdot H' = 0$ where $H' = 2\gamma H$) and the unit trace of the the density operator is preserved at all times (i.e., $\dot{\gamma}_D \cdot \gamma = 0$), then $\dot{\gamma}_H$ and $\dot{\gamma}_D$ must be orthogonal to each other.

Figure 7.1 shows the steepest-entropy-ascent geometrical representation given mathematically as

$$S' = S'_{L(\gamma,H')} + S'_{\perp L(\gamma,H')} \tag{7.6}$$

where $S' = -4k_B\gamma \ln \gamma$ represents the entropy gradient vector in state space; $S'_{L(\gamma,H')}$ the orthogonal projection of S' onto the plane or linear manifold $L(\gamma, H')$ formed by the real linear span of vectors γ and H' representing the conservation for the unit trace of the density operator and the energy of an isolated system, respectively; and $S'_{\perp L(\gamma,H')}$ the component of S' that is orthogonal to the plane $L(\gamma, H')$. The latter provides the direction of maximum entropy ascent or maximum entropy production, and is always tangent to the trajectory in state space that the system follows during its relaxation of state to stable equilibrium. Therefore, maximizing the expectation value of

the entropy of the system subject to the constraints $\dot{\gamma}_D \cdot \gamma = 0$ and $\dot{\gamma}_D \cdot H' = 0$, $S' = \dot{\gamma}$ is obtained, and assumming that γ_D is in the direction of $S'_{\perp L(\gamma,H')}$ (i.e., that of the steepest entropy ascent)

$$\dot{\gamma}_D = \frac{1}{4k_B\tau} S'_{\perp L(\gamma,H')} \tag{7.7}$$

where τ is the internal relaxation time which is a real constant or fuctional of ρ. Finally, the equation of motion can be expressed as

$$\dot{\gamma} = \frac{i}{\hbar}\gamma\Delta H + \frac{1}{4k_B\tau} S'_{\perp L(\gamma,H')} \tag{7.8}$$

A more detailed descfiption of the dissipative term, the second term on the right hand side of this equation is provided in Chapter 3 of this dissertation.

One of the contributions made by Beretta [297] is that of a perturbation method at constant system energy [297] to generate an initial non-equilibrium state matrix (in its diagonal form), $p(0)$, such that

$$p(0) = \lambda\, p^{pe} + (1-\lambda)\, p^{se} \tag{7.9}$$

which is a perturbation of the partially canonical distribution function p^{pe} that corresponds to some unstable equilibrium state of the system and is given by

$$p^{pe} = \frac{e^{-\beta^{pe} H}}{\mathrm{Tr}\left(e^{-\beta^{pe} H}\right)} \tag{7.10}$$

or each p_i^{pe} is expressed as

$$p_i^{pe} = \frac{e^{-\beta^{pe} e_i}}{\sum_{j=1}^{N} e^{-\beta^{pe} e_j}} \tag{7.11}$$

with the energy of the system and probabilities constrained by

$$E = \sum_{i=1}^{N} p_i^{pe} e_i \tag{7.12}$$

and

$$1 = \sum_{i=1}^{N} p_i^{pe} \tag{7.13}$$

where the e_i represent the energy eigenvalues of the system, p_i^{pe} is the occupation probability of the *i*-th eigenstate, and β^{pe} a constant which can be viewed as being inversely proportional to some not stable equilibrium temperature. The canonical form at this distribution, p^{pe}, that corresponds to the stable equilibrium state at energy E is given as

$$p^{pe} = \frac{e^{-H/k_B T}}{\mathrm{Tr}\left(e^{-H/k_B T}\right)} \tag{7.14}$$

where T is the stable equilibrium temperature and k_B Boltzmann's constant. It is the solution of Equations (7.11) and (7.12) which yields all the p_i^{pe} and β^{pe} at a given enrgy E. The partially canonical state represented by p^{pe} is then perturbated using Equation (7.9) into a non-equilibrium state to give $p(0)$.

The real positive constant λ in this equation satisfies the condition $0 < \lambda < 1$ where if $\lambda = 1$ the diagonal matrix, $p(0)$, generated reduces to the partially canonical distribution, p^{pe}.

Another important contribution provided by Beretta in [258, 300, 320] is that of establishing a lower bound for the internal-relaxation time, τ, of the equation of motion (Equation (7.8) based on the time-energy Heisenberg uncertainty principle such that for a dingle constituent isolated system

$$\tau^2(\rho) \geq \frac{\hbar^2(\tilde{D}|\tilde{D})}{4\left\langle \Delta H \Delta H \right\rangle} \tag{7.15}$$

where $\tilde{D}$ is a dissipation operator defined as

$$\tilde{D} = \frac{\begin{vmatrix} \sqrt{\rho}\ln\rho & \sqrt{\rho}\,R_0 & \sqrt{\rho}\,R_1 & \cdots & \sqrt{\rho}\,R_z \\ (R_0,\ln\rho) & (R_0,R_0) & (R_0,R_1) & \cdots & (R_0,R_z) \\ (R_1,\ln\rho) & (R_1,R_0) & (R_1,R_1) & \cdots & (R_1,R_z) \\ \vdots & \vdots & \vdots & \ddots & \vdots \\ (R_z,\ln\rho) & (R_z,R_0) & (R_z,R_1) & \cdots & (R_z,R_z) \end{vmatrix}}{\begin{vmatrix} (R_0,R_0) & (R_0,R_1) & \cdots & (R_0,R_z) \\ (R_1,R_0) & (R_1,R_1) & \cdots & (R_1,R_z) \\ \vdots & \vdots & \ddots & \vdots \\ (R_z,R_0) & (R_z,R_1) & \cdots & (R_z,R_z) \end{vmatrix}} \tag{7.16a}$$

whith

$$(F|G) = \frac{1}{2}\mathrm{Tr}\left(F^\dagger G + G^\dagger F\right) \tag{7.16b}$$

Furthermore, the term in the denominator of Equation (7.18) is given by

$$\langle \Delta H \Delta H \rangle = \frac{1}{2} \mathrm{Tr} \left(\rho \left\{ \Delta H, \Delta H \right\} \right) \tag{7.17}$$

where $\langle \Delta H \Delta H \rangle$ is the expectation value of the square of the deviation operator of H.

For the case of a composite isolated system, the lower bound for the internal-relaxation time for each constituent, J, is given as

$$\tau_J^2(\rho) \geq \frac{\hbar^2 (\tilde{D}_J | \tilde{D}_J)_J}{4 \langle \Delta H \Delta H \rangle^J} \tag{7.18}$$

where

$$\tilde{D}_J = \frac{\begin{vmatrix} \sqrt{\rho_J} \left(B \ln \rho \right)^J & \sqrt{\rho_J} \left(R_{0J} \right)^J & \sqrt{\rho_J} \left(R_{1J} \right)^J & \cdots & \sqrt{\rho_J} \left(R_{z(J)J} \right)^J \\ \left(R_{0J}, B \ln \rho \right)^J & \left(R_{0J}, R_{0J} \right)^J & \left(R_{0J}, R_{1J} \right)^J & \cdots & \left(R_{0J}, R_{z(J)J} \right)^J \\ \left(R_{1J}, B \ln \rho \right)^J & \left(R_{1J}, R_{0J} \right)^J & \left(R_{1J}, R_{1J} \right)^J & \cdots & \left(R_{1J}, R_{z(J)J} \right)^J \\ \vdots & \vdots & \vdots & \ddots & \vdots \\ \left(R_{z(J)J}, B \ln \rho \right)^J & \left(R_{z(J)J}, R_{0J} \right)^J & \left(R_{z(J)J}, R_{1J} \right)^J & \cdots & \left(R_{z(J)J}, R_{z(J)J} \right)^J \end{vmatrix}}{\begin{vmatrix} \left(R_{0J}, R_{0J} \right)^J & \left(R_{0J}, R_{1J} \right)^J & \cdots & \left(R_{0J}, R_{z(J)J} \right)^J \\ \left(R_{1J}, R_{0J} \right)^J & \left(R_{1J}, R_{1J} \right)^J & \cdots & \left(R_{1J}, R_{z(J)J} \right)^J \\ \vdots & \vdots & \ddots & \vdots \\ \left(R_{z(J)J}, R_{0J} \right)^J & \left(R_{z(J)J}, R_{1J} \right)^J & \cdots & \left(R_{z(J)J}, R_{z(J)J} \right)^J \end{vmatrix}} \tag{7.19}$$

with

$$\left(F_J | G_J \right)_J = \frac{1}{2} \mathrm{Tr}_J \left(F_J^\dagger G_J + G_J^\dagger F_J \right) \tag{7.20}$$

and

$$\langle \Delta H \Delta H \rangle^J = \frac{1}{2} \mathrm{Tr}_J \left(\rho_J \left\{ (\Delta H)^J, (\Delta H)^J \right\} \right) \tag{7.21a}$$

with

$$(\Delta H)^J = \mathrm{Tr}_{\bar{J}} [(I_J \otimes \rho_{\bar{J}}) \Delta H] \tag{7.21b}$$

Another contribution to the SEA-QT framework is that given by Beretta in [287] in which the equation of motion for an isolated single constituent system is extended to account for coupling

effects with a heat reservoir. The latter is treated on a phenomenological basis. The derivations and definitions are not repeated here. The extended equation of motion of a single constituent isolated system interacting with a heat reservoir expresed in a density operator representation is formulated as

$$\frac{d\rho}{dt} = -\frac{i}{\hbar}[H,\rho] + \frac{1}{2\tau_D\sqrt{\langle\Delta M\Delta M\rangle}}\{\Delta M,\rho\} + \frac{1}{2\tau_G\sqrt{\langle\Delta G\Delta G\rangle}}\{\Delta G,\rho\} \tag{7.22}$$

where

$$\langle\Delta M\Delta M\rangle = \mathrm{Tr}\rho(\Delta M)^2 \tag{7.23a}$$

$$M = S - \frac{H}{\theta_H} \tag{7.23b}$$

$$\Delta M = \Delta S - \frac{\Delta H}{\theta_H} \tag{7.23c}$$

$$\Delta S = S - (-k_B\mathrm{Tr}\rho\ln\rho)I \tag{7.23d}$$

$$\Delta H = H - \mathrm{Tr}(\rho H)I \tag{7.23e}$$

$$\theta_H = \frac{\langle\Delta H\Delta H\rangle}{\langle\Delta S\Delta H\rangle} \tag{7.23f}$$

$$\langle\Delta H\Delta H\rangle = \mathrm{Tr}\rho(\Delta H)^2 \tag{7.23g}$$

$$\langle\Delta S\Delta H\rangle = \frac{1}{2}\mathrm{Tr}\rho\{\Delta S,\Delta H\} \tag{7.23h}$$

$$G = S - \frac{H}{\theta} \tag{7.23i}$$

The first term on the right hand side of Equation (7.22) corresponds to the unitary evolution dynamics of the Schrödinger equation, the second term to the dissipative internal relaxation of the system, and the third term to the phenomenological description of the coupling between the system and reservoir. The operators M and G are defined as *"nonequilibrium Massieu operators"*, and θ_H is defined as a *"constant-energy, non-equilibrium temperature"*.

Finally, Equation (7.22) has been modified by Smith [303] and Smith and von Spakovsky [259] with respect to the heat interaction term to ensure that the system is brought into mutual stable equilibrium with the reservoir. In addition, an additional phenomenological term has been added to the equation of motion to allow for system interactions with a mass reservoir. The modified version with both types of interaction terms is expressed given as

$$\frac{d\rho}{dt} = -\frac{i}{\hbar}[H,\rho] + \frac{1}{2k_B\tau'_D}\{\Delta M,\rho\} + \frac{1}{2k_B\tau'_G}\{\Delta\tilde{G},\rho\} + \frac{1}{2k_B\tau'_M}\{\Delta\tilde{F},\rho\} \tag{7.24}$$

where $\tilde{G}$ in the third term on the righ hand side is a rotated version of the non-equilibrium Massieu heat interaction operator, G, appearing in Equation (7.22). The fourth term on the right hand side is the rotated version of the phenomenological mass interaction term, the details of which are found in Smith [303]. The $\tilde{F}$ in this term is a Massieu type mass interaction operator extended to include an appropriate number particle operator in addition to the entropy and Hamiltonian operators which normally appear in Massieu functions. Some results of the modeling developed generated using Equation (7.24) minus the heat interaction term are provided in a later section of this chapter.

7.2.2 Modeling hydrogen storage in and on a carbon nanotube

Smith [303], Smith et al. [301], and Sciacovelli et al. [302] develop the modeling of hydrogen storage in and on a carbon nanotube using the SEA-QT framework. The system is an isolated 3D tank with a volume of 250 nm^3, containing four H_2 molecules, and a carbon nanotube formed by 900 carbon atoms with a radius of 1.017 Å and a length of 3.56 Å located in the center of the tank.

In order to build the energy eigenstructure of the system, which establishes all possible quantum eigenstates for the system from which any given thermodynamic state is formed, the energy eigenvalue problems for translation and rotation are accounting for two particle interactions between $H_2 - H_2$ and $H_2 - C$ particles. The method of coarse graining based on density of states is used in order to scale the number of translational energy levels to values indicative of the physical system. Thus the scaled model is solved with $20,000$ energy eigenlevels representative of a system with 10^{15} energy eigenlevels. The Lennard-Jones potential function [321] is used to represent the interactions between pairs of particles. An initial non-equilibrium state is generated by finding a state with a high probability of finding the four H_2 molecules in one of the corners of the tank. The evolution of state of the system towards that of stable equilibrium is obtained by solving the system of first order differential equations generated by using the SEA-QT equation of motion for an isolated single constituent system.

Figure 7.2 shows the time evolution of the mass density of the hydrogen inside the carbon nanotube. Initially the nanotube is empty; but as time proceeds, the hydrogen molecules are attracted by the nanotube to be stored on and inside the tube. It is worth mentioning that the model and analysis is developed to study a possible methodology for modeling hydrogen storage at atomistic levels in the non-equilibrium regime only and not to determine the maximum allowable storage capability of the nanotube. Figure 7.3 shows a more detailed evolution of the hydrogen storage.

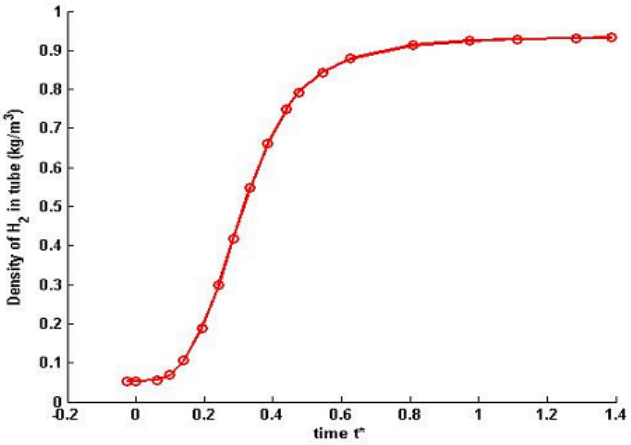

Figure 7.2. Time evolution of hydrogen mass density in the carbon nanotube by Smith [303]. Reprinted from [303] Copyright © 2012, with permission from the author.

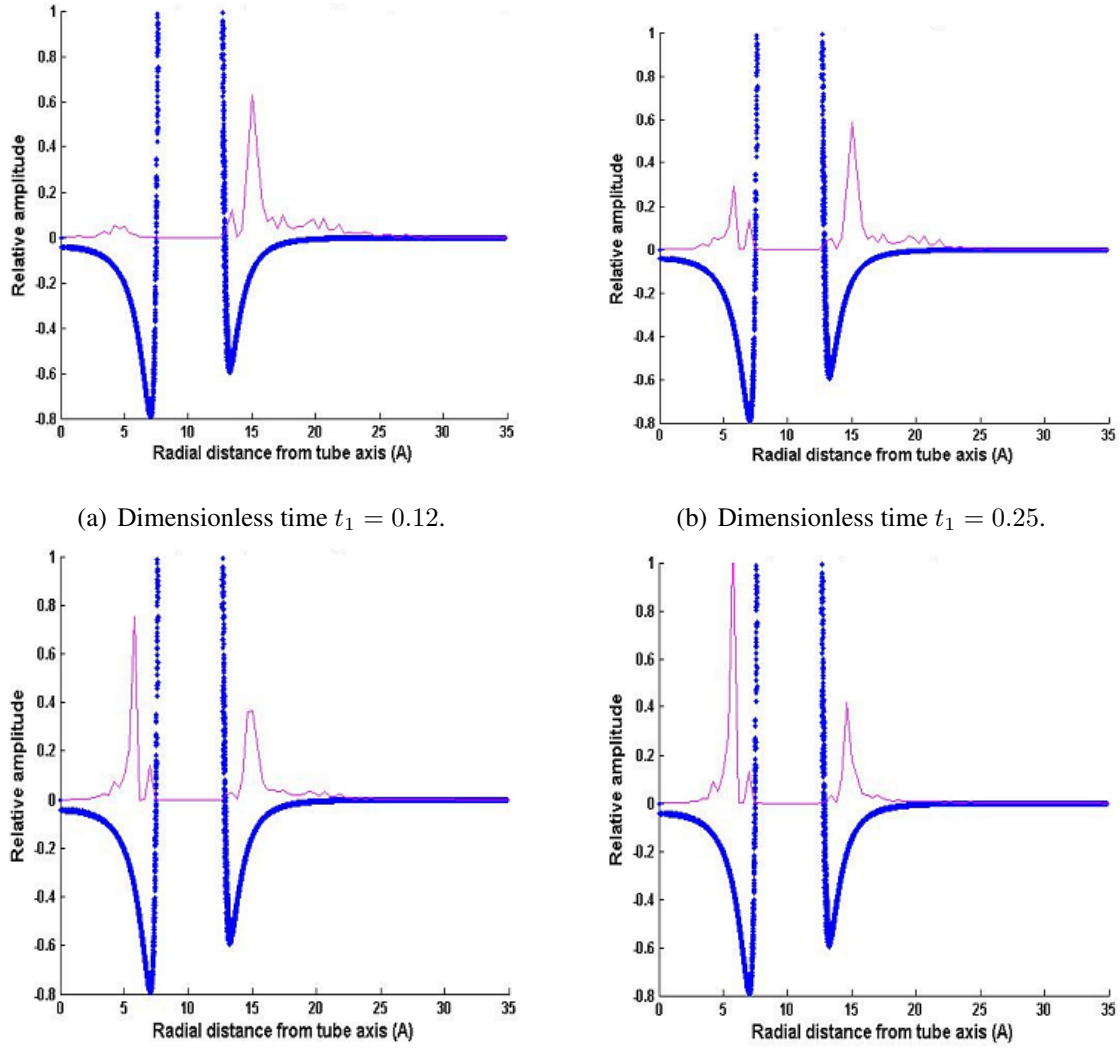

(a) Dimensionless time $t_1 = 0.12$.

(b) Dimensionless time $t_1 = 0.25$.

(c) Dimensionless time $t_3 = 0.46$.

(d) Dimensionless time $t_4 = 1.41$.

Figure 7.3. Hydrogen mass density time evolution in and around the carbon nanotube [303]. Reprinted from [303] Copyright © 2012, with permission from the author.

The vertical blue line in the left represent the potential of the inside wall of the tube, while the blue vertical line in the right represents that of the outside wall. The magenta line is indicative of the hydrogen density. It is observed that initially the probability amplitude is very low, but increases as the system evolves towards a state of stable equilibrium.

7.2.3 Modeling chemically reactive systems

The modeling of isolated chemically reactive systems has been developed by Al-Abbasi [306] and Al-Abbasi, Beretta and von Spakovsky [305] using the SEA-QT framework developed by Beretta and von Spakovsky [322]. Within this framework, the chemical kinetics of an isolated reactive system with one or more reaction mechanisms is predicted as the state of the system relaxes from a state of non-equilibrium to that of stable chemical equilibrium. As a first application, the single reaction for fluorine reacting with hydrogen, i.e.,

$$F + H_2 \rightleftharpoons FH + H \tag{7.25}$$

is modeled because of the extensive experimental and theoretical research that has been devoted to this particular reaction over the last several decades. To build the SEA-QT model, the energy and particle number eigenvalue problems are solved first in order to establish the energy and particle eigenstructure of the system and all possible available eigenstates of the system. The equation of motion of SEA-QT is then solved to obtain the unique thermodynamic path, i.e., the cloud of possible trajectories in state space that describe the relaxation of state of the system towards a state of stable chemical equilibrium. The modeling accounts for vibrational, rotational, and translational degrees of freedom, conserving the expectation values of system energy and the number of atomic particles of each species during the evolution. At every instant of time, the so-called reaction rates constants are obtained as a function of the kinetics of the reaction. Other expectation values such as entropy, entropy generation rate, particle number of each species, the reaction coordinate, etc., are calculated at every instant of time from the model.

Figure 7.4 shows the evolution of both the expectation value of the entropy and the entropy generation rate of the isolated chemically reactive system from an initial non-equilibrium state to that of stable chemical equilibrium. The initial mixture consists of 1 particle of H_2 and 1 particle of F at an initial temperature of 300 K. From the figure it is seen that the entropy of the system

increases in a very steep fashion at the early stage of the evolution after wich it asymptotically approaches its stable equilibrium value. Figure 7.5(a) shows the evolution in time of the expectation value of the particle number operator for each species where one can observe how the concentration of the ractants decrease in a fashion directly proportional to the increase in concentrations of the products. It is also seen that the reaction does not go to completion. This time evolution of the concentration of each species suggests that reaction rate constant is in fact changing in time. Figure 7.5(b) shows the evolution of the forward, backward, and net reaction rates (i.e., r_f, r_b and r, respectively) for the fluorine reaction. As can be seen,r_f dominates early in the evolution whith r_b effectively zero. However, after this initial stage, both raction forward and backward rates play a role as the system state evolves toward stable equilibrium.

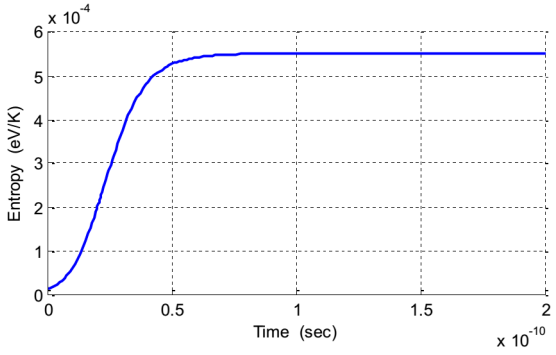

(a) Evolution of the expectation value of the entropy.

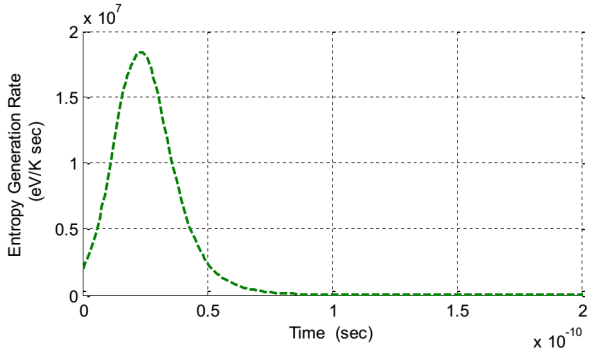

(b) Evolution of the expectation value of the entropy generation rate.

Figure 7.4. Evolution of the expectation value of the entropy of the fluorine reaction by Al-Abbasi [306]. Reprinted from [306] Copyright © 2013, with permission from the author.

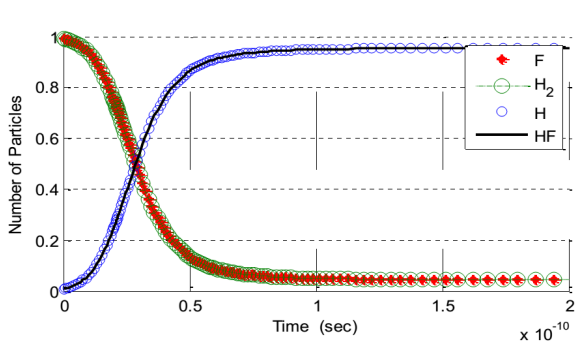

(a) Evolution of the expectation value of particle numbers for each species.

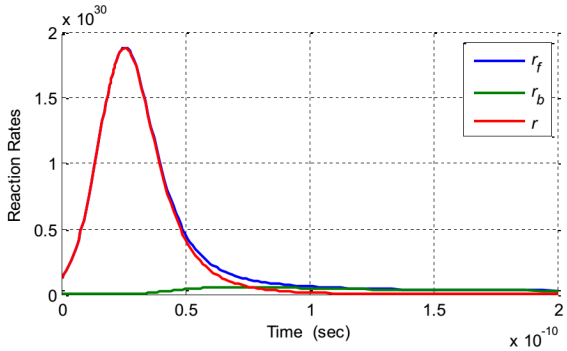

(b) Evolution of the forward, backward, and net (i.e., r_f, r_b and r, respectively) reaction rates.

Figure 7.5. SEA-QT modeling of the fluorine reaction corresponding to an initial stable equilibrium temperature of 298 K by Al-Abbasi [306]. Reprinted from [306] Copyright © 2013, with permission from the author.

7.3 Comparisons with experimental data from the literature

Experiments help to explain how nature behaves, but to date no experiment has been developed to conclusively prove the validity of the dynamical postulate of SEA-QT. Nonetheless, several comparison of SEA-QT predictions have been made to experimental data obtained from the literature among wich are comparisons with resonance fluorescence, absorption and stimulated emission data of a two-level atom; the relaxation of a Rb atom in a magnetic field; and the relaxation of Be^+ ion in a Paul trap interacting with a heat reservoir. A discussion of these comparisons is provided below.

7.3.1 Resonance fluorescence, absorption and stimulated emission

In [323] Beretta provide a SEA-QT description of resonance fluorescence, absorption and stimulated emission of a two-level atom in a magnetic field, driven near resonance by a monocromatic laser beam. The equation of motion of SEA-QT for a single constituent isolated system [284] is formulated to describe the evolution of the reduced state operator of the atom interacting with the magnetic field by including the Hamiltonian terms describing the effects of the atom-field state coupling obtained from the atom reduced state equations of Quantum Electrodynamics (QED) [324, 325]. The analsysis of the system is developed in the long time limit of $t \to \infty$ for non-equilibrium steady state solutions.

Figure 7.6(a) shows the effect of absorption for the weak field case and Figure 7.6(b) for the strong field case. Here δ is a measure of the iternal redistribution, which is a direct indicator of the internal-time dissipation of the system, τ_D, of the SEA-QT equation of motion. When $\delta = 0$, the SEA-QT equation of motion for the state of the atom reduces to that of QED obtained with the unitary dynamics of the Schrödinger equation of motion. The parameter η is an indicator of the strength of the field, θ of the detuning between the frequencies of the atom and the field, λ is the driving field bandwidth ($\lambda = 0$ for a monocromatic laser), and ξ is the assymetry corresponding to the ratio of one half of the Einstein A coefficient and the frequency between the two energy eigenstates of the atom. From Figures 7.6, it is interesting to see the broadening effect as a function of δ, that is, when dissipation is present, the absorption spectrum is broaden.

Figure 7.7(a) shows the resonance fluorescence sprectrum as a function of the dimensionless frequency, ν, when the atom is on resonance with the field, and Figure 7.7(b) shows the reso-

nanance fluorescence when the atom and the field are off-resonance. Both figures correspond to the strong-field limit ($\eta = 10$) case with a driving field bandwidth of $\lambda = 0.01$. In this case the assymetry ξ is set equal to zero. It is interesting to see that for the case when $\theta = 0$, the resonance fluorescence density spectrum is symmetric for all cases of different δ. For the case when $\theta \neq 0$, the density spectrum is never symmetric since as can be seen, the right hand side of the energy spectrum is larger than the left hand side. It is suggested in [323] that the internal energy redistribution due to dissipation contributes to this assymmetry. Finally, Figure 7.8 shows the absorption and stimulated emission as a function of the internal redistribution parameter, δ, for the case when the atom and the field are on resonance ($\eta = 2$, and $\lambda = 0.05$). As can be seen, the shape is assymmetric and broadens as the dissipation represented by δ is increased.

Several researchers have modeled the effects of resonance fluorescence, absorption and stimulated emission using the theory of QED [324–332]; and though QED experiments verify the theoretical predictions qualitatively, the quantitative predictions though good nenetheless differ from the experimental values sufficiently to question wether or not the difference and even perhaps a major portion of the difference may be attributable to a lacuna in the theory as suggested by IQT. Thus, developing a QED experiment sufficiently precise to distinguish the QED and SEA-QT predictions would be useful in verifying the existence or not of internal dissipations [333]. This experiment can also provide means of determining the internal-time relaxation constant, τ_D, of the SEA-QT equation of motion [323].

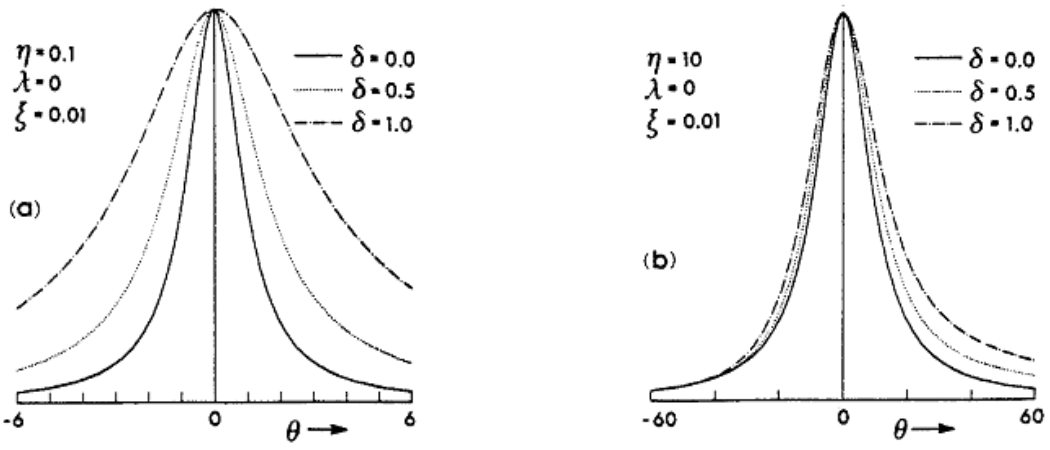

(a) Weak field, $\eta = 0.1$.

(b) Strong field, $\eta = 10$.

Figure 7.6. SEA-QT description of absorption spectrum of a two-level atom in a magnetic field by Beretta [323]. Reprinted from [323] with kind permission from Springer Science and Business Media.

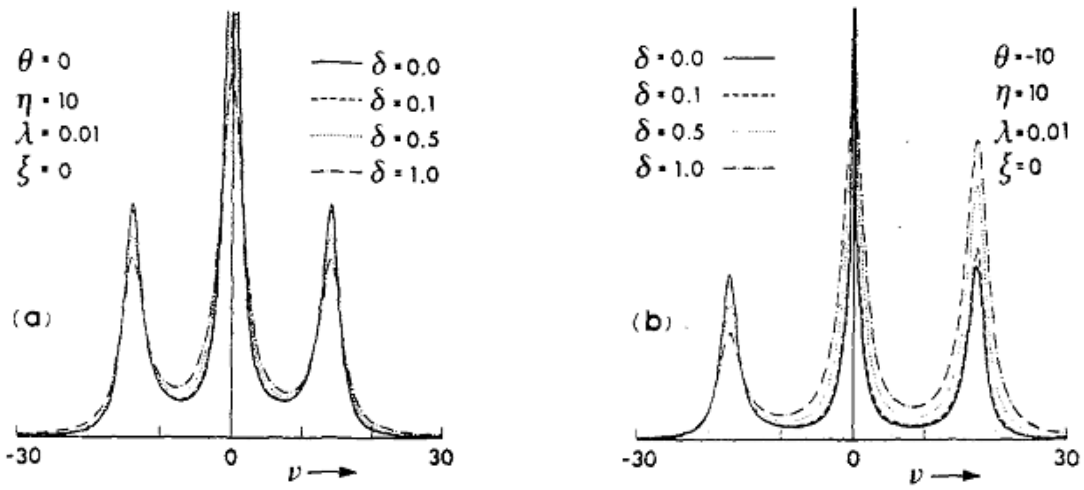

(a) On resonance, $\theta = 0$. (b) Off resonance, $\theta = -10$.

Figure 7.7. SEA-QT description of resonance fluorescence spectrum of a two-level atom in a magnetic field by Beretta [323]. Reprinted from [323] with kind permission from Springer Science and Business Media.

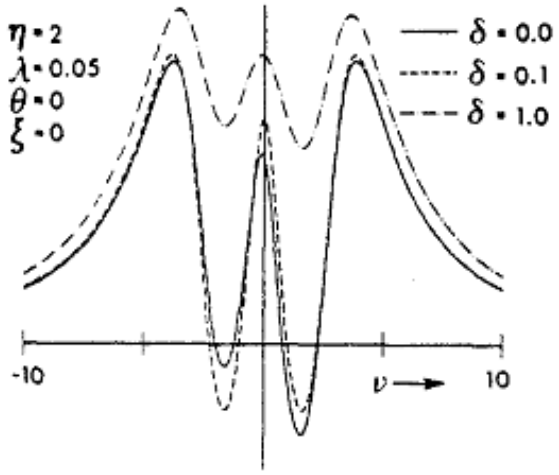

Figure 7.8. SEA-QT description of absorption and stimulated emission of a two-level atom in a magnetic field by Beretta [323]. Reprinted from [323] with kind permission from Springer Science and Business Media.

7.3.2 Relaxation of a Rb atom in a magnetic field

Smith [303] and Smith and von Spakovsky [259], model the realaxation of the state of a Rb atom using the SEA-QT framework, i.e., the change in state of the spin-1 (5-level) particle is considered to be due to spontaneous relaxation of the system only. The SEA-QT predictions are then compared with experimental observations of the relaxation of a Rb atoms in a magnetic field obtained by Nagel and Haworth [334] and Kukolich [335]. Nagel and Haworth use the earth's magnetic field

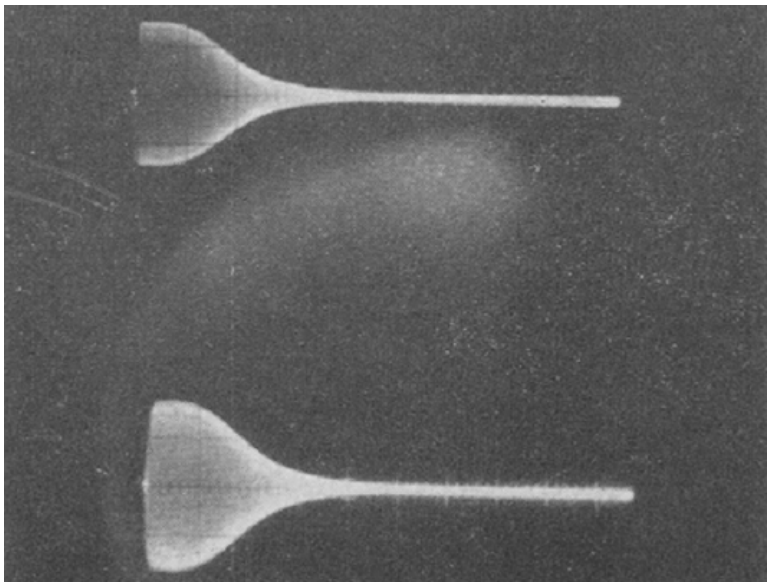

Figure 7.9. Results of the field switching experiment for the relaxation of Rb atoms by Nagel and Haworth [334] using a 10 ms sweep time signal. Reproduced with permission from [334] Copyright © 2005, American Association of Physics Teachers.

to obtain the thermodynamic state relaxation or spin attenuation of the atoms given in Figure 7.9 in terms of the changing light transmission intensity measured in the experiment. As can be seen, a very gradual decay in intensity occurs during the early stages of the relaxation followed by a much steeper decay after wich the decay becomes very gradual once more. In contrast, Kukolich obtains the precession decay of the atom's spin in an external magnetic field. In [335], the state of each Rb atom is initially prepared in a non-equilibrium state using the technique of optical pumping. The energy of each Rb atom is pumped to its highest energy eigenlevel ($|+2\rangle$); and subsequently, the orientation of the magnetic field is switched suddenly from the z- to the x- direction. The precession of the decay from the highest to the lowest energy eigenlevel is monitored in a photocell by measuring the intensity of the light emitted during the relaxation. Figure 7.10 shows the current measured by the photocell as a function of time for two different precession frequencies. As with the previous experiment a periodic decay takes place during the relaxation, including the variation in the amplitude of two succeeding wave crests. Clearly, the same gradual initial decay seen in Nagel and Haworth is not seen here, but it is believed that this is due to the fact that Kukolich only reports the latter part of the signal [259, 303].

The results obtain by Smith [303] and Smith and von Spakovsky [259] are depicted in Figure 7.11. It can be observed that the SEA-QT modeling captures the slow decay at the beginning of the relaxation, as well as the sudden decay and again a gradual decay towards a state of stable

equilibrium as seen in Figure 7.9. Moreover, the SEA-QT modeling also captures the features measured by Kukolich, that is, the uneven amplitude between two successive wave crests. The damping effects seen in Figure 7.10 is explained by Smith and von Spakovsky to be a direct indication of the existence of spontaneous relaxation.

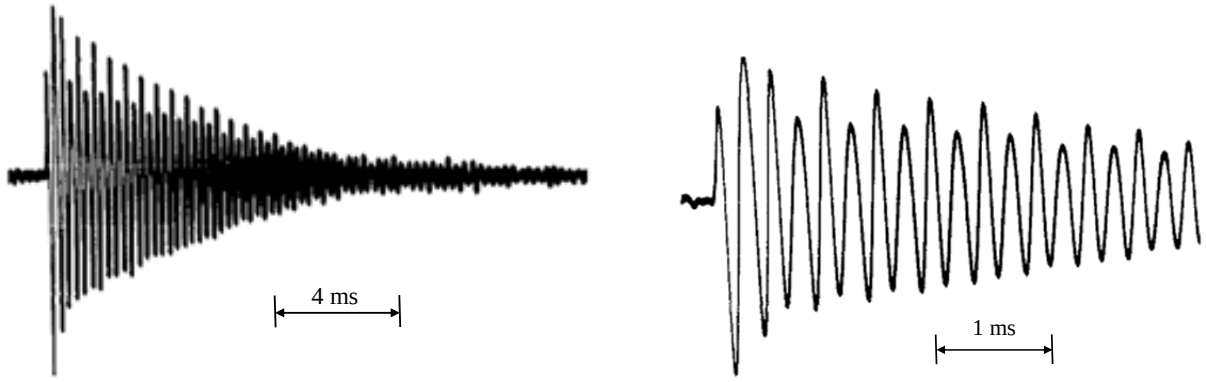

(a) Precession frequency of 4 ms. (b) Precession frequency of 1 ms.

Figure 7.10. Experimental measurements of the state relaxation (i.e., photocell current) of Rb atoms by Kukolich [335] for precession frequencies of 4 ms and 1 ms. Reproduced with permission from [335] Copyright ©2005, American Association of Physics Teachers.

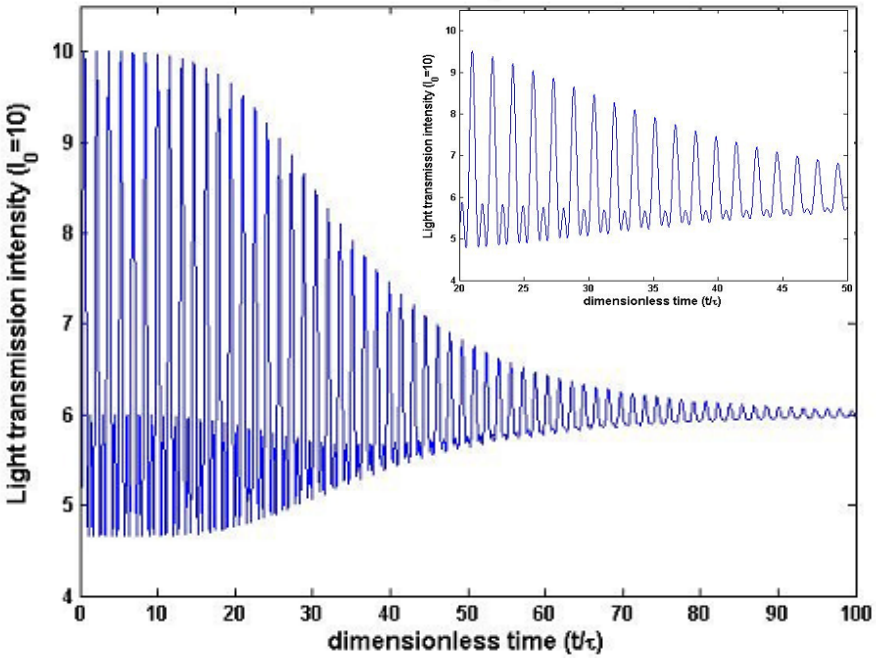

Figure 7.11. SEA-QT modeling of the relaxation of a Rb atom by Smith [303] and Smith and von Spakovsky [259]. Reprinted from [303] Copyright © 2012, with permission from the author.

7.3.3 Relaxation of a Be^+ ion as a particle in a box

Turchette et al. [336] experimentally obtain the relaxation of Be^+ ions combined with nuclear spins in a Paul trap. Be^+ ions behave as harmonic oscillators in a coherent state, $|\alpha\rangle$, where external radio frequencies are used to trap the ions and induce voltages to emmulate a high-temperature amplitude reservoir. The system is initially placed in a non-equilibrium state using optical pumping and laser cooling techniques. The decoherence of the Be^+ ion is indirectly measured with interferometer techniques by recording the decay of the nuclear spin state.

Smith and von Spakovsky [259] also model the relaxation of the Be^+ ion using a modified version of the equation of motion given in [287] to phenomenologically account for heat. This modified version of the equation of motion developed by Smith [303] and Smith and von Spakovsky [259] is given by Equation (7.24) minus the mass interaction term.

Figure 7.12(a) depicts the experimental and numerical results obtained by Turchete et al. [336] for the relaxation of the five lowest energy eigenlevels of the system for cat state $|1\rangle$. The experimental results are shown by the marks and the numerical results obtained using a QT master equation are shown as continuous lines. As can be seen the master equation predicts the relaxation of system state towards stable equilibrium very well. In this case, the dissipation of the relaxation is assumed to be due to a loss of information caused by weak interactions between the system and environment.

Figure 7.12(b) shows the same experimental results as in Figure 7.12(a), but now the continuous lines represent the numerical results obtained by Smith and von Spakovsky [259] using the SEA-QT framework. It is observed that SEA-QT predictions also fit the experimental results very well. In this case, it is assumed that the dissipation is intrinsic to the system. The deviations observed between the experimental and numerical results are attributed by Smith and von Spakovsky to a number of assumptions, such as approximating the values for the relaxation time constants τ_D and τ_Q, and the selection of the initial non-equilibrium state which had to be estimated from the experimental data.

7.4 Entanglement, coherence, and decoherence

Non-equilibrium phenomena is an important field of study within the scientific community and has as its general aim the development of a deeper understanding of how Nature behaves and

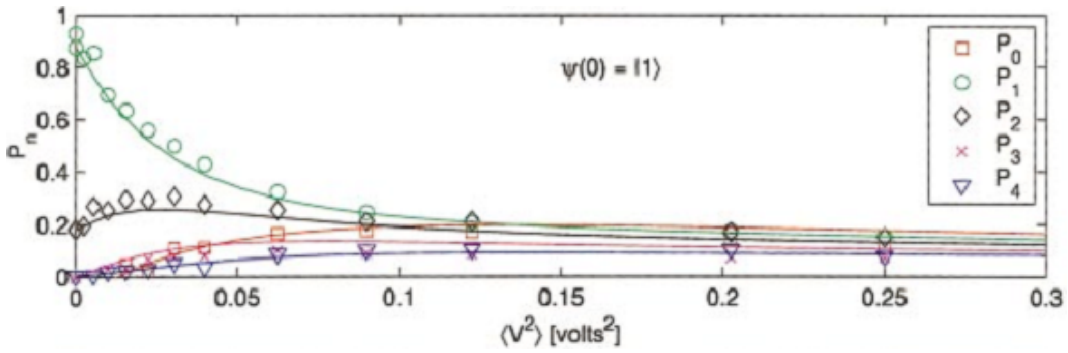

(a) Comparison with the results predicted using a QT master equation by Turchette et al. [336]. Reprinted from [336] Copyright © 2000 by The American Physical Society (APS), with permission from APS.

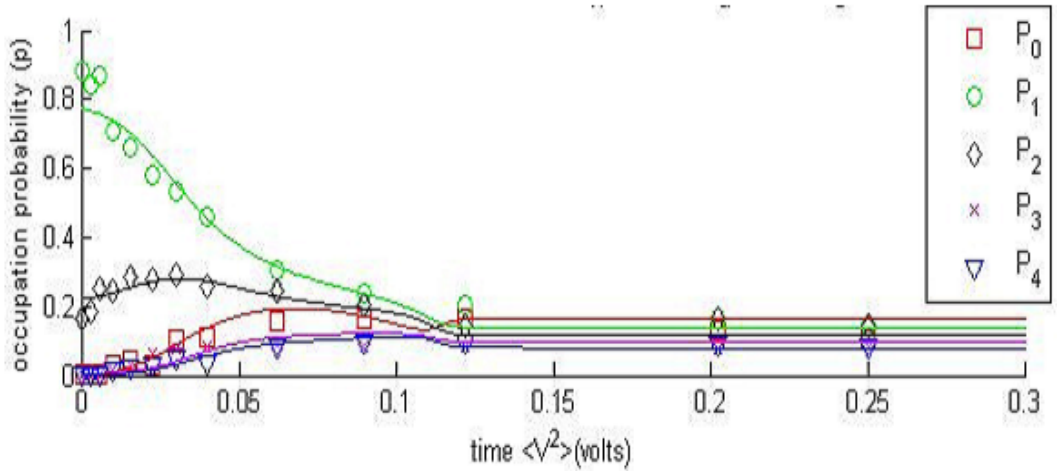

(b) Comparison with the results predicted using the SEA-QT equation of motion by Smith and von Spakovsky [259]. Reprinted from [303] Copyright © 2012, with permission from the author.

Figure 7.12. Relaxation of cat state $|1\rangle$ of Be^+ ion trapped in a box [336]. The marks represent experimental results and the continuous lines numerical results.

as a consequence, how new technologies can be more effectively developed. This applies at all spatial and temporal scales of analysis. Lately, of particular interest has been a consideration of the non-equilibrium phenomena which occur at the nanoscale, particularly in relation to quantum computing and nanometric devices [337–342] where entanglement, coherence, and decoherence are of great importance. The entanglement of zero-entropy states or the correlation of non-zero-entropy states is present when the state of one constituent is entangled or correlated to that of another and can no longer be described independently of the other, that is, only a single system state can be observed for the two constituents. The loss of entanglement or correlation among the so-called 'local states' of the constituents of a composite system occurs according to SEA-QT due to the presence of irreversibilities. The term 'states' is placed in quotes here to emphasize that

these are not actual states that can be observed or measured but instead so-called 'pseudo-states' represented by the reduced state operator of each constituent, which is found mathematically by taking the partial trace of the state operator of the composite system. To be an 'actual state', the 'local state' of each constituent would have to be uncorrelated or unentangled from that of the other constituent. According to the unitary dynamics of QM, the state of the composite system should evolve in a superposition of outcomes, i.e., entangled and coherent. Here the term 'coherent' refers to the fact that due to a phase difference between one quantum eigenstate and another, the one is able to interfere with the other and the greater the phase difference, the greater the interference and, thus, the coherence. Unitary dynamics suggestss that this coherence between quantum eigenstates, i.e., the states which comprise the thermodynamic state or simply state of the system, neither diminishes nor increases with time. In contrast, daily observations of Nature and experiments on microscopic systems [292, 336] indicate that a loss of entanglement or correlations as well as coherence (decoherence) is always present.

The analysis (both experimental and numerical) of the creation and loss of correlations and coherence has significance for explaining the transition between the microscopic and macroscopic worlds [343, 344]. For example, during the physical measurement of an indivisible microscopic system (e.g., a particle), the macroscopic measuring device (meter) becomes entangled or correlated with the state of the particle and thereafter behaves as a macroscopic system in a superposition of states. While an understanding the retention of entanglement or correlation and coherence between the constituents of the new-born particle-meter composite system is at the core of QM, the loss of entanglement or correlations and coherence of the constituents is at the core of non-equilibrium thermodynamics in general and SEA-QT in particular. In addition, the manipulation of communication-type phenomena such as entanglement, correlation, and coherence can be used for the development of nanometric devices (e.g., a quantum computer [345]), which rely for their operation on the correlation or entanglement of states among the different subsystems, which make up the composite system.

Plenty of work has been done on entanglement, correlation, coherence and decoherence phenomena [346–354] including that at the very start of QM such as the thought experiment of "Alice" and "Bob" of the Einstein, Podolsky and Rosen (EPR) paper [355], and the Schrödinger description of the strangeness of QM applied to the macroscopic world represented by the state of a cat being either dead or alive depending on the particular state of the atom with which the state of the cat is

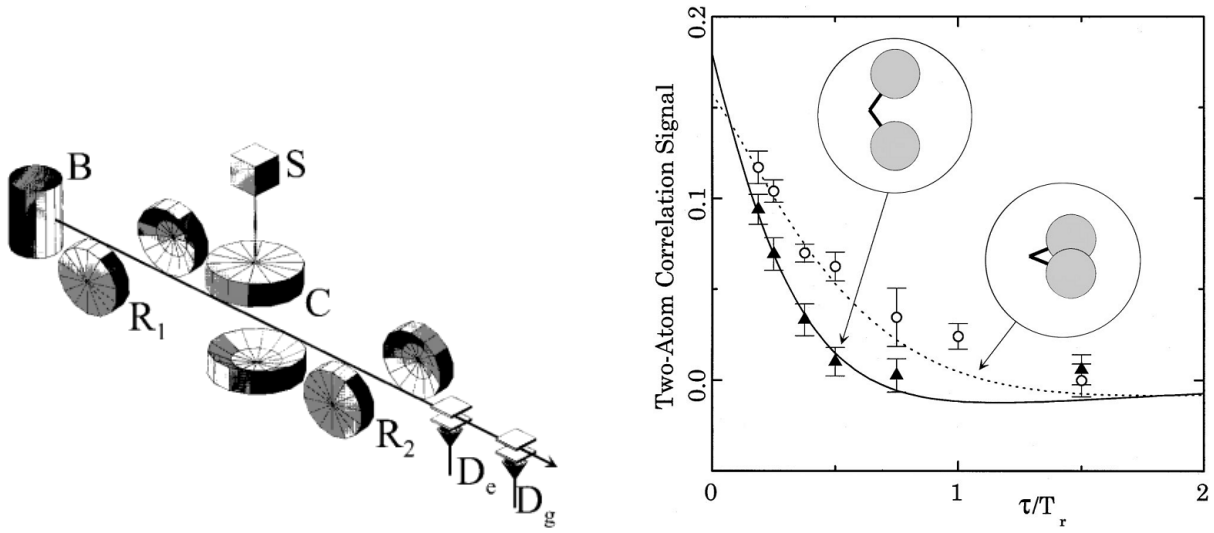

(a) CQED experimental setup by the group in Paris [371]. Reprinted from [371] Copyright © 1996 by The American Physical Society (APS), with permission from APS.

(b) Decoherence results by Brune et al. [292]. Reprinted from [292] Copyright © 1996 by The American Physical Society (APS), with permission from APS.

Figure 7.13. Decoherence phenomenon detected by the group in Paris [292, 371].

entangled [356]. However, despite all of these remarkable efforts, the most striking experimental and theoretical descriptions are those provided recently by the group of Haroche and co-workers in Paris [289–293, 339, 357–360], and the group of Wineland and co-workers [336, 361–370] at the National Institute of Standards and Technology (NIST) in Colorado.

The Cavity Quantum Electrodynamics (CQED) group of Paris lead by Serge Haroche have developed experimental measurements of decoherence for an atom entangled with a photon field contained in a high-Q cavity. Figure 7.13(a) shows the experimental setup used to monitor the decoherence between the atom and the photon field. Rb atoms are contained in a furnace (not ilustrated in the figure), and a single Rb atom is selected and sent through B, where it is prepared in an excited spin state $|0\rangle$. The atom then crosses the cavity R_1 where a microwave pulse prepares the state of the atom in a superposition of Rydeberg states. After that, the atom interacts with a photon field in a coherent state in the high-Q cavity, C. The photon field is generated and placed into the cavity by the source S just before the atom enters the cavity. The interaction of the atom with the field splits the field's phase, ϕ, creating an entanglement. Subsequently, the Rydberg states of the atom are mixed again by a microwave pulse at R_2 similar to that at R_1. Finally, the state of the atom is detected in either spin state $|0\rangle$ or spin state $|1\rangle$ by the detectors D_e and D_g, respectively. A second atom with identical charactaristics to the first atom is then send through the

expeimental set after a delay time, τ, undergoing the same process as the first atom, and its state is also recorded by detectors D_e and D_g. Measurig the state of the second atom uncovers the effects left by the first atom in the photon field. If the delay time τ is zero, the photon field has no time to lose any of its coherence; but as time goes on, the coherence of the photon field decays.

Figure 7.13(b) shows the experimental results obtained for two different field phases (i.e., the circles and triangles with error bars). For each particular phase representing a particular τ, each point in the figure is obtained by repeating the experiment 15,000 times and analyzing the change in the interference produced by the two atoms on the photon field. The same methodology is repeated for different delay times to obtain the different experimental points depicted in the figure.

It can also be observed that decoherence occurs faster if the phases have a bigger separation (i.e., the triangles in the figure as opposed to the circles). Figure 7.13(b) also shows the analytical description of decoherence for this particular experiment in terms of the correlation signal given by

$$\eta = \mathbb{P}(e_2|e_1) - \mathbb{P}(e_2|g_1) \qquad (0 \leq \eta \leq 0.5) \tag{7.26}$$

which is *"the difference between the conditional probability to detect the second atom in the excited state provided the first was in its excited state, and the conditional probability to detect the second atom in its excited state if the first was in its ground state"* [291].

These type of experiments are also modeled using linear Markovian quantum master equations (i.e., those of the Kossakowski-Lindblad-Gorini-Sudarshan type [272, 280, 372]), which are based on the so-called "open-system model", which assumes that the system is attached to (and weakly interacts with) a thermal bath or reservoir (environment). Under this "open-system model" approach of Quantum Thermodynamics (QT), it is assumed that entanglement or correlations periodically build up and dissipate due to the weak interactions between the system and the reservoir and do so in a time frame of creation and annihilation which is significantly shorter than that of the relaxation of system state to stable equilibrium. Under this assumption, the dissipation phenomenon is the result of a loss of information only and, thus, illusory (i.e., the so-called Loschmidt paradox [273]). The evolution of the reduced state operator of the atom interacting with a photon field described by the QT master equation [358, 359]

$$\frac{d\rho}{dt} = -\frac{i}{\hbar}[H, \rho] + \frac{\kappa}{2}(2a\rho a^\dagger - a^\dagger a\rho - \rho a^\dagger a) \tag{7.27}$$

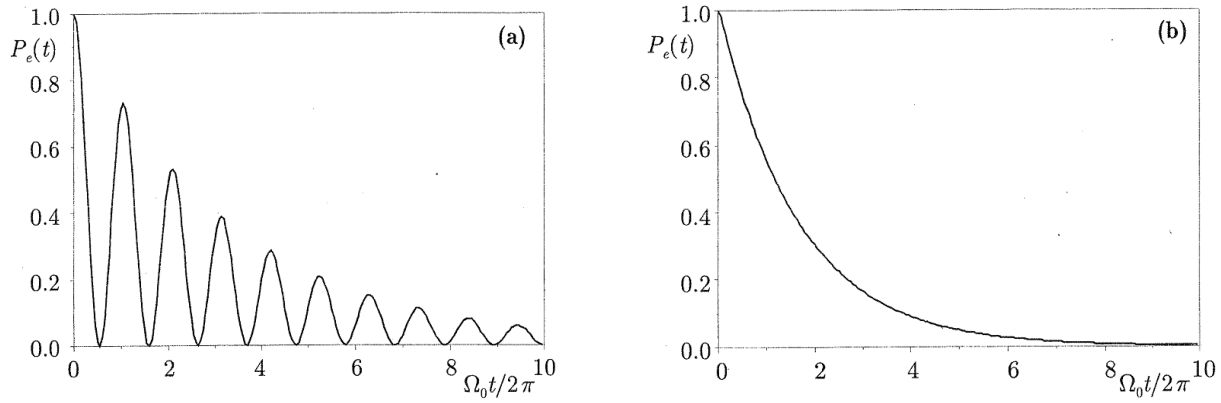

(a) Undamped case, $\kappa = 0.1\Omega_0$.

(b) Overdamped case, $\kappa = 10\Omega_0$.

Figure 7.14. Modeling of the spontaneous emission of an atom-field composite system [359]. $P_e(t)$ represents the probability of finding the atom in its excited spin state $|0\rangle$. Reprinted from [359] Copyright © 2006, with kind permission from Oxford University Press.

where the first term on the right descibes the unitary Hamiltonian evolution of the system and the second the emission of photons from the cavity to the environment. The a and $a^\dagger$ are the annihilation and creation operators of QM. Both terms to the right are linear, and, therefore, the equation only reresents a linear dynamics. The constant $\kappa = \omega_c/Q$ is the energy damping of the cavity and indicates how fast the photons are being dissipated, were ω_c is the cavity mode angular frequency and Q is the cavity quality factor with values on the order of 10^8.

Figure 7.14 shows the spontaneous emission of the photon field in the cavity. Figure 7.14(a) shows the probability of finding the atom in its excited state as a function of time (i.e., $P_e(t)$) for the case in which the cavity is underdamped, where Ω_0 is the vacuum Rabi frequency. As can be seen, many oscillations inside the cavity take place before the atom finally decays to its ground spin state $|1\rangle$. On the other hand, Figure 7.14(b) shows the overdamped case where the emission of a photon to the environment is very fast.

Independently of the Paris group, the group at NIST lead by David Wineland, provides experimental and theoretical descriptions for the relaxation of a Be^+ ion contained in a Paul trap. Figure 7.15 shows the creation of the cat state for the Be^+ ion. First, in (a) the wavepacket corresponding to spin state $|1\rangle$ of the Be^+ ion is placed in the ground state of the harmonic oscillator by cooling it to a very low temperature. Then, in (b) the wavepacket is split into two parts with a $\pi/2$ pulse creating a superposition of spin states $|0\rangle$ and $|1\rangle$. A force F is applied in (c) to spin state $|0\rangle$ allowing it to be excited (entangled) to coherent state $|-\alpha\rangle$ while keeping static spin state $|1\rangle$ at the center of the harmonic oscillator. Subsequently, in (d) the spins are flipped with a π pulse allowing

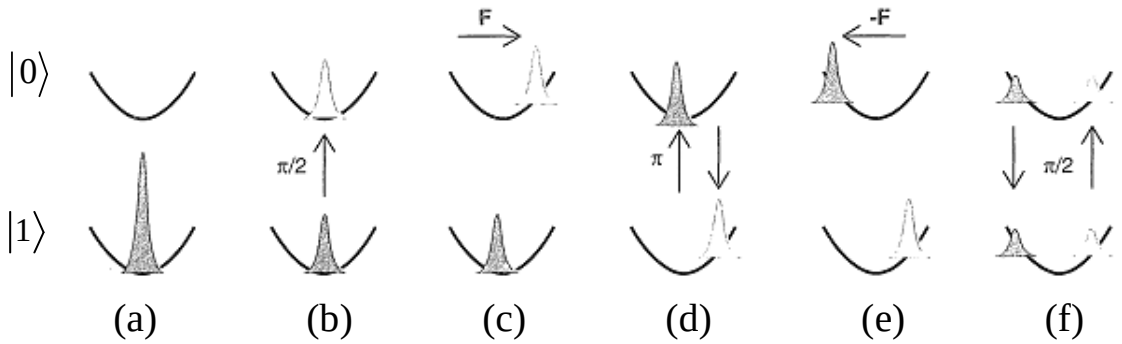

Figure 7.15. Schrödinger cat of a Be^+ ion created at NIST [361, 369]. Reprinted from [369] Copyright © 1996, with kind permission from The American Association for the Advancement of Science.

spin state $|1\rangle$ now to be entangled with the coherent state $|-\alpha\rangle$. A force $-F$ is applied in (e) to spin state $|0\rangle$ to excite it to coherent state $|\alpha\rangle$, obtaining cat state $|\psi\rangle = \frac{1}{\sqrt{2}}(|0\rangle|\alpha\rangle + |1\rangle|-\alpha\rangle)$. In an analogy with the thought exeriment of Schrödinger, $|\alpha\rangle$ represents the state of the cat being alive and $|-\alpha\rangle$ the cat being deceased, depending on the possible outcomes $|0\rangle$ or $|1\rangle$ of a measurement of the spin state of the atom with which the cat is entangled, respectively. Finally, in (f) another $\pi/2$ pulse is applied, and the two components representing the internal cat states of the Be^+ ion entangled or correlated with states that have phases in opposite directions are combined and allowed to relax to the ground state at the center of the oscillator. The coherence between the two components is monitored using interferometry techniques during the relaxation process.

Figure 7.16(a) shows the experimental results of the realaxation of different cat states for the Be^+ ion interacting with a high-temperature amplitude reservoir created by applying voltages that induce heating into the system. The fringe contrast is plotted with respect to the product of the mean squared voltage induced into the system and the squared size of the superposition $(\Delta n^2)\langle V^2\rangle$. The fringe contrast indicates the interference (i.e., coherence) between the two wavepackets and is obtained by recording the probability of finding the ion in spin state $|1\rangle$. Figure 7.16(b) shows the experimental results of the realaxation of different cat states for the Be^+ ion interacting with a zero-temperature reservoir for an undamped case (circles) and for an overdamped case (triangles) as a function of time. It is seen that the coherence existent in the system is lost in a very short time. As in the previous case, the probability of finding the ion in cat state $|1\rangle$ is measured, and the fringe contrast (i.e., coherence) plotted as a function of time.

Results from the modeling of this experiment using the QT master equation

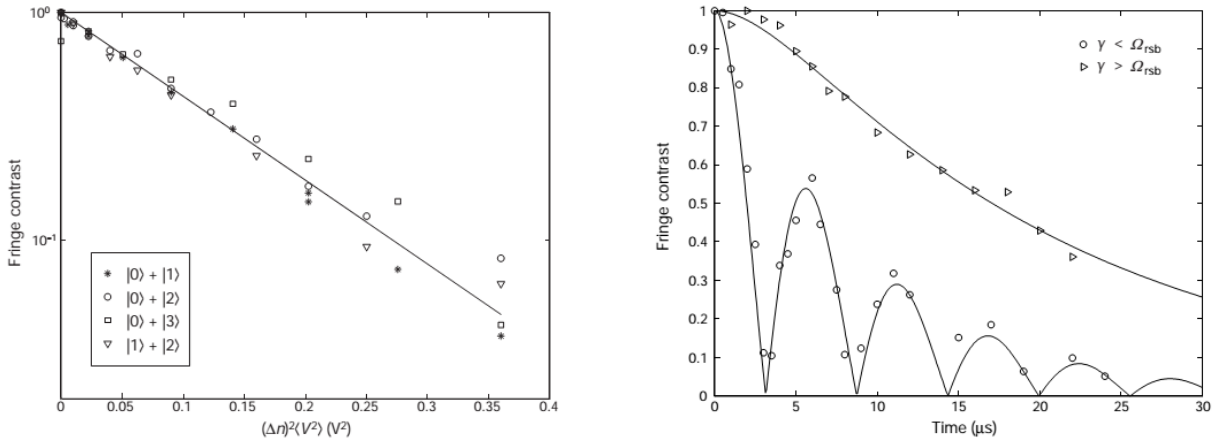

(a) High-temperature reservoir. (b) Zero-temperature reservoir.

Figure 7.16. Experimental results of decoherence of the state of a Be^+ ion [365]; the circles and triangles represent experimental data and the solid lines a fitting of the data. The fringe contrast is an indication of the coherence in the state of the ion. Reprinted by permission from Macmillan Publishers Ltd: Nature [365] Copyright © 2000.

$$\frac{d\rho}{dt} = \frac{\gamma}{2}(\bar{n}+1)(2a\rho a^\dagger - a^\dagger a\rho - \rho a^\dagger a) + \frac{\gamma}{2}\bar{n}(2a^\dagger \rho a - aa^\dagger \rho - \rho aa^\dagger) \tag{7.28}$$

are shown in Figure 7.12(a) for the case of the relaxation of the Be^+ ion inmersed in a high-temperature amplitude reservoir. The constant γ represents the decay rate of the system and $\bar{n}$ the average number of quanta in the reservoir.

Chapter 8

System Description and Modeling Scheme for SEA-QT

8.1 Bloch sphere representation of a two-level-type system

For the modeling of simple systems such as an isolated single particle, it is sufficient to know the transition between two neighboring energy eigenstates in order to fully understand its behavior. For example, the spin direction of a spin-$1/2$ in an external magnetic field can only be parallel or antiparallel to the external field so that it can be represented using a basis of only two orthogonal eigenstates. This makes it possible to model the particle as a two-level, single constituent microscopic system fully represented in a two-dimensional Hilbert space, $\mathscr{H}$. The geometrical representation of such space is a sphere with radius equal to one called a Bloch sphere. The Bloch sphere for a single two-level system (Quantum Bit or Qubit) is depicted in Figure 8.1(a). Here $\vec{r} = (r_x, r_y, r_z)$ is an arbitrary radius vector, such as $|\vec{r}| \leq 1$, with θ and ξ representing the rotation and azimuthal angles, repectively. In addition, $|0\rangle$ represents the high-energy eigenlevel state connected to the low-energy eigenlevel state, $|1\rangle$, by an electric dipole transistion at an angular frequency ω_{eg}[1] so that the energy between the two energy eigenlevel states is $E_{eg} = \hbar\,\omega_{eg}$, as depicted in Figure 8.1(b). For the case were $|\vec{r}\,| = 1$, the state of the qubit, $|\psi\rangle$, is the wave function

$$|\psi\rangle = c_0\,|0\rangle + c_1\,|1\rangle \tag{8.1}$$

[1] Subscript e stands for exited state, and the subscript g for ground state

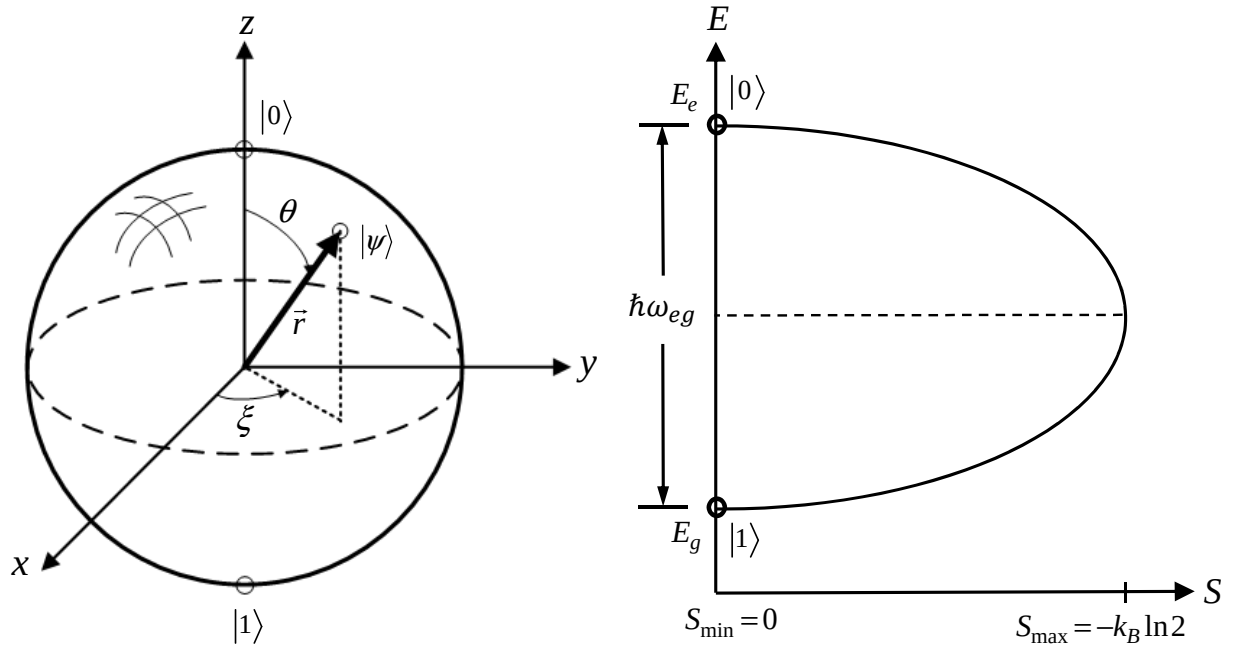

(a) Bloch sphere representation [345]. (b) Energy-entropy representation.

Figure 8.1. Geometrical representation of the state of a two-level system.

geometrically represented by a point on the surface of the Bloch sphere where c_0 and c_1 are the probability amplitudes. From the normalization condition ($|c_0|^2 + |c_1|^2 = 1$), it is found that $|c_0|^2$ and $|c_1|^2$ are the probabilities of finding the qubit in state $|0\rangle$ and $|1\rangle$, respectively, so that the quantum mechanical or thermodynamic state, which in this case is a pure state (i.e., zero-entropy state) can be represented as

$$|\psi\rangle = \frac{1}{\sqrt{2}}|0\rangle + \frac{1}{\sqrt{2}}|1\rangle \tag{8.2}$$

The pure state can be also represented by a density operator ρ obtained by the outer product of the wave function such that $\rho = |\psi\rangle\langle\psi|$. For this particular case, the density or state operator is idempotent, that is, $\rho^2 = \rho$. Non-pure or more accurately, non-zero entropy states of the two-level system are geometrically located inside the Bloch sphere ($|\vec{r}\,| < 1$) where the density or state opeator is non-idempotent ($\rho^2 < \rho$). The density operator for both, pure and non-pure staes, can also be generally represented in terms of the elements of the Bloch sphere such as

$$\rho = \frac{1}{2}(I + \vec{r}\cdot\vec{\sigma}) \tag{8.3}$$

where $\vec{\sigma} = (\sigma_x, \sigma_y, \sigma_z)$ is the vector of Pauli operators given by

$$\sigma_x = |e\rangle\langle g| + |g\rangle\langle e| \tag{8.4a}$$

$$\sigma_y = -i\left(|e\rangle\langle g| - |g\rangle\langle e|\right) \tag{8.4b}$$

$$\sigma_z = |e\rangle\langle e| + |g\rangle\langle g| \tag{8.4c}$$

with $|e\rangle$ and $|g\rangle$ the excited and ground energy states, respectively of a two-level system and I as the identity operator defined as

$$I = |0\rangle\langle 0| + |1\rangle\langle 1| \tag{8.5}$$

Here $|0\rangle$, and $|1\rangle$ are the eigenstates of σ_z with eigenvalues equal to $+1$ and -1, respectively. Important operators that can be constructed using Equation (8.4a) and Equation (8.4b) are the raising σ_+ and lowering σ_- ("spin-flip") operators expressed as

$$\sigma_\pm = \frac{1}{2}\left(\sigma_x \pm i\sigma_y\right) \tag{8.6}$$

which are used in subsequent sections to construct the models that represent the general composite systems used in this dissertation to analyze the phenomenon of decoherence.

The density or state operator of Equation (8.3) can also be represented in matrix form as

$$\rho = \begin{pmatrix} \rho_{00} & \rho_{01} \\ \rho_{10} & \rho_{11} \end{pmatrix} \tag{8.7}$$

where ρ_{00} and ρ_{11} represent the populations (i.e., the eigenlevel occupations) and $\rho_{01} = \rho_{10}^\dagger$ the coherences. Using these elements of Equation (8.7), the $x-$, $y-$ and $z-$components of the radius vector that represent the state of a two-level system can be given as

$$r_x = \rho_{01} + \rho_{10} \tag{8.8a}$$

$$r_y = \frac{1}{i}\left(\rho_{10} - \rho_{01}\right) \tag{8.8b}$$

$$r_z = \rho_{00} - \rho_{11} \tag{8.8c}$$

The state vector components r_x and r_y provide information about the evolution in time of the coherence of the density or state operator, while the state vector component r_z provides information about the evolution in time of the energy of the two-level system, which, for an isolated single constituent system, must remain constant at all times.

The Hamiltoninan of a two-level-type system is diagonal in the $|0\rangle$ and $|1\rangle$ basis and can be represented as

$$H = E_e \left|0\right\rangle \left\langle 0\right| + E_g \left|1\right\rangle \left\langle 1\right| \tag{8.9}$$

where from Figure 8.1(b) it can be observed that the energies of the excited and ground energy eigenstates are given as $E_e = \frac{1}{2}\hbar\,\omega_{eg}$ and $E_g = -\frac{1}{2}\hbar\,\omega_{eg}$, respectively. Substituting the values of E_e and E_g and the $z-$Pauli operator (Equation (8.4c)), the Hamiltonian on a two-dimensional Hilber space, $\mathscr{H}$, of a single two-level system is given as

$$H = \frac{1}{2}\hbar\,\omega_{eg}\sigma_z \tag{8.10}$$

This Hamiltonian is used in subsequent sections of this chapter to construct the overall Hamiltonian of a composite microscopic system.

8.2 Modeling of an electromagnetic field

8.2.1 The quantum Harmonic oscillator

The energy spectrum of a photon field is distributed among an infinite number of energy levels, with a Hamiltonian operator given as

$$H = T + V = -\frac{\hbar^2}{2m}\frac{d^2}{dx^2} + \frac{m\omega^2}{2}x^2 = \frac{1}{2m}\left[\left(\frac{\hbar}{i}\frac{d}{dx}\right)^2 + (m\omega x)^2\right] = \frac{1}{2m}(p^2 + \bar{x}^2) \tag{8.11}$$

where x represents the position operator, p the momentum operator, and $\bar{x} = m\omega x$. Other useful operators used below to reformulate x and p are the annihilation and creation operators defined as a and $a^\dagger$, respectively,

$$a = \frac{1}{\sqrt{2m\hbar\,\omega}}\,(m\omega x + i\,p) \tag{8.12a}$$

$$a^\dagger = \frac{1}{\sqrt{2m\hbar\,\omega}}\,(m\omega x - i\,p) \tag{8.12b}$$

A photon number operator, $N = a^\dagger a$, is obtained by combining the annihilation and creation operators. The position and momentum operators can be defined in terms of the annihilation and creation opperators such that

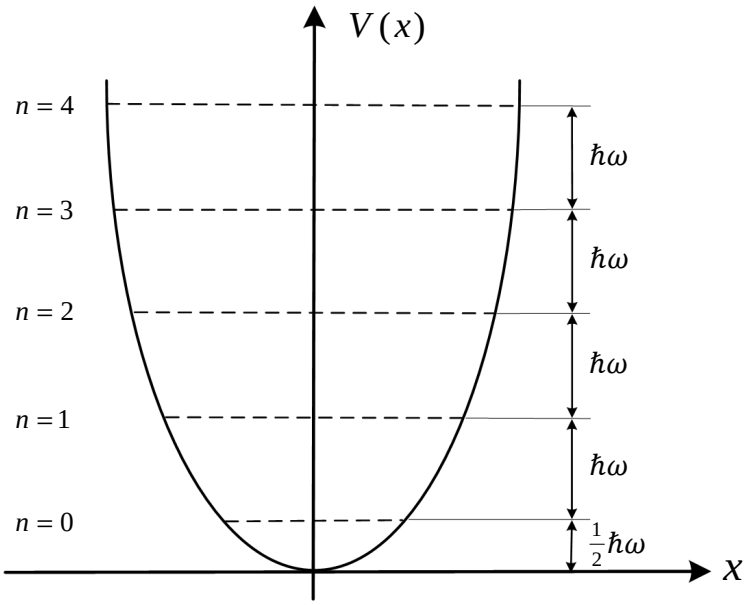

Figure 8.2. Schematic representation of a quantum Harmonic oscillator [373]. Only the first four energy eigenlevels and the ground energy eigenlevel are shown in the figure.

$$x = \sqrt{\frac{\hbar}{2m\omega}}\left(a + a^{\dagger}\right) \tag{8.13a}$$

$$p = i\sqrt{\frac{m\hbar\,\omega}{2}}\left(a^{\dagger} - a\right) \tag{8.13b}$$

Finally, the time independent Schrödinger equation or energy eigenvalue problem for the quantum harmonic oscillator is expressed as

$$\hbar\,\omega\left(N + \frac{1}{2}\right)\psi = \varepsilon\,\psi \tag{8.14}$$

where ψ is the energy eigenfunction and ε its energy eigenvalue. The solution to this equation provides the energy structure of the Harmonic oscillator for which each energy eigenvalue is given by

$$\varepsilon_n = \hbar\,\omega\left(n + \frac{1}{2}\right) \tag{8.15}$$

where n are the eigenvalues of the photon number operator, N, and $n = 0, 1, \ldots$

As seen from Equation (8.15), the energy eigenlevels of the harmonic oscillator are equally spaced with the ground or vacuum state equal to $\hbar\,\omega/2$. A schematic representation of the energy eigenstructure is depicted as a ladder of energy eigenlevels in Figure 8.2. The set of energy eigenstates represented by the set of eigenfunctions $\{\psi_n\}$, corresponding to the energy eigenlevels of

Equation (8.15), can be represented using the index number as the complete set of orthonormal vectors $\{|n\rangle\}$ in Fock space [373]. From Figure 8.2, it can also be observed that the annihilation operator, a, removes a quantum amount of energy $\hbar\omega$, lowering the eigenstate of the system to the next lower energy eigenlevel, while the creation operator, $a^\dagger$, adds a quantum amount of energy $\hbar\omega$ raising the state of the system to the next upper energy eigenlevel.

8.2.2 Coherent or Glauber states

A coherent or Glauber state [374], $|\alpha\rangle$, represents the state of a cloud of an indefinite number of photons behaving as randomly distributed classical particles with a particle number expectation value of $|\alpha|^2$. Examples of systems that have this characteristic are a laser beam and a photon field inside a quantum cavity. A Glauber state is defined as *"the eigenstate of the annihilation operator, a, with eigenvalues α"* [373] such that the eigenvalue problem for these eigenstates is written as

$$a\,|\alpha\rangle = \alpha\,|\alpha\rangle \tag{8.16}$$

Since the operator a is non-hermitian, the eigenvalue $\alpha = |\alpha|e^{i\phi}$ is a complex number with phase ϕ.

The set of eigenvectors $|\alpha\rangle$ is an overcomplete basis that is not orthonormal so that it is necessary to represent the Coherent states using the complete and orthonormal set of vectors $|n\rangle$ in Fock space. Since the vacuum state is a coherent state with $\alpha = 0$ (i.e., $a\,|0\rangle = 0$), a coherent state can be created in Fock space such that

$$|\alpha\rangle = D(\alpha)\,|0\rangle \tag{8.17}$$

where the displacement opeator $D(\alpha)$ is expressed as

$$D(\alpha) = e^{-\frac{1}{2}|\alpha|^2} e^{\alpha a^\dagger} e^{\alpha^* a} \tag{8.18}$$

where α^* is the complex conjugate off the eigenvalue α. $D(\alpha)$ has the function of creating coherent states from the ground state in a fashion similar to that the creation operator, $a^\dagger$, generating occupation number states. α^* is the complex conjugate of α.

For many cases as is the case for the particle system, it is sufficient to know the transition between two neighboring energy eigenstates in order to fully understand the behavior of the system.

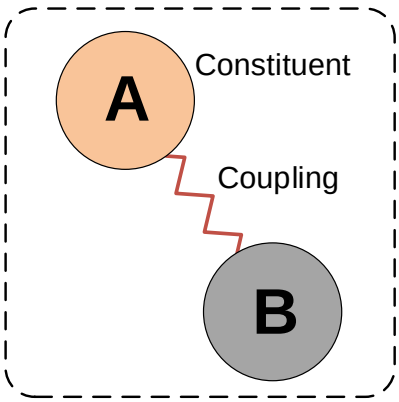

Figure 8.3. Schematic representation of a composite system of two spin-$^1/_2$ constituents. Reprinted from [262] Copyright © 2013 by ASME, with permission.

Taking this into account, the Hamiltonian for a system formed by a cloud of an indefinite number of photons can be written as

$$H = \hbar\omega N = \hbar\omega a^\dagger a \tag{8.19}$$

where the $\frac{1}{2}$ has been removed because the minimum energy of the reference eigenenergy has been taken as that of the ground state. This Hamiltonian will be used in a subsequent section of this chapter to construct the overal Hamiltonian of a composite microscopic system compraised of a particle and a photon field.

8.3 Two-particle spin-$^1/_2$ composite microscopic system

The two-particle composite system under analysis in this dissertation is depicted in Figure 8.3. It consists of two interacting, spin-$^1/_2$-type particles. This represents the smallest composite system that can be formed in Nature and can, for example, be used to analyze the entangled or correlated (thermodynamic) states obtained when physically measuring the state of a composite system in which one constituent represents the particle and the other the measuring device treated as a two-level-type subsystem [359].

It is assumed here that the state of spin-A and that of spin-B are fully represented in Hilbert subspaces $\mathscr{H}_A$ and $\mathscr{H}_B$, respectively. The Hilbert space corresponding to the composite system is given as the outer product of the two subspaces such that

$$\mathscr{H} = \mathscr{H}_A \otimes \mathscr{H}_B \tag{8.20}$$

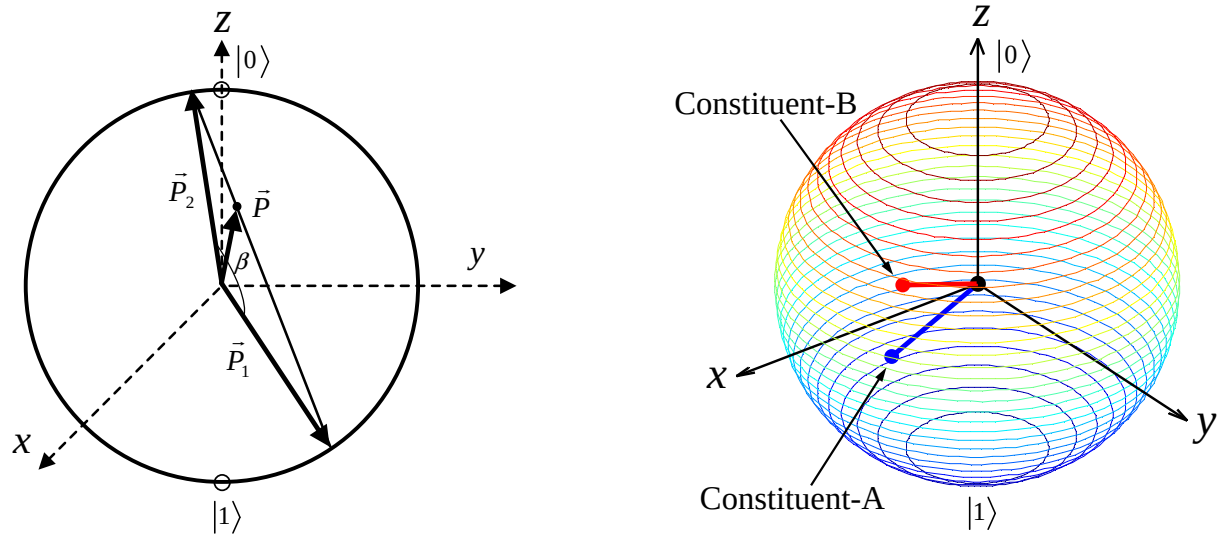

(a) Construction of a non-zero-entropy state [359].

(b) Initial state for the system under analysis.

Figure 8.4. Bloch sphere representation of a qubit [262]. Reprinted from [262] Copyright © 2013 by ASME, with permission.

Initially, the particles are independent of each other; but when an interaction occurs, their states can no longer be described independently, and a single nonseparable system behavior is observed for the states of the two constituents. In other words an entanglement or correlation of the now so-called local 'states' of the two particles is created.

The entangled or correlated density or state operator, ρ, for the composite system may be written as

$$\rho = \rho_A \otimes \rho_B + \zeta \tag{8.21}$$

Here ρ is formed from the outer product of the local or reduced operators represented by $\rho_A \equiv \mathrm{Tr}_B\, \rho$ and $\rho_B \equiv \mathrm{Tr}_A\, \rho$ and a correlation operator, ζ, which is the null operator only in the absence of entanglement or correlations.

8.3.1 Initial entangled and correlated density operators

The state (either of zero entropy or of non-zero entropy) of a spin-$^1/_2$ particle is represented as a vector on or in the Bloch sphere as depicted in Figure 8.1(a). If the state is a zero-entropy state, the tip of its vector representation, e.g., $\vec{P}_1$ or $\vec{P}_2$ in Figure 8.4(a), is on the surface of the sphere, i.e., $|\vec{P}_1| = 1$, or $|\vec{P}_2| = 1$, respectively. A non-zero-entropy state, on the other hand, lies within

the sphere and can, for example, be constructed as a statistical mixture of two zero-entropy states [359] such that

$$\rho = \frac{1}{2}[I + \omega\vec{P}_1 \cdot \vec{\sigma} + (1-\omega)\vec{P}_2 \cdot \vec{\sigma}] = \omega\,|\psi_1\rangle\,\langle\psi_1| + (1-\omega)\,|\psi_2\rangle\,\langle\psi_2| \tag{8.22}$$

where ω is a real constant satisfying $0 < \omega < 1$ and $|\psi_1\rangle$ and $|\psi_2\rangle$ are orthogonal, i.e., located in opposite directions of a diameter of the Bloch sphere because a non-zero-entropy state can also be obtained with a statistical mixture of two or more non-orthogonal zero-entropy states. However, the number of terms may exceed the size of the Hilbert space [359].

This approach can be applied to obtain non-zero-entropy state operators ρ_A and ρ_B for constituent-A and constituent-B, i.e., for spin-A the non-zero-entropy state ρ_A is given as

$$\rho_A = \omega_1^A \rho_1^A + \omega_2^A \rho_2^A \tag{8.23}$$

or equivalently in state vector representation as

$$\vec{P}_A = \omega_1^A \vec{P}_1^A + \omega_2^A \vec{P}_2^A \tag{8.24}$$

where

$$\rho_1^A = \left|\psi_1^A\right\rangle \left\langle\psi_1^A\right| = \frac{1}{2}(I + \vec{P_1^A} \cdot \vec{\sigma}) \tag{8.25a}$$

$$\rho_2^A = \left|\psi_2^A\right\rangle \left\langle\psi_2^A\right| = \frac{1}{2}(I + \vec{P_2^A} \cdot \vec{\sigma}) \tag{8.25b}$$

and the tip of the non-zero-entropy state vector, e.g., $\vec{P}_A$ ($|\vec{P}_A| < 1$) is on a line connecting the tips of the two zero-entropy or pure state vectors, $\vec{P}_1^A$ and $\vec{P}_2^A$. Here ω_1^A is a real constant satisfying $0 < \omega_1^A < 1$, and $\omega_2^A = 1 - \omega_1^A$. Note that Equation (8.23) represents the density operator for a non-zero-entropy state of constituent-A only. A similar procedure can be applied to obtain the non-zero-entropy state operator for constituent-B, resulting in

$$\rho_B = \omega_1^B \rho_1^B + \omega_2^B \rho_2^B \tag{8.26}$$

or equivalently in state vector representation

$$\vec{P}_B = \omega_1^B \vec{P}_1^B + \omega_2^B \vec{P}_2^B \tag{8.27}$$

where

$$\rho_1^B = \left|\psi_1^B\right\rangle \left\langle\psi_1^B\right| = \frac{1}{2}(I + \vec{P_1^B} \cdot \vec{\sigma}) \tag{8.28a}$$

$$\rho_2^B = \left|\psi_2^B\right\rangle \left\langle\psi_2^B\right| = \frac{1}{2}(I + \vec{P_2^B} \cdot \vec{\sigma}) \tag{8.28b}$$

and ω_1^B is also a real constant satisfying $0 < \omega_1^B < 1$, and $\omega_2^B = 1 - \omega_1^B$. Figure 8.4(b) shows the initial state vectors representing the reduced density operators ρ_A and ρ_B on $\mathscr{H}_A$ and $\mathscr{H}_B$ for particles A and B, respectively, obtained for a particular case provided in this dissertation.

If instead of a single qubit, the two distinguishable qubits constituent-A on $\mathscr{H}_A$ and constituent-B on $\mathscr{H}_B$ are considered, a non-zero-entropy state operator on $\mathscr{H}$ is obtained by the outer product of the non-zero-entropy state operators given by Equations (8.23) and (8.26) such as

$$\rho = \omega_1\rho_1^A \otimes \rho_1^B + \omega_2\rho_2^A \otimes \rho_2^B + \omega_3\rho_1^A \otimes \rho_2^B + \omega_4\rho_2^A \otimes \rho_1^B \tag{8.29}$$

In an attempt to preserve the generality of the above approach for generalizing a non-zero-entropy state, the zero-entropy sates ρ_1^A on $\mathscr{H}_A$, and ρ_1^B on $\mathscr{H}_B$ are obtained by randomly picking a point on the surface of the Bloch spheres using the *Point Picking* approach presented in [375]. In this randomization scheme, four real positive constants y_1, y_2, y_3, and y_4 between 0 and 1 are randomly obtained in order to calculate the rotational and azimutal angles (see Figure 8.1(a)) corresponding to the state vectors $\vec{P}_1^A$ and $\vec{P}_1^B$ such that

$$\theta_A = cos^{-1}(2y_2 - 1) \tag{8.30a}$$

$$\theta_B = cos^{-1}(2y_4 - 1) \tag{8.30b}$$

$$\xi_A = \frac{2}{\pi}y_1 \tag{8.30c}$$

$$\xi_B = \frac{2}{\pi}y_3 \tag{8.30d}$$

States ρ_2^A and ρ_2^B are in opposite directions to ρ_1^A and ρ_1^B, respectively, along a diameter of the Bloch sphere, that is, $\vec{P}_2^A(\theta_A + \pi, \xi_A + \pi)$ and $\vec{P}_2^B(\theta_B + \pi, \xi_B + \pi)$.

The weights ω_i in Equation (8.29) are obtained by randomly obtaining four real positive constants x_1, x_2, x_3, and x_4 between 0 and 1 and calculating the probabilities such as

$$\omega_i = \frac{x_i}{\sum_{i=1}^{4} x_i} \tag{8.31}$$

where the conditions

$$\sum_i \omega_i = 1 \text{ and } 0 < \omega_i < 1 \tag{8.32}$$

are satisfied.

The state operator obtained with Equation (8.29) is for the initial non-equilibrium state of the composite microscopic system given by Equation (8.21) [297]. In contrast, the final stable equilibrium state reached at the end of the state relaxation takes the canonical form

$$\rho_{se} = \frac{e^{-H/kT}}{\mathrm{Tr}\left(e^{-H/kT}\right)} \tag{8.33}$$

where the Hamiltonian operator, H, is defined in the next section below. The energy eigenlevel occupation probabilities showing the energy redistribution within the energy eigenlevels of the system are found from

$$p_j = \langle e_j \rangle = \mathrm{Tr}(e_j \rho) \tag{8.34}$$

where the e_j are the eigenprojectors of the Hamiltonian operator given by

$$e_j = |\varepsilon_j\rangle \langle \varepsilon_j| \tag{8.35}$$

8.3.2 Modeling of the energy structure

The Hamiltonian operator on $\mathscr{H}$, representing the total energy of the composite system, is written as

$$H = H_A \otimes I_B + I_A \otimes H_B + V \tag{8.36}$$

where the operators

$$H_A = \frac{1}{2}\hbar\, \omega_{eg} \sigma_A^{\mathrm{z}} \tag{8.37a}$$

$$H_B = \frac{1}{2}\hbar\, \omega_{eg} \sigma_B^{\mathrm{z}} \tag{8.37b}$$

are the Hamiltonians on subspaces $\mathscr{H}_A$ and $\mathscr{H}_B$, respectively, defined by Equation (8.10), ω_{eg} is the transition frequency between the exited and ground energy levels of each constituent, and $\hbar$ is the reduced or modified Planck constant. The interaction operator on $\mathscr{H}$ given by

$$V = -\Gamma\left(\vec{\sigma}_A \otimes \vec{\sigma}_B\right) \tag{8.38}$$

represents the interaction between constituents A and B, $\vec{\sigma}_J$ (where $J = A, B$) are three-dimensional vectors of Pauli operators defined by Equations (8.4a) to (8.4c), and Γ is the strength of the interaction or coupling between the subsystems. For the system under consideration, the Hamiltonian of Equation (8.36) becomes

$$H = -m\left(\sigma_A^z \otimes I_B + I_A \otimes \sigma_B^z\right) - \Gamma\left(\vec{\sigma}_A \otimes \vec{\sigma}_B\right) \tag{8.39}$$

where $m = \frac{1}{2}\hbar\,\omega_{eg}$ is the unit strength of a uniform externally applied magnetic field in the z-direction. The strength of the field given by $\vec{M} = m\hat{z}$ is small with respect to the Zeeman interaction splitting effects which are due to the interaction of the external magnetic field with the spin magnetic moment of the atom. If this interaction is big enough, the energy spectrum of the atom is split into two or more spectrums and can no longer be treated as a particle. For simplicity and without loss of generality, m and $\hbar$ are set to 1, while Γ is set to 0.02.

8.4 Particle-photon field composite microscopic system

The description of the experiments as well as the values used in the present modeling are based on the work developed by the CQED group of Haroche and co-workers in Paris [289–292, 339, 358, 359]. The reader is encouraged to visit these references for a thorough description of the theoretical background, experimental setup, and measurements developed on decoherence between the local 'states' of the atom and the electromagnetic field mode.

A schematic representation of the experimental configuration of Haroche and co-workers [289] is depicted in Figure 8.5. Rubidium atoms are contained in an oven **B** from which one atom in eigenstate $|\psi_B\rangle = |0\rangle$ (excited level) is selected and subsequently subjected to a classical resonant microwave $\pi/2$ pulse in $\mathbf{R}_1$ supplied by the source **S**'. This creates a state in a superposition of circular Rydberg eigenlevels $|0\rangle$ and $|1\rangle$ (ground eigenlevel) for the atom, corresponding to principal quantum numbers 51 and 50, respectively. Afterwards, the atom is allowed to enter

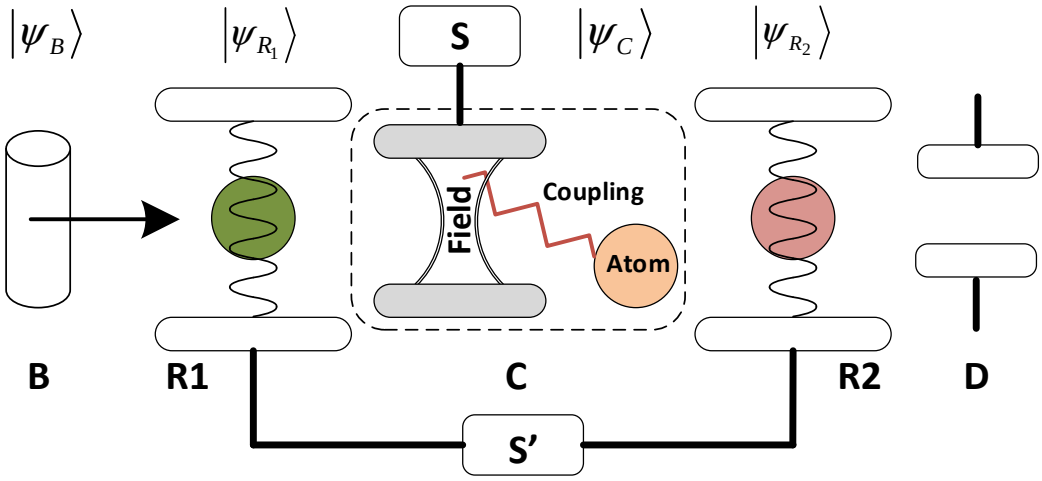

Figure 8.5. Schematic representation of an atom-field Cavity QED experiment [289]. Reprinted from [304], with permission.

the high-Q quantum cavity **C** that contains an electromagnetic field mode in a Fock state $|\alpha\rangle$ previously injected into the cavity by an external source **S**. The atom and cavity are off-resonant, and, therefore, absorption of photons is not exhibited during the interaction; and the atom shifts only the phase of the field mode by an amount ϕ. This dephasing provokes the coupling of the excited eigenlevel of the atom to the field mode state with phase $|\alpha_0\rangle \equiv \left|\alpha e^{i\phi}\right\rangle$ and the coupling of the ground state of the atom to the field mode state with phase $|\alpha_1\rangle \equiv \left|\alpha e^{-i\phi}\right\rangle$. In this manner, an entanglement between the eigenstates of the constituents is created such that

$$|\psi_C\rangle = \frac{1}{\sqrt{2}}\left(|0,\alpha_0\rangle + |1,\alpha_1\rangle\right) \tag{8.40}$$

After leaving the cavity, the atom is subjected again to a resonant microwave pulse in $\mathbf{R}_2$ equal to that at $\mathbf{R}_1$, mixing the atom energy eigenlevels and creating a "blurred" state for the composite, which preserves the quantum ambiguity of the field phase such that

$$|\psi_{R_2}\rangle = \frac{1}{2}e^{-i\phi}\,|0\rangle\left(|\alpha_0\rangle - |\alpha_1\rangle\right) + \frac{1}{2}\,|1\rangle\left(|\alpha_0\rangle + |\alpha_1\rangle\right) \tag{8.41}$$

Finally, the excited eigenlevel state of the Rb atom is observed and recorded by a detector **D**, projecting the state of the electromagnetic field into a superposition coherent states $|\alpha_0\rangle$ and $|\alpha_1\rangle$. Since at this point the state of the atom has been unveiled, the only coherence left in the composite system is that due to the phase difference between the shifted coherence states of the electromagnetic field.

8.4.1 Initial entangled and correlated density operator

In order to measure the decay of coherence left on the field mode state by the atom, a second atom of identical characteristics of that of the first one is put through the same path after a delay time of t_d. The reading of the state of the second atom at **D** uncovers the effects left by the first atom on the state of the field mode.

In order to monitor the decoherence in the CQED experiments, a second Rb atom of identical characteristics to that of the first one is put through the same path after a delay time of t_d. This second atom also shifts the phase of the electromagnetic field. If there is no decoherence, this phase shift produced by the second atom would be of the same magnitude as that produced by the first atom; and, thus, the probability of finding the second atom in the excited level eigenstate would be equal to one. On the other hand, if the system is allowed to relax for a certain period of time t_d, the interaction with the second Rb would cause a phase shift in the electromagnetic field of a value lower than that produced by the first atom, and, thus, the probability of finding the second atom in the excited level eigenstate would be lower than one.

In the modeling presented here, the initial thermodynamic state of the composite system is obtained when the first atom is detected in its excited level eigenstate, projecting the electromagnetic field in a superposition of coherent eigenstates so that the coherence of the composite is due to the phase difference on the states of the field only. Since the density operator that represents the thermodynamic state of the system can be known here, an equation of motion can be used to model the evolution in thermodynamic state of the composite system at every instant of time, and, of course, monitor the loss of coherence of the composite due to the phase different between the eigenstates of the electromagnetic field only. In this way, in a modeling scheme, a second atom is not needed to unveil the thermodynamic state of the field at every instant of time. The initial thermodynamic state operator for the composite system, i.e.,

$$\rho_0 = |\psi_{R_2}\rangle \langle \psi_{R_2}| \tag{8.42}$$

represents a pure (zero-entropy) state. In order for the state operator to evolve in time according to the the SEA-QT equation of motion, a slight perturbation in agreement with [297] is induced. The perturbation method at constant system energy is also described in Section 7.2.1 of this dissertation. A value of $\lambda = 0.95$ is used in the perturbation in order to start the evolution in a non-equilibrium

state very close to the original zero-entropy initial state ($\lambda = 1$) given by Equation (8.42). Values for the phase $2\phi = 100°$ and $2\phi = 50°$ [292] and the probability of the atom being in its excited eigenlevel state of $\mathbb{P}_e \approx 1$ are used for the two different cases presented.

The internal-relaxation time in the SEA-QT equation of motion for each constituent is considered to be a real positive constant with values of $\tau_A = \tau_F = 300$ ms. This value is chosen because it is long enough to show the various features of the state evolution in time of the composite system and its constituents well. As seen below in the comparison with the experimental results of [292], values of 0.26 ms and 0.36 ms are also used.

8.4.2 Modeling of the energy structure (Jaynes-Cummings Hamiltonian)

In the modeling of a field mode-atom composite system, it is common that the single mode of an electromagnetic field is assumed to be quantized and treated as a two-level-type harmonic oscillator fully represented in Hilbert subspace $\mathscr{H}_F$, while the atom is treated as a two-level-type spin-$1/2$ particle fully represented in Hilbert subspace $\mathscr{H}_A$ [376–378]. This represents the simplest model in which light and matter can interact.

The Hamiltonian on Hilbert space $\mathscr{H} = \mathscr{H}_A \otimes \mathscr{H}_F$ describes the total energy of the composite system and is the traditional Jaynes-Cummings Hamiltonian (in the rotating-wave approximation) [379–381] such that

$$H = \frac{1}{2}\hbar\,\omega_{eg}\,(\sigma_z \otimes I_F) + \hbar\,\omega_f\,(I_A \otimes N) + V \tag{8.43}$$

where the first term on the right hand side is the Hamiltonian of a particle on $\mathscr{H}_A$ given by Equation (8.10) spanned over the Hilbert space $\mathscr{H}$ while the second term is the Hamiltonian of a photon field on $\mathscr{H}_F$ given by Equation (8.19) spanned over the Hilbert space $\mathscr{H}$. The interaction operator on $\mathscr{H}$ is given as

$$V = \frac{1}{2}\hbar\,\Omega_0\left(a \otimes \sigma_+ + a^\dagger \otimes \sigma_-\right) \tag{8.44}$$

Here σ_z is the z-Pauli operator defined in Equation (8.4c), σ_+ and σ_- are the raising and lowering ("spin-flip") operators defined in Equation (8.6), $a^\dagger$ and a are the creation and annihilation operators, and $N = a^\dagger a$ is the photon number operator. ω_{eg} is the transition frequency between the excited and ground energy eigenlevels of the atom, ω_f the cavity frequency, and Ω_0 the Rabi

frequency, which indicates the strength of the atom-field interaction.

For the present model, values taken from [292] are used. The transition frequency between the excited and ground energy eigenlevels of the atom is given as $\omega_{eg}/2\pi = 51.099$ GHz, the Rabi frequency as $\Omega/2\pi = 24$ kHz , and detunings as $\delta/2\pi = 70$ kHz and $\delta/2\pi = 170$ kHz corresponding to phase shift of $2\phi = 100°$ and $2\phi = 50°$, respectively, where $\delta = \omega_{eg} - \omega_f$.

8.5 SEA-QT evolution dynamics

8.5.1 Isolated single constituent indivisible system

In the early 1980s, Beretta [257, 284, 288] completed the dynamical postulate of SEA-QT by providing an equation of motion capable of modeling the evolution of the state of a system from a non-equilibrium state to that of stable equilibrium, while keeping constant the expectation value of the energy of the system. This equation satisfies both the first and second law of thermodynamics and reduces to the Schrödinger equation for zero-entropy states and to the canonical form (or grand canonical form for the case of a grand system [382]) for stable equilibrium states (Equation (8.33)). This equation was "engineered" or postulated based on the *steepest-entropy-ascent ansatz* in which the system follows the path of local-maximum entropy generation during the relaxation of its state to stable equilibrium. For example, for a system composed of one two-level-type particle, its state evolution towards stable equilibrium is driven by both a Hamiltonian vector tangent to its trajectory through state space and a dissipative vector orthogonal to this trajectory as shown by the red vectors in Figure 8.6. The dissipative vector is the one which assures that the path is that of maximum entropy generation [295] represented by the blue spiral. For a system composed of two or more distinguishable constituents, the dissipation vector of the composite system corresponds to the contribution of the locally-perceived dissipation vectors of each individual subsystem where again the steepest entropy-ascent ansatz applies locally for every individual constituent and guarantees that the path to stable equilibrium followed by the composite system is also that of maximum entropy generation.

For an isolated, single constituent quantum system (single particle, a group of indistinguishable constituents, or a field) in a Hilbert space, $\mathscr{H}$, the SEA-QT quation of motion takes the form [257, 284]

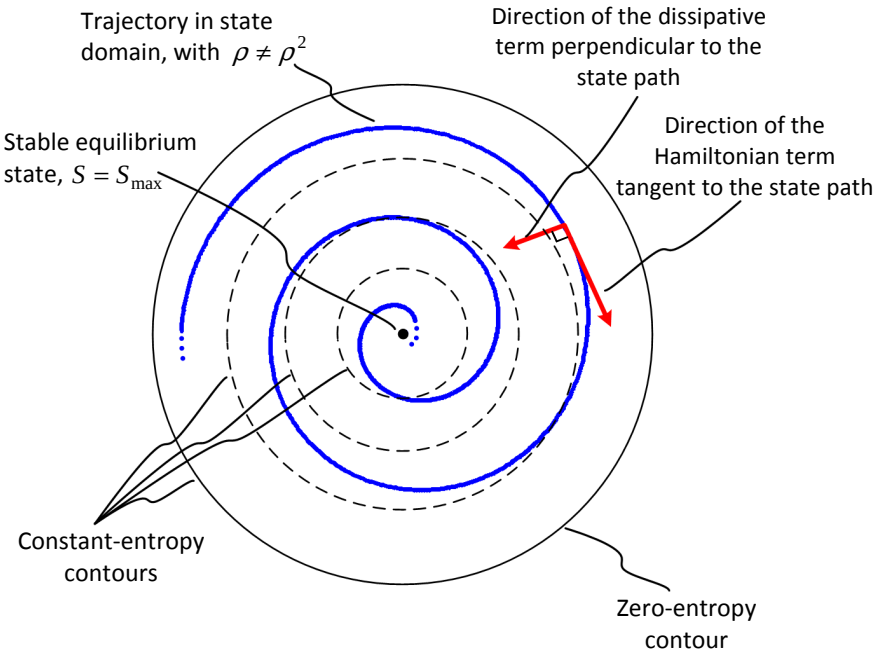

Figure 8.6. Steepest entropy ascent trajectory for the relaxation towards stable equilibrium [295].

$$\frac{d\rho}{dt} = -\frac{i}{\hbar}[H, \rho] - \frac{1}{\tau_D} D \tag{8.45}$$

where ρ is the density or state operator, H is the Hamiltonian operator that represents the total energy of the system, and the operator $[H, \rho] = H\rho - \rho H$ is the commutator between the Hamiltonian and density or state operator.

The density operator is mathematically redefined in [287] as the scalar product of the positive square root of the density operator, $\sqrt{\rho}$, and the Hermitian of the square root of the density operator, $(\sqrt{\rho})^\dagger$, such that

$$|\rho| = \sqrt{\rho^\dagger \rho} = (\sqrt{\rho})^\dagger \sqrt{\rho} = \gamma^\dagger \gamma \tag{8.46}$$

where γ is

$$\gamma = U\sqrt{\rho} \tag{8.47}$$

This is done to assure that the state operator is Hermitian, positive semi-definite, i.e., $\rho(t)^\dagger = \rho(t) \geq 0$, at all time. The operator U can be assumed to be the identity operator $(U = I)$.

The first term on the right-hand side of Equation (8.45) captures the unitary, Hamiltonian dynamics of the Schrödinger-von Neumann equation. When the system is in a zero-entropy state,

this term assures that the system evolves on the vertical axis of the energy-entropy diagram only (see Figure 8.1(b)) or for a two-level system on the surface of the Bloch diagram (see Figure 8.4).

The second term of Equation (8.45) models the non-linear dynamics of dissipative (irreversible) evolution in state based on the principle of SEA subject to the relevant dynamical constraints [284–287]. The internal-relaxation time particular to the system, τ_D, is considered to be a real constant or functional [294], and the operator D is the nonlinear functional constructed as a function of the overall density operator defined explicitly in [288] by

$$D = \frac{1}{2}\left(\sqrt{\rho}\tilde{D} + (\sqrt{\rho}\tilde{D})^{\dagger}\right) \tag{8.48}$$

where

$$\tilde{D} = \frac{\begin{vmatrix} \sqrt{\rho}\ln\rho & \sqrt{\rho}\,R_0 & \sqrt{\rho}\,R_1 & \cdots & \sqrt{\rho}\,R_z \\ (R_0,\ln\rho) & (R_0,R_0) & (R_0,R_1) & \cdots & (R_0,R_z) \\ (R_1,\ln\rho) & (R_1,R_0) & (R_1,R_1) & \cdots & (R_1,R_z) \\ \vdots & \vdots & \vdots & \ddots & \vdots \\ (R_z,\ln\rho) & (R_z,R_0) & (R_z,R_1) & \cdots & (R_z,R_z) \end{vmatrix}}{\begin{vmatrix} (R_0,R_0) & (R_0,R_1) & \cdots & (R_0,R_z) \\ (R_1,R_0) & (R_1,R_1) & \cdots & (R_1,R_z) \\ \vdots & \vdots & \ddots & \vdots \\ (R_z,R_0) & (R_z,R_1) & \cdots & (R_z,R_z) \end{vmatrix}} \tag{8.49}$$

Here $|\circ|$ denotes a determinant, and the determinant element (F,G) defined as

$$(F,G) = (G,F) \equiv \frac{1}{2}\mathrm{Tr}\left(|\rho|\,\{F,G\}\right) = (\sqrt{\rho}G|\sqrt{\rho}F) = (\sqrt{\rho}F|\sqrt{\rho}G) \tag{8.50}$$

is the inner product of the two operators F and G that can represent the entropy operator, $-k_B\ln\rho$, or one of the generators of the motion of the system represented by R_i. The term $(A|B)$ is the real scalar product of two linear operators given as

$$(A|B) = (B|A) \equiv \frac{1}{2}\mathrm{Tr}\left(A^{\dagger}B + B^{\dagger}A\right) \tag{8.51}$$

and $\{F,G\}$ is the anti-commutator operator $\{F,G\} = FG + GF$.

The dissipative term is highly non-linear, and the solution of Equation (8.45) must be obtained in numerical form for all but the simplest cases. An example of such a simplest case is given

in [323, 383]. For a petit system [382] such as a two-level, isolted and non-reactive system, a complete set of generators of the motion is represented by the set which includes the identity and Hamiltonian operators, i.e., $\{R_0, R_1\} = \{I, H\}$, so that Equation (8.49) reduces to

$$\tilde{D} = \frac{\begin{vmatrix} \sqrt{\rho}\ln\rho & \sqrt{\rho}\, I & \sqrt{\rho}\, H \\ (I, \ln\rho) & (I, I) & (I, H) \\ (H, \ln\rho) & (H, I) & (H, H) \end{vmatrix}}{\begin{vmatrix} (I, I) & (I, H) \\ (H, I) & (H, H) \end{vmatrix}} \tag{8.52}$$

and the equation of motion, Equation (8.45), takes the final form

$$\frac{d\rho}{dt} = -\frac{i}{\hbar}[H, \rho] - \frac{1}{\tau_D}\left(\rho\ln\rho + \alpha(\rho)\,\rho + \frac{1}{2}\beta(\rho)\,\{H, \rho\}\right) \tag{8.53}$$

where the terms $\alpha(\rho)$ and $\beta(\rho)$ are defined as

$$\alpha(\rho) = -\frac{\mathrm{Tr}\,(\rho\ln\rho)\,\mathrm{Tr}\,(\rho H^2) - \mathrm{Tr}\,(\rho H\ln\rho)\,\mathrm{Tr}\,(\rho H)}{\mathrm{Tr}\,(\rho H^2) - (\mathrm{Tr}\,(\rho H))^2} \tag{8.54}$$

$$\beta(\rho) = \frac{\mathrm{Tr}\,(\rho\ln\rho)\,\mathrm{Tr}\,(\rho H) - \mathrm{Tr}\,(\rho H\ln\rho)}{\mathrm{Tr}\,(\rho H^2) - (\mathrm{Tr}\,(\rho H))^2} \tag{8.55}$$

8.5.2 Isolated composite system

The SEA-QT equation of motion for an isolated and non-reactive composite system is given by [288]

$$\frac{d\rho}{dt} = -\frac{i}{\hbar}[H, \rho] + \frac{D\rho}{Dt} \tag{8.56}$$

where the first term on the right-hand side describes the unitary Hamiltonian dynamics of the system and the second the non-Hamiltonian dissipative (irreversible) dynamics. The second term is defined as

$$\frac{D\rho}{Dt} = -\sum_{J=1}^{M}\frac{1}{\tau_J} D_J \otimes \rho_{\bar{J}} \tag{8.57}$$

where subscript J represents a single indivisible constituent on $\mathscr{H}^J$ and subscript $\bar{J}$ represents the group of all constituents but the J-th on $\mathscr{H}^{\bar{J}}$. The internal-relaxation times, τ_J, are considered to

be real constants or functionals. The operators D_J are the nonlinear functions of the overall density operator defined explicitly in [288] by

$$D_J = \frac{1}{2}\left(\sqrt{\rho_J}\tilde{D}_J + (\sqrt{\rho_J}\tilde{D}_J)^\dagger\right) \tag{8.58}$$

with $\tilde{D}_J$ defined as

$$\tilde{D}_J = \frac{\begin{vmatrix} \sqrt{\rho_J}\,(B\ln\rho)^J & \sqrt{\rho_J}\,(R_{0J})^J & \sqrt{\rho_J}\,(R_{1J})^J & \cdots & \sqrt{\rho_J}\,(R_{z(J)J})^J \\ (R_{0J}, B\ln\rho)^J & (R_{0J}, R_{0J})^J & (R_{0J}, R_{1J})^J & \cdots & \left(R_{0J}, R_{z(J)J}\right)^J \\ (R_{1J}, B\ln\rho)^J & (R_{1J}, R_{0J})^J & (R_{1J}, R_{1J})^J & \cdots & \left(R_{1J}, R_{z(J)J}\right)^J \\ \vdots & \vdots & \vdots & \ddots & \vdots \\ \left(R_{z(J)J}, B\ln\rho\right)^J & \left(R_{z(J)J}, R_{0J}\right)^J & \left(R_{z(J)J}, R_{1J}\right)^J & \cdots & \left(R_{z(J)J}, R_{z(J)J}\right)^J \end{vmatrix}}{\begin{vmatrix} (R_{0J}, R_{0J})^J & (R_{0J}, R_{1J})^J & \cdots & \left(R_{0J}, R_{z(J)J}\right)^J \\ (R_{1J}, R_{0J})^J & (R_{1J}, R_{1J})^J & \cdots & \left(R_{1J}, R_{z(J)J}\right)^J \\ \vdots & \vdots & \ddots & \vdots \\ \left(R_{z(J)J}, R_{0J}\right)^J & \left(R_{z(J)J}, R_{1J}\right)^J & \cdots & \left(R_{z(J)J}, R_{z(J)J}\right)^J \end{vmatrix}} \tag{8.59}$$

Here B is the idempotent operator obtained by substituting unity for each nonzero eigenvalue of the density or state operator, ρ, $|\circ|$ denotes a determinant, $(F,G)^J = \left(\sqrt{\rho_J}(F)^J|\sqrt{\rho_J}(F)^J\right)^J$, and $(F_J|G_J)^J = \frac{1}{2}\mathrm{Tr}_J\left(F_J^\dagger G_J + G_J^\dagger F_J\right)$.

For a a general composite system to which its generators of the motion are given by the set $R = \{I, H\}$, Equation (8.59) reduces to

$$\tilde{D}_J = \frac{\begin{vmatrix} \sqrt{\rho_J}\,(B\ln\rho)^J & \sqrt{\rho_J}\,(I)^J & \sqrt{\rho_J}\,(H)^J \\ (I, B\ln\rho)^J & (I,I)^J & (I,H)^J \\ (H, B\ln\rho)^J & (H,I)^J & (H,H)^J \end{vmatrix}}{\begin{vmatrix} (I,I)^J & (I,H)^J \\ (H,I)^J & (H,H)^J \end{vmatrix}} \tag{8.60}$$

The generator of the motion representing the identity operator I is expressed as $I = I_J \otimes I_{\bar{J}}$, while the generator of the motion representing the Hamiltonian operator is given by Equation (8.39) for the particle-particle composite system and by Equation (8.43) for the particle-field composite system.

Finally, the SEA-QT equation of motion for the last two composite systems is expressed as [288]

$$\frac{d\rho}{dt} = -\frac{i}{\hbar}\left[H,\rho\right] - \left(\frac{1}{\tau_J}D_J \otimes \rho_{\bar{J}} + \frac{1}{\tau_{\bar{J}}}\rho_J \otimes D_{\bar{J}}\right) \tag{8.61}$$

where the internal-relaxation times τ_J and $\tau_{\bar{J}}$ are considered to be real constants for the models developed in this dissertation. For the case of the particle-particle composite system, it is assumed that $\tau_A = \tau_B = 1$. For the case of the particle-photon field compsite system, values for $\tau_A = \tau_F = 300$ ms are considered as are other values consistent with the Haroche and co-workers [292] experiments to which the SEA-QT predictions are compared. These former values are chosen because they are long enough to show the various features of the state evolution in time of the composite systems and their constituents well. As for the comparison with the experimental results of [292], value of 0.26 ms and 0.36 ms are used for the particle-photon field composite system.

The nonlinear operator D_J is represented as

$$D_J = \frac{1}{2}\left\{(B\ln\rho)^J, \rho_J\right\} - \alpha_J\rho_J + \frac{1}{2}\beta_J\left\{(H)^J, \rho_J\right\} \tag{8.62}$$

where the terms α_J and β_J are defined as

$$\alpha_J = -\mathrm{Tr}_J\left(\rho_J(B\ln\rho)^J\right) - \beta_J\mathrm{Tr}_J\left(\rho_J(H)^J\right) \tag{8.63}$$

and

$$\beta_J = \frac{-\frac{1}{2}\mathrm{Tr}_J\left(\rho_J\left\{(B\ln\rho)^J, (H)^J\right\}\right) + \mathrm{Tr}_J\left(\rho_J\left(B\ln\rho\right)^J\right)\mathrm{Tr}_J\left(\rho_J(H)^J\right)}{\mathrm{Tr}_J\left(\rho_J\left(H\right)^J(H)^J\right) - \left(\mathrm{Tr}_J\,\rho_J(H)^J\right)^2} \tag{8.64}$$

Important ingredients of the SEA-QT model are the local observables given by the linear local operators defined as follows [288]:

$$(H)^J = \mathrm{Tr}_{\bar{J}}\left((I_J \otimes \rho_{\bar{J}})H\right) \tag{8.65a}$$

$$(H)^{\bar{J}} = \mathrm{Tr}_J\left((\rho_J \otimes I_{\bar{J}})H\right) \tag{8.65b}$$

These locally perceived operators represent the *"local effective perception"* of the overall Hamiltonian operator. Their local mean values can be interpreted as the overall system's energy as *"locally perceived"* by each constituent. Analogously, the local observables given by the nonlinear local operators defined as follows [288]:

$$(S)^{J} = -k_B \mathrm{Tr}_{\bar{J}} \left((I_J \otimes \rho_{\bar{J}}) B \ln \rho \right) \tag{8.66a}$$

$$(S)^{\bar{J}} = -k_B \mathrm{Tr}_{A} \left((\rho_J \otimes I_{\bar{J}}) B \ln \rho \right) \tag{8.66b}$$

represent the *"local effective perception"* of the overall $-k_B \ln \rho$ operator. Their local mean values can also be interpreted as the overall system's entropy as *"locally perceived"* by each constituent.

Finally, the expectation value of the entropy for the overall, composite, microscopic system is given by the von Neumann entropy relation [283] using the density operator as defined in the SEA-QT framework, namely,

$$S = -k_B \mathrm{Tr}(\rho \ln \rho) \tag{8.67}$$

where k_B is Boltzmann's constant.

8.6 Measures of correlation and entanglement

Since part of the scope of this dissertation is to model decoherence, some measurements of entanglement and correlation as well as decoherence need to be described. There are several options in the literature. For example, a correlation functional, which in this case is the entropy correlation function, is written as [288]

$$\sigma_{AB}(\rho) = \mathrm{Tr}(\rho \ln \rho) - \mathrm{Tr}_A(\rho_A \ln \rho_A) - \mathrm{Tr}_B(\rho_B \ln \rho_B) \tag{8.68}$$

A measure of the coherence between the constituents of the system is the norm of the commutator operator given by

$$\|C\| = \mathrm{Tr}(CC^{\dagger}) \tag{8.69}$$

where $C = i[H, \rho]$. It can be used as an indicator of how phase difference between the off-diagonal elements of the matrix representing the state operator evolve towards zero. It can, as a cosequence, also be thought of as a measure of the evolution of the coherence of the constituents.

The rate of change of the correlation functional given by Equation (8.68) is expressed as

$$\frac{d(\sigma_{AB}(\rho))}{dt} = \dot{\sigma}_{AB}|_{H} - \dot{\sigma}_{AB}|_{D} \tag{8.70}$$

where the first term on the right-hand side represents the contribution, which the Hamiltonian term of Equation (8.56) makes to the rate of change of the correlation functional. The second term on the right-hand side represents the contribution of the dissipative term of Equation (8.56). Based on the characteristics of Equation (8.56), it is has been conjectured [288] that $\dot{\sigma}_{AB}|_D$ only destroys correlations between the constituents, namely, it should be non-negative at all times.

Another measurement of decoherence, which provides a theoretical description of the experimental observations for a composite system formed by an atom and an electromagnetic field mode, such as those of cavity quantum electrodynamics (CQED), is given by the correlation signal [291]

$$\eta(t_d) = \frac{1}{2} e^{-2n\left(1-e^{-\gamma t_d}\right)\sin^2\phi} \cos\left[n\left(1-e^{-\gamma t_d}\right)\sin 2\phi\right] \tag{8.71}$$

where n is the average number of photons in the field mode, $\gamma = 1/T_R$, T_R is the photon lifetime in the cavity, t_d is the delay for the second atom, and ϕ the field mode phase shift.

8.7 ODE45 Matlab® solver

The model for the two different microscopic composite systems is written using local functions in Matlab®. The system of first-order ordinary differential equations (ODEs) generated by the SEA-QT equation of motion, Equation (8.61), is solved with the *"ode45"* subroutine [384]. The subroutine *"ode45"* utilizes an explicit fourth order Runge-Kutta method of solution with a variable internal time step for efficiency purposes [385–387]. The absolute error tolerance is set here to 10^{-7}. This subroutine solves Equation (8.61) for the evolution in time of the density or state operator of the composite system. A post processing analysis is developed by creating local functions to obtain the value of the observables of the system at every instant of time such as the energy and entropy.

8.8 Verification of the model

In order to confirm that the model works properly, several of the conditions, which the equation of motion of SEA-QT must satisfy and which are explicitly defined in [296, 297], are monitored. The conditions applicable to the particular systems under analysis in this dissertation are as follow:

- for isolated composite systems with no chemical or nuclear reactions present among its constituents, the energy of the composite, $E = \langle E \rangle = \mathrm{Tr}(H\rho)$, must remain constant at all times; the time-invariant Hamiltonians are those defined by Equation (8.39) for the particle-particle composite system and by Equation (8.43) for the particle-photon field composite system;
- the rate of change of the entropy of the system $S = -k_B \mathrm{Tr}(\rho \ln \rho)$ (Equation (8.67)) must be nonnegative at all times;
- starting the evolution of the state of the system with a density operator that is not a projector operator, that is, $\rho(t_0) = \rho(t_0)^\dagger > \rho(t_0)^2$ and $\mathrm{Tr}(\rho(t_0)) = 1$, $\rho(t)$ must remain Hermitian ($\rho(t) = \rho(t)^\dagger$), nonnegative and unit trace $\mathrm{Tr}(\rho(t)) = 1$ at all times;
- since the energy, parameters, and amount of constituents are invariant in time, there must be one and only one stable equilibrium state for which $d\rho/dt = 0$ and $S_{\mathrm{se}} > S(t)$.

Chapter 9

Results and Discussion for SEA-QT

9.1 Two-particle spin-$^1/_2$ composite microscopic system

Figure 9.1 shows an energy-entropy ($\langle E\rangle$-$\langle S\rangle$) diagram for the state evolution of the two-particle spin-$^1/_2$ composite system. The four points depicted inside the curve are possible initial non-equilibrium states obtained with the approach described in Section 8.3.1 and illustrate the fact that the relaxation of any non-equilibrium state can be modeled with the approach used in this work. Although state A_1 together with states B_1, B_2, B_3, and B_4 are all modeled in terms of their evolution towards a state of stable equilibrium, the focus here is on the evolution in state A_1 only for which a complete set of results is presented. With this in mind, the system evolves at constant energy from state A_1 towards a state of stable equilibrium at A_{se} that for this case just happens to have a high negative absolute temperature. When the state of the system reaches A_{se}, the density operator takes the canonical form of Equation (8.33). This figure also confirms that the expectation value of the energy ($\langle E\rangle = \mathrm{Tr}(H\rho)$,) remains constant at all times and that there is one and only one stable equilibrium state for which $d\rho/dt = 0$ and $S_{\mathrm{se}} > S(t)$.

Figure 9.2 shows the norm of the commutator operator defined by Equation (8.69). The evolution of the norm is taken as an indicator of how the off-diagonal elements of the matrix representing the density or state operator decay; and as a result, it is also an indicator of how the coherence of the system disappears as the state of the system evolves towards A_{se}. A drastic descent is observed at the beginning of the evolution because the local coherence within each constituent is being annihilated by the dissipative term of the SEA-QT equation of motion. This drastic descent is in accordance with the locally-perceived steepest entropy ascent ansatz upon which the dynamic

model is constructed. As seen in Figure 9.3(a) where the evolution of the composite system entropy is given, the entropy increases very rapidly at the beginning of the evolution and then quickly slows its increase, asymptotically approaching its stable equilibrium value. Figure 9.3(b) depicts the entropy generation rate evolution of the composite system where it can be observed that $d\langle S\rangle/dt$ remains nonnegative at all times.

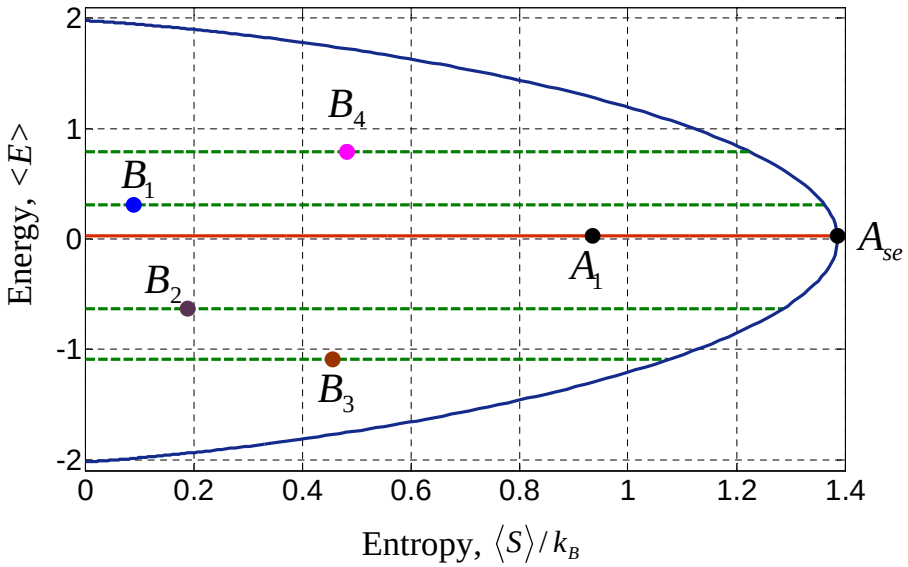

Figure 9.1. Energy-entropy diagram for the state evolution of the two-particle spin-$1/2$ composite system; states A_1 and A_{se} are for the particular case presented in detail in this work, while states B_i are other possible initial non-equilibrium states generated. Reprinted from [262] Copyright © 2013 by ASME, with permission.

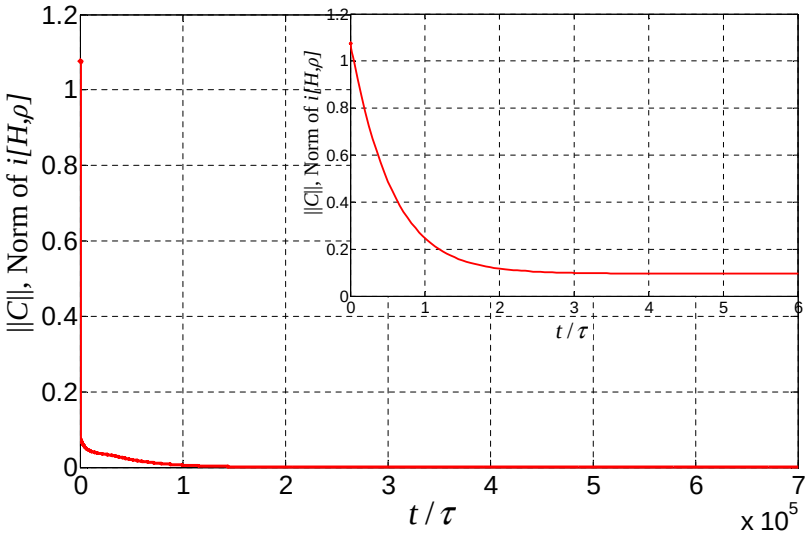

Figure 9.2. Evolution of $||C||$ which is the norm of the commutator term $C = i\,[H, \rho]$ for the two-particle composite system. Reprinted from [262] Copyright © 2013 by ASME, with permission.

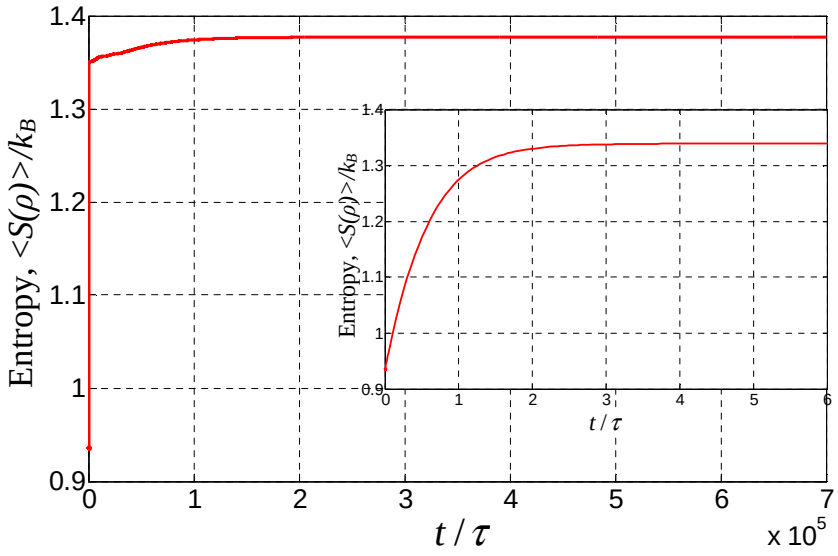

(a) Entropy. Reprinted from [262] Copyright © 2013 by ASME, with permission.

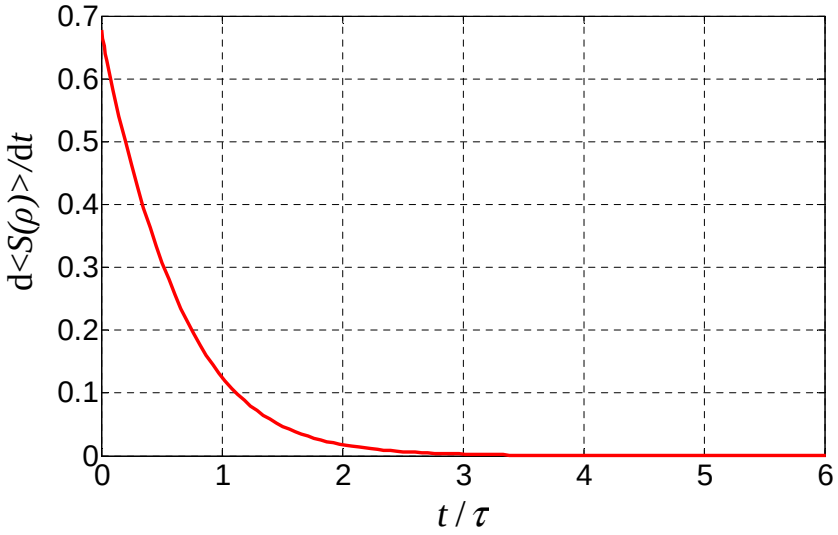

(b) Entropy generation rate.

Figure 9.3. Entropy and entropy generation rate evolution for the composite system.

Figure 9.4 shows the x-, y-, and z-components of the state vector representation for both constituents. It can be seen that constituent A starts its evolution closer to the surface of its corresponding unit Bloch sphere than constituent B (also see Figure 8.4(b)). The red line corresponds to the z-component of the vector, which shows how the two constituents are coherently exchanging energy, i.e., as the energy of constituent A decreases, that of constituent B increases. The x- and y-components evolve very fast towards a value of zero, which is reached at a dimensionless time of about 10. This evolution towards the center of the local-Bloch sphere for each constituent

represents the loss of local-coherence of these constituents. In contrast, the non-local coherence belonging to the off-diagonal elements of the density matrix of the composite system continues its decay but at a very gradual rate (see Figure 9.2 above) until it reaches a value of zero at which point the Hamiltonian and density operators commute and the state of the composite system is that of stable equilibrium. During this slow, non-linear and non-local decay, the constituents continue exchanging energy with each other.

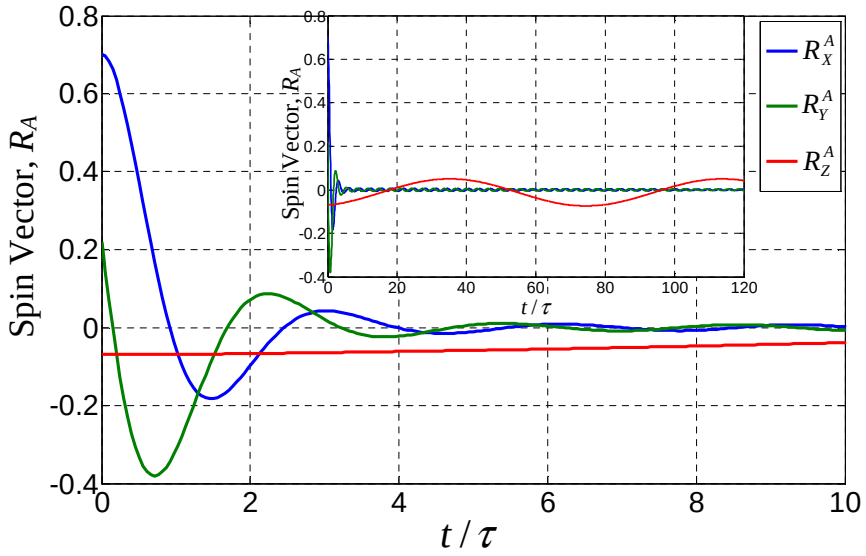

(a) Constituent A (Spin sub-system-A).

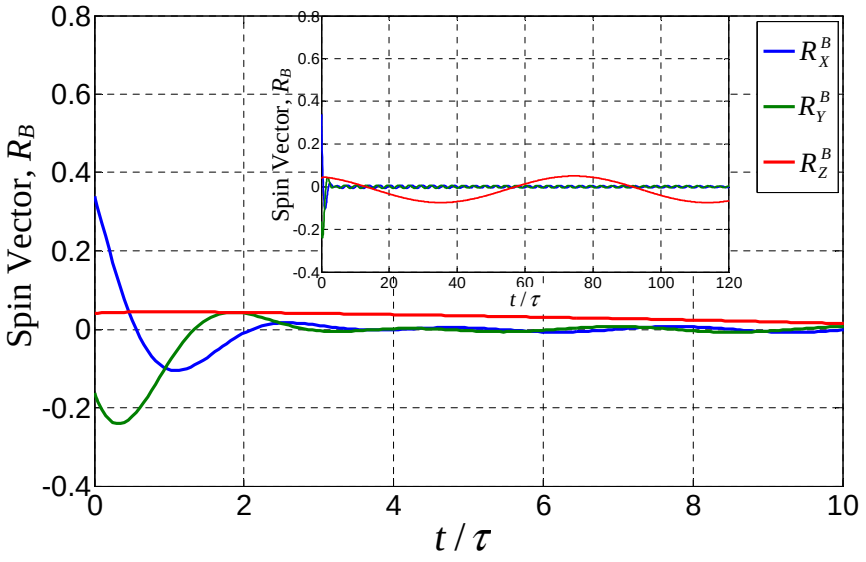

(b) Constituent B (Spin sub-system-B).

Figure 9.4. Evolution of the components of the state vector in their local Hilbert spaces. Reprinted from [262] Copyright © 2013 by ASME, with permission.

Figure 9.5 shows the evolution in time of the energy eigenlevel occupation probabilities given by Equation (8.34). As can be seen, the largest redistribution of system energy takes place primarily between two of the four energy eigenlevels of the system, the majority of which occurs during a short non-dimensional time interval corresponding to the decay of the local-coherence of the constituents. After this fast initial redistribution, the redistribution of energy represented by changes in the eigenlevel occupation probabilities occurs at a much slower rate. The sum of the four energy eigenlevel occupation probabilities is equal to one at all times.

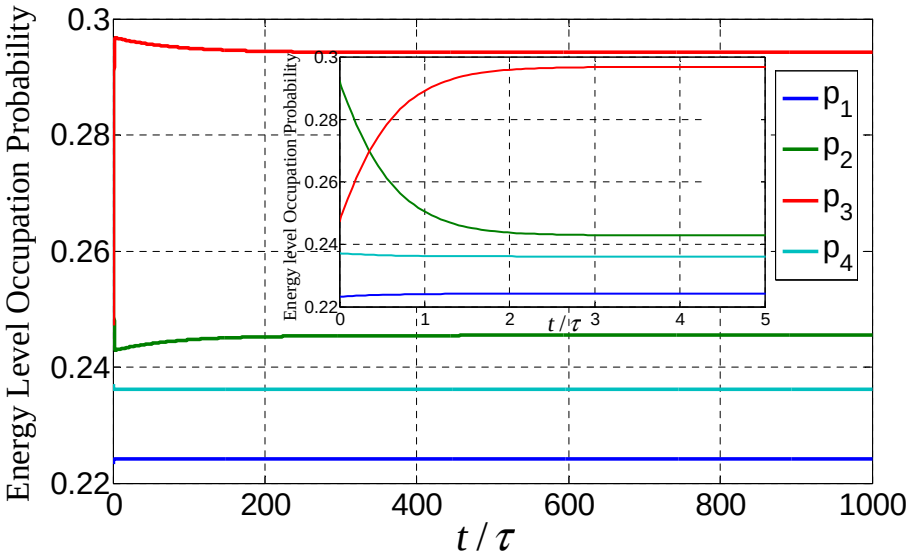

Figure 9.5. Evolution of the energy eigenlevel occupation probabilities of the composite system for a period of $t/\tau = 0 - 1,000$. Reprinted from [262] Copyright © 2013 by ASME, with permission.

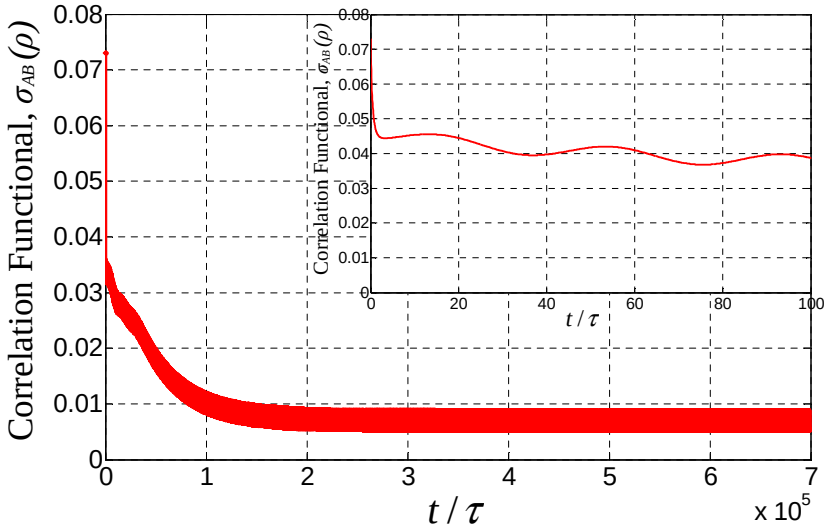

Figure 9.6. Evolution of the entropy correlation functional. Reprinted from [262] Copyright © 2013 by ASME, with permission.

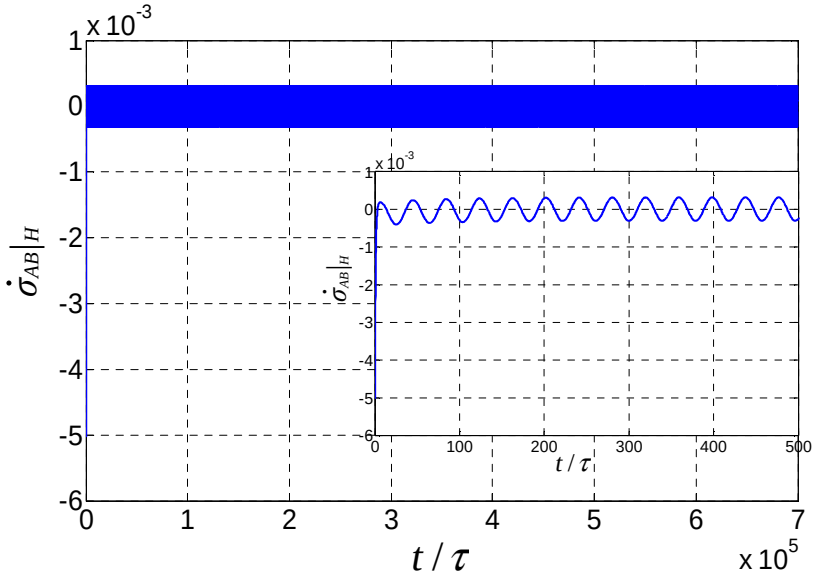

(a) Contribution of the Hamiltonian term.

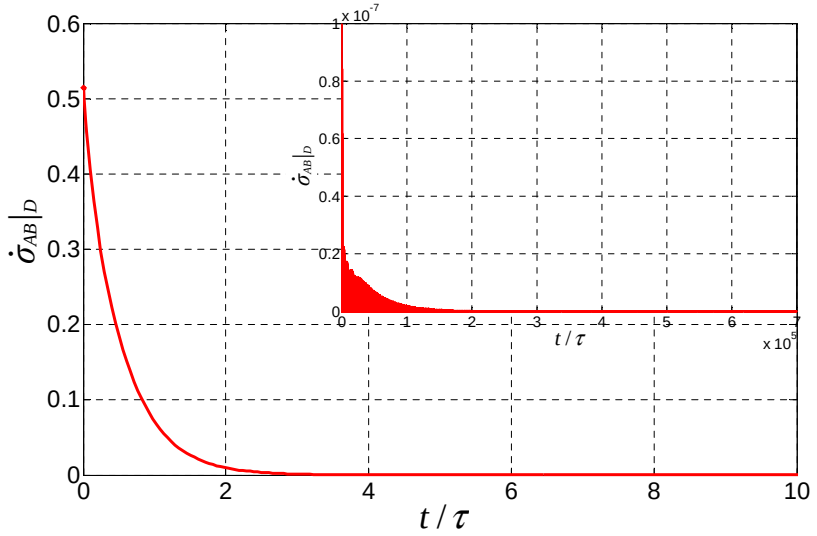

(b) Contribution of the dissipative term. Reprinted from [262] Copyright © 2013 by ASME, with permission.

Figure 9.7. Rate of change of the contribution of the Hamiltonian and dissipative terms to the rate of change of the entropy correlation functional.

Figure 9.6 depicts the evolution in time of the entropy correlation functional, which is a measurement of how the correlations between the constituents disappear when the composite system evolves towards a state of stable equilibrium. The correlation functional reaches a constant value when the composite is at stable equilibrium which occurs at about 7×10^5 dimensionless time units and at which the value of the correlation functional is $\sigma_{AB} = 0.0051$. The fact that the correlation functional does not reaches a value of zero at stable equilibrium, is because the interaction term, V,

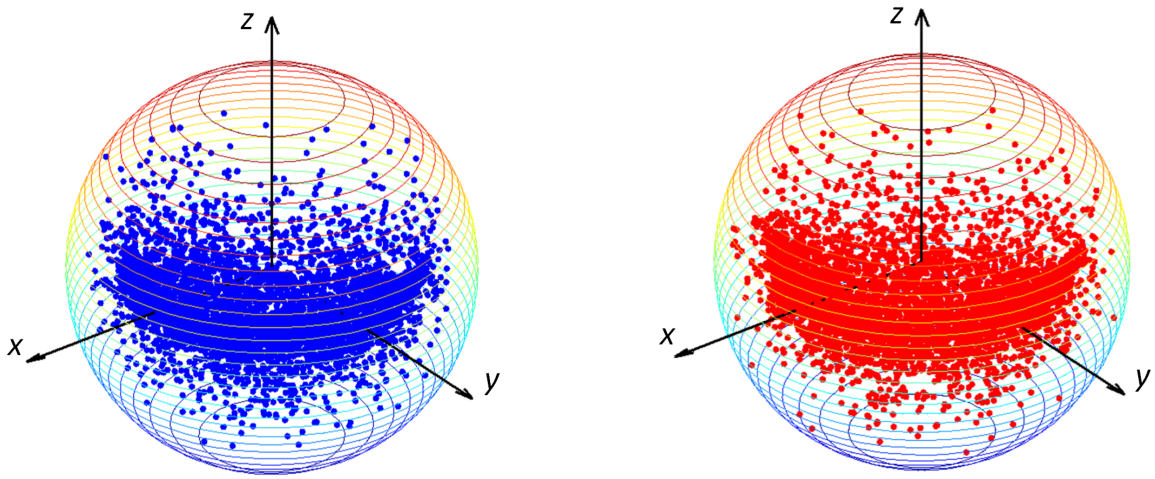

(a) Constituent A. (b) Constituent B.

Figure 9.8. Bloch sphere representation of 5,000 different random initial states.

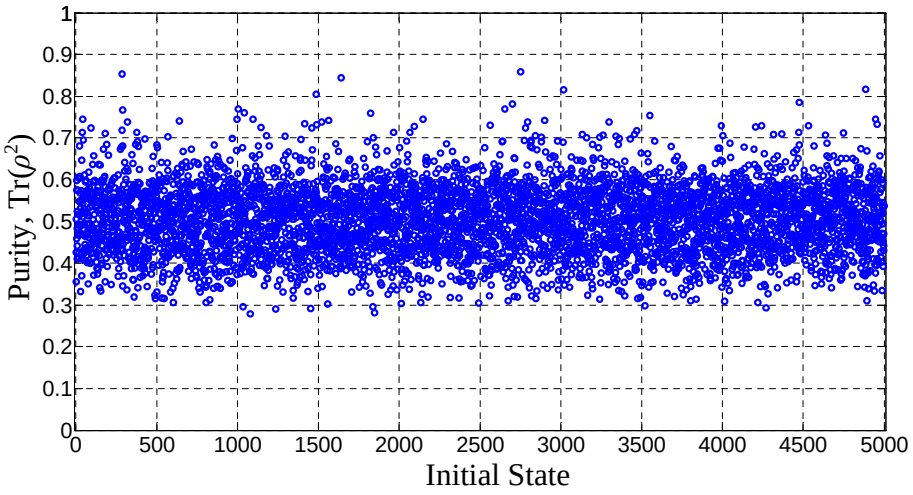

Figure 9.9. Degree of purity for the different 5,000 random initial non-equilibrium states tested.

of the Hamiltonian operator of Equation (8.36) is continuously creating correlations. This creation of correlations is described by the contribution of the Hamiltonian term of the equation of motion to the rate of change of the correlation functional, depicted in Figure 9.7(a), where it can be observed that this rate of change oscillates continuously at a fixed amplitude even when the composite system is at stable equilibrium. Figure 9.7(b) shows the rate of change of the correlation functional due to the dissipation term of the equation of motion and is consistent with the conjecture that the dissipation term can only destroy but never create correlations between constituents. Indeed, the rate of change of the entropy correlation is always non-negative, and this result is reproduced in all of the other thousands of simulations performed here, each beginning at a different initial state obtained randomly as described in Chapter 8.

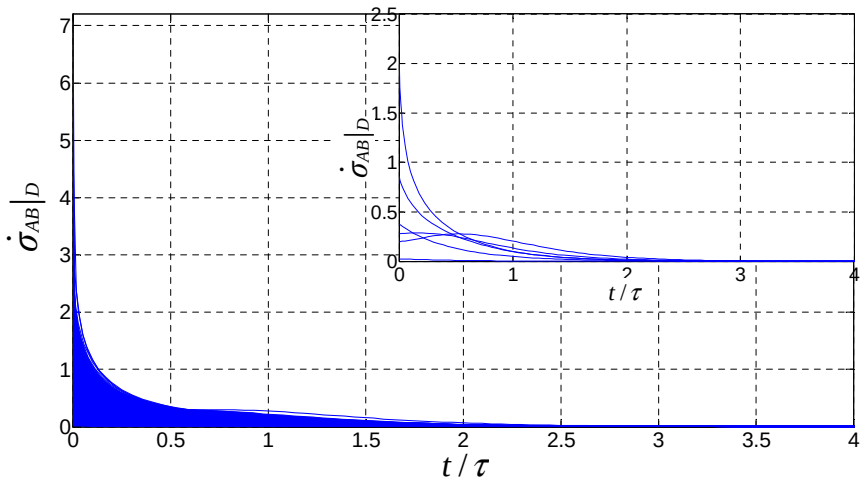

Figure 9.10. Rate of change of the contribution of the dissipative term to the rate of change of the entropy correlation functional for the different 5,000 random initial non-equilibrium states tested.

In an attempt to generalize the validity of this statement, many different initial non-zero-entropy states randomly generated as discussed above were tested (5,000) and in each case always resulted in non-negative values of $\dot{\sigma}_{AB|_D}$. The cloud of initial points tested is depicted in Figure 9.8 for constituents A and B in their local space. Figure 9.1 shows the degree of purity

$$\bar{\gamma}_p = \mathrm{Tr}(\rho^2) \tag{9.1}$$

of the density operator for the composite system for the 5,000 different cases tested. In the figure, a value of $\bar{\gamma}_p = 1$ defines a state which is a pure state (i.e., one of zero entropy), and a value of $\bar{\gamma}_p = 0$ defines a state which is a stable equilibrium state for which the entropy is a maximum, while the points in between represent non-zero-entropy non-equilibrium states with varying degrees of purity. It is observed that for this particular case, the majority of the state operators are located near a zone of purity of approximately 0.5. The closest state operator to stable equilibrium corresponds to one with a degree of purity of 0.28, and the state operator closest to the zero-entropy surface corresponds to one with a degree of purity of 0.86.

Figure 9.10 shows the rate of change of the contribution of the dissipative term to the rate of change of the entropy correlation functional for the different 5,000 random initial non-equilibrium states tested. It can be observed that $\dot{\sigma}_{AB|_D}$ evolves to zero for all cases and remains nonnegative at all times. In the inset of Figure 9.10, the evolution of six particular initial non-equilibrium states (i.e., with degrees of purity of 0.59, 0.58, 0.43, 0.68, 0.86, and 0.28) is depicted in order to show a more detailed evolution of $\dot{\sigma}_{AB|_D}$. The evolution of the initial non-equilibrium state located closer

to stable equilibrium shows the lowest correlation so that the destruction of correlations is very low, i.e., close to zero. The evolution of the initial non-equilibrium state closest to a pure state shows an increase in the destruction of correlations at the beginning of the evolution, reaching a maximum at about $t/\tau = 0.6$ and then decreasing to zero. This increase in the rate of destruction of correlations early during the evolution is caused by the maximum entropy production of the composite. In other words, the entropy generation of the composite increases for the first part of the evolution and then decreases evolving towards zero.

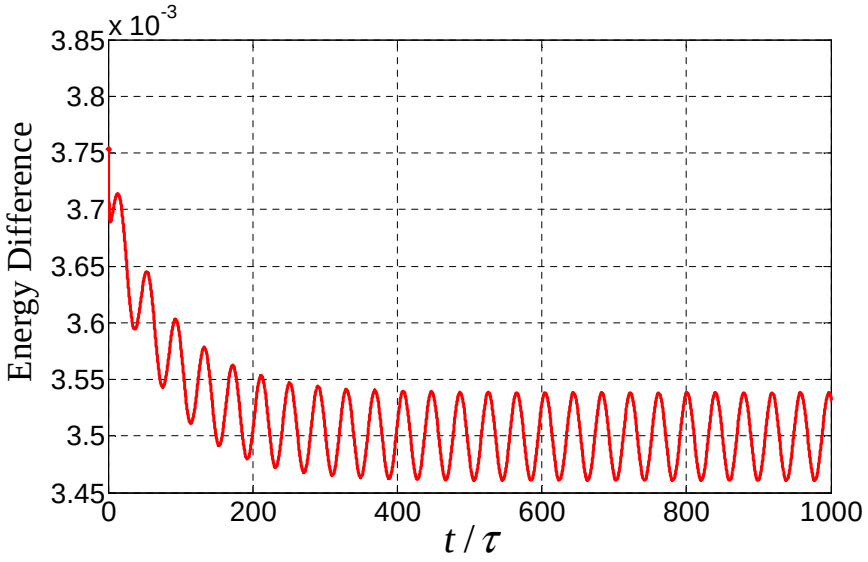

(a) Evolution of K^H.

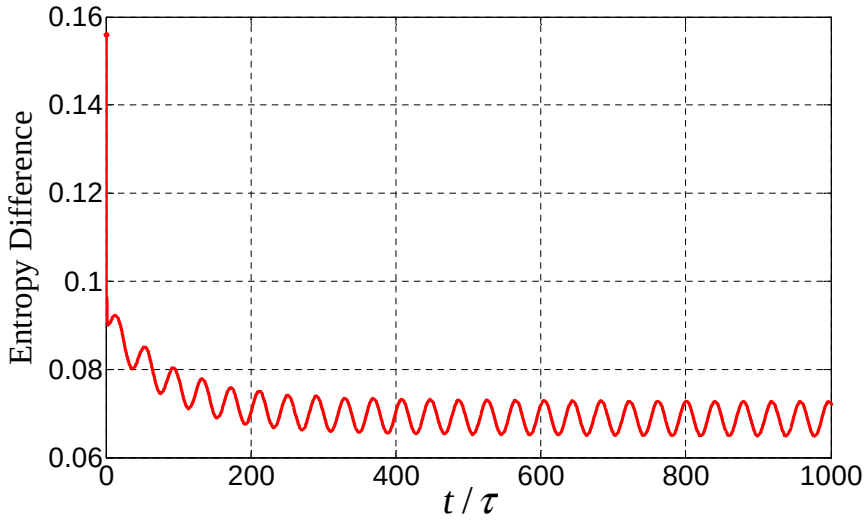

(b) Evolution of K^S.

Figure 9.11. Evolution of the difference between the "locally-perceived" energies and entropies of the constituents with respect to the energy and entropy of the composite. Reprinted from [262] Copyright © 2013 by ASME, with permission.

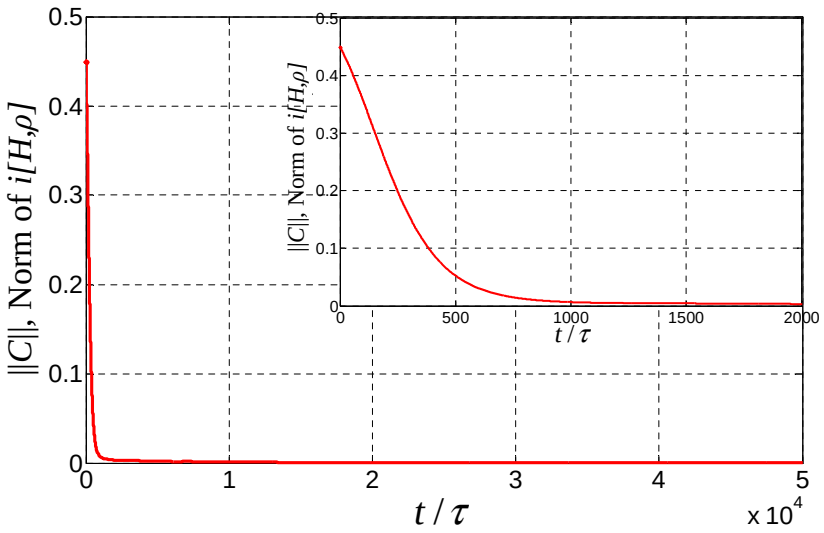

Figure 9.12. Evolution of $||C||$ which is the norm of the commutator term $C = i\,[H, \rho]$ for the atom-field composite system. Reprinted from [304], with permission.

Finally, additional possible measures of correlations are given by

$$K^H = \frac{1}{2}\left(\left\langle (H)^A \right\rangle + \left\langle (H)^B \right\rangle\right) - \langle H \rangle \tag{9.2a}$$

$$K^S = \frac{1}{2}\left(\left\langle (S)^A \right\rangle + \left\langle (S)^B \right\rangle\right) - \langle S \rangle \tag{9.2b}$$

which represent the difference in the locally perceived energies and the energy of the composite system and the difference in the locally perceived entropies and the entropy of the composite system, respectively. Figures 9.11(a) and 9.11(b) show the evolution of K^H and K^S, respectively, where it can be observed that these differences decay very quickly at first and then very gradually approaching zero but never quite getting there even at stable equilibrium, which occurs at about 7×10^5 dimensionless time units (not depicted in the figures).

9.2 Atom-field mode composite system

Figure 9.12 shows the evolution of the norm of the commutator operator formed by the Hamiltonian and density operator for the atom-field mode composite system. The figure shows how the off-diagonal elements in the overall density or state matrix are decaying with time as the system evolves towards a state of stable equilibrium. Thus, it is also an indicator on the degree to which the coherence of the composite system due to the shift on the phase of the field only is being dissipated in time. As seen in the figure, the steepest descent occurs at the beginning of the time

evolution. This is in accord with the steepest-entropy-ascent principle pictorially described in Figure 9.13 for the entropy evolution. Note that only the first part of the complete evolution in state of the composite system is depicted in Figures 9.12 and 9.13, i.e., that part from the initial perturbed state A_0 in Figure 9.14 to state A_1 which occurs at $t/\tau = 5 \times 10^4$. Both states are non-equilibrium states quite far from that of stable equilibrium, i.e., state A_{se}. The latter is estimated to occur at or after $t/\tau = 5.2 \times 10^6$ based on the simulation actually completed. The simulation was stopped at state A_2 after an elapsed time of $t/\tau = 6 \times 10^5$ (also a non-equilibrium state), since the state of the system at this point was evolving very slowly, i.e., asymptotically in a non-linear manner, towards A_{se} and the primary coherence and decoherence features of interest had already been captured.

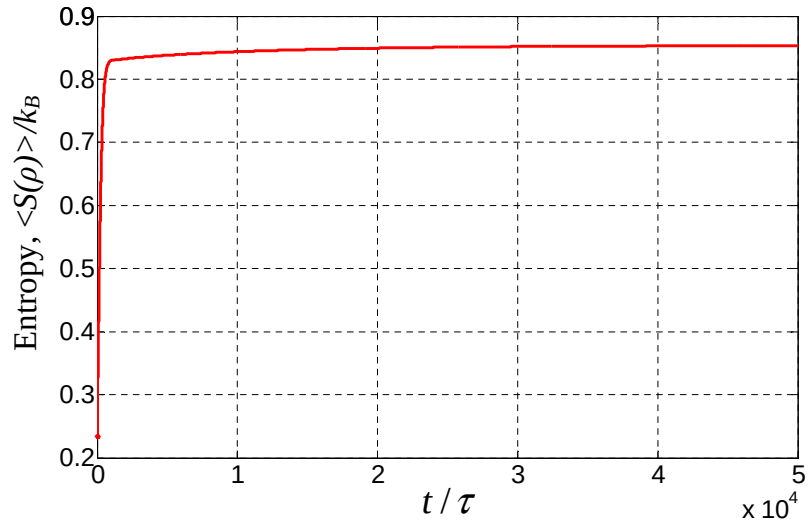

Figure 9.13. Entropy evolution of the atom-field composite system. Reprinted from [304], with permission.

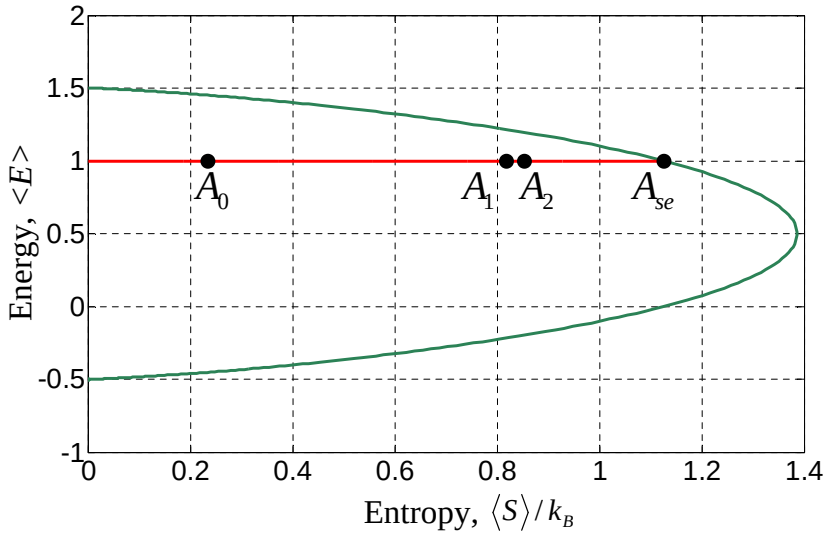

Figure 9.14. Energy-entropy diagram depicting the evolution in state of the composite system. Reprinted from [304], with permission.

Figure 9.15(a) depicts the evolution of the local density operator for the electromagnetic field mode. When the atom is detected in its excited level state, the state of the electromagnetic field is projected into a state of maximum local coherence. Subsequently, this local coherence represented by the off-diagonal elements of ρ_F decays in a steep fashion in accordance with the evolution of Equation (8.61). Figure 9.15(b) shows the evolution of the local density operator for the Rb atom where revival and death of its local coherence represented by the off-diagonal elements of ρ_A is observed during the evolution but with ever smaller amplitudes until the local coherence dies out at stable equilibrium.

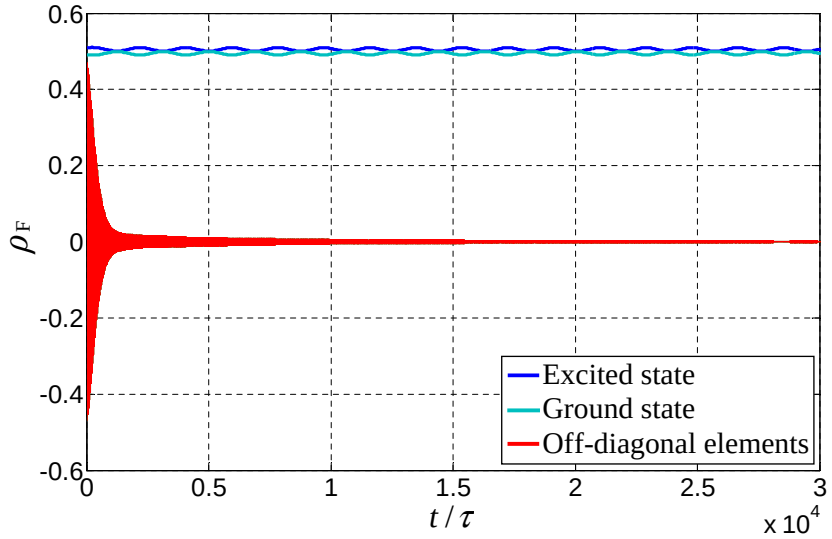

(a) Electromagnetic field mode.

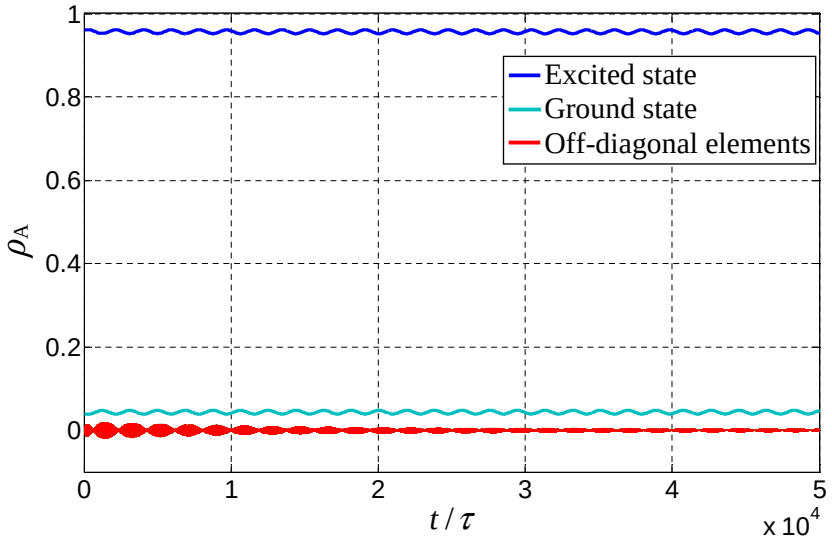

(b) Rb atom.

Figure 9.15. Evolution of the elements of the reduced density operators. Reprinted from [304], with permission.

Figure 9.16 depicts the evolution in time of the entropy correlation functional, which is a measurement of how the correlations between the constituents disappear when the composite system evolves towards a state of stable equilibrium. It it seen that the correlation functional decays early during the evolution and starts to reach a constant average value at state A_2 which occurs at 5×10^4 dimensionless time units. The fact that the correlation functional does not reaches a value of zero is because the interaction term, V, of the Hamiltonian operator given by Equation (8.44) is continuously creating correlations. This creation of correlations is described by the contribution of the Hamiltonian term of the equation of motion to the rate of change of the correlation functional, depicted in Figure 9.17(a), where it can be observed that this rate of change oscillates continuously at a fixed amplitude. Figure 9.17(b) shows the evolution of the rate of change of the contribution of the dissipation term of the equation of motion of SEA-QT to the rate of change of the entropy correlation functional. Its value is non-negative always, showing that the dissipative term of the equation of motion does not create correlations between the constituents but instead always destroys the correlations formed during the initial interaction between the constituents.

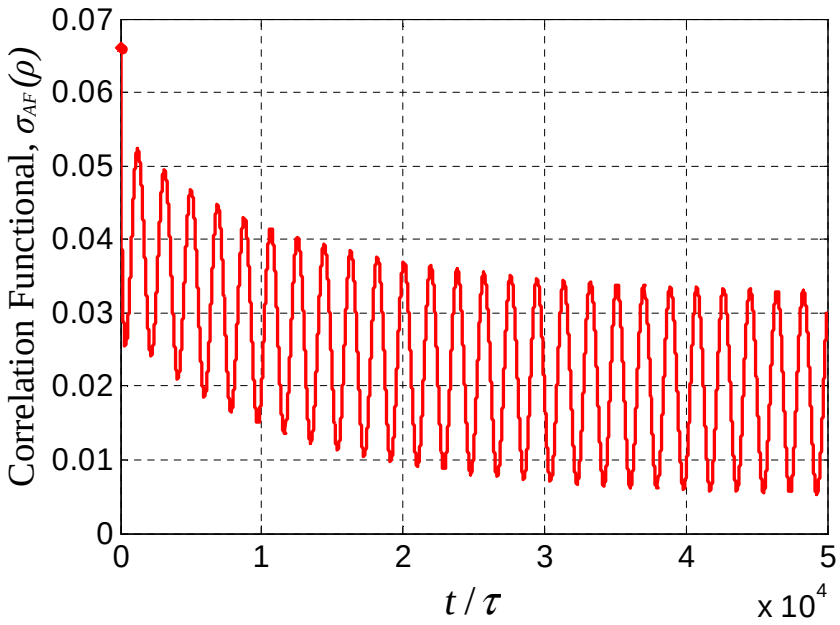

Figure 9.16. Evolution of the entropy correlation functional for the atom-field system.

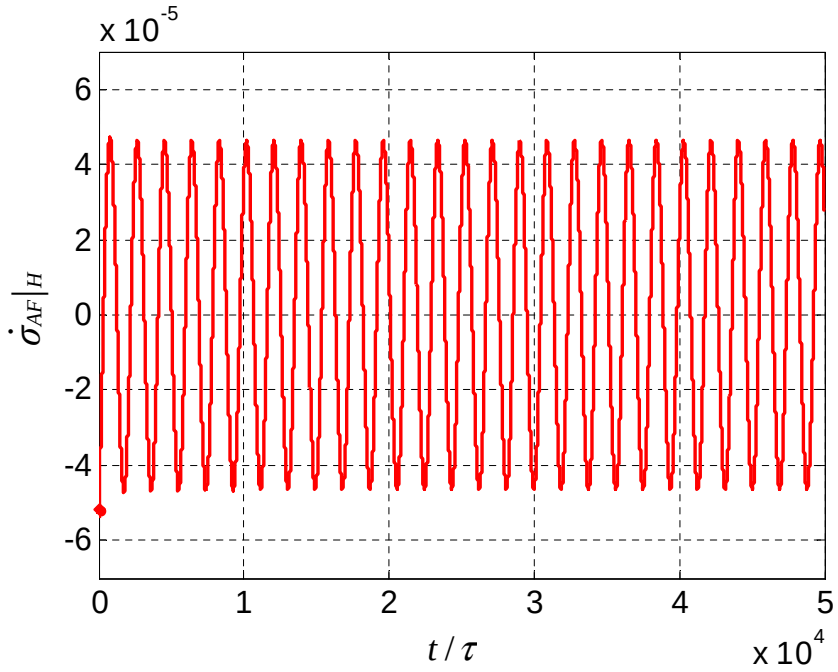

(a) Contribution of the Hamiltonian term.

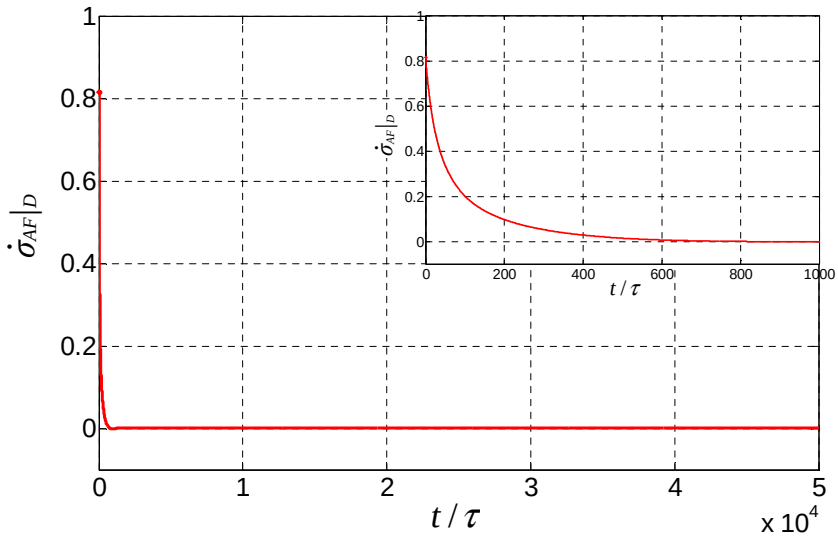

(b) Contribution of the dissipative term. Reprinted from [304], with permission.

Figure 9.17. Rate of change of the contribution of the Hamiltonian and dissipative terms to the rate of change of the entropy correlation functional.

In Figure 9.18, the results of the SEA-QT model are compared to the experimental data of [292] as well as to the theoretical prediction of the correlation signal η reported in the literature by Raimond, Brune and Haroche [291]. Figure 9.18(a) depicts the comparison for a case with the detuning parameter $\delta = 70/2\pi$ kHz. The solid triangles correspond to average values of experimental measurements obtained from [292]. The dashed line corresponds to the theoretical

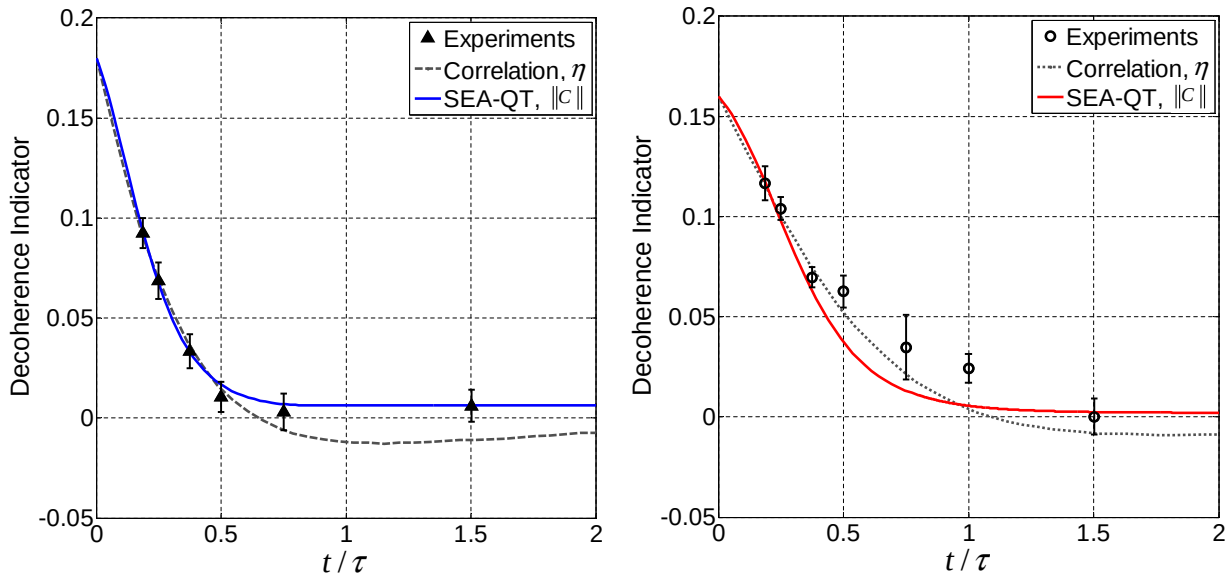

(a) Detuning parameter $\delta = 70/2\pi$ kHz [304].

(b) Detuning parameter $\delta = 170/2\pi$ kHz.

Figure 9.18. Comparison of the loss of coherence predicted by SEA-QT with the CQED experimental results of [292] and theoretically calculated correlation signal η from [291] for two different values of the detuning.

prediction made using the correlation signal η [291]. The initial point of the correlation has been moved in accord with [291, 292] from a value of 0.5 to 0.18 on the vertical axis to take into account experimental imperfections. The blue line represents the SEA-QT prediction using $\|C\|$ as a direct indicator of how the coherence of the electromagnetic field mode is dissipated in time. This SEA-QT prediction corresponds to a value of $\tau_A = \tau_F = 0.26$ ms for the internal-relaxation times of the constituents in the equation of motion. This is comparable to the characteristic coherence time reported for the CQED experiment in [360] which is 0.24 ms for the electromagnetic field mode. As in the case of the correlation signal, the maximum value for $\|C\|$ is moved to 0.18 on the vertical axis. As seen, SEA-QT predicts the experimental data well. A very slight deviation from the experimental values is observed with the fourth and fifth values but this is well within the error bars for the experimental values indicated in the figure. Thus, this deviation may well correspond to normal imperfections in the experimental equipment such as the quality of reflexion of the mirrors, which allows the leakage of photons from the cavity [293, 359].

Figure 9.18(b) depicts the comparison for a case with the detuning parameter $\delta = 170/2\pi$ kHz. The circles correspond to average values of the experimental measurements obtained from [292]. The dashed line corresponds to the theoretical prediction made using the correlation signal η [291]. The red solid line represents the SEA-QT prediction using a value of $\tau_A = \tau_F = 0.36$ ms for the

internal-relaxation times of the constituents in the equation of motion. An effective decoherence time for this case is not reported in the literature. As for the case of Figure 9.18(a), the maximum value of the theoretical predictions of η and the numerical predictions of SEA-QT have been corrected to take into account experimental imperfections. As seen, SEA-QT predicts the experimental data well at the beginning and at the end of the decoherence evolution. A deviation from the experimental values is observed with the third, fourth and fifth values, although it is also observed that the uncertainty associated with these measurements is higher than the rest of the experimental values reported. As for the previous case, this deviation may also correspond to normal imperfections in the experimental equipment such as the quality of reflexion of the mirrors, which allows a leakage of photons from the cavity [293, 359]. Another factor may be that the values chosen for the internal-relaxation times τ_A and τ_F do not completely take into account the physical characteristics of the constituents. For example, it may be that slightly differing values for each relaxation time are needed or that these times are instead functionals of the state operator as described in [257, 297]. Of course, the latter is still an open area of research.

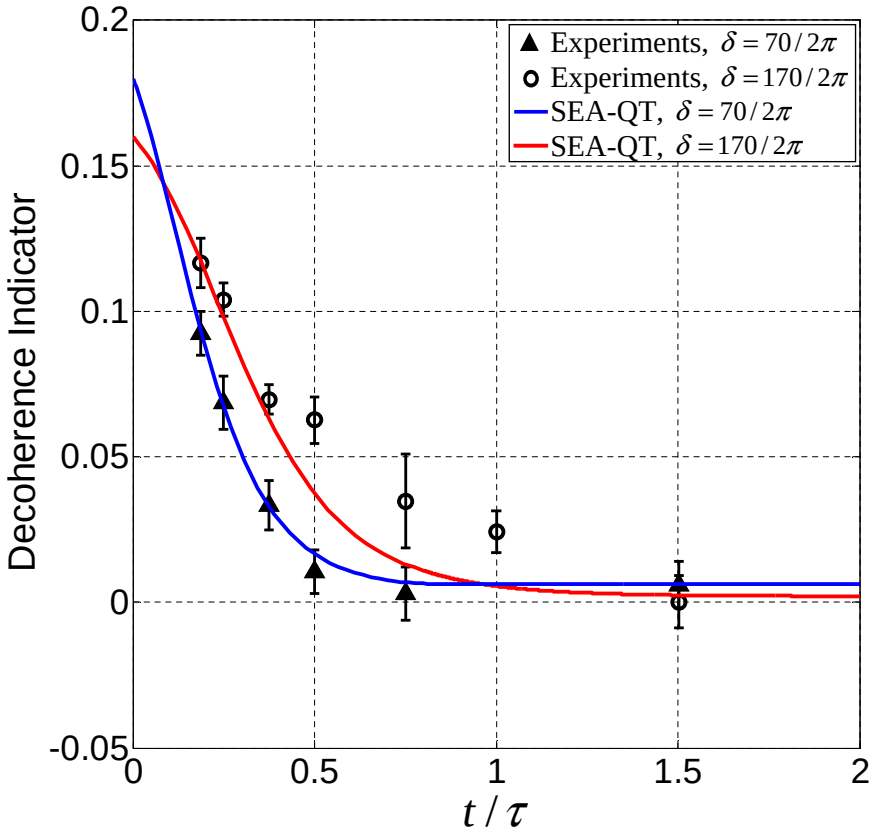

Figure 9.19. Comparison of the loss of coherence predicted by SEA-QT with the CQED experimental results of the group at Paris [292].

Figure 9.19 shows the SEA-QT decoherence prediction of the experimental data of [292] in a single figure for the two values of the detuning parameter. It is observed that decoherence takes place at a faster rate for smaller values of detuning when the separation of the two state components of the photon-field increase. In addition, the coherence for the case of a detuning of $170/2\pi$ kHz is smaller than for a detuning of $70/2\pi$ kHz at the end of the evolution. This behavior is also captured by the SEA-QT prediction. Note that neither the experimental values nor the SEA-QT predictions are ever negative; this contrast with the conventional quantum mechanical predictions of [291, 292]. This should not be and suggest that the predictions made with η are problematic.

Chapter 10

Conclusions for SEA-QT

In this dissertation, an approach called Steepest-Entropy-Ascent Quantum Thermodynamics (SEA-QT), whose equation of motion is able to model the non-linear model dynamics of state evolution, is used to describe in a thermodynamically consistent way the decoherence which occurs during relaxation to stable equilibrium of the two simplest composite systems found in Nature, namely, that of two interacting and correlated particles of type spin-$1/2$ and that of a particle and a photon field correlated via an interaction. For the particle-particle composite system, the results show that the local coherence within each constituent (particle) disappears in a very short period of time, whereas the non-local coherence belonging to the composite system takes a very long time to disappear. In addition, the conjecture previously stated by Beretta [288] that the dissipation term of the SEA-QT equation of motion is capable of destroying correlations only between constituents is heuristically confirmed (not proven) by randomly creating and modeling the state evolution of 5,000 initial non-equilibrium states. The closest random, initial non-equilibrium state to a pure state corresponds to a quantum purity of 0.86, and that closest to stable equilibrium corresponds to a quantum purity of 0.28.

For the atom-photon field composite system, results show how the coherence of the composite system is dissipated when the system evolves towards a state of stable equilibrium and how this affects the local coherence of each constituent. For the photon field, the local coherence decays from some maximum to zero. For the atom, since initially it is assumed that the atom has been detected in its excited state, its local coherence is zero at the beginning of the evolution; and subsequently exhibits many revivals and deaths of the coherence. Nevertheless, even the amplitudes of these revivals and deaths decay with time.

The decoherence phenomenon predicted with the SEA-QT model is compared to the experimental data of Haroche and co-workers [292] for two values of the detuning, i.e., $\delta/\pi = 70$ kHz and $\delta/\pi = 170$ kHz. The comparison for a detuning of $\delta/\pi = 70$ kHz shows that SEA-QT prediction is in good agreement with the experiments and is, in fact, in much better agreement than that for the correlation function developed for this experiment in [291]. On the other hand, the comparison for a detuning of $\delta/\pi = 170$ kHz shows that the SEA-QT predicts the decoherence at the beginning of the evolution well followed by a slightly higher deviation from experimental values than was previously observed. However, this is probably due to the fact that the uncertainty associated with these measurements is higher than that for the rest of the experimental values reported.

As a final remark, the results obtained demonstrate that the dynamic SEA-QT approach utilized in this dissertation is a robust and comprehensive framework for simulating the non-linear dynamics encountered in complex composite quantum systems. This suggests that at least one way of controlling decoherence may be to judiciously choose the initial state in such a way that the spontaneous loss of correlations between constituents is so slow as to be almost negligible. Another possibility as suggested by Levin et al. [388] may be to induce a steady state of the composite system via a set of constant energy fluxes with the environment. Limits to this control or any other must also be understood [389]. Of course, the first step in any control is the ability to simulate the process of loss of coherence, something which has been demonstrated here using the SEA-QT framework.

The study of controlling decoherence for its use in devices such as quantum computing, quantum communication, atomic clocks, etc. or in applications of modeling chemically reactive systems and mass diffusion through porous media is an on-going area of research that is being explored using the SEA-QT framework and the predictions obtained from the modeling of decoherence presented in this dissertation. In addition, the development of a framework to obtain an internal-relaxation time constant or functional of the state operator that captures all the physical phenomena of these type of systems is an open area of research.

Bibliography

[1] G. H. Brundtland, "World commission on environment and development," *Our common future*, 1987.

[2] G. P. Hammond, "Engineering sustainability: thermodynamics, energy systems, and the environment," *International Journal of Energy Research*, vol. 28, no. 7, pp. 613–639, 2004.

[3] J.-J. Wang, Y.-Y. Jing, C.-F. Zhang, and J.-H. Zhao, "Review on multi-criteria decision analysis aid in sustainable energy decision-making," *Renewable and Sustainable Energy Reviews*, vol. 13, no. 9, pp. 2263–2278, 2009.

[4] E. P. Gyftopoulos and G. P. Beretta, *Thermodynamics: Foundations and Applications*. Mineola, New York: Courier Dover Publications, 2005.

[5] A. Valero, M. Lozano, L. Serra, and C. Torres, "Application of the exergetic cost theory to the CGAM problem," *Energy*, vol. 19, no. 3, pp. 365–381, 1994.

[6] A. Valero, F. Lerch, L. Serra, and J. Royo, "Structural theory and thermoeconomic diagnosis: Part ii: Application to an actual power plant," *Energy conversion and management*, vol. 43, no. 9, pp. 1519–1535, 2002.

[7] A. Valero, L. Correas, A. Zaleta, A. Lazzaretto, V. Verda, M. Reini, and V. Rangel, "On the thermoeconomic approach to the diagnosis of energy system malfunctions: Part 1: the tadeus problem," *Energy*, vol. 29, no. 12, pp. 1875–1887, 2004.

[8] A. Valero, L. Correas, A. Zaleta, A. Lazzaretto, V. Verda, M. Reini, and V. Rangel, "On the thermoeconomic approach to the diagnosis of energy system malfunctions: Part 2. malfunction definitions and assessment," *Energy*, vol. 29, no. 12, pp. 1889–1907, 2004.

[9] V. Verda, L. Serra, and A. Valero, "Thermoeconomic diagnosis: zooming strategy applied to highly complex energy systems. part 1: detection and localization of anomalies," *Journal of energy resources technology*, vol. 127, no. 1, pp. 42–49, 2005.

[10] V. Verda, L. Serra, and A. Valero, "Thermoeconomic diagnosis: zooming strategy applied to

highly complex energy systems. part 2: on the choice of the productive structure," *Journal of energy resources technology*, vol. 127, no. 1, pp. 50–58, 2005.

[11] A. Lazzaretto and G. Tsatsaronis, "Speco: A systematic and general methodology for calculating efficiencies and costs in thermal systems," *Energy*, vol. 31, no. 8, pp. 1257–1289, 2006.

[12] T. Morosuk and G. Tsatsaronis, "A new approach to the exergy analysis of absorption refrigeration machines," *Energy*, vol. 33, no. 6, pp. 890–907, 2008.

[13] G. Tsatsaronis and M.-H. Park, "On avoidable and unavoidable exergy destructions and investment costs in thermal systems," *Energy Conversion and Management*, vol. 43, no. 9, pp. 1259–1270, 2002.

[14] G. Tsatsaronis, "Definitions and nomenclature in exergy analysis and exergoeconomics," *Energy*, vol. 32, no. 4, pp. 249–253, 2007.

[15] M. R. von Spakovsky and C. A. Frangopoulos, "Analysis and optimization of energy systems with sustainability considerations," in *Enciclopedia of Life Suport Systems (Exergy, Energy System Analysis and Optimization)* (C. A. Frangopoulos, ed.), vol. 3, EOLSS, 2009.

[16] C. A. Frangopoulos, "Functional analysis," in *Enciclopedia of Life Suport Systems (Exergy, Energy System Analysis and Optimization)* (C. A. Frangopoulos, ed.), vol. 3, EOLSS, 2009.

[17] C. A. Frangopoulos, "Introduction to environomics," in *Winter Annual Meeting of the American Society of Mechanical Engineers*, (Atlanta, GA, USA), ASME, 1991.

[18] C. A. Frangopoulos, "Application of the thermoeconomic functional approach to the CGAM problem," *Energy*, vol. 19, no. 3, pp. 323–342, 1994.

[19] C. A. Frangopoulos, *Thermoeconomical Functional Analysis: a Method for Optimal Design or Improvement of Complex Thermal Systems*. PhD thesis, Mechanical Engineering Dept., Georgia Institute of Technology, Atlanta, Georgia, USA, 1983.

[20] C. A. Frangopoulos and Y. C. Caralis, "A method for taking into account environmental impacts in the economic evaluation of energy systems," *Energy conversion and management*, vol. 38, no. 15, pp. 1751–1763, 1997.

[21] V. Curti, M. R. von Spakovsky, and D. Favrat, "An environomic approach for the modeling and optimization of a district heating network based on centralized and decentralized heat pumps, cogeneration and/or gas furnace. Part I: Methodology," *International Journal of Thermal Sciences*, vol. 39, no. 7, pp. 721–730, 2000.

[22] V. Curti, D. Favrat, and M. R. von Spakovsky, "An environomic approach for the modeling and optimization of a district heating network based on centralized and decentralized heat pumps, cogeneration and/or gas furnace. Part II: Application," *International Journal of Thermal Sciences*, vol. 39, no. 7, pp. 731–741, 2000.

[23] S. Pelster, D. Favrat, and M. R. von Spakovsky, "The thermoeconomic and environomic modeling and optimization of the synthesis design, and operation of combined cycles with advanced options," *ASME Journal of engineering for gas turbines and power*, vol. 123, no. 4, pp. 717–726, 2001.

[24] S. Pelster, D. Favrat, and M. R. von Spakovsky, "Centrales de production d'électricité à cycles combinés: Optimisation thermoéconomique et environomique," *Journal des Eaux et des Gaz*, vol. 80, no. 8, pp. 590–598, 2000.

[25] M. R. von Spakovsky, "Application of engineering functional analysis to the analysis and optimization of the CGAM problem," *Energy*, vol. 19, no. 3, pp. 343–364, 1994.

[26] M. R. von Spakovsky, "Sustainability considerations in the modeling of energy systems," in *Enciclopedia of Life Suport Systems (Exergy, Energy System Analysis and Optimization)* (C. A. Frangopoulos, ed.), vol. 3, EOLSS, 2009.

[27] L. Meyer, G. Tsatsaronis, J. Buchgeister, and L. Schebek, "Exergoenvironmental analysis for evaluation of the environmental impact of energy conversion systems," *Energy*, vol. 34, no. 1, pp. 75–89, 2009.

[28] F. Petrakopoulou, A. Boyano, M. Cabrera, and G. Tsatsaronis, "Exergoeconomic and exergoenvironmental analyses of a combined cycle power plant with chemical looping technology," *International Journal of Greenhouse Gas Control*, vol. 5, no. 3, pp. 475–482, 2011.

[29] G. Tsatsaronis and T. Morosuk, "A general exergy-based method for combining a cost analysis with an environmental impact analysis: Part I, theoretical development," No. IMECE2008-67218, (Boston, Massachusetts, USA), ASME, ASME International Mechanical Engineering Congress and Exposition, November 2-6, 2008.

[30] G. Tsatsaronis and T. Morosuk, "A general exergy-based method for combining a cost analysis with an environmental impact analysis, part ii - application to a cogeneration system," No. IMECE2008-67219, (Boston, Massachusetts, USA), ASME, ASME International Mechanical Engineering Congress and Exposition, November 2-6, 2008.

[31] A. J. Wood and B. F. Wollenberg, *Power generation, operation, and control*. John Wiley and Sons, Inc., 2nd ed., 1996.

[32] J. Nanda, L. Hari, and M. Kothari, "Economic emission load dispatch with line flow constraints using a classical technique," *IEEE Proceedings - Generation Transmission and Distribution*, vol. 141, no. 1, pp. 1–10, 1994.

[33] D. Streiffert, "Multi-area economic dispatch with tie line constraints," *IEEE Transactions on Power Systems*, vol. 10, no. 4, pp. 1946–1951, 1995.

[34] B. F. Hobbs, G. Drayton, E. Bartholomew Fisher, and W. Lise, "Improved transmission representations in oligopolistic market models: Quadratic losses, phase shifters, and DC lines," *IEEE Transactions on Power Systems*, vol. 23, no. 3, pp. 1018–1029, 2008.

[35] M. Basu, "Dynamic economic emission dispatch using nondominated sorting genetic algorithm-ii," *International Journal of Electrical Power & Energy Systems*, vol. 30, no. 2, pp. 140–149, 2008.

[36] P. M. Costa and M. A. Matos, "Assessing the contribution of microgrids to the reliability of distribution networks," *Electric Power Systems Research*, vol. 79, no. 2, pp. 382–389, 2009.

[37] C. Lo Prete, B. F. Hobbs, C. S. Norman, S. Cano-Andrade, A. Fuentes, M. R. von Spakovsky, and L. Mili, "Sustainability and reliability assessment of microgrids in a regional electricity market," *Energy*, vol. 41, no. 1, pp. 192–202, 2012.

[38] M. Pipattanasomporn, M. Willingham, and S. Rahman, "Implications of on-site distributed generation for commercial/industrial facilities," *IEEE Transactions on Power Systems*, vol. 20, no. 1, pp. 206–212, 2005.

[39] K. Kim, *Dynamic Proton Exchange Membrane Fuel Cell System Synthesys/Design and Operation/Control Optimization under Uncertainty*. Ph.D. Thesis, Mechanical Engineering Dept., Virginia Polytechnic Institute and State University, Blacksburg, VA, 2008.

[40] M. Wang, *The Integration of State Space into the Dynamic Synthesis/Design and Operational/Control Optimization of a PEMFC System*. Ph.D. Thesis, Mechanical Engineering Dept., Virginia Polytechnic Institute and State University, Blacksburg, VA, 2008.

[41] R. Munos, *Optimization Strategies for the Synthesis / Design of Highly Coupled, Highly Dynamic Energy Systems*. Ph.D. Thesis, Mechanical Engineering Dept., Virginia Polytechnic Institute and State University, Blacksburg, VA, 2000.

[42] D. F. Rancruel, *Dynamic Synthesis/Design and Operation/Control Optimization Approach*

applied to a Solid Oxide Fuel Cell based Auxiliary Power Unit under Transient Conditions. Ph.D. Thesis, Mechanical Engineering Dept., Virginia Polytechnic Institute and State University, Blacksburg, VA, 2005.

[43] A. Fuentes, *Title to be defined*. Ph.D. Thesis, Mechanical Engineering Dept., Virginia Polytechnic Institute and State University, Blacksburg, VA, 2014.

[44] J. L. Cohon, *Multiobjective programming and planning*. Mineola, New York: Courier Dover Publications, 2004.

[45] B. F. Hobbs and P. Meier, *Energy decisions and the environment: a guide to the use of multicriteria methods*. Boston: Kluwer Academic Publishers, 2000.

[46] B. F. Hobbs and G. T. F. Horn, "Building public confidence in energy planning: a multimethod mcdm approach to demand-side planning at bc gas," *Energy policy*, vol. 25, no. 3, pp. 357–375, 1997.

[47] G. Tsatsaronis and T. Morosuk, "Advanced exergoeconomic evaluation and its application to compression refrigeration machines," No. IMECE2007-41202, (Seattle, Washington, USA), ASME, ASME International Mechanical Engineering Congress and Exposition, 2007.

[48] G. Tsatsaronis, K. Kapanke, and A. María Blanco Marigorta, "Exergoeconomic estimates for a novel zero-emission process generating hydrogen and electric power," *Energy*, vol. 33, no. 2, pp. 321–330, 2008.

[49] D. M. Paulus and G. Tsatsaronis, "Auxiliary equations for the determination of specific exergy revenues," *Energy*, vol. 31, no. 15, pp. 3232–3247, 2006.

[50] E. Sciubba and G. Wall, "A brief commented history of exergy from the beginnings to 2004," *International Journal of Thermodynamics*, vol. 10, no. 1, pp. 1–26, 2007.

[51] S. Carnot, "Réflexions sur la puissance motrice du feu et sur les machines propres à développer cette puissance," in *Annales scientifiques de l'École Normale Supérieure*, vol. 1, pp. 393–457, Société mathématique de France, 1824.

[52] B. P. E. Clapeyron vol. 4, (Paris), p. 153, Ecole Polytechnique, 1832.

[53] R. J. E. Clausius, "On the motive power of heat," in *Poggendorf Ann.*, vol. 79, p. 369, 1850.

[54] R. J. E. Clausius, *The Mechanical Theory of Heat*. 1867.

[55] W. Thomson, "On the dynamical theory of heat," *Trans. Roy. Soc. Edinburgh*, March 1851.

[56] W. Rankine, "On the dynamical theory of heat," *Trans. Roy. Soc. Edinburgh*, March 1850.

[57] P. G. Tait, *Sketch of Thermodynamics*. Edinburgh: Edinburgh University Press, 1868.

[58] J. W. Gibbs, "A method of geometrical representation of the thermodynamic properties of substances by means of surfaces," *Trans. Conn. Acad. Arts Sci.*, vol. 3, pp. 108–248 (and 343–524), 1876 (and 1878). also in The Collected Works of J. Willard Gibbs, Longmans Green and Co., 1906 and 1931.

[59] J. C. Maxwell, *Theory of Heat*. London: Longmans Green and Co., 1871.

[60] J. C. Maxwell, "Tait's thermodynamics," *Nature*, vol. 17, p. 278, 1878.

[61] L. G. Gouy, "Sur une loi générale relative aux effects des transformations réversibles," *Compt. Rend. Acad. des Sciences*, vol. 108, 1889.

[62] L. G. Gouy, "Sur les transformations et l'equilibre en thermodynamique," *Compt. Rend. Paris*, vol. 108, 1889.

[63] L. G. Gouy, "Sur les transformations et l'equilibre en thermodynamique. note de m. gouy," *Compt. Rend. Paris*, vol. 108, 1889.

[64] L. G. Gouy, "Sur l'energie utilisable," *J. de Physique*, vol. 8, pp. 501–518, 1889.

[65] A. Stodola, *Die Kreisprozesse der Gasmaschine*. 1898.

[66] G. Goodenough, *Principles of Thermodynamics*. New York: Henry Holt and Company, 1911.

[67] G. Darrieus, "Definition of steam turbine efficiencies," *Engineering*, vol. 130, pp. 283–285, 1930.

[68] G. Darrieus, "L'evolution des centrales thermiques et la notation d'energie utilisable," *Science at Industrie*, vol. 15, pp. 122–126, 1931. In French.

[69] P. Duhem, "Sur la stabilite de lâequilibre en thermodynamique et les recherches de j. w. gibbs au sujet de ce probleme," *Procés-verbaux des séances de la Soc. des Sciences Phys. et Natur. de Bordeaux*, pp. 112–130, 21 July 1904. In French.

[70] C. Carathéodory, "Untersuchungen uber die grundlage der thermodynamik," *Mathematische Annalen*, vol. 67, pp. 355–386, 1909. In German.

[71] H. Lorenz, "Beitrage zur beurteilung von kühlmaschinen," *Zeitschr. des VDI*, vol. 38, pp. 62–68, 98–102, and 124–130, 1894. In German.

[72] H. Lorenz, "Die beurteilung der dampfkessel," *Zeitschr. des VDI*, vol. 38, pp. 1450–1452, 1894. In German.

[73] F. Bosnjakovic, *Technische Thermodynamik*. Dresden und Leipzig: Theodor Steinkopf, 1935. Reprint Dresden und Leipzig, 1948.

[74] F. Bosnjakovic, "Kampf den nichtumkehrbarkeiten," *Arch. WÃ□rmewirtsch. Dampfkesselwes*, vol. 19, pp. 1–2, 1938.

[75] J. H. Keenan, *Thermodynamics*. N.Y.: Wiley, 1941. also 1st MIT Press Ed., Cambridge, MA, 1970.

[76] J. H. Keenan, "A steam chart for second law analysis," *ASME*, vol. 54, pp. 195–204, 1932.

[77] P. Grassmann, "Energie und exergie," *BWK*, vol. 13, no. 11, pp. 482–486, 1961.

[78] V. M. Brodyansky, "A single criterion for assessing the performance of power plants," *Teploenergetika*, vol. 14, no. 3, pp. 71–74, 1968.

[79] E. A. Bruges, "Applications of second law analysis," *The Engineer*, pp. 341–344, 1954.

[80] M. Tribus, "Thermodynamic and economic considerations in the preparation of fresh water from sea water," tech. rep., University of California at Los Angeles, 1956.

[81] M. Tribus and R. Evans, "Thermoeconomics," tech. rep., University of California at Los Angeles, 1962.

[82] M. Tribus and R. Evans, "Thermoeconomics in the design of desalination plants," tech. rep., Thayer School of Engineering, Dartmouth College, Hanover, New Hampshire, 1969.

[83] Y. El-Sayed, "In the use of exergy and thermoeconomics in the design of desalination plants," *J. Eng. Power*, vol. 92, pp. 17–26, 1970.

[84] R. L. El-Sayed, Y.M. ans Evans, "Thermoeconomics and the design of heat systems," *J. Eng. Gas Power*, vol. 92, pp. 27–35, 1969.

[85] E. F. Obert, *Concepts of thermodynamic*. New York: McGraw-Hill, 1960.

[86] R. A. Gaggioli, *Thermodynamics and the Non-equilibrium System*. PhD thesis, Mechanical Engineering Dept., University of Wisconsin-Madison, Madison, Wisconsin, USA, 1961.

[87] H. D. Baehr, "Ein exergie-entropie-diagramm für luft," *Chem. Ing. Techn.*, vol. 33, no. 5, pp. 335–338, 1961.

[88] W. Fratzscher, "Exergetische beurteilung technischer verbrennungsreaktionen," *Energietechn*, vol. 12, no. 4, pp. 153–161, 1962.

[89] J. Szargut, "The potential balance of chemical processes," *Arch. Budowy Maszyn*, vol. 4, pp. 87–117, 1957.

[90] J. Szargut, "Exergy balance of metallurgical processes," *Arch. Hutnictwa*, vol. 6, pp. 23–60, 1961.

[91] R. Petela, "Exergy of heat radiation," *J. Heat Transfer*, vol. 86, no. 2, pp. 187–192, 1964.

[92] K. Knoche, "Exergetische bewertung thermochemischer wasserzersetsungsprozesse," *BWK*, vol. 19, pp. 48–53, 1967.

[93] Z. Rant, "Exergie, ein neues wort fÃ¼r âtechnische arbeitsfÃ¤higkeitâ (exergy, a new word for technical available work)," *Forschungen im Ingenieurwesen*, vol. 22, pp. 36–37, 1956.

[94] T. J. Kotas, *The exergy method of thermal plant analysis*. Stoneham, MA: Butterworth Publishers, 1985.

[95] J. Szargut, D. Morris, and F. Steward, "Exergy analysis of thermal, chemical, and metallurgical processes," 1988.

[96] M. J. Moran, *Availability analysis: a guide to efficient energy use*. Englewood Cliffs, NJ: Prentice-Hall, 1982.

[97] G. N. Hatsopoulos and E. P. Gyftopoulos, "A unified quantum theory of mechanics and thermodynamics. part i. postulates," *Foundations of Physics*, vol. 6, no. 1, pp. 15–31, 1976.

[98] G. N. Hatsopoulos and E. P. Gyftopoulos, "A unified quantum theory of mechanics and thermodynamics. part iia. available energy," *Foundations of Physics*, vol. 6, no. 2, pp. 127–141, 1976.

[99] G. N. Hatsopoulos and E. P. Gyftopoulos, "A unified quantum theory of mechanics and thermodynamics. part iib. stable equilibrium states," *Foundations of Physics*, vol. 6, no. 4, pp. 439–455, 1976.

[100] G. N. Hatsopoulos and E. P. Gyftopoulos, "A unified quantum theory of mechanics and thermodynamics. part iii. irreducible quantal dispersions," *Foundations of Physics*, vol. 6, no. 5, pp. 561–570, 1976.

[101] A. Bejan, G. Tsatsaronis, and M. J. Moran, *Thermal Design and Optimization*. New York: John Wiley Sons, Inc., 1996.

[102] M. Anheden and G. Svedberg, "Exergy analysis of chemical-looping combustion systems," *Energy Conversion and Management*, vol. 39, no. 16, pp. 1967–1980, 1998.

[103] E. Bergmann and K. Schmidt, "Second law analysis for process costing and process design of steam power plants," *Mitt. d. G. B.*, vol. 108, pp. 151–160, 1967. In German.

[104] J. Szargut, "Standard chemical exergy of some elements and their compunds, based upon the concentration in the earth's crust," *Bull. Acad. Pol. Tech.*, vol. 35, pp. 53–60, 1987.

[105] J. Szargut, "Standard chemical exergy of typical aqueous solutions," *Bull. Acad. Pol. Tech.*, vol. 35, pp. 481–483, 1987.

[106] J. Szargut and D. Morris, "Calculation of the standard chemical exergy of some elements and their compounds, based upon sea water as the level substance," *Bull. Acad. Pol. Tech.*, vol. 33, pp. 293–305, 1985.

[107] N. Georgescu-Roegen, *The Entropy Law and the Economic Process*. Cambridge, MA: Harvard University Press, 1971.

[108] G. Tsatsaronis, "Thermoeconomic analysis and optimization of energy systems," *Progress in energy and combustion science*, vol. 19, no. 3, pp. 227–257, 1993.

[109] G. Tsatsaronis, "Energy economics and management in industry," in *Proc. European Conference*, vol. 1, p. 151, 1984.

[110] A. Valero, M. A. Lozano, L. Serra, G. Tsatsaronis, J. Pisa, C. Frangopoulos, and M. R. von Spakovsky, "CGAM problem: Definition and conventional solution," *Energy*, vol. 19, pp. 279–286, 1994.

[111] G. Tsatsaronis and J. Pisa, "Exergoeconomic evaluation and optimization of energy systemsâapplication to the CGAM problem," *Energy*, vol. 19, no. 3, pp. 287–321, 1994.

[112] A. Valero, M. A. Lozano, and M. Muñoz, "A general theory of exergy saving. i. on the exergetic cost," in *Computer-aided engineering and energy systems: second law analysis and modelling*, vol. 3, pp. 1–8, 1986.

[113] A. Valero, M. A. Lozano, and M. Muñoz, "A general theory of exergy savings ii. on the thermoeconomic cost," in *Computer-aided engineering and energy systems: second law analysis and modelling*, 1986.

[114] A. Valero, M. A. Lozano, and M. Muñoz, "A general theory of exergy savings iii. energy savings and thermoeconomics," in *Computer-aided engineering and energy systems: second law analysis and modelling*, 1986.

[115] A. Valero and A. Carreras, "On causality in organized energy systems i. purpose, cause, irreversibility, cost," in *A Future for Energy*, (Florence, Italy), 1990.

[116] A. Valero and C. Torres, "On causality in organized energy systems ii. symbolic exergoeconomics," in *A Future for Energy*, (Florence, Italy), 1990.

[117] A. Valero, M. Lozano, and C. Torres, "On causality in organized energy systems iii. theory of perturbations," in *A Future for Energy*, (Florence, Italy), 1990.

[118] A. Valero, C. Torres, and L. Serra, "A general theory of thermoeconomics part i. structural analysis," in *ECOS 92*, (Zaragoza, Spain), 1992.

[119] A. Valero and M. Lozano, "A general theory of thermoeconomics part ii. the relative free energy function," in *ECOS 92*, (Zaragoza, Spain), 1992.

[120] C. Torres, A. Valero, L. Serra, and J. Royo, "Structural theory and thermoeconomic diagnosis part i. on malfunction and dysfunction analysis," *Energy conversion and management*, vol. 43, no. 9, pp. 1503–1518, 2002.

[121] A. Valero, L. Correas, A. Lazzaretto, V. H. Rangel-Hernandez, M. Reini, R. Taccani, A. Toffolo, V. Verda, and A. Zaleta-Aguilar, "Thermoeconomic philosophy applied to the operating analysis and diagnosis of energy utility systems," *International Journal of Thermodynamics*, vol. 7, no. 2, pp. 33–39, 2004.

[122] A. Zaleta-Aguilar, A. Gallegos-Muñoz, V. H. Rangel-Hernandez, and A. Valero, "A reconciliation method based on a module simulator, an approach to the diagnosis ofenergy system malfunctions," *International Journal of Thermodynamics*, vol. 7, no. 2, pp. 51–60, 2004.

[123] L. Correas, "On the thermoeconomic approach to the diagnosis of energy system malfunctions, suitability to real-time monitoring," *International Journal of Thermodynamics*, vol. 7, no. 2, pp. 85–94, 2010.

[124] G. Tsatsaronis and M. Winhold, "Exergoeconomic analysis and evaluation of energy-conversion plantsâii. analysis of a coal-fired steam power plant," *Energy*, vol. 10, no. 1, pp. 81–94, 1985.

[125] M. R. von Spakovsky, *Practical Generalized Analysis Approach to the Optimal Thermoeconomic Design and Improvement of Real-world Thermal Systems*. Ph.D. Thesis, Mechanical Engineering Dept., Georgia Institute of Technology, Atlanta, GA, 1986.

[126] M. R. von Spakovsky and R. B. Evans, "Engineering functional analysis - Part I," *Journal of Energy Resources Technology*, vol. 115, pp. 86–92, 1993.

[127] R. B. Evans and M. R. von Spakovsky, "Engineering functional analysis - Part II," *Journal of Energy Resources Technology*, vol. 115, pp. 93–99, 1993.

[128] M. R. von Spakovsky and R. B. Evans, "The design and performance optimization of thermal systems," *ASME Journal of Engineering for Gas Turbines and Power*, vol. 112, pp. 86–93, 1990.

[129] M. R. von Spakovsky and R. B. Evans, "The design and performance optimization of thermal system components," *Journal of Energy Resources Technology*, vol. 111, pp. 231–238, 1989.

[130] F. Cziesla, G. Tsatsaronis, and Z. Gao, "Avoidable thermodynamic inefficiencies and costs in an externally fired combined cycle power plant," *Energy*, vol. 31, no. 10, pp. 1472–1489, 2006.

[131] S. Kelly, G. Tsatsaronis, and T. Morosuk, "Advanced exergetic analysis: Approaches for splitting the exergy destruction into endogenous and exogenous parts," *Energy*, vol. 34, no. 3, pp. 384–391, 2009.

[132] T. Morosuk and G. Tsatsaronis, "Advanced exergetic evaluation of refrigeration machines using different working fluids," *Energy*, vol. 34, no. 12, pp. 2248–2258, 2009.

[133] M. Ameri, P. Ahmadi, and A. Hamidi, "Energy, exergy and exergoeconomic analysis of a steam power plant," *International Journal of Energy Research*, vol. 33, pp. 499–512, 2009.

[134] A. Ucar and M. Inalli, "Exergoeconomic analysis and optimization of a solar-assisted heating system for residential buildings," *Building and Environment*, vol. 41, pp. 1551–1556, 2006.

[135] O. Balli, H. Aras, and A. Hepbasli, "Exergoeconomic analysis of a combined heat and power (chp) system," *International Journal of Energy Research*, vol. 32, pp. 273–289, 2008.

[136] M. Rosen and I. Dincer, "Thermoeconomic analysis of power plants: An apllication to coal fired electrical generating station," *Energy Conversion and Management*, vol. 44, pp. 2743–2761, 2003.

[137] M. Orhan, I. Dincer, and M. Rosen, "Exergoeconomic analysis of a thermochemical copper-chlorine cycle for hydrogen production using specific costs (speco) method," *Termochimica Acta*, vol. 497, pp. 60–66, 2010.

[138] A. Kazim, "Exergoeconomic analysis of a pem fuel cell at various operating conditions," *Energy Conversion and Management*, vol. 46, pp. 1073–1081, 2005.

[139] R. River, C. Rendon, and S. Gallegos, "Exergy and exergoeconomic analysis of a crude oil combined distillation unit," *Energy*, vol. 29, pp. 1909–1927, 2004.

[140] L. Ozgener, A. Hepbasli, I. Dincer, and M. A. Rosen, "Exergoeconomic analysis of geothermal district heating systems: A case study," *Applied Thermal Engineering*, vol. 27, no. 8, pp. 1303–1310, 2007.

[141] O. Ozgener and L. Ozgener, "Exergoeconomic analysis of an underground air tunnel system for greenhouse cooling system," *International Journal of Refrigeration*, vol. 33, pp. 995–1005, 2010.

[142] O. Ozgener and A. Hepbasli, "Exergoeconomic analysis of a solar assisted ground-source heat pump greenhouse heating system," *Applied Thermal Engineering*, pp. 1459–1471, 2005.

[143] F. Calise, M. Dentice dâAccadia, L. Vanoli, and M. R. von Spakovsky, "Single-level optimization of a hybrid sofc–gt power plant," *Journal of Power Sources*, vol. 159, no. 2, pp. 1169–1185, 2006.

[144] F. Calise, M. D. dâAccadia, A. Palombo, and L. Vanoli, "A detailed one dimensional finite-volume simulation model of a tubular sofc and a pre-reformer," *International Journal of Thermodynamics*, vol. 10, no. 3, pp. 87–96, 2010.

[145] C. A. Frangopoulos, M. R. von Spakovsky, and E. Sciubba, "A brief review of methods for the design and synthesis optimization of energy systems," *International Journal of Applied Thermodynamics*, vol. 5, no. 4, pp. 151–160, 2002.

[146] B. Olsommer, M. R. von Spakovsky, and D. Favrat, "An approach for the time-dependent thermoeconomic modeling and optimization of energy system synthesis, design and operation part i: Methodology and results," *International Journal of Applied Thermodynamics*, vol. 2, no. 3, pp. 97–114, 1999.

[147] B. Olsommer, D. Favrat, and M. R. von Spakovsky, "An approach for the time-dependent thermoeconomic modeling and optimization of energy system synthesis, design and operation part ii: Reliability and availability," *International Journal of Applied Thermodynamics*, vol. 2, no. 4, pp. 177–186, 1999.

[148] D. F. Rancruel and M. R. von Spakovsky, "Decomposition with thermoeconomic isolation applied to the optimal synthesis/design and operation of an advanced tactical aircraft system," *Energy*, vol. 31, no. 15, pp. 3327–3341, 2006.

[149] D. Rancruel and M. R. von Spakovsky, "A decomposition strategy based on thermoeconomic isolation applied to the optimal synthesis/design operation of an advanced tactical aircraft system," *Energy: The international journal*, vol. 31, no. 15, pp. 3327–3341, 2006.

[150] J. R. Muñoz and M. R. von Spakovsky, "A decomposition approach for the large scale synthesis design optimization of highly coupled, highly dynamic energy systems," *International Journal of Thermodynamics*, vol. 4, no. 1, pp. 19–33, 2001.

[151] J. Muños and M. R. von Spakovsky, "Decomposition in energy systems synthesis/design

optimization for stationary and aerospace applications," *AIAA Journal of Aircraft*, vol. 40, no. 1, pp. 35–42, 2003.

[152] J. R. Muñoz and M. R. von Spakovsky, "The application of decomposition to the large scale synthesis/design optimization of aircraft systems," *International Journal of Thermodynamics*, vol. 4, no. 2, pp. 19–33, 2001.

[153] M. Wang, K. Kim, M. R. von Spakovsky, and D. J. Nelson, "Multi-versus single-level dynamic synthesis/design and operation/control optimizations of a PEMFC system," in *Proceedings of ASME International Mechanical Engineering Congress and Exposition*, no. IMECE2008-68073, New York, N. Y., USA: ASME, Oct.-Nov. 2008.

[154] M. Wang, K. Kim, M. R. von Spakovsky, and D. J. Nelson, "Use of state space in the dynamic synthesis/design and operation/control optimization of a PEMFC system," in *Proceedings of ASME International Mechanical Engineering Congress and Exposition*, no. IMECE2008-68076, New York, N. Y., USA: ASME, Oct.-Nov. 2008.

[155] A. Lazzaretto, A. Toffolo, M. Morandin, and M. R. von Spakovsky, "Criteria for the decomposition of energy systems in local/global optimizations," *Energy*, vol. 35, no. 2, pp. 1157–1163, 2010.

[156] K. Kim, M. R. von Spakovsky, M. Wang, and D. J. Nelson, "A hybrid multi-level optimization approach for the dynamic synthesis/design and operation/control under uncertainty of a fuel cell system," *Energy*, vol. 36, no. 6, pp. 3933–3943, 2011.

[157] A. Toffolo, A. Lazzaretto, and M. R. von Spakovsky, "On the nature of the heat transfer feasibility constraint in the optimal synthesis/design of complex energy systems," *Energy*, vol. 41, no. 1, pp. 236–243, 2012.

[158] K. Kim, M. Wang, M. R. von Spakovsky, and D. J. Nelson, "Dynamic optimization under uncertainty of the synthesis/design and operation/control of a PEMFC system," *Journal of Power Sources*, vol. 205, pp. 252–263.

[159] M. R. von Spakovsky, "Chapter 10 - MIS/DO applied to high performance aerospace vehicles," in *Exergy Analysis and Design optimization for Aerospace Vehicles and Systems* (J. Camberos and D. Moorhouse, eds.), AIAA book series, 2011.

[160] M. R. von Spakovsky, "Chapter 9 - Mission-Integrated Synthesis and Design Optimization MIS/DO of Aerospace Vehicles," in *Exergy Analysis and Design optimization for Aerospace Vehicles and Systems* (J. Camberos and D. Moorhouse, eds.), AIAA book series, 2011.

[161] G. Wall and M. Gong, "On exergy and sustainable developmentâpart 1: Conditions and concepts," *Exergy, An International Journal*, vol. 1, no. 3, pp. 128–145, 2001.

[162] M. Gong and G. Wall, "On exergy and sustainable developmentâpart 2: Indicators and methods," *Exergy, an International journal*, vol. 1, no. 4, pp. 217–233, 2001.

[163] C. A. Frangopoulos and M. R. von Spakovsky, "A global environomic approach for energy systems analysis and optimization. Part I," *Energy systems and ecology, ENSEC 93*, pp. 123–132, 1993.

[164] M. R. von Spakovsky and C. A. Frangopoulos, "A global environomic approach for energy systems analysis and optimization. Part II," *Energy systems and ecology, ENSEC 93*, pp. 133–144, 1993.

[165] M. R. von Spakovsky and C. A. Frangopoulos, "The environomic analysis and optimization of a gas turbine cycle with cogeneration," *AES-Thermodynamic and the design, analysis, and improvement of energy systems*, vol. 33, pp. 15–26, 1994.

[166] A. Agazzani, A. F. Massardo, and C. A. Frangopoulos, "Environmental influence on the thermoeconomic optimization of a combined plant with nox abatement," *Trans. ASME, J. Eng. Gas Turbines Power*, vol. 120, pp. 557–565, 1998.

[167] M. Goedkoop and R. Spriensma, "The Eco-indicator 99: A damage oriented method for Life Cycle Impact Assessment.," Methodology Report. Amersfoort, Netherlands, 2000. www.pre.nl.

[168] A. Valero-Delgado, *Exergy Evolution of the mineral capital on earth*. Ph.D. Thesis, University of Zaragoza, Zaragoza, Spain, 2008.

[169] A. Valero and A. Valero, "Exergoecology: A thermodynamic approach for accounting the earth's mineral capital. the case of bauxite–aluminium and limestone–lime chains," *Energy*, vol. 35, no. 1, pp. 229–238, 2010.

[170] G. E. A. of Natural Resources, "Valero, a. and botero, e. and valero, a.," in *Enciclopedia of Life Suport Systems (Exergy, Energy System Analysis and Optimization)* (C. A. Frangopoulos, ed.), vol. 3, EOLSS, 2009.

[171] A. Valero, A. Valero, and I. Arauzo, "Evolution of the decrease in mineral exergy throughout the 20th century. the case of copper in the us," *Energy*, vol. 33, no. 2, pp. 107–115, 2008.

[172] A. Valero, A. Agudelo, and A. Valero, "The crepuscular planet. a model for the exhausted atmosphere and hydrosphere," *Energy*, vol. 36, no. 6, pp. 3745–3753, 2011.

[173] A. Valero, A. Valero, and A. Martínez, "Inventory of the exergy resources on earth including its mineral capital," *Energy*, vol. 35, no. 2, pp. 989–995, 2010.

[174] A. Valero and A. Valero, "The crepuscular planet. part ii. a model for the exhausted continental crust," in *22nd international conference on efficiency, cost, optimization simulation and environmental impact of energy systems ECOS â09, Foz do Iguaçu, Paraná, Brazil*, 2009.

[175] International Standard Organization. International Standard ISO 14040, "Environmental management – Lyfe Cycle Assessment – Principles and framework," *Paris*, 1997.

[176] International Standard Organization. International Standard ISO 14040, "Environmental management – Lyfe Cycle Assessment – Goal and scope definition and life cycle inventory analysis," *Paris*, 1998.

[177] International Standard Organization. International Standard ISO 14040, "Environmental management – Lyfe Cycle Assessment – Life cycle impact assessment," *Paris*, 2000.

[178] International Standard Organization. International Standard ISO 14040, "Environmental management – Lyfe Cycle Assessment – Life cycle interpretation," *Paris*, 2000.

[179] US-EPA, "U.S. Life Cycle Inventory database." National Renewable Energy Laboratory NREL. Available from: http://www.nrel.gov/lci/database/. Access Date [12-22-2013].

[180] Ecoinvent Centre, "Ecoinvent." Swiss Centre for Life Cycle Inventories. Available from: http://www.ecoinvent.ch/. Access Date [12-22-2013].

[181] J. Dewulf, M. Bösch, B. D. Meester, G. V. d. Vorst, H. V. Langenhove, S. Hellweg, and M. Huijbregts, "Cumulative exergy extraction from the natural environment (ceene): a comprehensive life cycle impact assessment method for resource accounting," *Environmental science & technology*, vol. 41, no. 24, pp. 8477–8483, 2007.

[182] J. Dewulf, H. Van Langenhove, J. Mulder, M. Van den Berg, H. Van der Kooi, and J. de Swaan Arons, "Illustrations towards quantifying the sustainability of technology," *Green Chemistry*, vol. 2, no. 3, pp. 108–114, 2000.

[183] B. De Meester, J. Dewulf, A. Janssens, and H. Van Langenhove, "An improved calculation of the exergy of natural resources for exergetic life cycle assessment (elca)," *Environmental science & technology*, vol. 40, no. 21, pp. 6844–6851, 2006.

[184] G. Van der Vorst, H. Van Langenhove, F. De Paep, W. Aelterman, J. Dingenen, and J. Dewulf, "Exergetic life cycle analysis for the selection of chromatographic separation

processes in the pharmaceutical industry: preparative HPLC versus preparative SFC," *Green Chemistry*, vol. 11, no. 7, pp. 1007–1012, 2009.

[185] A. Zvolinschi, S. Kjelstrup, O. Bolland, and H. J. Kooi, "Exergy sustainability indicators as a tool in industrial ecology," *Journal of Industrial Ecology*, vol. 11, no. 4, pp. 85–98, 2007.

[186] H. A. Udo de Haes and R. Heijungs, "Life-cycle assessment for energy analysis and management," *Applied Energy*, vol. 84, no. 7, pp. 817–827, 2007.

[187] G. Wall, "Life cycle exergy analysis of renewable energy systems," *Open Renew Energy Journal*, vol. 4, no. 1, pp. 1–6, 2011.

[188] E. Sciubba, "Extended exergy accounting applied to energy recovery from waste: The concept of total recycling," *Energy*, vol. 28, no. 13, pp. 1315–1334, 2003.

[189] A. Gasparatos, M. El-Haram, and M. Horner, "A critical review of reductionist approaches for assessing the progress towards sustainability," *Environmental Impact Assessment Review*, vol. 28, no. 4, pp. 286–311, 2008.

[190] A. L. Mayer, "Strengths and weaknesses of common sustainability indices for multidimensional systems," *Environment international*, vol. 34, no. 2, pp. 277–291, 2008.

[191] E. Sciubba and S. Ulgiati, "Emergy and exergy analyses: complementary methods or irreducible ideological options?," *Energy*, vol. 30, no. 10, pp. 1953–1988, 2005.

[192] A. Gasparatos, M. El-Haram, and M. Horner, "The argument against a reductionist approach for measuring sustainable development performance and the need for methodological pluralism," *Accounting Forum*, vol. 33, no. 3, pp. 245–256, 2009.

[193] J. S. Heslin and B. F. Hobbs, "A multiobjective production costing model for analyzing emissions dispatching and fuel switching," *IEEE Transactions on Power Systems*, vol. 4, no. 3, pp. 836–842, 1989.

[194] C. J. Day, B. F. Hobbs, and J.-S. Pang, "Oligopolistic competition in power networks: a conjectured supply function approach," *IEEE Transactions on Power Systems*, vol. 17, no. 3, pp. 597–607, 2002.

[195] B. F. Hobbs and F. A. M. Rijkers, "Strategic generation with conjectured transmission price responses in a mixed transmission pricing system-part i: formulation," *IEEE Transactions on Power Systems*, vol. 19, no. 2, pp. 707–717, 2004.

[196] B. F. Hobbs, F. A. M. Rijkers, and A. F. Wals, "Strategic generation with conjectured trans-

mission price responses in a mixed transmission pricing system-part II: Application," *IEEE Transactions on Power Systems*, vol. 19, no. 2, pp. 872–879, 2004.

[197] B. F. Hobbs, F. A. Rijkers, and M. G. Boots, "The more cooperation, the more competition? a cournot analysis of the benefits of electric market coupling," *The Energy Journal*, vol. 26, no. 4, pp. 69–97, 2005.

[198] K. Neuhoff, J. Barquin, M. G. Boots, A. Ehrenmann, B. F. Hobbs, F. A. M. Rijkers, and M. Vazquez, "Network-constrained cournot models of liberalized electricity markets: the devil is in the details," *Energy Economics*, vol. 27, no. 3, pp. 495–525, 2005.

[199] W. Lise, B. F. Hobbs, and S. Hers, "Market power in the european electricity marketâthe impacts of dry weather and additional transmission capacity," *Energy Policy*, vol. 36, no. 4, pp. 1331–1343, 2008.

[200] D. Eager, B. F. Hobbs, and J. W. Bialek, "Dynamic modeling of thermal generation capacity investment: Application to markets with high wind penetration," *IEEE Transactions on Power Systems*, pp. 1–11, 2012.

[201] I. Vera and L. Langlois, "Energy indicators for sustainable development," *Energy*, vol. 32, no. 6, pp. 875–882, 2007.

[202] U. N. D. o. E. a. S. A. International Atomic Energy Agency, I. E. Agency, Eurostat, and E. E. Agency, "Energy indicators for sustainable development: Guidelines and methodologies," 2005.

[203] N. H. Afgan, M. G. Carvalho, and N. V. Hovanov, "Modeling of energy system under sustainability index," *Thermal Science*, vol. 9, pp. 3–16, 2005.

[204] N. H. Afgan and M. da Graça Carvalho, "Multi-criteria assessment of new and renewable energy power plants," *Energy*, vol. 27, no. 8, pp. 739–755, 2002.

[205] N. H. Afgan, M. da Graça Carvalho, and N. V. Hovanov, "Energy system assessment with sustainability indicators," *Energy Policy*, vol. 28, pp. 603–612, 2000.

[206] A. Evans, V. Strezov, and T. J. Evans, "Assessment of sustainability indicators for renewable energy technologies," *Renewable and sustainable energy reviews*, vol. 13, no. 5, pp. 1082–1088, 2009.

[207] C. A. Frangopoulos and D. E. Keramioti, "Multi-criteria evaluation of energy systems with sustainability considerations," *Entropy*, vol. 12, no. 5, pp. 1006–1020, 2010.

[208] C. Sheinbaum-Pardo, B. J. Ruiz-Mendoza, and V. Rodríguez-Padilla, "Mexican energy policy and sustainability indicators," *Energy Policy*, vol. 46, pp. 278–283, 2012.

[209] OLADE, CEPAL, and GTZ, *Energía y Desarrollo Sustentable en América Latina y el Caribe: Enfoques para la Política Energética*. Quito, Ecua: United Nations Publications, 1997.

[210] D. Gallego Carrera and A. Mack, "Sustainability assessment of energy technologies via social indicators: Results of a survey among european energy experts," *Energy policy*, vol. 38, no. 2, pp. 1030–1039, 2010.

[211] D. Gallego Carrera and A. Mack, "Quantification of social indicators for the assessment of energy system related effects," Report, NEEDS Integrated project, ISSN 1614-3035, ISBN 978-3-938245-11-8, 2009.

[212] S. Cano-Andrade, M. R. von Spakovsky, A. Fuentes, C. Lo Prete, B. F. Hobbs, and L. Mili, "Multiobjective optimization for the sustainable-resilient synthesis/design/operation of a power network coupled to distributed power producers via microgrids," in *Proceedings of ASME International Mechanical Engineering Congress and Exposition*, vol. 6, Energy: Sustainable Technologies, pp. 1393–1408, Houston, Texas, USA: ASME, November 9-15, 2012.

[213] European Network of Transmission System Operators for Electricity, "Hourly load values for a specific country for a specific month." Available from: www.entsoe.eu/index.php?id=137. Access date: [09-12-2013].

[214] Energy Research Centre of the Netherlands, "Competes input data." Available from: www.ecn.nl/fileadmin/ecn/units/bs/COMPETES/costfunctions.xls. Access date: [09-12-2013].

[215] X-RatesTM, "Currency calculator historic lookup." Available from: www.x-rates.com/d/USD/EUR/hist2010.html. Access date: [09-12-2013].

[216] European Nuclear Society, "Capacity operating hours (2012)." Available from: www.euronuclear.org/info/encyclopedia/capacityoperation hours.htm. Access date: [09-12-2013].

[217] World Nuclear Association, "Nuclear Power Reactors." Available online from: http://world-nuclear.org/info/Nuclear-Fuel-Cycle/Power-Reactors/Nuclear-Power-Reactors/#.Uijdhj_N3zs. Access date: [11-12-2013].

[218] K. Flury and R. Frischknecht, "Life cycle inventories of hydroelectric generation," ESU-Services Ltd., 2012.

[219] C. Lo Prete, B. F. Hobbs, C. S. Norman, S. Cano-Andrade, A. Fuentes, M. R. von Spakovsky, and L. Mili, "Sustainability assessment of microgrids in the northwestern european electricity market," in *Proceedings of the Efficiency, Cost, Optimization, Simulation and Environmental Impact of Energy Systems Conference, ECOS 2010*, ASME, June 14-17, 2010. Lausanne, Switzerland.

[220] R. A. King and H. C. Rughooputh, "Elitist multiobjective evolutionary algorithm for environmental/economic dispatch," in *The 2003 Congress on Evolutionary Computation CEC'03*, vol. 2, pp. 1108–1114, IEEE, 2003.

[221] Y. Sumio, S. Masuto, and M. Fumihiro, "Thermoselect waste gasification and reforming process," *JFE Technical Report*, no. 3, 2004.

[222] R. Kehlhofer, F. Hannemann, F. Stirnimann, and B. Rukes, *Combined-cycle gas & steam turbine power plants*. Tulsa, Oklahoma: PennWell Corporation, 2009.

[223] Y. Smeers, L. Bolle, and O. Squilbin, "Coal options, evaluation of coal-based power generation in an uncertain context," 2001. Report UCL-CORE, UCL-TERM, CG/DD/231-G/DD/232.

[224] P. Lako, "Coal-fired power technologies," in *ECN project on Clean Coal Technologies*, 2004.

[225] D. King, *Electric Power Micro-grids: Opportunities and Challenges for an Emerging Distributed Energy Architecture*. Ph.D. Thesis, Carnegie Mellon University, Pittsburgh, PA, 2006.

[226] G. Erdmann, "Future economics of the fuel cell housing market," *International Journal of Hydrogen Energy*, vol. 28, no. 7, pp. 685–694, 2003.

[227] US EPA, "Technology characterization: Gas turbines," Climate Protection Partnership Division, 2008.

[228] US EPA, "Combined heat and power at comercial supermarket capstone 60 kW microturbine CHP system," No. SRI/USEPA-GHG-VR-27, Environmental Technology Verification Report, 2003.

[229] V. I. Kuprianov, W. Kaewboonsong, and P. Douglas, "Minimizing fuel and environmental

costs for a variable-load power plant (co-) firing fuel oil and natural gas part 2. Optimization of load dispatch," *Fuel Processing Technology*, vol. 89, no. 1, pp. 55–61, 2008.

[230] US EPA, "Technology characterization: Reciprocating engines," US EPA Climate protection Partnership Division, 2002.

[231] US EPA, "Biomass combined heat and power catalog of technologies," Combined Heat and Power Partnership, 2007.

[232] G. P. Beretta, P. Iora, and A. F. Ghoniem, "Novel approach for fair allocation of primary energy consumption among cogenerated energy-intensive products based on the actual local area production scenario," *Energy*, vol. 44, no. 1, pp. 1107–1120, 2012.

[233] R. Billinton and R. N. Allan, *Reliability Evaluation of Power Systems*. New York: Plenum Press, 2nd ed., 1996.

[234] G. Gross, N. V. Garapic, and B. McNutt, "The mixture of normals approximation technique for equivalent load duration curves," *IEEE Transactions on Power Systems*, vol. 3, no. 2, pp. 368–374, 1988.

[235] "Renewable energy in the netherlands," p. 39, The Hague: Statistics Netherlands, 2011.

[236] Q. Chen and L. Mili, "Resiliency metrics for electric power systems," Report, ECE Department, Virginia Tech: Northern Virginia Center, Falls Church, VA, 2011.

[237] T. Yalcinoz and O. Köksoy, "A multiobjective optimization method to environmental economic dispatch," *Electrical Power and Energy Systems*, vol. 29, no. 1, pp. 42–50, 2007.

[238] J. Arora, *Introduction to Optimum Design*. Waltham, MA, USA: Academic Press, 3rd ed., 2011.

[239] K. Deb, A. Pratap, S. Agarwal, and T. Meyarivan, "A fast and elitist multiobjective genetic algorithm: NSGA-II," *IEEE Transactions on Evolutionary Computation*, vol. 6, no. 2, pp. 182–197, 2002.

[240] M. Abido, "Multiobjective particle swarm optimization for environmental/economic dispatch problem," *Electric Power Systems Research*, vol. 79, no. 7, pp. 1105–1113, 2009.

[241] A. Abraham, L. C. Jain, and R. Goldberg, *Evolutionary Multiobjective Optimization: Theoretical Advances and Applications*. Springer, 2005.

[242] A. L. Tits. Personal webpage, available from: http://www.ece.umd.edu/ andre/. Access Date [08-18-2013].

[243] J. L. Zhou and A. L. Tits, "An SQP algorithm for finely discretized continuous minimax

problems and other minimax problems with many objective functions," *SIAM Journal on Optimization*, vol. 6, no. 2, pp. 461–487, 1996.

[244] C. T. Lawrence and A. L. Tits, "Feasible sequential quadratic programming for finely discretized problems from SIP," in *Semi-Infinite Programming*, pp. 159–193, Springer, 1998.

[245] W. Zhang and R. A. Gaggioli, "Multiobjective optimization with aid of fuzzy-set concepts," in *Proceedings of Efficiency, Cost, Optimization, Simulation and Environmental Impact of Energy Systems Conference (ECOS 1992)*, Zagaroza, Spain: ASME, June 15-18, 1992.

[246] D. von Winterfeldt and W. Edwards, *Decision analysis and behavioral research*. Cambridge: Cambridge University Press, 1986.

[247] A. J. Wood and B. F. Wollenberg, *Power generation, operation, and control*. John Wiley & Sons, 1984.

[248] D. Streiffert, "Multi-area economic dispatch with tie line constraints," *IEEE Transactions on Power Systems*, vol. 10, no. 4, pp. 1946–1951, 1995.

[249] K. Deb. Available from: http://www.iitk.ac.in/kangal/codes.shtml. Access Date [08-29-2013].

[250] International Business Machines Corporation(IBM), "Ilog opl 6.3." Available from: http://www-01.ibm.com/software/websphere/ilog/. Access date: [09-18-2013].

[251] G. N. Hatsopoulos and J. H. Keenan, *Principles of general thermodynamics*. New York: Wiley, 1965.

[252] G. N. Hatsopoulos and E. P. Gyftopoulos, "A unified quantum theory of mechanics and thermodynamics. Part I. Postulates," *Foundations of Physics*, vol. 6, no. 1, pp. 15–31, 1976.

[253] G. N. Hatsopoulos and E. P. Gyftopoulos, "A unified quantum theory of mechanics and thermodynamics. Part IIa. Available energy," *Foundations of Physics*, vol. 6, no. 2, pp. 127–141, 1976.

[254] G. N. Hatsopoulos and E. P. Gyftopoulos, "A unified quantum theory of mechanics and thermodynamics. Part IIb. Stable equilibrium states," *Foundations of Physics*, vol. 6, no. 4, pp. 439–455, 1976.

[255] G. N. Hatsopoulos and E. P. Gyftopoulos, "A unified quantum theory of mechanics and thermodynamics. Part III. Irreducible quantal dispersions," *Foundations of Physics*, vol. 6, no. 5, pp. 561–570, 1976.

[256] J. L. Park, "Nature of quantum states," *American Journal of Physics*, vol. 36, pp. 211–226, 1968.

[257] G. P. Beretta, *On the general equation of motion of quantum thermodynamics and the distinction between quantal and nonquantal uncertainties*. Ph.D. Thesis, Mechanical Engineering Dept., Massachusetts Institute of Technology, Boston, MA, 1981. arXiv:quant-ph/0509116.

[258] G. P. Beretta, "Maximal-entropy-production-rate nonlinear quantum dynamics compatible with second law, reciprocity, fluctuation-dissipation, and time-energy uncertainty relations," *arXiv preprint quant-ph/0112046*, 2001.

[259] C. E. Smith and M. R. von Spakovsky, "Comparison of the non-equilibrium predictions of Quantum Thermodynamics at the atomistic level with experimental evidence," *Journal of Physics, Institute of Physics (IOP)*, vol. 380, p. 012015, 2012.

[260] U. Weiss, *Quantum Dissipative Systems*, vol. 13. Singapore-London: World Scientific Publishing Company, Series in Modern Condensed Matter Physics, 2008.

[261] K. Blum, *Density Matrix Theory and Applications*. New York: Plenum Publishing Corporation, 2nd ed., 1996.

[262] S. Cano-Andrade, G. P. Beretta, and M. R. von Spakovsky, "Steepest-entropy-ascent quantum thermodynamic non-equilibrium modeling of decoherence of a composite system of two interacting spin-1/2 systems," in *Proceedings of ASME International Mechanical Engineering Congress and Exposition*, no. IMECE2013-63596, San Diego, California, USA: ASME, November 15-21, 2013.

[263] C. R. Wylie and L. C. Barrett, *Advanced engineering mathematics*. New York: McGraw-Hill, 6th ed., 1995.

[264] E. Zanchini and G. P. Beretta, "Removing heat and conceptual loops from the definition of entropy," *International Journal of Thermodynamics*, vol. 12, no. 2, pp. 67–76, 2010. ISSN 1301-9724.

[265] G. P. Beretta and E. Zanchini, "Rigorous and general definition of thermodynamic entropy," in *Thermodynamics* (M. Tadashi, ed.), InTech, January 2011. ISBN 978-953-307-544-0.

[266] J. von Neumann, *Mathematical Foundations of Quantum Mechanics (English translation by R.T. Beyer)*. Princeton, New Jersey: Princeton University Press, 1955.

[267] G. C. Schatz and M. A. Ratner, *Quantum Mechanics in Chemistry*. Courier Dover Publications, 1993.

[268] C. Hampel and H. J. Werner, "Local treatment of electron correlation in coupled cluster theory," *The Journal of chemical physics*, vol. 104, pp. 6286–6297, 1996.

[269] M. Schütz, "A new, fast, semi-direct implementation of linear scaling local coupled cluster theory," *Physical Chemistry Chemical Physics*, vol. 4, no. 16, pp. 3941–3947, 2002.

[270] T. D. Crawford, "Ab initio calculation of molecular chiroptical properties," *Theoretical Chemistry Accounts*, vol. 115, no. 4, pp. 227–245, 2006.

[271] N. J. Russ and T. D. Crawford, "Local correlation in coupled cluster calculations of molecular response properties," *Chemical physics letters*, vol. 400, no. 1, pp. 104–111, 2004.

[272] M. Nakatani and T. Ogawa, "Quantum master equations for composite systems: Is Born-Markov approximation really valid?," *Journal of the Physical Society of Japan*, vol. 79, no. 8, p. 084401, 2010.

[273] J. Loschmidt, "Sitzungsber. kais. akad. wiss. wien," *Math. Naturwiss*, vol. 73, pp. 128–142, 1876.

[274] K. Hornberger, "Master equation for a quantum particle in a gas," *Physical review letters*, vol. 97, no. 6, p. 060601, 2006.

[275] V. Gorini, A. Frigerio, M. Verri, A. Kossakowski, and E. Sudarshan, "Properties of quantum markovian master equations," *Reports on Mathematical Physics*, vol. 13, no. 2, pp. 149–173, 1978.

[276] D. Rodrigues and A. Armour, "Quantum master equation descriptions of a nanomechanical resonator coupled to a single-electron transistor," *New Journal of Physics*, vol. 7, no. 1, p. 251, 2005.

[277] X.-Q. Li, W.-K. Zhang, P. Cui, J. Shao, Z. Ma, and Y. Yan, "Quantum measurement of a solid-state qubit: A unified quantum master equation approach," *Physical Review B*, vol. 69, no. 8, p. 085315, 2004.

[278] C.-H. Chou, T. Yu, and B.-L. Hu, "Exact master equation and quantum decoherence of two coupled harmonic oscillators in a general environment," *Physical Review E*, vol. 77, no. 1, p. 011112, 2008.

[279] A. Kossakowski, "On quantum statistical mechanics of non-Hamiltonian systems," *Reports on Mathematical Physics*, vol. 3, no. 4, pp. 247–274, 1972.

[280] G. Lindblad, "On the generators of quantum dynamical semigroups," *Communications in Mathematical Physics*, vol. 48, no. 2, pp. 119–130, 1976.

[281] G. Lindblad, *Non-equilibrium entropy and irreversibility*. Dordrecht, Holland: D. Reidel Publishing Company, 1983.

[282] H. Haken, *Synergetics*. Berlin: Springer, 1978.

[283] E. P. Gyftopoulos and E. Cubukcu, "Entropy: Thermodynamic definition and quantum expression," *Physical Review E*, vol. 55, pp. 3851–3858, 1997.

[284] G. P. Beretta, E. P. Gyftopoulos, J. L. Park, and G. N. Hatsopoulos, "Quantum thermodynamics. A new equation of motion for a single constituent of matter," *Il Nuovo Cimento B Series 11*, vol. 82, no. 2, pp. 169–191, 1984.

[285] G. P. Beretta, "Steepest entropy ascent in quantum thermodynamics," *Lecture Notes in Physics*, vol. 278, 1986.

[286] G. P. Beretta, "Nonlinear model dynamics for closed-system, constrained, maximal-entropy-generation relaxation by energy redistribution," *Physical Review E*, vol. 73, no. 2, p. 026113, 2006.

[287] G. P. Beretta, "Nonlinear quantum evolution equations to model irreversible adiabatic relaxation with maximal entropy production and other nonunitary processes," *Reports on Mathematical Physics*, vol. 64, no. 1, pp. 139–168, 2009.

[288] G. P. Beretta, E. P. Gyftopoulos, and J. L. Park, "Quantum thermodynamics. A new equation of motion for a general quantum system," *Il Nuovo Cimento B Series 11*, vol. 87, no. 1, pp. 77–97, 1985.

[289] S. Haroche, M. Brune, and J.-M. Raimond, "Atomic clocks for controlling light fields," *Physics today*, vol. 66, no. 1, p. 27, 2013.

[290] S. Deleglise, I. Dotsenko, C. Sayrin, J. Bernu, M. Brune, J.-M. Raimond, and S. Haroche, "Reconstruction of non-classical cavity field states with snapshots of their decoherence," *Nature*, vol. 455, no. 7212, pp. 510–514, 2008.

[291] J. M. Raimond, M. Brune, and S. Haroche, "Reversible decoherence of a mesoscopic superposition of field states," *Physical Review Letters*, vol. 79, pp. 1964–1967, 1997.

[292] M. Brune, E. Hagley, J. Dreyer, X. Maitre, A. Maali, C. Wunderlich, J. M. Raimond, and S. Haroche, "Observing the progressive decoherence of the meter in a quantum measurement," *Physical Review Letters*, vol. 77, pp. 4887–4890, 1996.

[293] J. Raimond, M. Brune, and S. Haroche, "Colloquium: Manipulating quantum entanglement with atoms and photons in a cavity," *Reviews of Modern Physics*, vol. 73, no. 3, pp. 565–582, 2001.

[294] G. P. Beretta, "Quantum thermodynamics of nonequilibrium. Onsager reciprocity and dispersion-dissipation relations," *Foundations of Physics*, vol. 17, no. 4, pp. 365–381, 1987.

[295] G. P. Beretta, "Quantum thermodynamics: Microscopic foundations of entropy and of maximal entropy generation by irreversibility," in *XXII Congresso Nazionale sulla Trasmissione del Calore*, 2004.

[296] G. P. Beretta, "Nonlinear extensions of schrödinger-von newmann quantum dynamics: A set of necessary conditions for compatibility with thermodynamics," *Modern Physics Letters A*, vol. 20, no. 13, pp. 977–984, 2005.

[297] G. P. Beretta, "Steepest-Entropy-Ascent irreversible relaxation towards thermodynamic equilibrium: The dynamical ansatz that completes the gyftopoulos-hatsopoulos unified theory with a general quantal law of causal evolution," *International Journal of Thermodynamics*, vol. 9, no. 3, pp. 117–128, 2006.

[298] G. P. Beretta, "Well-behaved nonlinear evolution equation for steepest-entropy-ascent dissipative quantum dynamics," *International Journal of Quantum Information*, vol. 5, no. 1 and 2, pp. 249–255, 2007.

[299] G. P. Beretta, "Modeling non-equilibrium dynamics of a discrete probability distribution: General rate equation for maximal entropy generation in a maximum-entropy landscape with time-dependent constraints," *Entropy*, vol. 10, pp. 160–182, 2008.

[300] G. P. Beretta, "Maximum entropy production rate in quantum thermodynamics," *Journal of Physics: Conference Series, Symmetries in Science XIV*, vol. 237, p. 012004, 2010.

[301] C. E. Smith, A. Sciacovelli, M. R. von Spakovsky, and V. Verda, "3d quantum thermodynamic description of the nonequilibrium behavior of an unbounded system at an atomistic level," *Journal of Physics, Institute of Physics (IOP)*, vol. 237, p. 012022, 2010. doi:10.1088/1742-6596/237/1/012022.

[302] A. Sciacovelli, C. E. Smith, M. R. von Spakovsky, and V. Verda, "Quantum thermodynamics: Non-equilibrium 3D description of an unbounded system at an atomistic level," *International Journal of Thermodynamics*, vol. 13, no. 1, pp. 23–33, 2010. ISSN 1301-9724.

[303] C. E. Smith, *Intrinsic Quantum Thermodynamics: Application to Hydrogen Storage on a*

Carbon Nanotube and Theoretical Consideration of Non-Work Interactions. Ph.D. Thesis, Mechanical Engineering Dept., Virginia Polytechnic Institute and State University, Blacksburg, VA, 2012.

[304] S. Cano-Andrade, G. P. Beretta, and M. R. von Spakovsky, "Intrinsic quantum thermodynamic non-equilibrium modeling of CQED atom-field evolution with comparison to published data," in *Proceedings of the 12th Joint European Thermodynamics Conference* (M. Pilotelli and G. P. Beretta, eds.), pp. 430–435, Brescia, Italy: Snoopy, July 1-5, 2013. ISBN 978-88-89252-22-2.

[305] O. Al-Abbasi, G. P. Beretta, and M. R. von Spakovsky, "Intrinsic quantum thermodynamic prediction of the non-equilibrium atomistic level behavior of chemically reactive systems," in *Proceedings of the 12th Joint European Thermodynamics Conference* (M. Pilotelli and G. P. Beretta, eds.), pp. 573–578, Brescia, Italy: Snoopy, July 1-5, 2013. ISBN 978-88-89252-22-2.

[306] O. Al-Abbasi, *Modeling the non-equilibrium phenomena of chemically reactive atomistic level systems using steepest-entropy-ascent quantum thermodynamics*. Ph.D. Thesis, Mechanical Engineering Dept., Virginia Polytechnic Institute and State University, Blacksburg, VA, USA, 2013.

[307] G. N. Hatsopoulos and G. P. Beretta, "Where is the entropy challenge?," in *Meeting the Entropy Challenge, AIP Conf. Proc. Series*, vol. 1033, pp. 34–54, 2008.

[308] S. Carnot, "Réflexions sur la puissance motrice du feu et sur les machines propres à développer cette puissance," in *Annales scientifiques de l'École Normale Supérieure*, vol. 1, pp. 393–457, Société mathématique de France, 1872.

[309] G. N. Hatsopoulos and J. H. Keenan, *Principles of general thermodynamics*. New York: Wiley, 1965.

[310] R. F. Simmons Jr. and J. L. Park, "The essential nonlinearity of n-level quantum thermodynamics," *Foundations of Physics*, vol. 11, no. 3/4, pp. 297–305, 1981.

[311] Z. Daróczy, "Generalized information functions," *Information and control*, vol. 16, no. 1, pp. 36–51, 1970.

[312] R. V. Hartley, "Transmission of information," *Bell System Technical Journal*, vol. 7, no. 3, pp. 535–563, 1928.

[313] A. Rényi, *Wahrscheinlichkeitsrechnung*. Berlin: VEB Deutcher Verlag der Wissenschaften, 1966.

[314] J. von Newmann *Z. Phys.*, vol. 57, no. 30, 1929.

[315] S. Gheorghiu-Svirschevski, "Nonlinear quantum evolution with maximal entropy production," *Physical Review A*, vol. 63, p. 022105, 2001.

[316] S. Gheorghiu-Svirschevski, "Addendum to: Nonlinear quantum evolution with maximal entropy production," *Physical Review A*, vol. 63, p. 054102, 2001.

[317] A. Caticha, "Change, time and information geometry," in *Bayesian Methods and Maximum Entropy in Science and Engineering, AIP Conf. Proc.* (A. Mohammad-Djafari, ed.), vol. 568. Available online: arXiv.org/abs/mathph/0008018.

[318] M. Lemanska and Z. Jaeger, "A nonlinear model for relaxation in excited closed physical systems," *Physica D*, vol. 170, pp. 72–86, 2002.

[319] G. P. Beretta, "Mechanics and thermodynamics fundamentally united by density operators with an ontic status obeying a locally maximum entropy production dynamics. But at what price?," in *PIAF '09 New Perspectives on Quantum State*, Perimeter Institute, 2009.

[320] G. P. Beretta, "Time-energy and time-entropy uncertainty relations in dissipative quantum dynamics," *arxiv.org*, pp. 1–16, 2006. Available from: arXiv:quant-ph/0511091v3.

[321] C. L. Tien and J. H. Lienhard, *Statistical thermodynamics/Revised printing*. Washington, D.C.: Hemisphere Publishing Corp., 1979.

[322] G. P. Beretta and M. R. von Spakovsky, "Steepest-entropy-ascent quantum thermodynamic framework for describing the non-equilibrium behavior of a chemically reactive system at an atomistic level," To be published.

[323] G. P. Beretta, "Effect of irreversible atomic relaxation on resonance fluorescence, absorption, and stimulated emission," *International journal of theoretical physics*, vol. 24, no. 12, pp. 1233–1258, 1985.

[324] H. Kimble and L. Mandel, "Resonance fluorescence with excitation of finite bandwidth," *Physical Review A*, vol. 15, no. 2, p. 689, 1977.

[325] C. Cohen-Tannoudji and S. Reynaud, "Dressed-atom description of resonance fluorescence and absorption spectra of a multi-level atom in an intense laser beam," *Journal of Physics B: Atomic and Molecular Physics*, vol. 10, no. 3, p. 345, 1977.

[326] B. R. Mollow, "Power spectrum of light scattered by two-level systems," *Physical Review*, vol. 188, pp. 1969–1975, 1969.

[327] B. R. Mollow, "Stimulated emission and absorption near resonance for driven systems," *Physical Review A*, vol. 5, pp. 2217–2222, 1972.

[328] B. R. Mollow, "Elastic and inelastic collisional and radiative damping effects on saturated line shapes in the limit of well-separated spectral lines," *Physical Review A*, vol. 15, pp. 1023–1028, 1977.

[329] B. R. Mollow, *Progress in Optics*, vol. XIX. N.Y.: North-Holland, 1981.

[330] J. R. Ackerhalt and J. H. Eberly, "Quantum electrodynamics and radiation reaction: Nonrelativistic atomic frequency shifts and lifetimes," *Phys. Rev. D*, vol. 10, pp. 3350–3375, 1974.

[331] J. R. Ackerhalt, P. L. Knight, and J. H. Eberly, "Radiation reaction and radiative frequency shifts," *Phys. Rev. Lett.*, vol. 30, pp. 456–460, Mar 1973.

[332] H. J. Kimble and L. Mandel, "Theory of resonance fluorescence," *Physical Review A*, vol. 13, pp. 2123–2144, 1976.

[333] M. von Spakovsky, L. Winfrey, C. Smith, K. Yerkes, J. Scofield, G. Levine, G. Panasyuk, and K. Walczak, "White paper: Non-equilibrium thermodynamics at atomistic scales and the phenomenon of "spontaneous decoherence": Theory and experiment." ME Department, Virginia Tech, Blacksburg, VA, 2012.

[334] M. Nagel and F. Haworth, "Advanced laboratory experiments on optical pumping of rubidium atoms-part II: Free precession," *American Journal of Physics*, vol. 34, p. 559, 1966. http://dx.doi.org/10.1119/1.1973112.

[335] S. G. Kukolich, "Time dependence of quantum-state amplitudes demonstrated by free precession of spins," *American Journal of Physics*, vol. 36, pp. 420–425, 1968. http://dx.doi.org/10.1119/1.1974553.

[336] Q. A. Turchette, C. J. Myatt, B. E. King, C. A. Sackett, D. Kielpinski, W. M. Itano, C. Monroe, and D. J. Wineland, "Decoherence and decay of motional quantum states of a trapped atom coupled to engineered reservoirs," *Phys. Rev. A*, vol. 62, p. 053807, 2000.

[337] C. H. Bennett and D. P. DiVincenzo, "Quantum information and computation," *Nature*, vol. 404, no. 6775, pp. 247–255, 2000.

[338] B. Lanyon, M. Barbieri, M. Almeida, and A. White, "Experimental quantum computing without entanglement," *Physical Review Letters*, vol. 101, no. 20, p. 200501, 2008.

[339] X. Zhou, I. Dotsenko, B. Peaudecerf, T. Rybarczyk, C. Sayrin, S. Gleyzes, J. Raimond, M. Brune, and S. Haroche, "Field locked to a fock state by quantum feedback with single photon corrections," *Physical Review Letters*, vol. 108, no. 24, p. 243602, 2012.

[340] A. Ardavan, O. Rival, J. J. Morton, S. J. Blundell, A. M. Tyryshkin, G. A. Timco, and R. E. Winpenny, "Will spin-relaxation times in molecular magnets permit quantum information processing?," *Physical review letters*, vol. 98, no. 5, p. 057201, 2007.

[341] W. Tittel, H. Zbinden, and N. Gisin, "Experimental demonstration of quantum secret sharing," *Physical Review A*, vol. 63, no. 4, p. 042301, 2001.

[342] D. Naik, C. Peterson, A. White, A. Berglund, and P. Kwiat, "Entangled state quantum cryptography: Eavesdropping on the Ekert protocol," *Physical Review Letters*, vol. 84, no. 20, p. 4733, 2000.

[343] W. H. Zurek, "Decoherence, einselection, and the quantum origins of the classical," *Reviews of Modern Physics*, vol. 75, no. 3, p. 715, 2003.

[344] W. H. Zurek, "Decoherence and the transition from quantum to classical-revisited," *Los Alamos Science*, vol. 27, pp. 86–109, 2002.

[345] M. A. Nielsen and I. L. Chuang, *Quantum computation and quantum information*. Cambridge, U.K.: Cambridge university press, 2010.

[346] V. Buzek, H. Moya-Cessa, P. Knight, and S. Phoenix, "Schrödinger-cat states in the resonant Jaynes–Cummings model: Collapse and revival of oscillations of the photon-number distribution," *Physical review A*, vol. 45, no. 11, pp. 8190–8203, 1992.

[347] V. Buzek, "Jaynes–Cummings model with intensity-dependent coupling interacting with Holstein–Primakoff SU (1,1) coherent state," *Physical review A*, vol. 39, no. 6, pp. 3196–3199, 1989.

[348] J. Eberly, N. B. Narozhny, and J. Sanchez-Mondragon, "Periodic spontaneous collapse and revival in a simple quantum model," *Physical Review Letters*, vol. 44, no. 20, pp. 1323–1326, 1980.

[349] D. F. Walls, "Higher order effects in the master equation for coupled systems," *Zeitschrift für Physik*, vol. 234, no. 3, pp. 231–241, 1970.

[350] H. Carmichael and D. Walls, "Master equation for strongly interacting systems," *Journal of Physics A: Mathematical, Nuclear and General*, vol. 6, no. 10, p. 1552, 1973.

[351] J. Sanchez-Mondragon, N. B. Narozhny, and J. Eberly, "Theory of spontaneous-emission line shape in an ideal cavity," *Physical Review Letters*, vol. 51, no. 7, pp. 550–553, 1983.

[352] S. Phoenix and P. Knight, "Establishment of an entangled atom-field state in the jaynes-cummings model," *Physical Review A*, vol. 44, no. 9, pp. 6023–6029, 1991.

[353] D. Walls and G. Milburn, "Effect of dissipation on quantum coherence," *Physical review A*, vol. 31, no. 4, pp. 2403–2408, 1985.

[354] P. Goetsch, R. Graham, and F. Haake, "Schrödinger cat states and single runs for the damped harmonic oscillator," *Physical Review A*, vol. 51, pp. 136–142, 1995.

[355] A. Einstein, B. Podolsky, and N. Rosen, "Can quantum-mechanical description of physical reality be considered complete?," *Physical review*, vol. 47, no. 10, pp. 777–780, 1935.

[356] E. Schrödinger, "Die gegenwärtige situation in der quantenmechanik," *Naturwissenschaften*, vol. 23, no. 49, pp. 823–828, 1935. In German.

[357] S. Haroche, "Nobel lecture: Controlling photons in a box and exploring the quantum to classical boundary," *Reviews of Modern Physics*, vol. 85, no. 3, pp. 1083–1102, 2013.

[358] J.-M. Raimond and S. Haroche, "Monitoring the decoherence of mesoscopic quantum superpositions in a cavity," in *Quantum Decoherence*, pp. 33–83, Springer, 2007.

[359] S. Haroche and J.-M. Raimond, *Exploring the Quantum*. Oxford, UK: Oxford University Press, 2006.

[360] M. Brune, F. Schmidt-Kaler, A. Maali, J. Dreyer, E. Hagley, J. Raimond, and S. Haroche, "Quantum rabi oscillation: A direct test of field quantization in a cavity," *Physical Review Letters*, vol. 76, no. 11, p. 1800, 1996.

[361] D. Wineland, "Nobel lecture: Superposition, entanglement, and raising schrödingerâs cat," *Reviews of Modern Physics*, vol. 85, pp. 1103–1114, 2013.

[362] U. Warring, C. Ospelkaus, Y. Colombe, R. Jördens, D. Leibfried, and D. Wineland, "Individual-ion addressing with microwave field gradients," *Physical review Letters*, vol. 110, no. 17, p. 173002(5), 2013.

[363] D. Leibfried, B. DeMarco, V. Meyer, D. Lucas, M. Barrett, J. Britton, W. Itano, B. Jelenkovic, C. Langer, T. Rosenband, and D. Wineland, "Experimental demonstration of a

robust, high-fidelity geometric two ion-qubit phase gate," *Nature*, vol. 422, pp. 412–415, 2003.

[364] D. Leibfried, R. Blatt, C. Monroe, and D. Wineland, "Quantum dynamics of single trapped ions," *Reviews of Modern Physics*, vol. 75, no. 1, pp. 281–324, 2003.

[365] C. Myatt, B. E. King, Q. A. Turchette, C. A. Sackett, D. Kielpinski, W. M. Itano, C. Monroe, and D. J. Wineland, "Decoherence of quantum superpositions through coupling to engineered reservoirs," *Nature*, vol. 403, no. 20, pp. 269–273, 2000.

[366] C. Sackett, D. Kielpinski, B. King, C. Langer, V. Meyer, C. Myatt, M. Rowe, Q. A. Turchette, W. Itano, D. Wineland, and C. Monroe, "Experimental entanglement of four particles," *Nature*, vol. 404, pp. 256–259, 2000.

[367] Q. A. Turchette, C. S. Wood, B. E. King, C. J. Myatt, D. Leibfried, W. M. Itano, C. Monroe, and D. J. Wineland, "Deterministic entanglement of two trapped ions," *Physical Review Letters*, vol. 81, no. 17, pp. 3631–3634, 1998.

[368] D. Meekhof, C. Monroe, B. King, W. Itano, and D. Winelan, "Generation of nonclassical motional states of a trapped atom," *Physical Review Letters*, vol. 76, no. 11, pp. 1796–1799, 1996.

[369] C. Monroe, D. Meekhof, B. King, and D. Wineland, "A schrödinger cat superposition state of an atom," *Science*, vol. 272, pp. 1131–1136, 1996.

[370] C. Monroe, D. Meekhof, B. King, W. Itano, and D. Winelan, "Demonstration of a fundamental quantum logic gate," *Physical Review Letters*, vol. 75, no. 25, pp. 4714–4717, 1995.

[371] L. Davidovich, M. Brune, J. M. Raimond, and S. Haroche, "Mesoscopic quantum coherences in cavity QED: Preparation and decoherence monitoring schemes," *Physical Review A*, vol. 53, pp. 1295–1309, 1996.

[372] X.-Z. Yuan, H.-S. Goan, and K.-D. Zhu, "Non-markovian reduced dynamics and entanglement evolution of two coupled spins in a quantum spin environment," *Physical Review B*, vol. 75, no. 4, p. 045331, 2007.

[373] R. Shankar, *Principles of quantum mechanics*. New York, N.Y.: Plenum Press, 2nd ed., 1994.

[374] R. J. Glauber, "Coherent and incoherent states of the radiation field," *Physical Review Letters*, vol. 10, no. 84, pp. 2766–2788, 1963.

[375] E. Weisstein, "Sphere point picking." Available: MathWorld - A Wolfram Web Resource, 2013. http://mathworld.wolfram.com/SpherePointPicking.html.

[376] J. Fink, M. Göppl, M. Baur, R. Bianchetti, P. Leek, A. Blais, and A. Wallraff, "Climbing the Jaynes-Cummings ladder and observing its nonlinearity in a cavity QED system," *Nature*, vol. 454, no. 7202, pp. 315–318, 2008.

[377] K. Fujii and T. Suzuki, "An approximate solution of the Jaynes-Cummings model with dissipation II: Another approach," *International Journal of Geometric Methods in Modern Physics*, vol. 9, no. 4, 2012.

[378] M. A. Marchiolli, "Quantitative aspects of entanglement in the driven Jaynes-Cummings model," *Journal of Modern Optics*, vol. 53, no. 18, pp. 2733–2751, 2006.

[379] E. T. Jaynes and F. W. Cummings, "Comparison of quantum and semiclassical radiation theories with application to the beam maser," *Proceedings of the IEEE*, vol. 51, no. 1, pp. 89–109, 1963.

[380] F. Cummings, "Stimulated emission of radiation in a single mode," *Physical Review*, vol. 140, no. 4A, p. A1051, 1965.

[381] E. Jaynes, "Some aspects of maser theory," *Microwave Laboratory, Stanford University, Stanford, CA, Report*, no. 502, 1958.

[382] G. N. Hatsopoulos and E. P. Gyftopoulos, *Thermionic Energy Conversion Vol II: Theory, technology and application*. Cambridge, Massachusetts: The MIT press, 1979.

[383] G. P. Beretta, "Entropy and irreversibility for a single isolated two level system: New individual quantum states and new nonlinear equation of motion," *International journal of theoretical physics*, vol. 24, no. 2, pp. 119–134, 1985.

[384] MathWorks, "R2013b documentation: ode45." Available from: http://www.mathworks.com/help/matlab/ref/ode45.html?searchHighlight=ode45, 2013. Access date: [10-22-2013].

[385] E. Fehlberg, "Low-order classical runge-kuttaformulas with step size control and their application to some heat transfer problems." NASA Technical Report 315, 1969.

[386] E. Fehlberg Computing (Arch. Elektron. Rechnen) 661â71, 1970.

[387] G. Hairer, S. Norsett, and W. E., *Solving ordinary differential equations I: Nonstiff Problems*. Berlin: Springer, 1993.

[388] G. Levin, W. Jones, K. Walczak, and K. Yerkes, "Energy transport in closed quantum systems," *Physical Review E*, vol. 85, no. 3, p. 031109, 2012.

[389] N. Khaneja, B. Luy, and S. J. Glaser, "Boundary of quantum evolution under decoherence," *Proceedings of the National Academy of Sciences*, vol. 100, no. 23, pp. 13162–13166, 2003.

Appendix A

Configuration synthesis/design decision variable values for COMPETES, *Scenario 1.*

MAIN GRID:

Technology (Fuel Type)	CONFIG. 1 (MWh)	CONFIG. 2 (MWh)	CONFIG. 3 (MWh)	CONFIG. 4 (MWh)	CONFIG. 5 (MWh)	CONFIG. 6 (MWh)	CONFIG. 7 (MWh)	CONFIG. 8 (MWh)
Hydroelectric	0.18	0.18	0.18	0.18	0.18	0.18	0.18	0.17
Coal	343.86	340.25	329.84	283.44	329.09	259.30	330.72	293.65
Natural gas	718.94	718.94	718.94	718.94	718.94	718.94	718.94	718.94
Oil	51.16	39.80	0.73	0.02	4.86	20.20	82.66	76.63
Nuclear	2918.82	2918.82	2918.82	2918.82	2918.82	2918.82	2918.82	2918.82
Coal	1119.28	1119.26	1119.28	1119.28	1119.10	1093.01	1112.85	1113.38
Oil	2609.19	2608.29	2598.49	2609.28	2609.34	2607.89	2609.41	2609.41
Natural gas	0.37	141.44	173.60	173.60	173.60	173.60	173.53	173.60
Oil	0.20	24.28	0.15	0.05	40.06	81.40	121.18	121.23
Waste	472.32	472.32	472.32	471.66	472.32	304.15	12.00	311.68
Waste	20.58	0.97	0.81	0.00	0.02	1.37	1.91	1.51
Natural gas	235.17	462.34	656.48	656.48	656.48	656.48	656.29	656.48
Natural gas	0.00	1.86	22.63	75.75	4.52	100.67	126.29	116.08
Waste	8.52	10.11	8.64	0.42	10.86	9.57	4.04	9.97
Waste	15.21	33.66	29.94	4.11	36.35	23.73	17.31	33.25
Nuclear	3510.04	3510.04	3510.04	3510.04	3510.04	3510.04	3510.04	3509.99
Coal	840.23	281.54	0.19	0.00	0.07	4.07	7.12	22.25
Natural gas	0.00	11.76	154.91	173.38	154.84	163.13	173.31	173.37
Oil	0.00	0.14	0.00	0.00	0.15	0.97	9.45	7.62
Oil	0.00	3.81	0.00	0.00	0.00	0.14	20.03	29.62
Nuclear	431.92	431.92	431.92	431.92	431.92	431.92	431.92	431.92
Coal	590.00	590.00	590.00	590.00	590.00	577.28	564.12	549.49
Natural gas	1009.56	1067.63	855.63	953.33	923.96	1051.27	1545.45	1513.31
Oil	0.06	0.34	0.91	0.00	1.30	0.88	0.65	0.13
Waste	102.41	102.41	102.41	102.41	102.41	102.40	95.05	62.16
Coal	1169.02	1169.02	1169.02	1169.02	1169.02	1150.57	1135.28	1110.84
Natural gas	519.55	519.55	519.55	519.55	519.55	519.55	519.55	519.55
Waste	21.66	21.66	21.66	21.66	21.66	21.10	10.48	14.70
Waste	20.68	20.68	20.68	20.68	20.68	20.36	9.82	13.39
Natural gas	84.88	84.88	84.88	84.88	84.88	84.88	84.88	84.88
Coal	1444.52	1444.52	1444.52	1444.52	1444.52	1443.75	1443.36	1420.52
Natural gas	309.88	309.88	309.88	309.88	309.88	309.88	309.88	309.88

Waste	166.41	166.41	166.41	166.41	166.41	166.37	161.77	73.94
Coal	766.08	766.08	766.08	766.08	766.08	745.68	710.45	660.76
Natural gas	2316.24	2316.24	2316.24	2316.24	2316.24	2316.24	2316.24	2316.24
Hydroelectric	24.40	24.40	24.40	24.40	24.40	24.40	24.38	22.96
Coal	314.58	314.01	314.58	314.58	273.14	285.79	295.21	127.15
Natural gas	67.71	217.26	222.12	225.80	168.85	225.79	225.78	225.80
Waste	87.78	87.78	87.78	87.78	87.78	87.78	86.90	77.13
Natural gas	1442.55	1445.29	1453.98	1453.98	1453.88	1453.91	1453.94	1453.98
Waste	51.19	51.19	51.19	51.19	50.72	24.10	48.96	13.77
Coal	144.70	11.00	0.65	0.00	0.22	0.12	9.70	2.80
Natural gas	1.07	17.13	7.27	0.56	1.57	60.27	1187.12	196.07
Coal	738.34	164.71	22.69	0.09	1.40	99.47	536.21	13.09
Natural gas	2605.12	3402.26	3624.11	3626.16	3624.63	3524.35	1365.76	3110.85
Nuclear	7749.46	7749.46	7749.46	7749.46	7749.46	7749.46	7749.46	7711.66
Coal	20666.85	20525.54	16949.74	17322.23	17472.97	17578.61	18118.79	17535.66
Natural gas	0.00	0.17	2042.74	817.03	3156.49	4543.85	7110.32	8655.71
Oil	0.00	0.00	0.00	0.00	0.04	0.03	1.76	28.89
Oil	0.01	0.01	0.00	0.00	4.00	1.21	6.66	373.81
Nuclear	7988.20	7988.20	7988.20	7988.20	7988.20	7988.20	7988.20	7970.70
Coal	703.91	515.55	19.83	0.44	19.95	2.06	6.13	18.35
Natural gas	0.00	1.00	2504.47	1211.15	3834.66	5316.73	6544.39	6550.19
Oil	0.00	0.00	0.00	0.02	0.15	0.38	0.91	8.45
Oil	0.00	0.00	0.00	0.00	0.45	0.52	2.79	164.77
Hydroelectric	59.81	59.81	59.81	59.81	59.81	59.81	59.73	39.87
Nuclear	3159.28	3159.28	3159.28	3159.28	3159.28	3159.28	3159.28	3140.10
Coal	3673.54	3589.06	1222.70	1114.98	1245.34	815.04	1405.15	1032.42
Natural gas	0.00	0.30	3.68	852.91	513.03	808.77	850.12	845.53
Oil	0.00	0.00	0.00	0.00	0.00	0.11	0.85	4.85
Oil	0.00	0.00	0.00	0.00	3.72	0.70	1.51	145.26
Nuclear	5018.29	5018.29	5018.29	5018.29	5018.29	5018.29	5018.29	4996.64
Coal	13365.97	13364.09	13365.08	13366.03	13009.28	11949.07	12172.51	10576.31
Natural gas	0.00	79.13	3454.26	3889.53	3867.07	3826.21	1805.38	3848.29
Oil	0.00	0.25	0.00	0.01	0.00	0.00	0.29	1.66
Oil	0.00	0.00	0.00	0.00	1.90	0.32	0.48	45.60
Nuclear	2106.97	2106.97	2106.97	2106.97	2106.97	2106.97	2106.97	2087.65
Coal	6989.94	6991.21	6428.89	5862.97	5768.42	4111.58	4413.60	3764.61
Natural gas	0.00	18.99	41.13	798.72	776.23	790.07	796.38	788.96
Oil	0.00	0.00	0.00	0.00	0.00	0.29	1.58	8.58
Oil	0.00	0.61	0.00	0.00	0.56	0.13	2.25	96.71
Hydroelectric	4588.78	4588.78	4588.78	4588.78	4588.78	4588.73	4577.90	4108.28
Coal	2062.45	1712.08	0.11	1.14	1.48	115.52	456.37	284.90
Natural gas	7.03	811.82	2687.64	2720.23	2666.04	2476.53	1040.03	2357.91
Oil	0.12	1.15	0.11	21.53	2.56	78.42	312.74	7.76
Oil	0.00	0.00	29.24	0.08	2.94	1.52	0.48	92.18

Nuclear	68700.53	68700.53	68700.53	68700.53	68700.53	68700.53	68697.97	68581.31
Coal	651.22	285.04	0.00	0.00	0.00	0.12	11.78	13.91
Oil	0.64	0.28	4.51	0.00	2.89	47.43	23.51	395.66
Oil	0.68	4.68	0.04	0.00	0.55	15.57	507.21	45.43
Oil	0.01	0.02	0.40	0.00	0.74	6.70	395.34	166.40
Hydroelectric	49.00	43.22	49.00	49.00	47.03	48.69	49.00	48.98
LONN - AVEL	1159.39	1162.23	1159.43	1159.66	1160.10	1162.91	1163.99	1165.40
D - DIEL	257.53	170.97	232.65	177.08	340.34	401.63	423.98	465.96
D - EICH	764.12	686.85	792.57	725.25	952.17	1015.07	972.32	996.57
D - ROMM	429.30	350.54	429.25	370.22	552.04	621.49	563.84	612.42
D - UCHT	719.98	646.29	743.62	679.44	894.34	960.09	914.66	941.65
DIEL - ROMM	113.89	119.06	130.34	128.06	140.37	145.79	92.77	97.16
DIEL - ZWOL	107.55	35.47	72.64	31.68	136.44	166.61	231.09	245.24
UCHT - EICH	49.04	45.05	54.40	50.90	64.24	61.04	64.01	60.93
F - AVEL	999.28	1023.13	999.87	1004.73	990.93	1006.32	977.53	983.25
F - LONN	437.82	460.30	439.53	443.10	429.10	448.79	443.66	439.51
F - MOUL	16.54	37.82	16.28	21.36	3.24	20.08	14.91	13.61
MUHL - F	183.03	163.48	185.45	178.67	199.44	186.72	191.25	189.42
GRAM - LONN	860.59	791.58	821.71	828.60	843.40	773.48	798.04	868.90
GRAM - MOUL	125.07	104.78	113.25	115.69	118.75	97.70	104.64	125.94
KRIM - MERC	770.69	789.34	747.56	786.71	766.03	851.57	873.09	741.79
MOUL - LONN	712.75	714.80	716.10	713.53	720.53	725.38	726.44	724.94
MAAS - GRAM	164.28	270.37	252.50	249.02	254.35	306.82	349.71	209.47
MAAS - KRIM	112.09	104.75	178.51	144.95	132.97	142.75	-5.82	59.05
MAAS - MERC	485.19	492.13	503.92	509.84	492.54	545.10	486.30	443.66
MERC - AVEL	757.30	774.57	771.56	768.13	803.48	729.23	846.38	846.39
GRAM - MERC	731.70	602.60	649.78	666.07	624.94	657.59	485.36	589.45
MUHL - MOUL	239.49	241.58	242.08	240.05	243.23	248.21	247.46	243.72
EICH - MUHL	467.17	447.92	474.41	462.21	491.62	483.89	489.20	483.69
ROMM - MAAS	121.95	74.76	109.58	80.04	144.67	176.46	100.04	142.83
ROMM - UCHT	310.65	316.09	335.98	330.46	365.83	361.90	374.97	351.93
UCHT - MOUL	650.58	638.55	666.45	652.22	691.91	690.68	696.75	683.60
ZWOL - KRIM	401.67	392.33	496.92	452.47	484.26	520.26	189.31	286.95
ZWOL - MAAS	200.31	198.42	224.63	214.77	242.77	260.89	128.58	155.41

Appendix B

Configuration synthesis/design decision variable values for COMPETES, *Scenario 2.*

MAIN GRID:

Technology (Fuel Type)	CONFIG. 1 (MWh)	CONFIG. 2 (MWh)	CONFIG. 3 (MWh)	CONFIG. 4 (MWh)	CONFIG. 5 (MWh)	CONFIG. 6 (MWh)	CONFIG. 7 (MWh)	CONFIG. 8 (MWh)
Hydroelectric	0.18	0.18	0.18	0.18	0.18	0.18	0.18	0.18
Coal	342.45	340.77	212.94	49.98	247.96	257.77	190.41	190.41
Natural gas	650.33	709.90	717.42	717.18	710.19	709.85	712.23	712.23
Oil	1.34	1.37	6.50	16.93	24.06	21.74	37.74	37.74
Nuclear	2918.82	2918.82	2918.82	2918.82	2918.82	2918.82	2918.82	2918.82
Coal	1119.28	1119.28	1074.61	984.35	1049.35	1068.02	964.13	964.13
Oil	2259.85	2345.40	2287.95	2434.78	2419.81	2412.31	2464.03	2464.03
Natural gas	0.04	5.41	151.64	148.30	47.75	42.77	77.10	77.10
Oil	2.13	2.18	25.47	88.53	35.42	32.03	55.44	55.44
Waste	472.32	472.32	260.37	135.48	467.31	472.32	431.50	431.50
Waste	6.35	1.74	0.29	0.34	1.68	1.75	1.29	1.29
Natural gas	28.21	39.06	536.13	539.29	171.36	152.30	301.78	301.78
Natural gas	0.08	3.51	69.01	103.83	34.80	31.18	56.15	56.15
Waste	8.00	10.86	2.72	3.15	10.86	10.86	10.75	10.75
Waste	26.84	36.43	9.13	10.57	36.43	36.42	36.07	36.07
Nuclear	3508.11	3510.04	3510.04	3509.95	3510.04	3510.04	3510.04	3510.04
Coal	568.17	498.36	334.65	182.02	378.90	397.84	310.64	310.64
Natural gas	0.18	4.87	148.72	143.03	47.82	42.86	77.11	77.11
Oil	0.11	0.11	0.80	2.53	5.60	5.15	9.17	9.17
Oil	0.00	0.00	1.51	4.13	9.78	9.70	17.49	17.49
Nuclear	431.92	431.92	431.92	431.92	431.92	431.92	431.92	431.92
Coal	590.00	590.00	571.62	550.28	577.77	574.89	552.43	552.43
Natural gas	0.14	0.14	9.46	194.92	217.76	212.94	657.67	657.67
Oil	4.64	4.75	1.07	1.66	8.41	8.56	9.97	9.97
Waste	102.41	102.41	102.41	101.52	102.41	102.41	91.64	91.64
Coal	1169.02	1169.02	1130.85	1100.26	1132.66	1134.78	1101.15	1101.15
Natural gas	216.01	267.61	468.47	478.76	324.39	316.42	378.19	378.19
Waste	21.66	21.66	21.66	18.74	21.66	21.66	17.86	17.86
Waste	20.68	20.68	20.68	18.14	20.68	20.68	17.59	17.59
Natural gas	72.66	84.88	84.88	84.88	84.88	84.88	84.88	84.88
Coal	1444.52	1444.52	1404.86	1380.14	1401.50	1405.94	1374.88	1374.88
Natural gas	265.64	304.41	309.13	309.01	305.55	305.38	306.56	306.56
Waste	166.41	166.41	166.41	165.69	166.41	166.41	158.10	158.10

Coal	766.08	766.08	726.05	686.17	724.19	729.18	687.87	687.87
Natural gas	2315.95	2315.98	2316.20	2316.19	2315.99	2315.98	2316.05	2316.05
Hydroelectric	24.40	24.40	24.40	24.40	24.40	24.40	23.51	23.51
Coal	314.58	314.58	288.66	142.20	228.13	237.15	180.23	180.23
Natural gas	131.88	179.53	218.87	219.00	192.32	190.99	200.13	200.13
Waste	87.78	87.78	87.78	81.79	87.78	87.78	57.19	57.19
Natural gas	774.83	856.76	918.35	1092.23	1020.56	1003.41	1121.65	1121.65
Waste	51.18	51.18	46.35	21.89	37.11	38.58	28.46	28.46
Coal	38.75	0.05	0.01	0.02	0.04	0.05	0.03	0.03
Natural gas	0.00	0.00	0.00	6.20	6.70	14.09	220.39	220.39
Coal	464.44	394.74	332.69	244.26	302.46	328.86	344.50	344.50
Natural gas	2666.22	2769.65	2855.59	2989.81	2919.94	2889.26	2917.93	2917.93
Nuclear	7749.46	7749.46	7749.46	7749.46	7749.46	7749.46	7749.46	7749.46
Coal	15898.23	15931.35	15820.17	15714.70	15867.66	15873.42	15845.32	15845.32
Natural gas	0.00	0.00	334.05	1221.11	693.01	700.52	1982.73	1982.73
Oil	0.00	0.00	25.30	84.73	195.23	175.13	315.85	315.85
Oil	0.00	0.00	29.84	130.52	217.57	194.86	351.44	351.44
Nuclear	7988.20	7988.20	7988.20	7988.20	7988.20	7988.20	7988.20	7988.20
Coal	645.48	673.54	563.65	452.89	609.72	617.16	599.09	599.09
Natural gas	0.05	0.05	412.73	1386.74	809.49	751.49	2211.35	2211.35
Oil	0.00	0.00	19.42	28.78	82.67	75.03	135.32	135.32
Oil	0.00	0.00	14.17	30.76	64.78	58.02	104.65	104.65
Hydroelectric	59.81	59.81	59.81	59.81	59.81	59.81	59.81	59.81
Nuclear	3159.28	3159.28	3159.28	3159.28	3159.28	3159.28	3159.28	3159.28
Coal	322.66	349.66	283.02	206.72	323.07	326.57	299.77	299.77
Natural gas	0.00	0.00	451.86	719.31	234.43	209.96	378.71	378.71
Oil	0.00	0.00	10.45	13.63	48.72	46.51	83.89	83.89
Oil	0.00	0.00	15.75	44.38	56.89	50.97	91.79	91.79
Nuclear	5018.29	5018.29	5018.29	5018.29	5018.29	5018.29	5018.29	5018.29
Coal	13038.05	13041.85	13008.86	12995.67	12988.31	12986.39	13003.25	13003.25
Natural gas	2.32	2.51	611.13	1416.46	601.23	488.23	1430.22	1430.22
Oil	0.00	0.00	3.89	5.52	22.16	19.85	35.78	35.78
Oil	0.00	0.00	4.22	9.17	18.96	16.98	30.62	30.62
Nuclear	2106.97	2106.97	2106.97	2106.97	2106.97	2106.97	2106.97	2106.97
Coal	6993.67	6993.26	6980.96	6825.89	6991.20	6993.66	6968.72	6968.72
Natural gas	0.00	0.00	586.16	679.68	218.32	195.20	354.64	354.64
Oil	0.00	0.00	13.32	35.18	99.91	92.11	166.15	166.15
Oil	0.00	0.00	8.95	19.88	38.70	34.67	62.40	62.40
Hydroelectric	3525.55	3355.07	3349.57	3304.05	3344.67	3339.52	3324.04	3324.04
Coal	55.10	69.30	9.81	10.61	52.77	54.86	44.15	44.15
Natural gas	0.00	0.00	0.00	25.92	16.72	36.67	815.11	815.11
Oil	0.00	0.00	0.00	37.51	103.66	118.23	245.23	245.23
Oil	0.00	0.00	5.09	12.27	33.66	38.03	68.59	68.59
Nuclear	68627.56	68673.38	68696.99	68687.59	68680.26	68679.46	68684.99	68684.99

Coal	1428.54	1470.73	1311.64	1079.43	1404.38	1412.15	1374.52	1374.52
Oil	0.00	0.00	1.01	219.84	47.01	74.58	392.62	392.62
Oil	0.00	0.00	1.67	63.84	63.44	93.01	184.98	184.98
Oil	0.00	0.00	43.01	28.14	92.56	100.23	177.51	177.51
Hydroelectric	16.38	5.03	33.52	40.11	6.17	4.70	9.08	9.08
LONN - AVEL	1201.71	1205.03	1198.42	1193.64	1203.50	1203.97	1204.06	1204.06
D - DIEL	273.35	267.36	259.57	245.98	258.93	263.07	258.98	258.98
D - EICH	450.60	458.01	464.51	460.22	455.21	457.04	454.44	454.44
D - ROMM	342.36	332.38	328.88	319.23	326.57	329.36	326.41	326.41
D - UCHT	464.96	469.10	472.07	466.41	465.47	467.58	465.00	465.00
DIEL - ROMM	45.76	43.11	45.97	48.60	44.85	43.96	44.71	44.71
DIEL - ZWOL	179.28	180.71	173.74	160.08	174.33	178.05	175.22	175.22
EICH - UCHT	15.98	12.33	8.43	6.94	11.40	11.73	11.79	11.79
F - AVEL	1189.49	1192.81	1167.57	1149.92	1188.56	1190.21	1191.37	1191.37
F - LONN	609.39	609.30	587.93	582.19	605.79	607.22	608.61	608.61
F - MOUL	178.69	176.13	160.41	156.85	174.09	174.91	176.35	176.35
MUHL - F	25.73	28.92	40.97	42.87	29.74	29.41	27.75	27.75
GRAM - LONN	796.73	805.91	818.44	817.79	807.12	806.54	805.74	805.74
GRAM - MOUL	103.86	105.79	111.06	111.51	106.57	106.33	106.00	106.00
KRIM - MERC	411.32	415.70	426.77	422.61	421.96	418.22	424.70	424.70
MOUL - LONN	728.71	732.87	723.34	719.71	730.39	731.40	731.33	731.33
GRAM - MAAS	88.37	57.22	62.91	55.42	56.42	56.97	55.63	55.63
MAAS - KRIM	50.09	51.27	49.97	55.25	50.56	50.87	50.92	50.92
MAAS - MERC	254.30	257.32	262.89	263.06	260.49	258.54	262.20	262.20
MERC - AVEL	785.41	814.85	811.97	815.00	812.33	813.77	810.10	810.10
GRAM - MERC	619.00	582.28	600.91	591.20	587.43	584.35	589.80	589.80
MUHL - MOUL	245.33	246.08	241.69	239.73	244.62	245.21	244.93	244.93
EICH - MUHL	301.44	306.23	315.08	314.44	306.52	306.66	305.63	305.63
ROMM - MAAS	185.93	160.35	153.44	145.66	157.88	159.29	158.83	158.83
ROMM - UCHT	131.05	146.12	153.05	157.34	148.45	147.73	148.12	148.12
UCHT - MOUL	478.97	488.21	491.91	491.04	487.65	488.07	487.09	487.09
ZWOL - KRIM	232.65	205.75	207.24	215.80	209.01	207.24	209.06	209.06
ZWOL - MAAS	124.67	106.19	107.94	110.56	108.75	107.41	108.88	108.88

MICROGRIDS:

Technology (Fuel Type)	Config. 1 (MWh)	Config. 2 (MWh)	Config. 3 (MWh)	Config. 4 (MWh)	Config. 5 (MWh)	Config. 6 (MWh)	Config. 7 (MWh)	Config. 8 (MWh)
SOFC	20.39	0.11	0.02	35.49	0.94	0.11	9.36	9.36
REs	10.73	8.36	16.50	15.97	6.62	5.90	6.54	6.54
MT	8.86	0.17	13.36	23.13	0.52	0.17	2.01	2.01
Wind	7.84	0.55	0.09	0.11	0.53	0.55	1.13	1.13
SOFC	9.16	0.04	0.01	3.85	0.09	0.04	3.40	3.40
REs	91.84	86.33	80.36	90.62	63.77	66.18	58.72	58.72
MT	6.45	0.02	0.00	7.43	0.02	0.02	0.62	0.62
PV	89.87	90.00	90.00	90.00	90.00	90.00	90.00	90.00
NGCC	222.00	222.00	222.00	222.00	222.00	222.00	222.00	222.00
Coal	180.00	180.00	179.70	180.00	174.77	175.12	180.00	180.00
SOFC	9.12	0.06	0.01	11.55	0.17	0.06	1.94	1.94
REs	8.89	7.60	9.85	10.08	5.59	5.68	5.48	5.48
MT	5.60	0.43	0.07	10.26	0.44	0.43	1.40	1.40
NGCC	74.00	74.00	74.00	74.00	74.00	74.00	74.00	74.00
Coal	59.69	59.63	59.30	58.18	47.67	48.56	51.40	51.40
IGCC	200.00	200.00	200.00	200.00	199.21	198.57	199.44	199.44
SOFC	8.54	0.38	0.06	0.17	0.47	0.38	6.50	6.50
REs	6.49	5.24	5.13	5.42	2.87	2.82	2.89	2.89
MT	6.33	1.04	0.03	3.36	0.23	0.20	1.57	1.57
Wind	9.64	4.34	0.73	0.84	4.19	4.36	3.42	3.42
SOFC	0.00	0.00	0.00	0.00	0.00	0.00	0.14	0.14
REs	24.05	13.45	1.79	10.21	9.54	9.92	7.80	7.80
MT	3.10	0.08	0.01	0.11	0.08	0.08	0.37	0.37
PV	35.92	45.00	45.00	45.00	45.00	45.00	45.00	45.00
NGCC	111.00	111.00	111.00	111.00	111.00	111.00	111.00	111.00
Coal	81.50	78.61	69.30	73.06	60.07	62.21	53.30	53.30
SOFC	2.58	0.02	0.00	0.00	0.01	0.02	0.01	0.01
REs	6.37	4.37	0.53	2.43	3.02	3.14	2.44	2.44
MT	4.89	0.03	0.04	0.01	0.03	0.03	0.21	0.21
NGCC	74.00	74.00	74.00	73.99	74.00	74.00	74.00	74.00
Coal	44.03	39.54	30.56	37.25	28.77	29.80	28.19	28.19
IGCC	199.99	199.99	199.97	199.15	184.60	186.28	182.33	182.33
SOFC	17.64	0.07	0.01	1.39	0.07	0.07	1.94	1.94
REs	9.93	7.89	3.12	3.29	5.50	5.72	4.26	4.26
MT	7.78	0.17	0.19	1.79	0.17	0.17	0.31	0.31
Wind	6.56	0.26	0.04	0.05	0.25	0.26	0.19	0.19
SOFC	7.50	0.00	0.00	0.00	0.00	0.00	0.00	0.00
REs	56.10	44.09	13.63	7.94	31.75	33.00	25.23	25.23
MT	5.40	0.04	0.01	0.81	0.04	0.04	0.03	0.03
PV	74.92	75.00	75.00	75.00	75.00	75.00	75.00	75.00
NGCC	185.00	185.00	185.00	184.99	185.00	185.00	185.00	185.00

Coal	150.00	150.00	147.08	130.47	131.47	136.14	137.88	137.88
SOFC	16.62	0.40	0.07	0.08	0.38	0.40	2.44	2.44
REs	14.96	11.64	1.42	1.64	8.15	8.47	6.40	6.40
MT	10.57	0.21	0.04	0.04	0.20	0.21	0.16	0.16
NGCC	148.00	148.00	148.00	147.99	148.00	148.00	148.00	148.00
Coal	119.89	119.86	110.40	89.39	95.58	100.71	101.36	101.36
IGCC	400.00	400.00	400.00	399.65	400.00	400.00	400.00	400.00
SOFC	23.57	0.21	0.04	0.04	0.20	0.21	1.78	1.78
REs	13.84	10.48	2.36	3.93	7.52	7.82	5.82	5.82
MT	10.65	0.17	0.04	0.70	0.16	0.17	0.35	0.35
Wind	9.40	0.41	0.07	0.08	0.39	0.41	0.30	0.30
SOFC	2.34	0.76	0.13	0.15	0.73	0.76	0.60	0.60
REs	11.44	9.05	1.15	1.32	6.57	6.83	5.04	5.04
MT	1.50	0.44	0.07	0.09	0.43	0.44	0.33	0.33
PV	15.00	15.00	15.00	14.97	15.00	15.00	15.00	15.00
NGCC	37.00	37.00	37.00	35.10	32.31	33.12	28.35	28.35
Coal	27.09	25.87	15.72	3.85	18.88	19.62	14.47	14.47
SOFC	21.55	0.04	0.65	35.67	0.04	0.04	1.21	1.21
REs	6.81	0.67	2.13	1.73	0.57	0.59	0.48	0.48
MT	10.76	0.02	0.26	6.03	0.02	0.02	0.02	0.02
Wind	9.01	0.01	0.00	0.34	0.01	0.01	0.01	0.01
SOFC	6.02	0.02	0.49	0.00	0.02	0.02	0.02	0.02
REs	19.25	0.08	0.01	0.38	0.08	0.08	0.06	0.06
MT	4.02	0.00	0.00	0.00	0.00	0.00	0.00	0.00
PV	56.01	60.00	60.00	59.96	60.00	60.00	60.00	60.00
NGCC	148.00	148.00	148.00	147.31	142.44	143.69	144.54	144.54
Coal	78.59	63.29	40.60	9.31	46.08	47.90	37.67	37.67
SOFC	4.16	0.02	0.55	0.00	0.02	0.02	0.02	0.02
REs	1.68	0.00	0.00	0.00	0.00	0.00	0.00	0.00
MT	2.51	0.08	0.08	0.02	0.08	0.08	0.06	0.06
NGCC	37.00	37.00	37.00	33.36	28.33	29.35	22.63	22.63
Coal	7.95	0.14	0.02	0.71	0.14	0.14	0.11	0.11
IGCC	63.04	49.60	30.81	7.23	35.97	37.39	28.26	28.26
SOFC	0.01	0.02	0.01	0.01	0.01	0.02	0.01	0.01
REs	84.51	60.19	30.51	12.37	43.66	45.39	34.27	34.27
MT	13.16	3.24	0.50	0.59	2.86	2.98	2.20	2.20
Wind	0.10	0.10	0.02	0.02	0.09	0.10	0.17	0.17
SOFC	22.06	0.00	0.00	0.00	0.00	0.00	0.00	0.00
REs	223.17	54.52	14.97	8.01	39.83	41.41	30.75	30.75
MT	61.03	7.02	1.18	1.38	6.79	7.06	5.20	5.20
PV	771.81	966.47	973.79	973.59	968.05	967.77	969.67	969.67
NGCC	2391.69	2387.07	2402.00	2390.14	2389.84	2389.44	2393.62	2393.62
Coal	231.73	24.39	5.71	3.67	18.11	18.82	17.91	17.91
SOFC	0.00	0.00	0.00	0.00	0.00	0.00	6.65	6.65

REs	15.04	2.65	0.35	0.41	2.02	2.10	1.55	1.55
MT	0.15	0.15	0.03	0.03	0.15	0.15	0.11	0.11
NGCC	1291.75	1295.00	1295.00	1295.00	1295.00	1295.00	1295.00	1295.00
Coal	10.80	14.50	2.16	2.14	10.66	11.08	10.36	10.36
IGCC	3312.28	3295.23	3280.41	3258.20	3274.31	3278.01	3273.42	3273.42
SOFC	0.26	0.26	0.13	0.42	0.25	0.26	0.22	0.22
REs	15.66	0.74	3.20	3.97	0.70	0.73	0.70	0.70
MT	2.07	0.03	0.01	0.01	0.03	0.03	0.02	0.02
Wind	0.40	0.41	0.07	0.55	0.39	0.41	0.30	0.30
SOFC	0.00	0.00	0.00	0.00	0.00	0.00	0.00	0.00
REs	5.87	2.16	0.36	0.66	2.09	2.17	1.60	1.60
MT	0.12	0.00	0.00	0.00	0.00	0.00	0.00	0.00
PV	34.63	44.49	84.40	354.78	250.75	226.27	406.91	406.91
NGCC	33.44	42.59	5.78	6.75	31.14	32.37	23.88	23.88
Coal	0.00	0.00	0.00	0.00	0.00	0.00	0.00	0.00
SOFC	0.00	0.00	0.00	0.00	0.00	0.00	0.00	0.00
REs	1.84	0.03	0.01	0.01	0.03	0.03	0.02	0.02
MT	0.03	0.03	0.14	0.01	0.03	0.03	0.02	0.02
NGCC	1173.28	1183.97	1183.99	1183.97	1183.97	1183.97	1183.98	1183.98
Coal	0.24	0.25	0.04	0.05	0.24	0.25	0.20	0.20
IGCC	1529.12	1529.87	1494.68	1451.77	1499.42	1501.99	1494.58	1494.58
Merc - Res	118.60	147.62	136.39	131.22	145.50	146.84	138.60	138.60
Com - Merc	127.59	109.27	105.06	105.54	83.19	85.77	87.47	87.47
Ind - Merc	49.93	33.73	35.85	39.81	22.38	22.47	31.04	31.04
Gram - Res	108.45	114.11	113.90	110.98	114.02	114.11	113.34	113.34
Gram - Com	14.14	20.28	22.96	23.38	32.52	30.97	37.59	37.59
Gram - Ind	(2.61)	3.54	6.50	8.12	23.97	21.46	27.21	27.21
Krim - Res	94.25	120.29	123.09	122.34	121.31	121.20	121.76	121.76
Com - Krim	83.43	61.22	30.92	6.62	32.19	37.95	32.94	32.94
Ind - Krim	102.54	76.16	66.67	44.57	52.63	57.68	60.21	60.21
Maas - Res	155.53	187.42	187.97	186.45	187.42	187.42	187.42	187.42
Maas - Com	18.92	35.44	35.99	37.27	38.62	37.87	40.75	40.75
Zwol - Res	187.18	190.08	190.08	190.19	190.08	190.08	190.08	190.08
Zwol - Com	38.08	41.00	62.70	97.44	63.05	60.08	68.85	68.85
Zwol - Ind	69.80	72.72	83.03	112.48	91.64	89.55	103.05	103.05
D - Res	1522.03	1533.69	1554.19	1573.26	1546.69	1545.34	1553.89	1553.89
D - Com	1594.47	1604.43	1632.12	1655.69	1617.85	1616.54	1620.56	1620.56
D - Ind	559.63	571.29	585.44	608.57	591.20	587.61	589.35	589.35
F - Res	1468.08	1469.39	1445.27	1441.60	1467.27	1468.70	1469.39	1469.39
F - Com	4420.84	4405.61	4413.41	4368.91	4401.75	4402.85	4405.00	4405.00
F - Ind	1473.03	1463.17	1499.20	1543.17	1493.51	1490.98	1498.20	1498.20

Appendix C

Configuration operation decision variable values of the most desirable optimum configuration obtained using value functions for COMPETES, *Scenario 1*.

MAIN GRID:

Technology (Fuel Type)	HOUR 1 (MWh)	HOUR 2 (MWh)	HOUR 3 (MWh)	HOUR 4 (MWh)	HOUR 5 (MWh)	HOUR 6 (MWh)	HOUR 7 (MWh)	HOUR 8 (MWh)	HOUR 9 (MWh)
Hydroelectric	0.17	0.17	0.17	0.17	0.17	0.17	0.17	0.17	0.17
Coal	0.39	0.39	0.02	0.00	0.00	0.02	0.39	0.39	1.23
Natural gas	718.94	718.94	718.94	718.94	718.94	718.94	718.94	718.94	718.94
Oil	0.01	0.01	0.01	0.01	0.01	0.01	0.01	0.01	0.01
Nuclear	2918.82	2918.82	2918.82	2918.82	2918.82	2918.82	2918.82	2918.82	2918.82
Coal	1119.28	1119.28	1119.24	1065.19	1063.74	1119.24	1119.28	1119.28	1119.28
Oil	1307.93	955.03	677.87	537.79	482.28	684.41	1456.42	1969.48	2234.63
Natural gas	173.60	173.60	173.60	173.60	173.60	173.60	173.60	173.60	173.60
Oil	0.01	0.01	0.01	0.01	0.01	0.01	0.01	0.01	0.01
Waste	51.44	1.11	0.97	0.08	0.00	1.41	87.01	266.40	393.41
Waste	0.00	0.00	0.00	0.00	0.00	0.00	0.00	0.00	0.00
Natural gas	656.48	656.48	656.48	656.48	656.48	656.48	656.48	656.48	656.48
Natural gas	8.65	1.46	1.79	0.03	0.00	1.58	7.74	13.86	23.68
Waste	0.13	0.13	0.13	0.13	0.13	0.12	0.13	0.14	0.13
Waste	0.11	0.09	0.05	0.09	0.04	0.08	0.03	0.08	0.10
Nuclear	3510.04	3510.04	3510.04	3510.04	3510.04	3510.04	3510.04	3510.04	3510.04
Coal	0.00	0.00	0.00	0.00	0.00	0.00	0.00	0.00	0.00
Natural gas	171.91	172.70	119.12	60.73	44.69	122.72	173.10	173.32	173.38
Oil	0.00	0.00	0.00	0.00	0.00	0.00	0.00	0.00	0.00
Oil	0.00	0.00	0.00	0.00	0.00	0.00	0.00	0.00	0.00
Nuclear	431.92	431.92	431.92	431.92	431.92	431.92	431.92	431.92	431.92
Coal	489.55	447.97	428.76	408.66	419.12	422.69	551.73	590.00	590.00
Natural gas	0.00	0.00	0.00	0.00	0.00	0.00	0.00	0.00	170.77
Oil	0.00	0.00	0.00	0.00	0.00	0.00	0.00	0.00	0.00
Waste	102.41	102.41	102.41	102.41	102.41	102.41	102.41	102.41	102.41
Coal	479.36	380.40	356.30	320.46	356.98	359.95	547.37	942.09	1168.95
Natural gas	72.21	20.34	13.01	11.27	20.16	30.08	84.29	519.55	519.55
Waste	21.66	21.65	21.65	21.65	21.60	21.65	21.66	21.66	21.66
Waste	20.52	20.52	20.52	20.52	20.52	20.52	20.52	20.52	20.68
Natural gas	84.88	84.88	84.88	84.88	84.88	84.88	84.88	84.88	84.88
Coal	1214.73	1092.62	1094.44	1126.56	1089.35	1220.75	1347.08	1444.52	1444.52

Natural gas	228.92	200.57	138.64	129.47	140.60	165.19	309.55	309.88	309.88
Waste	166.41	166.41	166.41	166.41	166.41	166.41	166.41	166.41	166.41
Coal	331.41	313.34	254.69	249.48	251.89	280.92	371.38	635.63	766.08
Natural gas	2316.24	2316.24	2316.20	2315.08	2316.21	2316.20	2316.24	2316.24	2316.24
Hydroelectric	24.40	24.40	24.40	24.40	24.40	24.40	24.40	24.40	24.40
Coal	192.36	180.72	189.02	171.14	171.17	176.27	203.65	292.13	314.57
Natural gas	3.74	0.28	1.70	1.70	1.70	2.15	9.31	70.39	225.78
Waste	87.78	87.78	87.78	87.78	87.78	87.78	87.78	87.78	87.78
Natural gas	1338.75	1265.05	1210.39	1215.50	1219.29	1257.34	1399.71	1453.98	1453.98
Waste	50.53	50.48	50.70	50.90	50.86	50.79	50.59	51.00	51.19
Coal	0.02	0.02	0.02	0.02	0.02	0.02	0.02	0.02	0.02
Natural gas	0.06	0.06	0.06	0.06	0.06	0.06	0.06	0.06	0.22
Coal	0.02	0.02	0.02	0.02	0.02	0.02	0.02	0.02	0.02
Natural gas	2790.19	2654.08	2590.73	2575.21	2588.39	2664.70	2947.96	3423.19	3625.97
Nuclear	7749.46	7749.46	7749.46	7749.46	7749.46	7749.46	7749.46	7749.46	7749.46
Coal	1152.34	197.95	79.50	120.72	240.54	681.90	5277.07	10344.72	11825.49
Natural gas	100.65	0.76	0.64	0.00	0.04	78.06	347.37	817.03	817.03
Oil	0.00	0.00	0.00	0.00	0.00	0.00	0.00	0.00	0.00
Oil	0.00	0.00	0.00	0.00	0.00	0.00	0.00	0.00	0.00
Nuclear	7988.20	7988.20	7988.20	7988.20	7988.20	7988.20	7988.20	7988.20	7988.20
Coal	0.18	0.18	0.18	0.17	0.17	0.17	0.24	0.32	0.28
Natural gas	1193.68	568.96	560.27	188.96	565.27	1152.00	1211.13	1211.15	1211.15
Oil	0.00	0.00	0.00	0.00	0.00	0.00	0.00	0.00	0.00
Oil	0.00	0.00	0.00	0.00	0.00	0.00	0.00	0.00	0.00
Hydroelectric	59.81	59.81	59.81	59.81	59.81	59.81	59.81	59.81	59.81
Nuclear	3159.28	3159.28	3159.28	3159.28	3159.28	3159.28	3159.28	3159.28	3159.28
Coal	763.95	432.14	354.15	355.72	446.40	740.65	1114.98	1114.98	1114.98
Natural gas	852.91	852.91	852.91	852.91	852.91	852.91	852.91	852.91	852.91
Oil	0.00	0.00	0.00	0.00	0.00	0.00	0.00	0.00	0.00
Oil	0.00	0.00	0.00	0.00	0.00	0.00	0.00	0.00	0.00
Nuclear	5018.29	5018.29	5018.29	5018.29	5018.29	5018.29	5018.29	5018.29	5018.29
Coal	13366.03	13366.03	13364.84	13363.17	13366.03	13366.03	13366.03	13366.03	13366.03
Natural gas	3889.53	3889.53	3889.53	3889.53	3889.53	3889.53	3889.53	3889.53	3889.53
Oil	0.00	0.00	0.00	0.00	0.00	0.00	0.00	0.00	0.00
Oil	0.00	0.00	0.00	0.00	0.00	0.00	0.00	0.00	0.00
Nuclear	2106.97	2106.97	2106.97	2106.97	2106.97	2106.97	2106.97	2106.97	2106.97
Coal	5837.05	5830.92	5822.28	5792.91	5818.35	5837.05	5854.83	5857.44	5862.97
Natural gas	798.72	798.72	798.72	798.72	798.72	798.72	798.72	798.72	798.72
Oil	0.00	0.00	0.00	0.00	0.00	0.00	0.00	0.00	0.00
Oil	0.00	0.00	0.00	0.00	0.00	0.00	0.00	0.00	0.00
Hydroelectric	0.00	0.00	0.00	0.00	0.00	0.00	652.04	4588.78	4588.78
Coal	0.03	0.03	0.03	0.03	0.03	0.02	0.00	0.07	0.09
Natural gas	0.00	0.00	0.00	0.00	0.00	0.00	0.01	69.99	0.02
Oil	0.00	0.00	0.00	0.00	0.00	0.00	0.00	0.00	0.00

Oil	0.02	0.02	0.02	0.02	0.02	0.02	0.02	0.02	0.02
Nuclear	63486.84	63421.54	62081.29	60472.46	60623.91	63877.03	68700.53	68700.53	68700.53
Coal	0.00	0.00	0.00	0.00	0.00	0.00	0.00	0.00	0.00
Oil	0.00	0.00	0.00	0.00	0.00	0.00	0.00	0.00	0.00
Oil	0.00	0.00	0.00	0.00	0.00	0.00	0.00	0.00	0.00
Oil	0.00	0.00	0.00	0.00	0.00	0.00	0.00	0.00	0.00
Hydroelectric	1.33	1.33	1.33	1.33	1.33	1.33	3.22	49.00	41.71
AVEL - LONN	-1223.76	-1224.70	-1225.29	-1225.52	-1225.43	-1225.23	-1217.47	-1186.52	-1207.60
D - DIEL	-104.87	-102.68	-101.99	-101.41	-102.07	-104.24	-108.07	-90.17	-44.31
D - EICH	279.83	276.07	273.21	272.60	272.12	272.18	284.98	356.79	305.57
D - ROMM	76.79	77.16	76.82	77.09	76.72	75.31	76.52	110.31	112.52
D - UCHT	286.30	283.24	280.81	280.36	279.88	279.70	289.37	346.79	310.13
DIEL - ROMM	120.44	119.23	118.55	118.34	118.54	119.04	122.38	132.92	103.98
DIEL - ZWOL	-231.45	-227.81	-226.37	-225.51	-226.45	-229.36	-236.97	-227.69	-149.56
EICH - UCHT	7.20	7.97	8.44	8.62	8.61	8.36	4.89	-11.12	5.07
F - AVEL	1268.39	1269.72	1270.56	1271.02	1270.71	1270.56	1251.00	1147.74	1221.60
F - LONN	675.72	676.59	677.14	677.50	677.23	677.17	661.38	573.10	636.75
F - MOUL	240.28	241.55	242.42	242.79	242.67	242.58	229.38	154.66	210.44
F - MUHL	41.74	43.84	45.33	45.80	45.86	45.69	32.87	-35.29	16.18
GRAM - LONN	758.95	769.74	777.46	779.35	780.41	778.19	756.15	765.39	760.31
GRAM - MOUL	91.55	94.78	97.11	97.66	98.01	97.36	91.75	98.40	94.62
KRIM - MERC	793.77	793.30	791.86	791.13	790.85	791.79	792.28	804.50	627.56
LONN - MOUL	-736.71	-736.03	-735.50	-735.47	-735.21	-735.27	-730.89	-707.94	-721.26
MAAS - GRAM	187.76	167.30	153.60	149.73	148.06	153.76	193.80	210.49	144.51
MAAS - KRIM	127.26	124.82	124.53	124.10	124.06	124.89	129.56	128.91	253.35
MAAS - MERC	505.36	503.94	503.00	502.38	502.20	503.12	505.63	512.16	472.38
MERC - AVEL	695.68	690.97	688.21	687.60	687.37	688.77	695.12	695.65	693.99
MERC - GRAM	-739.71	-764.44	-781.03	-785.03	-786.91	-781.05	-732.12	-722.49	-733.13
MOUL - MUHL	-238.25	-237.26	-236.51	-236.39	-236.19	-236.28	-235.81	-227.95	-233.13
MUHL - EICH	-223.28	-220.07	-217.73	-217.15	-216.84	-217.11	-228.82	-287.57	-241.82
ROMM - MAAS	-41.91	-38.88	-37.52	-36.66	-36.72	-38.93	-44.18	-30.71	-10.56
ROMM - UCHT	223.90	220.24	218.01	217.23	217.12	218.44	227.48	252.73	211.18
UCHT - MOUL	447.37	443.18	440.23	439.49	439.06	439.72	449.95	490.63	451.48
ZWOL - KRIM	413.87	410.46	409.40	409.00	409.67	410.65	420.07	449.66	486.96
ZWOL - MAAS	199.55	198.71	198.18	198.17	198.64	198.80	202.31	222.25	174.50

HOUR 10 (MWh)	HOUR 11 (MWh)	HOUR 12 (MWh)	HOUR 13 (MWh)	HOUR 14 (MWh)	HOUR 15 (MWh)	HOUR 16 (MWh)	HOUR 17 (MWh)	HOUR 18 (MWh)	HOUR 19 (MWh)	HOUR 20 (MWh)
0.17	0.17	0.17	0.17	0.17	0.17	0.17	0.17	0.18	0.18	0.18
1.27	1.10	1.27	0.48	1.27	1.26	1.26	1.52	283.44	283.44	2.08
718.94	718.94	718.94	718.94	718.94	718.94	718.94	718.94	718.94	718.94	718.94
0.01	0.01	0.01	0.01	0.01	0.01	0.01	0.01	0.02	0.02	0.01
2918.82	2918.82	2918.82	2918.82	2918.82	2918.82	2918.82	2918.82	2918.82	2918.82	2918.82
1119.28	1119.28	1119.28	1119.28	1119.28	1119.28	1119.28	1119.28	1119.28	1119.28	1119.28
2255.06	2214.34	2270.18	2175.80	2269.17	2258.93	2246.80	2397.63	2609.28	2609.28	2541.25
173.60	173.60	173.60	173.60	173.60	173.60	173.60	173.60	173.60	173.60	173.60
0.01	0.01	0.01	0.01	0.01	0.01	0.01	0.01	0.03	0.05	0.01
427.04	426.65	443.72	405.37	441.19	435.16	430.94	452.36	471.66	471.66	461.43
0.00	0.00	0.00	0.00	0.00	0.00	0.00	0.00	0.00	0.00	0.00
656.48	656.48	656.48	656.48	656.48	656.48	656.48	656.48	656.48	656.48	656.48
19.75	16.81	16.80	18.07	18.85	16.68	14.56	36.07	75.75	75.75	25.28
0.13	0.13	0.12	0.13	0.14	0.14	0.13	0.11	0.32	0.42	0.12
0.07	0.05	0.14	0.11	0.20	0.19	0.12	0.44	3.91	4.11	0.61
3510.04	3510.04	3510.04	3510.04	3510.04	3510.04	3510.04	3510.04	3510.04	3510.04	3510.04
0.00	0.00	0.00	0.00	0.00	0.00	0.00	0.00	0.00	0.00	0.00
173.32	173.38	173.38	173.38	173.38	173.38	173.38	173.38	173.38	173.38	173.38
0.00	0.00	0.00	0.00	0.00	0.00	0.00	0.00	0.00	0.01	0.00
0.00	0.00	0.00	0.00	0.00	0.00	0.00	0.00	0.00	0.00	0.00
431.92	431.92	431.92	431.92	431.92	431.92	431.92	431.92	431.92	431.92	431.92
590.00	590.00	590.00	590.00	590.00	590.00	590.00	590.00	590.00	590.00	590.00
433.88	558.21	585.29	503.64	479.02	388.54	347.48	634.92	953.33	953.33	472.61
0.00	0.00	0.00	0.00	0.00	0.00	0.00	0.00	0.00	0.00	0.00
102.41	102.41	102.41	102.41	102.41	102.41	102.41	102.41	102.41	102.41	102.41
1169.02	1169.02	1169.02	1169.02	1169.02	1169.02	1169.02	1169.02	1169.02	1169.02	1169.02
519.55	519.55	519.55	519.55	519.55	519.55	519.55	519.55	519.55	519.55	519.55
21.66	21.66	21.66	21.66	21.66	21.66	21.66	21.66	21.66	21.66	21.66
20.68	20.68	20.68	20.68	20.68	20.68	20.68	20.68	20.68	20.68	20.68
84.88	84.88	84.88	84.88	84.88	84.88	84.88	84.88	84.88	84.88	84.88
1444.52	1444.52	1444.52	1444.52	1444.52	1444.52	1444.52	1444.52	1444.52	1444.52	1444.52
309.88	309.88	309.88	309.88	309.88	309.88	309.88	309.88	309.88	309.88	309.88
166.41	166.41	166.41	166.41	166.41	166.41	166.41	166.41	166.41	166.41	166.41
766.08	766.08	766.08	766.08	766.08	766.08	766.08	766.08	766.08	766.08	766.08
2316.24	2316.24	2316.24	2316.24	2316.24	2316.24	2316.24	2316.24	2316.24	2316.24	2316.24
24.40	24.40	24.40	24.40	24.40	24.40	24.40	24.40	24.40	24.40	24.40
314.58	314.58	314.58	314.58	314.58	314.58	314.58	314.58	314.58	314.58	314.58
225.80	225.80	225.80	225.80	225.80	225.80	225.80	225.80	225.80	225.80	225.80
87.78	87.78	87.78	87.78	87.78	87.78	87.78	87.78	87.78	87.78	87.78
1453.98	1453.98	1453.98	1453.98	1453.98	1453.98	1453.98	1453.98	1453.98	1453.98	1453.98
51.19	51.19	51.19	51.19	51.19	51.19	51.19	51.19	51.19	51.19	51.19
0.02	0.02	0.02	0.02	0.02	0.02	0.02	0.02	0.03	0.03	0.02

0.18	0.14	0.16	0.17	0.18	0.19	0.17	0.13	0.50	0.56	0.16
0.02	0.02	0.03	0.03	0.04	0.03	0.03	0.03	0.07	0.09	0.03
3611.91	3626.11	3626.14	3626.10	3626.15	3626.12	3626.13	3626.16	3626.16	3626.16	3626.04
7749.46	7749.46	7749.46	7749.46	7749.46	7749.46	7749.46	7749.46	7749.46	7749.46	7749.46
11706.46	12585.39	13530.89	13307.19	13421.61	12847.75	13096.69	14587.31	17253.83	17322.23	14832.68
817.03	817.03	817.03	817.03	817.03	817.03	817.03	817.03	817.03	817.03	817.03
0.00	0.00	0.00	0.00	0.00	0.00	0.00	0.00	0.00	0.00	0.00
0.00	0.00	0.00	0.00	0.00	0.00	0.00	0.00	0.00	0.00	0.00
7988.20	7988.20	7988.20	7988.20	7988.20	7988.20	7988.20	7988.20	7988.20	7988.20	7988.20
0.32	0.27	0.25	0.27	0.27	0.27	0.25	0.28	0.37	0.44	0.27
1211.15	1211.15	1211.15	1211.15	1211.15	1211.15	1211.15	1211.15	1211.15	1211.15	1211.15
0.00	0.00	0.00	0.00	0.00	0.00	0.00	0.00	0.00	0.02	0.00
0.00	0.00	0.00	0.00	0.00	0.00	0.00	0.00	0.00	0.00	0.00
59.81	59.81	59.81	59.81	59.81	59.81	59.81	59.81	59.81	59.81	59.81
3159.28	3159.28	3159.28	3159.28	3159.28	3159.28	3159.28	3159.28	3159.28	3159.28	3159.28
1114.98	1114.98	1114.98	1114.98	1114.98	1114.98	1114.98	1114.98	1114.98	1114.98	1114.98
852.91	852.91	852.91	852.91	852.91	852.91	852.91	852.91	852.91	852.91	852.91
0.00	0.00	0.00	0.00	0.00	0.00	0.00	0.00	0.00	0.00	0.00
0.00	0.00	0.00	0.00	0.00	0.00	0.00	0.00	0.00	0.00	0.00
5018.29	5018.29	5018.29	5018.29	5018.29	5018.29	5018.29	5018.29	5018.29	5018.29	5018.29
13366.03	13366.03	13366.03	13366.03	13366.03	13366.03	13366.03	13366.03	13366.03	13366.03	13366.03
3889.53	3889.53	3889.53	3889.53	3889.53	3889.53	3889.53	3889.53	3889.53	3889.53	3889.53
0.00	0.00	0.00	0.00	0.00	0.00	0.00	0.00	0.00	0.01	0.00
0.00	0.00	0.00	0.00	0.00	0.00	0.00	0.00	0.00	0.00	0.00
2106.97	2106.97	2106.97	2106.97	2106.97	2106.97	2106.97	2106.97	2106.97	2106.97	2106.97
5862.97	5862.97	5862.97	5862.97	5862.97	5862.97	5862.97	5862.97	5862.97	5862.97	5862.97
798.72	798.72	798.72	798.72	798.72	798.72	798.72	798.72	798.72	798.72	798.72
0.00	0.00	0.00	0.00	0.00	0.00	0.00	0.00	0.00	0.00	0.00
0.00	0.00	0.00	0.00	0.00	0.00	0.00	0.00	0.00	0.00	0.00
4335.62	3848.75	3823.52	3286.79	2067.24	760.23	106.89	1643.57	4588.78	4588.78	4588.78
0.00	0.00	0.00	0.00	0.00	0.00	0.00	0.00	0.09	1.14	0.07
0.00	0.00	0.00	0.01	0.00	0.01	0.01	0.00	1421.08	2720.23	1109.33
0.00	0.00	0.00	0.00	0.00	0.00	0.00	0.00	0.00	21.53	0.00
0.02	0.02	0.02	0.02	0.02	0.02	0.02	0.02	0.03	0.08	0.03
68700.53	68700.53	68700.53	68700.53	68700.53	68700.53	68700.53	68700.53	68700.53	68700.53	68700.53
0.00	0.00	0.00	0.00	0.00	0.00	0.00	0.00	0.00	0.01	0.00
0.00	0.00	0.00	0.00	0.00	0.00	0.00	0.00	0.00	0.01	0.00
0.00	0.00	0.00	0.00	0.00	0.00	0.00	0.00	0.00	0.01	0.00
0.00	0.00	0.00	0.00	0.00	0.00	0.00	0.00	0.00	0.02	0.00
3.46	3.22	3.22	3.22	3.22	3.43	3.26	3.22	49.00	49.00	49.00
-1220.78	-1218.62	-1218.34	-1218.53	-1218.51	-1217.81	-1217.37	-1217.82	-1205.19	-1159.66	-1188.73
-214.90	-16.18	-13.81	-21.71	-24.59	-32.61	-36.05	-9.32	170.19	177.08	-0.19
332.53	295.26	296.13	294.03	293.86	293.20	292.85	298.60	445.33	725.25	366.43
195.62	121.48	122.83	118.55	117.29	113.50	111.82	125.84	281.95	370.22	153.56

348.72	305.32	306.23	303.82	303.47	302.16	301.52	308.71	451.89	679.44	362.34
12.30	91.27	90.59	93.00	94.07	96.88	98.03	89.61	74.09	128.06	101.94
-252.39	-107.79	-104.70	-115.16	-119.18	-130.26	-134.98	-99.18	80.25	31.68	-102.33
18.00	11.19	11.22	10.88	10.67	9.97	9.63	11.23	7.29	-50.90	-4.54
1257.57	1254.42	1253.73	1254.31	1254.16	1252.17	1250.93	1252.63	1199.00	1004.73	1156.85
666.34	664.23	663.68	664.17	664.03	662.38	661.35	662.83	615.32	443.10	581.14
230.91	232.30	231.85	232.33	232.17	230.91	230.17	231.00	178.86	21.36	161.56
26.62	34.34	33.85	34.57	34.43	33.58	33.09	32.68	-32.88	-178.67	-31.01
747.20	762.47	761.68	762.59	762.45	762.35	762.54	758.43	696.50	828.60	758.02
88.16	93.60	93.40	93.66	93.61	93.70	93.83	92.46	73.21	115.69	95.93
572.15	625.31	625.02	625.64	628.40	629.43	629.14	625.35	596.70	786.71	650.86
-736.69	-730.77	-730.61	-730.61	-730.65	-729.99	-729.51	-730.61	-738.43	-713.53	-709.89
96.42	119.89	119.59	122.94	125.11	130.24	132.05	121.71	139.07	249.02	157.35
255.49	228.83	226.54	231.79	232.19	237.87	240.72	221.04	255.19	144.95	222.12
442.35	459.41	458.17	461.02	462.76	466.04	467.24	455.73	455.96	509.84	470.54
685.35	695.86	696.26	696.46	696.06	695.95	695.98	697.67	654.91	768.13	696.26
-738.89	-740.80	-738.76	-739.86	-740.35	-739.90	-739.80	-731.14	-708.22	-666.07	-712.25
-245.15	-237.56	-237.60	-237.33	-237.30	-236.81	-236.50	-237.97	-254.10	-240.05	-231.08
-246.24	-229.53	-230.05	-229.03	-229.12	-229.35	-229.45	-231.62	-316.90	-462.21	-286.91
23.28	1.28	2.35	-1.32	-2.49	-6.07	-7.70	4.67	126.74	80.04	10.93
163.61	196.47	196.00	198.00	198.97	201.62	202.73	195.44	181.60	330.46	223.11
450.56	442.67	442.93	442.59	442.92	443.45	443.57	444.15	513.29	652.22	484.36
363.74	433.45	429.78	440.15	443.25	455.17	460.45	422.83	458.47	452.47	456.14
91.80	153.39	152.30	156.10	157.92	162.48	164.32	150.91	154.59	214.77	172.29

HOUR 21 (MWh)	HOUR 22 (MWh)	HOUR 23 (MWh)	HOUR 24 (MWh)
0.17	0.17	0.18	0.17
0.39	0.39	0.39	0.39
718.94	718.94	718.94	718.94
0.01	0.01	0.01	0.01
2918.82	2918.82	2918.82	2918.82
1119.28	1119.28	1119.28	1119.28
2138.52	1724.67	1958.44	1957.37
173.60	173.60	173.60	173.60
0.01	0.01	0.01	0.01
363.61	201.52	273.61	282.47
0.00	0.00	0.00	0.00
656.48	656.48	656.48	656.48
17.40	15.58	10.89	12.54
0.14	0.13	0.13	0.14
0.09	0.10	0.11	0.09
3510.04	3510.04	3510.04	3510.04
0.00	0.00	0.00	0.00
173.38	172.16	173.38	173.38
0.00	0.00	0.00	0.00
0.00	0.00	0.00	0.00
431.92	431.92	431.92	431.92
590.00	590.00	590.00	567.50
31.60	0.00	0.00	0.00
0.00	0.00	0.00	0.00
102.41	102.41	102.41	102.41
1166.45	1088.87	761.43	674.67
519.55	519.55	467.55	191.42
21.66	21.66	21.66	21.66
20.68	20.52	20.52	20.52
84.88	84.88	84.88	84.88
1444.52	1444.52	1444.52	1389.10
309.88	309.88	309.80	309.80
166.41	166.41	166.41	166.41
765.68	735.86	499.42	350.17
2316.24	2316.24	2316.24	2316.24
24.40	24.40	24.40	24.40
314.56	295.09	267.85	204.50
225.75	92.94	24.04	11.29
87.78	87.78	87.78	87.78
1453.98	1453.98	1453.93	1444.66
51.17	50.51	50.96	50.90
0.02	0.02	0.02	0.02

0.25	0.07	0.06	0.06
0.02	0.02	0.02	0.02
3624.46	3460.55	3278.27	3050.69
7749.46	7749.46	7749.46	7749.46
12170.09	9875.63	8288.32	5675.01
817.03	817.03	813.41	456.43
0.00	0.00	0.00	0.00
0.00	0.00	0.00	0.00
7988.20	7988.20	7988.20	7988.20
0.27	0.31	0.31	0.24
1211.15	1211.15	1211.15	1211.15
0.00	0.00	0.00	0.00
0.00	0.00	0.00	0.00
59.81	59.81	59.81	59.81
3159.28	3159.28	3159.28	3159.28
1114.98	1114.98	1114.98	1114.98
852.91	852.91	852.91	852.91
0.00	0.00	0.00	0.00
0.00	0.00	0.00	0.00
5018.29	5018.29	5018.29	5018.29
13366.03	13366.03	13366.03	13366.03
3889.53	3889.53	3889.53	3889.53
0.00	0.00	0.00	0.00
0.00	0.00	0.00	0.00
2106.97	2106.97	2106.97	2106.97
5862.97	5854.83	5854.83	5854.83
798.72	798.72	798.72	798.72
0.00	0.00	0.00	0.00
0.00	0.00	0.00	0.00
2577.11	0.00	1140.54	0.00
0.00	0.03	0.00	0.03
0.00	0.00	0.00	0.00
0.00	0.00	0.00	0.00
0.02	0.02	0.02	0.02
68700.53	68282.36	68700.53	68296.30
0.00	0.00	0.00	0.00
0.00	0.00	0.00	0.00
0.00	0.00	0.00	0.00
0.00	0.00	0.00	0.00
3.22	1.33	3.22	1.33
-1218.39	-1223.62	-1217.53	-1223.15
-62.05	-101.79	-111.49	-111.73
289.42	279.32	284.93	278.66
100.13	79.16	77.10	73.22

296.99	286.27	289.46	284.70
107.53	119.97	125.03	122.62
-171.86	-227.57	-243.45	-241.30
8.42	7.73	5.04	6.71
1253.80	1268.66	1251.43	1267.24
663.73	676.06	661.78	674.86
231.70	240.87	229.74	239.76
34.45	42.44	33.16	41.56
760.30	759.48	755.65	758.01
92.94	91.78	91.59	91.38
633.21	777.82	788.09	792.62
-730.93	-736.29	-730.96	-736.12
151.15	180.46	191.55	193.04
260.66	131.01	128.45	130.51
479.03	498.22	502.75	506.27
696.01	698.41	696.21	697.64
-737.24	-735.51	-729.49	-734.39
-236.71	-238.12	-235.90	-237.85
-228.38	-222.43	-228.64	-222.96
-17.80	-37.56	-40.99	-45.54
210.39	221.34	226.94	226.01
445.36	445.91	449.75	447.42
502.87	418.50	429.78	421.86
180.75	200.42	209.37	202.94

Appendix D

Configuration operation decision variable values of the most desirable optimum configuration obtained using value functions for COMPETES, *Scenario 2*.

MAIN GRID:

Technology (Fuel Type)	HOUR 1 (MWh)	HOUR 2 (MWh)	HOUR 3 (MWh)	HOUR 4 (MWh)	HOUR 5 (MWh)	HOUR 6 (MWh)	HOUR 7 (MWh)	HOUR 8 (MWh)	HOUR 9 (MWh)
Hydroelectric	0.17	0.17	0.17	0.17	0.17	0.17	0.17	0.17	0.17
Coal	329.89	322.47	319.85	307.46	309.80	317.34	332.41	339.98	337.56
Natural gas	121.28	100.81	74.64	37.46	36.58	75.58	145.12	369.84	436.24
Oil	0.06	0.06	0.05	0.05	0.06	0.05	0.05	0.05	0.05
Nuclear	2918.82	2918.82	2918.82	2918.82	2918.82	2918.82	2918.82	2918.82	2918.82
Coal	1119.28	1119.28	1119.28	1119.28	1119.28	1119.28	1119.28	1119.28	1119.28
Oil	1365.19	1025.97	806.26	608.85	565.61	809.12	1553.03	1818.37	1939.88
Natural gas	0.01	0.01	0.01	0.01	0.01	0.01	0.01	0.01	0.01
Oil	0.09	0.09	0.08	0.08	0.09	0.08	0.08	0.08	0.08
Waste	472.32	472.32	472.32	472.32	472.32	472.32	472.32	472.32	472.32
Waste (Lower Efficiency)	2.70	2.30	1.93	2.03	2.03	2.22	2.47	2.80	2.80
Natural gas	0.44	0.65	0.00	0.01	0.00	0.44	0.44	1.14	1.31
Natural gas	0.01	0.01	0.01	0.01	0.01	0.01	0.01	0.01	0.01
Waste	6.27	5.68	6.02	5.90	5.90	6.02	6.27	6.74	6.74
Waste	20.43	14.09	20.19	19.39	19.38	20.19	21.02	21.02	21.02
Nuclear	3480.79	3471.10	3469.93	3474.14	3470.50	3472.43	3481.73	3496.71	3502.48
Coal	182.84	174.51	170.34	284.55	299.51	178.68	183.07	276.33	329.41
Natural gas	0.02	0.03	0.03	0.04	0.04	0.03	0.04	0.03	0.03
Oil	0.02	0.02	0.02	0.02	0.02	0.02	0.02	0.02	0.02
Oil	0.00	0.00	0.00	0.00	0.00	0.00	0.00	0.00	0.00
Nuclear	431.92	431.92	431.92	431.92	431.92	431.92	431.92	431.92	431.92
Coal	590.00	590.00	590.00	590.00	590.00	590.00	590.00	590.00	590.00
Natural gas	0.03	0.03	0.03	0.03	0.03	0.03	0.03	0.03	0.03
Oil	0.03	0.11	0.11	0.11	0.11	0.11	0.86	0.92	0.96
Waste	102.41	102.41	102.41	102.41	102.41	102.41	102.41	102.41	102.41
Coal	1151.87	1064.13	977.86	928.12	923.78	1071.98	1169.02	1169.02	1169.02
Natural gas	0.00	0.04	0.00	0.02	0.05	0.00	0.00	0.01	0.07
Waste	21.66	21.66	21.66	21.66	21.66	21.66	21.66	21.66	21.66
Waste	20.68	20.68	20.68	20.68	20.68	20.68	20.68	20.68	20.68
Natural gas	52.75	52.76	52.22	50.62	52.22	52.22	72.66	72.66	72.66
Coal	1433.93	1371.68	1317.40	1286.49	1319.15	1380.96	1444.52	1444.52	1444.52

Natural gas	0.00	0.05	0.00	0.03	0.07	0.00	0.00	0.01	17.63
Waste	166.41	166.41	166.41	166.41	166.41	166.41	166.41	166.41	166.41
Coal	766.08	699.03	676.19	665.20	648.59	704.28	766.08	766.08	766.08
Natural gas	0.00	3.38	0.00	2.24	4.51	0.00	99.04	1394.56	2266.83
Hydroelectric	24.40	24.40	24.40	24.40	24.40	24.40	24.40	24.40	24.40
Coal	314.58	314.58	312.27	305.41	303.04	312.27	314.58	314.58	314.58
Natural gas	0.00	0.00	0.00	0.01	0.00	0.00	0.00	2.91	37.84
Waste	87.78	87.78	87.78	87.78	87.78	87.78	87.78	87.78	87.78
Natural gas	265.22	176.82	147.74	136.77	142.06	170.47	395.94	592.35	711.62
Waste	51.18	51.18	51.18	51.18	51.18	51.18	51.18	51.18	51.18
Coal	16.58	16.58	16.58	16.58	16.58	16.58	16.58	16.58	16.30
Natural gas	0.01	0.01	0.01	0.01	0.01	0.01	0.01	0.01	0.01
Coal	137.46	151.09	164.71	140.97	141.05	144.27	140.98	161.30	161.32
Natural gas	1655.51	1406.17	1288.78	1313.20	1317.31	1403.23	1848.65	2261.67	2383.45
Nuclear	7749.46	7749.46	7749.46	7749.46	7749.46	7749.46	7749.46	7749.46	7749.46
Coal	5762.48	4399.33	3342.70	3691.51	4185.15	4552.65	8911.68	11620.05	12073.28
Natural gas	0.01	0.01	0.01	0.01	0.01	0.01	0.01	0.01	0.01
Oil	0.01	0.01	0.01	0.01	0.01	0.01	0.01	0.01	0.01
Oil	0.00	0.00	0.00	0.00	0.00	0.00	0.00	0.00	0.00
Nuclear	7988.20	7988.20	7988.20	7988.20	7988.20	7988.20	7988.20	7988.20	7988.20
Coal	14.21	0.03	4.73	0.08	0.00	0.00	129.84	169.89	172.11
Natural gas	0.01	0.01	0.01	0.01	0.01	0.01	0.01	0.02	0.02
Oil	0.00	0.00	0.00	0.00	0.00	0.00	0.00	0.00	0.00
Oil	0.00	0.00	0.00	0.00	0.00	0.00	0.00	0.00	0.00
Hydroelectric	59.81	59.81	59.81	59.81	59.81	59.81	59.81	59.81	59.81
Nuclear	3159.28	3159.28	3159.28	3159.28	3159.28	3159.28	3159.28	3159.28	3159.28
Coal	237.75	211.73	234.26	227.18	235.39	228.29	276.18	322.66	322.66
Natural gas	0.00	0.00	0.00	0.00	0.00	0.00	0.00	0.00	0.00
Oil	0.00	0.00	0.00	0.00	0.00	0.00	0.00	0.00	0.00
Oil	0.00	0.00	0.01	0.00	0.00	0.01	0.01	0.00	0.00
Nuclear	5018.29	5018.29	5018.29	5018.29	5018.29	5018.29	5018.29	5018.29	5018.29
Coal	10746.76	10085.95	10743.24	10202.17	9978.30	11030.09	11508.17	13038.05	13038.05
Natural gas	0.12	0.09	0.10	0.10	0.10	0.10	0.10	0.10	0.10
Oil	0.00	0.00	0.00	0.00	0.00	0.00	0.00	0.00	0.00
Oil	0.00	0.00	0.00	0.00	0.00	0.00	0.00	0.00	0.00
Nuclear	2106.97	2106.97	2106.97	2106.97	2106.97	2106.97	2106.97	2106.97	2106.97
Coal	6993.67	6993.67	6993.67	6993.67	6993.67	6993.67	6993.67	6993.67	6993.67
Natural gas	0.01	0.01	0.01	0.01	0.01	0.01	0.01	0.01	0.01
Oil	0.00	0.00	0.00	0.00	0.00	0.00	0.00	0.00	0.00
Oil	0.04	0.04	0.04	0.04	0.04	0.04	0.04	0.04	0.04
Hydroelectric	935.94	936.16	936.26	937.28	935.98	935.94	933.78	2728.16	2491.34
Coal	5.23	5.34	5.55	5.43	5.43	5.43	5.34	5.76	5.11
Natural gas	0.02	0.02	0.02	0.02	0.02	0.02	0.02	0.02	0.02
Oil	0.00	0.00	0.00	0.00	0.00	0.00	0.00	0.00	0.00

Oil	0.00	0.00	0.00	0.00	0.00	0.00	0.00	0.00	0.00
Nuclear	60816.68	60957.24	59593.52	58067.60	57976.71	60789.89	66239.55	68243.70	68170.44
Coal	0.00	0.04	0.05	0.00	0.00	0.00	0.00	0.74	0.00
Oil	0.00	0.00	0.00	0.00	0.00	0.00	0.00	0.00	0.00
Oil	0.00	0.00	0.00	0.00	0.00	0.00	0.00	0.00	0.00
Oil	0.19	0.20	0.20	0.20	0.19	0.20	0.20	0.22	0.20
Hydroelectric	5.81	5.81	5.81	5.81	5.81	5.81	5.81	5.81	5.69
AVEL - LONN	-1207.85	-1211.80	-1215.75	-1207.66	-1207.16	-1214.90	-1211.02	-1194.69	-1194.45
D - DIEL	193.00	210.36	219.58	224.17	226.45	219.27	198.19	192.72	212.59
D - EICH	309.48	305.56	300.18	304.67	304.65	299.92	310.34	332.38	334.37
D - ROMM	254.61	256.39	257.23	259.78	260.79	258.23	258.94	261.68	266.75
D - UCHT	339.97	337.82	334.20	336.38	336.42	334.08	341.98	356.79	359.20
DIEL - ROMM	40.86	30.53	24.97	23.62	22.77	25.84	40.29	45.73	35.92
DIEL - ZWOL	131.25	155.14	167.77	172.63	175.20	166.68	135.90	126.16	151.47
EICH - UCHT	33.97	35.86	37.81	35.25	35.29	37.97	35.51	27.69	28.28
F - AVEL	1230.64	1242.12	1253.41	1226.15	1224.80	1250.95	1240.38	1188.71	1187.93
F - LONN	653.86	662.06	671.01	649.18	648.22	669.12	661.86	619.69	619.54
F - MOUL	243.63	249.47	256.12	239.33	238.30	255.62	249.65	215.00	214.86
F - MUHL	46.81	52.13	58.37	45.99	45.39	58.19	50.84	21.32	20.97
GRAM - LONN	773.94	783.29	793.91	813.87	815.34	794.26	767.97	768.44	768.54
GRAM - MOUL	99.87	101.97	104.66	112.10	113.67	104.91	97.54	100.42	99.93
KRIM - MERC	393.35	425.19	411.37	396.49	387.91	404.72	321.18	347.24	350.94
LONN - MOUL	-714.62	-717.14	-719.40	-709.63	-708.92	-718.48	-718.55	-704.69	-704.32
MAAS - GRAM	-151.41	-162.75	-180.69	-213.50	-218.52	-185.29	-148.30	-133.83	-133.35
MAAS - KRIM	24.09	-15.05	-3.70	15.77	19.74	-1.28	95.92	70.62	63.20
MAAS - MERC	231.86	232.09	229.42	229.65	226.71	227.05	225.68	228.22	226.75
MERC - AVEL	746.84	743.98	744.10	733.33	733.99	743.01	752.11	754.32	756.29
MERC - GRAM	-658.99	-680.50	-698.55	-741.00	-741.60	-700.40	-643.17	-628.23	-624.70
MOUL - MUHL	-236.19	-236.83	-237.32	-232.02	-231.50	-236.93	-238.59	-232.44	-232.69
MUHL - EICH	-216.52	-212.26	-207.00	-212.28	-212.22	-206.68	-215.61	-236.51	-237.15
ROMM - MAAS	166.99	162.75	162.86	163.76	164.71	165.57	172.07	166.22	163.50
ROMM - UCHT	91.24	87.04	82.24	81.88	80.85	81.08	88.77	101.65	98.82
UCHT - MOUL	397.05	393.68	388.87	387.44	386.57	387.89	397.56	410.84	410.35
ZWOL - KRIM	200.30	132.50	126.30	139.57	141.16	132.96	265.70	253.42	214.65
ZWOL - MAAS	118.89	96.37	85.66	83.11	81.85	88.65	119.85	126.45	105.15

HOUR 10 (MWh)	HOUR 11 (MWh)	HOUR 12 (MWh)	HOUR 13 (MWh)	HOUR 14 (MWh)	HOUR 15 (MWh)	HOUR 16 (MWh)	HOUR 17 (MWh)	HOUR 18 (MWh)	HOUR 19 (MWh)	HOUR 20 (MWh)
0.18	0.17	0.18	0.18	0.18	0.18	0.18	0.18	0.18	0.18	0.18
337.51	337.43	332.47	337.61	337.43	335.02	340.04	339.94	342.45	342.45	342.45
459.88	445.25	488.41	421.06	488.18	488.58	459.95	502.48	650.33	650.33	555.67
0.05	0.05	0.05	0.05	0.05	0.05	0.05	0.05	0.85	1.34	0.05
2918.82	2918.82	2918.82	2918.82	2918.82	2918.82	2918.82	2918.82	2918.82	2918.82	2918.82
1119.28	1119.28	1119.28	1119.28	1119.28	1119.28	1119.28	1119.28	1119.28	1119.28	1119.28
1906.13	1936.60	1943.11	1914.66	1935.21	1919.80	1929.54	2026.92	2251.49	2259.85	2088.55
0.01	0.01	0.01	0.01	0.01	0.01	0.01	0.01	0.02	0.04	0.01
0.08	0.09	0.08	0.08	0.08	0.08	0.08	0.08	1.14	2.13	0.08
472.32	472.32	472.32	472.32	472.32	472.32	472.32	472.32	472.32	472.32	472.32
2.80	2.80	2.80	2.80	2.80	2.80	2.80	2.80	4.27	6.35	3.22
1.52	1.31	1.31	1.31	1.31	1.31	1.31	1.31	21.13	28.21	4.16
0.01	0.01	0.01	0.01	0.01	0.01	0.01	0.01	0.05	0.08	0.01
6.74	6.74	6.74	6.74	6.74	6.74	6.74	6.74	6.37	8.00	6.27
21.02	21.02	21.02	21.02	21.02	21.02	21.02	21.09	21.02	26.84	21.02
3506.39	3503.26	3505.86	3499.97	3504.24	3503.05	3502.40	3508.11	3508.11	3508.11	3508.11
358.29	333.59	346.38	304.24	336.86	333.57	329.39	376.32	568.17	568.17	442.71
0.03	0.03	0.03	0.03	0.03	0.03	0.03	0.03	0.11	0.18	0.04
0.02	0.02	0.02	0.02	0.02	0.02	0.02	0.02	0.06	0.11	0.02
0.00	0.00	0.00	0.00	0.00	0.00	0.00	0.00	0.00	0.00	0.00
431.92	431.92	431.92	431.92	431.92	431.92	431.92	431.92	431.92	431.92	431.92
590.00	590.00	590.00	590.00	590.00	590.00	590.00	590.00	590.00	590.00	590.00
0.03	0.04	0.04	0.04	0.04	0.04	0.04	0.04	0.08	0.14	0.04
0.99	1.23	1.16	1.06	1.03	0.99	0.99	1.13	4.12	4.64	1.03
102.41	102.41	102.41	102.41	102.41	102.41	102.41	102.41	102.41	102.41	102.41
1169.02	1169.02	1169.02	1169.02	1169.02	1169.02	1169.02	1169.02	1169.02	1169.02	1169.02
0.00	4.75	16.38	0.00	0.05	0.00	0.00	28.93	216.01	216.01	0.30
21.66	21.66	21.66	21.66	21.66	21.66	21.66	21.66	21.66	21.66	21.66
20.68	20.68	20.68	20.68	20.68	20.68	20.68	20.68	20.68	20.68	20.68
71.47	72.66	72.66	72.66	72.66	72.66	72.66	72.66	72.66	72.66	72.66
1444.52	1444.52	1444.52	1444.52	1444.52	1444.52	1444.52	1444.52	1444.52	1444.52	1444.52
31.17	233.47	244.50	201.44	177.46	107.53	82.17	253.28	265.64	265.64	165.57
166.41	166.41	166.41	166.41	166.41	166.41	166.41	166.41	166.41	166.41	166.41
766.08	766.08	766.08	766.08	766.08	766.08	766.08	766.08	766.08	766.08	766.08
2288.10	2315.95	2315.95	2315.95	2315.95	2315.78	2315.47	2315.95	2315.95	2315.95	2315.95
24.40	24.40	24.40	24.40	24.40	24.40	24.40	24.40	24.40	24.40	24.40
314.58	314.58	314.58	314.58	314.58	314.58	314.58	314.58	314.58	314.58	314.58
42.73	47.39	48.36	47.52	45.58	40.79	39.80	49.34	131.42	131.88	46.42
87.78	87.78	87.78	87.78	87.78	87.78	87.78	87.78	87.78	87.78	87.78
737.50	753.35	755.47	742.98	743.44	731.88	728.60	756.67	774.83	774.83	753.35
51.18	51.18	51.18	51.18	51.18	51.18	51.18	51.18	51.18	51.18	51.18
16.30	16.30	16.30	16.30	16.30	16.30	16.30	16.30	28.80	38.75	16.30

0.01	0.01	0.01	0.01	0.01	0.01	0.01	0.01	0.04	0.06	0.01
174.93	198.99	202.18	191.97	185.14	174.98	178.33	208.99	464.44	464.44	185.14
2451.98	2484.88	2501.05	2472.75	2470.88	2445.10	2436.54	2507.47	2599.45	2666.22	2465.67
7749.46	7749.46	7749.46	7749.46	7749.46	7749.46	7749.46	7749.46	7749.46	7749.46	7749.46
11957.22	12648.35	13466.35	13491.94	13455.23	12816.35	13067.17	14455.45	15898.23	15898.23	14979.69
0.01	0.01	0.01	0.01	0.01	0.01	0.01	0.01	0.01	0.01	0.01
0.01	0.01	0.01	0.01	0.01	0.01	0.01	0.01	0.01	0.03	0.01
0.00	0.00	0.00	0.00	0.00	0.00	0.00	0.00	0.01	0.03	0.00
7988.20	7988.20	7988.20	7988.20	7988.20	7988.20	7988.20	7988.20	7988.20	7988.20	7988.20
169.92	328.35	404.07	389.94	389.86	347.25	361.56	470.33	645.48	645.48	640.76
0.02	0.02	0.02	0.02	0.02	0.02	0.02	0.02	0.02	0.05	0.02
0.00	0.00	0.00	0.00	0.00	0.00	0.00	0.00	0.00	0.01	0.00
0.00	0.00	0.00	0.00	0.00	0.00	0.00	0.00	0.00	0.00	0.00
59.81	59.81	59.81	59.81	59.81	59.81	59.81	59.81	59.81	59.81	59.81
3159.28	3159.28	3159.28	3159.28	3159.28	3159.28	3159.28	3159.28	3159.28	3159.28	3159.28
322.66	322.66	322.66	322.66	322.66	322.66	322.66	322.66	322.66	322.66	322.66
0.00	0.00	0.00	0.00	0.00	0.00	0.00	0.00	0.00	0.01	0.00
0.00	0.00	0.00	0.00	0.00	0.00	0.00	0.00	0.00	0.00	0.00
0.00	0.00	0.00	0.00	0.00	0.00	0.00	0.00	0.08	0.12	0.00
5018.29	5018.29	5018.29	5018.29	5018.29	5018.29	5018.29	5018.29	5018.29	5018.29	5018.29
13038.05	13038.05	13038.05	13038.05	13038.05	13038.05	13038.05	13038.05	13038.05	13038.05	13038.05
0.10	0.10	0.10	0.10	0.10	0.10	0.10	0.10	1.57	2.32	0.10
0.00	0.00	0.00	0.00	0.00	0.00	0.01	0.00	0.01	0.01	0.01
0.00	0.00	0.00	0.00	0.00	0.00	0.00	0.00	0.00	0.01	0.00
2106.97	2106.97	2106.97	2106.97	2106.97	2106.97	2106.97	2106.97	2106.97	2106.97	2106.97
6993.67	6993.67	6993.67	6993.67	6993.67	6993.67	6993.67	6993.67	6993.67	6993.67	6993.67
0.01	0.01	0.01	0.01	0.01	0.01	0.01	0.01	0.02	0.05	0.01
0.00	0.00	0.00	0.00	0.00	0.00	0.00	0.00	0.00	0.00	0.00
0.04	0.04	0.04	0.04	0.04	0.04	0.04	0.04	0.07	0.13	0.04
2133.22	1818.61	1750.28	1432.02	964.16	933.78	935.59	933.76	3318.71	3525.55	3370.42
5.76	5.34	5.76	5.34	5.75	5.34	5.34	5.34	12.26	55.10	5.83
0.02	0.02	0.02	0.02	0.02	0.02	0.02	0.02	0.02	0.09	0.02
0.00	0.00	0.00	0.00	0.00	0.00	0.00	0.00	0.00	0.00	0.00
0.00	0.00	0.00	0.00	0.00	0.00	0.00	0.00	0.00	0.00	0.00
68074.06	67973.56	67964.44	67850.35	67622.07	66261.48	65595.64	67008.65	68496.47	68627.56	68449.99
0.69	0.00	1.56	0.13	0.00	0.00	0.00	0.00	20.95	1428.54	0.00
0.00	0.00	0.00	0.00	0.00	0.00	0.00	0.00	0.00	0.00	0.00
0.00	0.00	0.00	0.00	0.00	0.00	0.00	0.00	0.00	0.00	0.00
0.21	0.21	0.20	0.21	0.20	0.19	0.20	0.20	0.21	1.17	0.21
5.81	5.81	5.81	5.69	6.17	5.81	5.81	5.81	7.85	16.38	6.53
-1189.51	-1194.67	-1194.58	-1200.21	-1206.72	-1207.04	-1207.24	-1204.57	-1174.52	-1201.71	-1185.01
139.63	214.35	213.83	214.90	213.96	214.00	213.58	214.53	176.76	273.35	209.17
355.85	334.97	334.90	327.31	318.27	318.32	317.93	320.61	398.84	450.60	358.17
294.89	270.02	269.84	269.10	266.67	266.29	265.66	268.31	280.11	342.36	270.57

380.97	360.42	360.33	355.48	349.48	349.23	348.84	350.94	408.70	464.96	376.34
14.30	36.92	37.14	35.94	34.96	34.68	34.54	35.66	68.51	45.76	40.72
114.06	151.82	151.19	153.23	153.47	153.79	153.60	153.21	90.62	179.28	144.03
27.93	28.86	28.83	31.83	34.65	34.92	34.83	34.26	10.97	15.98	20.82
1169.82	1188.73	1188.46	1207.16	1227.55	1228.54	1229.13	1221.00	1106.64	1189.49	1153.17
604.40	619.80	619.71	635.60	652.75	653.46	653.87	647.76	548.59	609.39	587.35
201.02	215.29	215.28	228.49	242.64	243.14	243.44	238.95	149.79	178.69	185.79
7.40	21.31	21.30	32.28	44.21	44.60	44.85	41.22	-37.77	-25.73	-4.90
769.40	768.80	768.48	761.80	759.59	758.98	759.16	759.34	801.16	796.73	786.61
102.49	100.51	100.46	97.41	95.38	95.36	95.38	96.03	113.30	103.86	106.71
336.15	325.93	325.37	330.04	332.75	337.26	340.04	321.47	329.09	411.32	344.16
-701.23	-704.54	-704.50	-709.82	-715.66	-716.11	-716.27	-713.69	-692.65	-728.71	-697.04
-149.72	-141.86	-141.54	-139.01	-139.30	-137.97	-137.25	-142.59	-121.11	-88.37	-129.67
66.63	80.38	80.74	77.86	77.89	74.50	72.42	84.53	131.22	50.09	73.90
220.21	220.93	220.79	222.04	223.56	224.47	225.04	220.41	247.19	254.30	228.05
749.84	756.57	756.67	753.72	752.64	752.28	752.42	752.84	760.67	785.41	765.34
-633.89	-624.74	-624.03	-623.59	-626.96	-626.94	-627.11	-624.70	-650.14	-619.00	-622.31
-232.37	-232.81	-232.79	-235.47	-238.14	-238.26	-238.33	-237.28	-227.16	-245.33	-228.85
-250.11	-236.97	-236.96	-229.55	-221.36	-221.13	-220.98	-223.17	-289.68	-301.44	-258.10
169.12	168.95	168.94	171.67	172.86	172.17	171.32	174.87	166.37	185.93	156.48
92.01	96.63	96.73	92.33	88.51	88.66	88.92	88.33	135.21	131.05	113.05
416.91	409.68	409.69	405.66	401.19	401.43	401.35	401.56	454.45	478.97	426.13
189.74	236.41	237.48	233.96	232.85	228.58	225.79	241.98	367.71	232.65	230.89
87.52	109.53	109.99	109.37	108.62	107.78	107.14	110.80	166.74	124.67	109.65

HOUR 21 (MWh)	HOUR 22 (MWh)	HOUR 23 (MWh)	HOUR 24 (MWh)
0.17	0.17	0.17	0.17
335.03	334.92	337.54	334.96
390.95	226.83	385.55	359.91
0.05	0.06	0.05	0.05
2918.82	2918.82	2918.82	2918.82
1119.28	1119.28	1119.28	1119.28
1893.31	1722.71	1786.86	1818.14
0.01	0.01	0.01	0.01
0.09	0.09	0.08	0.08
472.32	472.32	472.32	472.32
2.80	2.80	2.80	2.80
1.31	0.44	1.01	0.88
0.01	0.01	0.01	0.01
6.74	6.27	6.74	6.74
21.02	21.02	21.02	21.02
3499.12	3489.84	3494.59	3494.06
295.85	220.42	254.53	251.23
0.03	0.03	0.03	0.03
0.02	0.02	0.02	0.02
0.00	0.00	0.00	0.00
431.92	431.92	431.92	431.92
590.00	590.00	590.00	590.00
0.03	0.03	0.03	0.03
0.96	0.92	0.92	0.86
102.41	102.41	102.41	102.41
1169.02	1169.02	1169.02	1169.02
0.00	0.01	0.00	0.08
21.66	21.66	21.66	21.66
20.68	20.68	20.68	20.68
72.66	72.66	72.66	72.66
1444.52	1444.52	1444.52	1444.52
0.00	0.01	0.00	0.10
166.41	166.41	166.41	166.41
766.08	766.08	766.08	766.08
2152.48	1648.03	1020.29	407.88
24.40	24.40	24.40	24.40
314.58	314.58	314.58	314.58
31.13	6.84	0.02	0.00
87.78	87.78	87.78	87.78
689.13	614.39	545.88	457.63
51.18	51.18	51.18	51.18
16.30	16.87	16.58	16.58

0.01	0.01	0.01	0.01
147.68	157.90	147.68	140.89
2379.45	2316.38	2172.85	1953.86
7749.46	7749.46	7749.46	7749.46
13750.70	12133.62	10787.30	8694.44
0.01	0.01	0.01	0.01
0.01	0.01	0.01	0.01
0.00	0.00	0.00	0.00
7988.20	7988.20	7988.20	7988.20
432.46	172.20	169.85	102.45
0.02	0.02	0.02	0.02
0.00	0.00	0.00	0.00
0.00	0.00	0.00	0.00
59.81	59.81	59.81	59.81
3159.28	3159.28	3159.28	3159.28
322.66	322.66	322.66	276.18
0.00	0.00	0.00	0.00
0.00	0.00	0.00	0.00
0.00	0.00	0.00	0.00
5018.29	5018.29	5018.29	5018.29
13038.05	13038.05	13038.05	12655.58
0.10	0.10	0.10	0.10
0.00	0.00	0.00	0.00
0.00	0.00	0.00	0.00
2106.97	2106.97	2106.97	2106.97
6993.67	6993.67	6993.67	6993.67
0.01	0.01	0.01	0.01
0.00	0.00	0.00	0.00
0.04	0.04	0.04	0.04
1063.64	936.38	935.58	936.38
5.34	5.75	5.34	5.11
0.02	0.02	0.02	0.02
0.00	0.00	0.00	0.00
0.00	0.00	0.00	0.00
67723.41	64890.62	66916.69	65554.55
0.00	0.00	0.00	0.00
0.00	0.00	0.00	0.00
0.00	0.00	0.00	0.00
0.19	0.20	0.20	0.20
6.17	5.81	5.81	5.81
-1204.14	-1211.26	-1208.87	-1208.54
207.81	199.87	189.50	191.45
318.91	312.33	314.01	314.86
261.69	261.56	256.62	257.09

348.24	344.11	344.21	344.91
35.74	40.91	44.51	43.53
147.96	136.60	124.83	127.35
33.07	35.76	33.95	33.80
1219.57	1241.10	1234.00	1232.95
646.07	662.90	657.50	656.68
237.32	250.38	246.04	245.33
40.21	50.86	47.10	46.38
761.35	763.88	758.76	758.04
96.63	95.97	94.99	94.82
355.37	340.68	346.26	343.93
-713.11	-719.38	-717.98	-717.81
-133.98	-144.41	-129.43	-127.62
61.95	71.09	78.51	84.24
228.64	224.76	231.43	232.86
751.46	752.80	751.63	750.69
-629.77	-636.16	-629.11	-629.49
-236.55	-239.43	-238.76	-238.76
-223.24	-216.61	-219.37	-220.03
166.05	175.06	169.47	168.65
92.50	88.24	93.62	93.87
402.51	398.68	401.87	402.39
216.65	247.44	261.07	262.43
107.19	122.22	126.92	124.48

MICROGRIDS

Technology (Fuel Type)	HOUR 1 (MWh)	HOUR 2 (MWh)	HOUR 3 (MWh)	HOUR 4 (MWh)	HOUR 5 (MWh)	HOUR 6 (MWh)	HOUR 7 (MWh)	HOUR 8 (MWh)	HOUR 9 (MWh)
SOFC	8.13	8.28	8.28	8.13	8.28	8.28	8.13	8.43	8.43
REs	4.43	4.35	4.51	4.28	4.28	4.35	4.51	4.51	4.51
MT	4.05	3.99	3.99	4.05	4.05	3.99	4.05	3.92	3.92
Wind	3.59	3.57	3.54	3.54	3.54	3.54	3.69	3.41	3.47
SOFC	4.07	4.34	4.34	4.34	4.34	4.34	4.14	4.07	4.14
REs	25.83	27.88	26.62	25.83	25.83	26.66	26.51	27.18	29.94
MT	3.36	3.38	3.38	3.42	3.41	3.42	3.37	3.33	3.33
PV	89.87	89.87	89.87	89.87	89.87	89.87	89.87	89.87	89.87
NGCC	222.00	222.00	222.00	222.00	222.00	222.00	222.00	222.00	222.00
Coal	172.08	177.46	176.50	176.04	176.04	176.66	173.40	174.72	176.32
SOFC	4.84	4.71	4.71	4.71	4.71	4.71	4.84	5.04	5.24
REs	3.28	2.76	2.57	2.63	2.50	2.63	3.48	3.87	4.13
MT	2.32	2.36	2.32	2.32	2.32	2.32	2.40	2.48	2.68
NGCC	74.00	74.00	74.00	74.00	74.00	74.00	74.00	74.00	74.00
Coal	39.13	28.20	25.55	27.74	25.61	27.30	40.43	42.62	46.12
IGCC	200.00	197.34	195.60	198.53	196.34	197.07	200.00	200.00	200.00
SOFC	3.39	3.45	3.39	3.39	3.39	3.26	3.83	3.45	3.89
REs	2.31	2.30	2.48	2.07	2.12	2.57	2.69	2.31	2.98
MT	2.86	2.63	2.86	2.67	2.67	2.86	2.77	2.72	2.81
Wind	3.89	4.25	3.68	3.47	3.47	3.82	3.97	3.47	3.89
SOFC	0.00	0.00	0.00	0.00	0.00	0.00	0.00	0.00	0.00
REs	6.28	7.25	6.54	6.02	6.01	6.37	6.02	6.28	6.42
MT	1.76	1.60	1.51	1.35	1.23	1.48	1.55	1.65	1.65
PV	35.92	35.92	35.92	34.21	34.21	35.92	35.92	35.92	35.92
NGCC	110.32	107.74	109.37	96.45	94.64	108.73	111.00	111.00	111.00
Coal	45.79	45.73	40.28	22.24	21.57	39.18	39.91	66.07	71.48
SOFC	0.96	0.70	0.88	0.85	0.85	0.88	1.05	1.28	1.17
REs	1.87	1.49	1.41	1.15	1.15	1.49	1.92	1.92	1.94
MT	2.63	2.19	2.11	2.11	2.11	2.11	2.89	2.90	2.99
NGCC	74.00	73.87	71.55	69.31	67.96	71.79	74.00	74.00	74.00
Coal	11.02	11.02	11.02	9.65	9.19	11.02	13.38	29.42	32.74
IGCC	173.27	139.11	113.46	93.54	80.99	113.53	191.19	199.99	199.99
SOFC	8.61	7.29	7.29	7.11	7.04	6.67	7.84	7.72	8.20
REs	2.88	2.98	2.91	2.91	2.91	2.83	6.58	6.58	7.75
MT	3.57	3.71	3.48	3.62	3.59	3.70	3.39	3.45	3.56
Wind	3.15	2.62	3.00	2.97	3.02	3.08	3.15	3.15	3.25
SOFC	3.64	3.58	3.20	3.64	3.20	3.58	3.60	3.35	3.23
REs	14.07	14.03	14.03	14.03	14.06	14.07	24.42	24.01	21.95
MT	2.67	2.45	2.45	2.45	2.50	2.50	2.82	3.10	2.39
PV	74.92	74.92	74.92	74.92	74.92	74.92	74.92	74.92	74.92
NGCC	185.00	185.00	185.00	185.00	185.00	185.00	185.00	185.00	185.00

Coal	130.11	125.50	123.25	125.49	130.26	124.81	150.00	150.00	150.00
SOFC	7.14	5.52	5.52	5.52	5.52	5.52	7.36	7.48	7.36
REs	3.79	3.94	3.74	3.75	3.74	3.74	9.26	9.59	8.93
MT	3.46	2.45	2.45	2.45	2.45	2.45	4.91	4.76	4.29
NGCC	148.00	148.00	148.00	148.00	148.00	148.00	148.00	148.00	148.00
Coal	98.98	88.98	73.93	73.40	71.55	74.84	118.13	118.13	119.01
IGCC	400.00	400.00	400.00	400.00	400.00	400.00	400.00	400.00	400.00
SOFC	9.61	9.43	10.12	9.95	9.43	11.33	9.61	9.26	9.95
REs	4.81	4.63	5.03	4.73	4.53	5.99	4.81	4.89	6.23
MT	4.65	4.57	4.65	4.65	4.73	4.81	4.65	4.65	4.81
Wind	4.24	4.17	4.17	4.11	4.17	4.38	4.24	4.11	4.31
SOFC	1.07	1.09	1.09	1.07	1.07	1.07	1.07	0.98	1.00
REs	7.58	7.58	7.16	7.25	7.33	7.16	7.75	8.42	8.42
MT	1.00	0.77	0.81	0.80	0.80	0.78	1.00	1.01	1.00
PV	15.00	15.00	15.00	15.00	15.00	15.00	15.00	15.00	15.00
NGCC	37.00	37.00	37.00	37.00	37.00	37.00	37.00	37.00	37.00
Coal	24.51	24.70	23.71	23.91	24.31	23.71	24.70	25.70	25.90
SOFC	11.00	12.74	13.84	13.53	13.68	13.53	10.05	11.31	14.16
REs	2.03	2.28	2.29	2.18	2.23	2.28	2.18	2.43	3.46
MT	7.35	6.49	6.19	6.19	6.11	6.35	7.41	6.95	6.36
Wind	4.63	4.54	4.74	4.75	4.75	4.67	4.57	4.26	4.54
SOFC	3.82	3.77	3.91	3.77	3.77	3.77	3.82	3.77	3.81
REs	7.00	7.00	6.44	7.00	7.00	7.14	7.00	6.86	8.66
MT	1.49	1.66	1.80	1.76	1.76	1.76	1.49	1.53	1.60
PV	56.01	56.01	56.01	56.01	56.01	56.01	56.01	56.01	56.01
NGCC	137.27	136.24	142.57	139.32	138.49	138.23	137.34	143.92	148.00
Coal	25.08	23.90	33.97	26.85	26.90	25.65	25.10	38.75	76.86
SOFC	2.63	2.63	2.48	2.48	2.44	2.48	2.63	2.51	2.66
REs	1.09	1.16	1.16	1.16	1.16	1.16	1.09	1.16	1.15
MT	1.23	1.23	1.24	1.24	1.24	1.24	1.23	1.23	1.25
NGCC	36.46	36.48	32.93	32.93	33.49	32.93	36.46	33.81	37.00
Coal	3.94	3.47	3.59	3.65	4.12	3.12	3.94	3.47	4.28
IGCC	31.04	19.31	21.98	21.99	25.82	18.67	31.04	23.09	57.95
SOFC	0.01	0.01	0.01	0.01	0.01	0.01	0.01	0.01	0.01
REs	24.77	24.11	24.30	24.11	25.47	27.28	53.98	26.69	22.87
MT	4.36	4.03	4.25	3.49	2.84	3.27	2.73	3.38	2.51
Wind	0.04	0.04	0.04	0.04	0.04	0.04	0.04	0.04	0.04
SOFC	14.97	14.97	14.42	14.79	14.97	14.97	14.97	14.05	18.73
REs	32.15	32.15	32.16	32.16	32.15	32.15	32.16	32.15	58.08
MT	7.61	7.61	7.61	7.61	7.61	7.61	7.16	6.71	22.64
PV	520.39	567.36	579.33	573.48	533.18	561.68	744.41	771.81	760.42
NGCC	253.49	34.78	40.43	38.72	36.30	34.61	184.49	1124.63	2237.13
Coal	54.32	54.32	54.33	54.32	54.32	54.32	54.33	54.32	63.49
SOFC	0.00	0.00	0.00	0.00	0.00	0.00	0.00	0.00	0.00

REs	2.61	2.61	2.61	2.61	4.20	4.20	2.61	2.61	2.61
MT	0.06	0.06	0.06	0.06	0.06	0.06	0.06	0.06	0.06
NGCC	1239.65	1238.76	1250.16	1239.01	1287.47	1286.02	1265.60	1280.51	1280.26
Coal	1.64	1.64	1.64	1.64	2.78	2.78	1.64	1.80	1.79
IGCC	2953.45	2949.07	3066.61	2949.33	3287.66	3264.22	3159.59	3238.02	3237.99
SOFC	0.11	0.11	0.14	0.12	0.14	0.10	0.12	0.11	0.14
REs	6.33	6.33	6.95	6.87	6.73	6.33	6.90	5.64	7.36
MT	1.07	1.10	0.97	1.02	0.93	1.14	1.02	1.11	1.27
Wind	0.14	0.14	0.11	0.10	0.10	0.14	0.11	0.14	0.14
SOFC	0.00	0.00	0.00	0.00	0.00	0.00	0.00	0.00	0.00
REs	1.15	1.15	1.15	1.15	1.15	1.15	1.19	1.11	1.06
MT	0.05	0.05	0.05	0.05	0.05	0.05	0.05	0.05	0.05
PV	5.48	5.48	5.48	5.48	5.48	5.48	5.99	9.96	9.59
NGCC	4.86	4.86	4.86	4.86	4.86	4.86	4.86	7.16	6.59
Coal	0.00	0.00	0.00	0.00	0.00	0.00	0.00	0.00	0.00
SOFC	0.00	0.00	0.00	0.00	0.00	0.00	0.00	0.00	0.00
REs	0.82	0.82	0.82	0.82	0.82	0.82	0.82	0.88	0.88
MT	0.01	0.01	0.01	0.01	0.01	0.01	0.01	0.01	0.01
NGCC	1157.10	1157.10	1157.10	1157.10	1157.10	1157.10	1157.10	1166.28	1166.27
Coal	0.10	0.10	0.11	0.11	0.11	0.10	0.10	0.10	0.10
IGCC	1193.50	1193.50	1309.29	1193.50	1388.70	1364.25	1364.26	1449.18	1449.18
Merc - Res	30.79	17.83	14.69	13.99	13.86	20.84	57.67	91.77	94.72
Merc - Com	-347.24	-379.09	-388.86	-383.45	-355.83	-338.11	-295.55	-201.50	-4.76
Merc - Ind	-59.70	-45.50	-29.01	-45.39	-9.62	9.20	22.74	9.92	5.91
Gram - Res	25.50	16.40	13.56	14.31	14.29	18.43	45.67	72.01	73.35
Gram - Com	-115.27	-124.99	-125.18	-89.89	-73.36	-98.84	-82.58	-61.12	34.36
Gram - Ind	5.34	46.54	90.41	107.39	156.89	132.01	66.32	28.52	24.99
Krim - Res	26.58	16.73	14.57	13.60	13.60	19.76	46.96	77.00	78.16
Krim - Com	-268.11	-279.29	-286.40	-285.97	-268.48	-245.61	-254.29	-174.10	6.60
Krim - Ind	-134.38	-119.41	-81.37	-102.07	-36.98	2.52	8.66	-12.70	-12.11
Maas - Res	39.52	24.03	18.86	18.37	20.00	24.26	73.51	115.92	118.58
Maas - Com	-57.22	-61.29	-61.91	-61.19	-57.56	-52.80	-48.56	-34.21	-0.38
Zwol - Res	37.90	20.85	15.84	15.25	16.13	24.08	72.69	113.94	115.41
Zwol - Com	-116.69	-130.61	-154.34	-141.45	-123.96	-108.31	-81.78	-37.88	53.04
Zwol - Ind	56.57	68.58	74.71	69.64	79.57	99.52	98.51	103.59	64.73
D - Res	529.13	385.67	350.63	341.65	346.86	418.96	802.32	1204.27	1248.12
D - Com	1258.27	921.04	768.77	822.47	1183.10	1355.70	1374.98	1453.68	2484.61
D - Ind	440.22	454.70	482.67	450.27	588.26	970.71	1669.82	1386.85	1388.51
F - Res	496.41	368.31	336.93	328.13	334.70	398.06	768.45	1101.19	1134.69
F - Com	2218.40	2218.40	2218.40	2218.40	2218.40	2218.40	2225.30	3063.42	5022.25
F - Ind	1918.72	1918.72	1937.56	1918.72	2180.98	2549.04	3053.85	2776.64	2776.69

HOUR 10 (MWh)	HOUR 11 (MWh)	HOUR 12 (MWh)	HOUR 13 (MWh)	HOUR 14 (MWh)	HOUR 15 (MWh)	HOUR 16 (MWh)	HOUR 17 (MWh)	HOUR 18 (MWh)	HOUR 19 (MWh)	HOUR 20 (MWh)
8.28	8.13	8.28	8.43	8.43	8.28	8.28	8.43	15.00	20.39	8.57
4.51	4.51	4.51	4.51	4.51	4.51	4.51	4.51	10.57	10.73	7.50
3.92	3.99	3.86	3.92	3.92	3.92	3.99	3.92	6.20	8.86	4.70
3.53	3.70	3.64	3.47	3.47	3.70	3.64	3.41	2.95	7.84	3.76
4.08	4.08	4.09	4.14	4.09	4.08	4.08	4.25	7.48	9.16	4.26
31.89	31.22	32.68	29.20	31.91	31.89	31.22	42.00	91.84	91.84	50.16
3.38	3.38	3.38	3.33	3.38	3.38	3.38	3.42	5.18	6.45	3.38
89.87	89.87	89.87	89.87	89.87	89.87	89.87	89.87	89.87	89.87	89.87
222.00	222.00	222.00	222.00	222.00	222.00	222.00	222.00	222.00	222.00	222.00
177.36	177.36	177.80	176.04	177.42	177.36	177.36	180.00	180.00	180.00	180.00
5.18	5.18	5.18	5.18	5.18	5.18	5.18	5.18	6.98	9.12	4.91
4.13	4.13	3.74	4.13	4.00	4.07	4.13	3.61	7.65	8.89	4.13
2.68	2.73	2.56	2.44	2.60	2.60	2.73	2.52	4.57	5.60	2.56
74.00	74.00	74.00	74.00	74.00	74.00	74.00	74.00	74.00	74.00	74.00
47.87	47.43	48.75	45.25	48.31	47.87	47.56	54.44	59.32	59.69	55.75
200.00	200.00	200.00	200.00	200.00	200.00	200.00	200.00	200.00	200.00	200.00
3.51	3.39	3.51	3.64	3.64	3.45	3.89	3.45	6.82	8.54	4.50
2.79	2.45	2.69	2.98	3.02	2.41	3.02	3.07	6.15	6.49	3.73
2.77	2.72	2.77	2.81	2.81	2.77	2.81	2.81	4.71	6.33	3.73
3.89	3.82	3.89	3.89	3.89	3.68	3.97	3.89	6.50	9.64	4.60
0.00	0.00	0.00	0.00	0.00	0.00	0.00	0.00	0.00	0.00	0.00
6.42	6.42	6.43	6.41	6.44	6.43	6.42	6.46	23.87	24.05	7.29
1.65	1.65	1.65	1.65	1.65	1.65	1.65	1.65	2.91	3.10	1.66
35.92	35.92	35.92	35.92	35.92	35.92	35.92	35.92	35.92	35.92	35.92
111.00	111.00	111.00	111.00	111.00	111.00	111.00	111.00	111.00	111.00	111.00
71.94	71.94	72.07	71.94	72.16	72.04	71.94	73.13	81.50	81.50	74.93
1.17	1.17	1.17	1.32	1.17	1.17	1.17	1.16	1.60	2.58	1.22
1.99	1.99	1.99	1.99	1.99	1.99	1.99	1.99	6.13	6.37	2.40
2.99	2.99	2.99	2.99	3.00	3.00	2.99	3.03	4.60	4.89	3.11
74.00	74.00	74.00	74.00	74.00	74.00	74.00	74.00	74.00	74.00	74.00
33.07	33.01	33.33	33.01	33.43	33.33	33.33	34.30	44.03	44.03	35.34
199.99	199.99	199.99	199.99	199.99	199.99	199.99	199.99	199.99	199.99	199.99
7.91	7.93	7.94	8.20	8.07	7.94	7.90	7.64	15.18	17.64	8.02
7.82	8.19	8.19	7.97	7.68	7.97	7.89	8.19	9.93	9.93	6.66
3.62	3.56	3.33	3.56	3.56	3.62	3.56	3.50	6.93	7.78	4.02
3.25	3.15	3.15	3.25	3.20	3.25	3.20	3.15	3.00	6.56	2.86
3.23	3.23	3.23	3.23	3.23	3.23	3.23	3.23	4.67	7.50	3.23
21.54	17.02	17.84	17.02	18.25	20.72	21.13	22.78	56.10	56.10	18.66
2.39	2.74	2.67	2.67	2.59	2.43	2.39	2.86	4.41	5.40	2.59
74.92	74.92	74.92	74.92	74.92	74.92	74.92	74.92	74.92	74.92	74.92
185.00	185.00	185.00	185.00	185.00	185.00	185.00	185.00	185.00	185.00	185.00
150.00	150.00	150.00	150.00	150.00	150.00	150.00	150.00	150.00	150.00	150.00

7.36	7.36	7.24	7.11	7.36	7.36	7.36	7.36	14.31	16.62	7.24
9.04	9.15	9.15	9.26	9.15	8.93	8.93	9.37	14.96	14.96	9.15
4.14	4.21	4.68	4.06	4.14	4.14	4.14	4.68	6.62	10.57	4.14
148.00	148.00	148.00	148.00	148.00	148.00	148.00	148.00	148.00	148.00	148.00
119.01	119.01	119.01	119.01	119.01	119.01	119.01	119.01	119.89	119.89	119.01
400.00	400.00	400.00	400.00	400.00	400.00	400.00	400.00	400.00	400.00	400.00
9.61	10.12	10.12	9.95	8.91	9.43	9.26	10.12	18.56	23.57	10.61
5.84	6.33	6.43	5.62	5.59	5.82	5.82	6.03	13.74	13.84	12.42
4.65	4.65	4.65	4.65	4.65	4.73	4.73	4.65	8.93	10.65	6.74
4.24	4.45	4.45	4.45	4.04	4.17	4.17	4.45	4.44	9.40	4.17
1.07	1.02	1.02	1.02	1.02	1.02	1.00	1.09	1.77	2.34	1.00
7.50	7.92	8.34	8.25	8.34	8.34	8.34	8.17	10.18	11.44	8.42
1.01	1.00	1.00	1.00	1.00	1.00	1.01	1.00	0.70	1.50	1.00
15.00	15.00	15.00	15.00	15.00	15.00	15.00	15.00	15.00	15.00	15.00
37.00	37.00	37.00	37.00	37.00	37.00	37.00	37.00	36.73	37.00	37.00
26.29	26.49	26.49	26.49	26.49	26.49	26.49	26.49	27.09	27.09	25.30
14.01	13.83	13.87	14.16	14.16	13.97	14.16	14.13	13.20	21.55	16.34
4.41	4.46	4.46	4.26	4.16	4.41	4.26	4.41	6.51	6.81	5.51
7.21	7.29	7.29	6.77	6.69	7.29	6.69	6.78	6.97	10.76	6.35
4.63	4.63	4.56	4.65	4.58	4.63	4.58	4.57	4.24	9.01	6.46
3.77	3.73	3.73	3.55	3.55	3.81	3.81	3.73	3.31	6.02	3.77
8.66	8.81	8.81	8.66	8.81	8.95	11.06	8.95	16.62	19.25	8.81
1.63	2.34	2.34	2.24	1.49	1.53	1.66	2.34	2.81	4.02	1.56
56.01	56.01	56.01	56.01	56.01	56.01	56.01	56.01	56.01	56.01	56.01
148.00	148.00	148.00	148.00	148.00	148.00	148.00	148.00	148.00	148.00	148.00
77.44	77.44	77.44	77.44	77.44	77.05	72.98	77.44	78.59	78.59	77.44
2.66	2.57	2.57	2.60	2.60	2.72	2.72	2.57	2.51	4.16	2.69
1.15	1.10	1.10	1.10	1.10	1.16	1.16	1.12	0.69	1.68	1.15
1.25	1.28	1.28	1.28	1.28	1.28	1.28	1.28	1.83	2.51	1.28
37.00	37.00	37.00	37.00	37.00	37.00	37.00	37.00	37.00	37.00	37.00
4.28	4.51	4.51	4.45	4.45	4.22	4.28	4.51	7.54	7.95	4.39
57.49	58.42	58.42	58.42	58.42	58.50	58.48	58.42	63.04	63.04	58.42
0.01	0.01	0.01	0.01	0.01	0.01	0.01	0.01	0.01	0.01	0.01
56.66	59.04	59.75	31.13	27.96	61.57	60.93	63.44	83.89	84.51	60.94
2.73	2.84	2.84	2.62	2.84	2.84	2.84	2.84	10.59	13.16	2.84
0.04	0.04	0.04	0.04	0.04	0.04	0.04	0.04	0.05	0.10	0.04
14.77	12.37	14.85	14.40	18.54	18.36	14.48	11.15	18.92	22.06	13.31
58.51	57.62	55.80	55.80	61.15	62.78	61.15	57.42	219.90	223.17	32.15
16.38	17.55	21.98	16.38	23.44	23.88	23.44	22.19	44.47	61.03	6.71
761.45	760.95	760.98	759.75	753.18	751.25	749.04	754.96	653.81	771.81	771.81
2163.56	2178.65	2213.88	2058.86	2288.34	2303.99	2290.32	2231.06	2391.69	2391.69	1557.37
60.98	60.98	60.48	57.94	66.89	70.28	68.59	63.49	230.03	231.73	54.32
0.00	0.00	0.00	0.00	0.00	0.00	0.00	0.00	0.00	0.00	0.00
2.61	2.61	2.61	2.61	2.61	2.61	2.61	2.61	14.37	15.04	5.66

0.06	0.06	0.06	0.06	0.06	0.06	0.06	0.06	0.12	0.15	0.08
1283.37	1281.00	1282.00	1276.00	1267.14	1270.33	1271.10	1273.67	1291.75	1291.75	1291.75
2.14	1.86	2.06	1.64	1.64	1.64	1.64	1.64	9.66	10.80	5.89
3241.62	3238.07	3238.18	3212.59	3160.41	3173.30	3186.32	3190.93	3312.28	3312.28	3312.28
0.13	0.13	0.11	0.14	0.08	0.12	0.11	0.11	0.10	0.26	0.15
7.13	7.13	6.79	7.59	4.94	6.33	6.44	6.33	4.60	15.66	9.37
1.19	1.22	1.22	1.25	0.78	1.18	1.16	1.16	1.19	2.07	1.47
0.14	0.13	0.13	0.12	0.12	0.14	0.14	0.14	0.14	0.40	0.15
0.00	0.00	0.00	0.00	0.00	0.00	0.00	0.00	0.00	0.00	0.00
1.35	1.02	1.95	1.06	1.06	1.10	1.06	1.06	2.16	5.87	1.41
0.05	0.05	0.05	0.05	0.05	0.05	0.05	0.05	0.05	0.12	0.05
15.97	14.76	25.74	9.56	11.58	9.34	9.55	9.83	21.64	34.63	15.59
12.59	9.06	15.29	6.73	6.24	5.14	5.41	5.14	21.80	33.44	10.00
0.00	0.00	0.00	0.00	0.00	0.00	0.00	0.00	0.00	0.00	0.00
0.00	0.00	0.00	0.00	0.00	0.00	0.00	0.00	0.00	0.00	0.00
0.91	0.88	0.88	0.79	0.82	0.82	0.82	0.82	1.20	1.84	0.97
0.01	0.01	0.01	0.01	0.01	0.01	0.01	0.01	0.01	0.03	0.01
1166.90	1166.59	1166.81	1165.85	1157.10	1157.10	1157.10	1157.10	1173.28	1173.28	1172.14
0.12	0.10	0.11	0.10	0.10	0.12	0.11	0.11	0.14	0.24	0.15
1449.26	1449.22	1449.24	1442.91	1317.25	1340.03	1309.29	1309.30	1506.59	1529.12	1484.33
85.77	79.69	81.73	92.71	91.69	79.60	70.61	70.77	76.20	118.60	136.47
104.44	114.40	131.03	83.78	-20.81	-50.43	-0.89	13.50	-32.53	-127.59	-226.79
-7.00	4.38	3.69	17.14	67.01	25.20	-58.75	-64.75	-77.75	-49.93	-56.32
66.98	63.56	64.09	71.64	70.59	62.64	54.26	55.72	59.75	108.45	104.41
89.93	95.11	103.75	77.24	27.66	11.79	36.91	49.76	27.55	14.14	-68.93
13.60	24.71	24.38	34.63	87.24	45.37	-38.51	-39.56	-55.52	-2.61	-31.23
70.32	65.15	67.36	76.02	75.51	64.20	56.35	57.46	61.81	94.25	119.33
-108.95	102.23	117.70	74.64	-9.57	-38.09	2.53	24.29	-5.25	-83.43	-163.98
-33.07	-12.52	-12.83	9.05	113.77	29.89	-139.08	-140.21	-155.92	-102.54	-118.11
108.47	99.30	102.23	116.14	115.63	99.70	88.86	88.57	93.22	155.53	167.03
17.95	19.46	22.01	13.09	-2.96	-9.02	0.00	4.16	3.30	18.92	-32.88
102.72	94.78	97.81	111.10	109.35	93.68	83.25	84.05	108.14	187.18	166.51
126.68	132.75	144.75	109.18	43.82	23.61	58.40	74.61	70.57	38.08	-79.44
60.13	64.12	64.11	70.16	96.19	74.95	32.91	33.00	25.21	69.80	38.00
1114.22	1045.68	1064.86	1213.54	1204.59	1034.96	935.95	936.14	1130.19	1522.03	1717.82
3784.58	3876.65	4041.33	3622.84	2295.87	1950.22	2501.41	2877.79	2637.88	1594.47	1061.97
1184.44	1383.86	1377.50	1600.88	2581.21	1822.82	343.58	326.70	161.69	559.63	361.27
1047.68	986.66	1004.96	1110.42	1114.97	983.66	893.49	896.62	1095.23	1468.08	1590.93
6109.18	6208.98	6337.75	5861.03	4962.91	4649.58	5137.51	5406.14	5411.10	4420.84	3105.19
2604.77	2774.68	2773.43	2949.04	3948.59	3249.57	1937.56	1937.55	1698.53	1473.03	1890.11

HOUR 21 (MWh)	HOUR 22 (MWh)	HOUR 23 (MWh)	HOUR 24 (MWh)
8.43	8.13	8.28	8.28
4.35	4.43	4.43	4.43
3.99	3.99	3.99	3.99
3.30	3.64	3.64	3.64
4.07	4.14	4.07	4.14
27.18	26.65	27.18	27.18
3.33	3.37	3.33	3.33
89.87	89.87	89.87	89.87
222.00	222.00	222.00	222.00
174.72	173.98	174.72	174.72
5.04	4.91	5.04	5.04
4.00	3.55	4.00	3.87
2.48	2.60	2.48	2.48
74.00	74.00	74.00	74.00
42.67	41.84	42.62	42.62
200.00	200.00	200.00	200.00
3.89	3.58	3.32	3.89
3.12	2.55	2.31	3.07
2.91	2.77	2.77	3.00
3.97	3.89	3.54	3.97
0.00	0.00	0.00	0.00
6.39	6.27	6.28	6.27
1.67	1.65	1.65	1.65
35.92	35.92	35.92	35.92
111.00	111.00	111.00	111.00
70.74	56.18	66.60	66.55
1.32	1.07	1.27	1.27
1.94	1.97	1.92	1.92
2.94	2.89	2.91	2.91
74.00	74.00	74.00	74.00
32.35	21.20	30.07	29.76
199.99	199.99	199.99	199.99
9.09	9.14	7.58	8.11
4.54	4.98	6.73	4.91
3.67	3.33	3.45	3.33
2.77	3.11	3.11	3.11
3.23	3.35	3.60	3.60
20.72	23.60	23.60	23.60
2.43	3.10	3.06	2.86
74.92	74.92	74.92	74.92
185.00	185.00	185.00	185.00
150.00	150.00	150.00	150.00

7.60	7.48	7.60	7.60
9.48	9.59	9.48	9.37
4.83	4.76	4.83	4.91
148.00	148.00	148.00	148.00
118.13	118.13	118.13	118.13
400.00	400.00	400.00	400.00
11.51	9.26	9.43	9.61
6.53	4.99	4.81	4.91
4.75	4.57	4.65	4.65
4.11	4.11	4.17	4.24
1.00	1.00	1.07	1.07
8.42	8.25	8.17	7.75
1.00	1.01	1.00	1.00
15.00	15.00	15.00	15.00
37.00	37.00	37.00	37.00
25.90	26.10	25.30	24.70
13.53	12.42	10.21	10.36
2.03	2.08	2.28	2.18
5.86	6.41	7.01	7.42
4.12	4.78	4.15	4.57
3.77	3.73	3.77	3.82
8.38	7.71	7.00	7.00
1.60	1.56	1.49	1.49
56.01	56.01	56.01	56.01
148.00	145.83	138.46	137.38
73.98	47.47	26.31	25.11
2.66	2.57	2.60	2.63
1.15	1.16	1.09	1.09
1.24	1.23	1.24	1.23
37.00	34.56	36.73	36.46
4.22	4.12	3.94	3.94
49.63	31.93	27.75	31.06
0.01	0.01	0.01	0.01
61.01	44.47	57.78	52.71
2.84	2.73	2.73	2.73
0.04	0.04	0.04	0.04
15.16	14.97	14.97	14.97
32.17	32.15	32.16	32.15
6.71	6.71	7.61	7.61
771.81	771.81	721.34	664.16
587.74	222.53	139.60	67.31
54.33	54.32	54.33	54.32
0.00	0.00	0.00	0.00
4.20	4.20	2.61	2.61

0.06	0.06	0.06	0.06
1288.31	1285.93	1266.88	1243.63
2.88	2.78	1.64	1.64
3287.79	3263.11	3160.21	3006.58
0.12	0.10	0.12	0.10
6.67	6.33	6.33	6.33
1.16	1.02	1.12	1.10
0.14	0.13	0.14	0.14
0.00	0.00	0.00	0.00
1.06	1.32	1.15	1.15
0.05	0.05	0.05	0.05
11.58	10.43	5.48	5.48
6.24	7.04	4.86	4.86
0.00	0.00	0.00	0.00
0.00	0.00	0.00	0.00
0.87	0.82	0.82	0.82
0.01	0.01	0.01	0.01
1157.74	1157.10	1157.10	1157.10
0.12	0.12	0.11	0.11
1400.98	1376.76	1309.29	1193.50
124.96	101.82	80.68	54.69
-255.79	-288.17	-309.65	-324.18
-22.34	-21.04	-53.12	-63.97
95.05	78.18	64.01	42.01
-92.79	-94.05	-115.65	-122.45
-6.63	5.53	-35.26	-46.03
106.83	86.38	67.07	46.43
-215.21	-245.78	-263.96	-274.62
-75.94	-75.73	-139.91	-160.79
153.96	128.90	102.74	69.47
-43.44	-48.40	-51.69	-52.58
155.37	126.22	102.27	68.38
-114.73	-107.02	-92.06	-98.84
57.99	78.42	64.72	56.43
1538.53	1297.19	1051.08	768.44
1394.77	1407.18	1308.34	1299.23
764.84	788.02	371.60	373.61
1435.57	1201.09	994.37	734.40
2606.74	2248.92	2221.13	2218.40
2332.65	2359.89	1937.56	1918.72